A STUDY OF LIQUID-LIQUID EXTRACTION IN A SIEVE PLATE COLUMN

by

JIMMY OLATOKUNBO OLOIDI

Doctor of Philosopy

THE UNIVERSITY OF ASTON IN BIRMINGHAM

October 1987

The University of Aston in Birmingham

"A STUDY OF LIQUID-LIQUID EXTRACTION IN A SIEVE PLATE COLUMN"

Jimmy Olatokunbo Oloidi

Doctor of Philosophy 1987

SUMMARY

The literature relating to sieve plate liquid extraction columns and relevant hydrodynamic phenomena have been surveyed. Mass transfer characteristics during drop formation, rise and coalescence, and related models were also reviewed.

Important design parameters i.e flooding, dispersed phase hold-up ,drop size distribution, mean drop size, coalescence/flocculation zone height beneath a plate and jetting phenomena were investigated under non-mass transfer and mass transfer conditions in a 0.45m diameter, 2.3m high sieve plate column. This column had provision for four different plate designs, and variable plate spacing and downcomer heights, and the system used was Clairsol '350'(dispersed) - acetone - deionised water (continuous) with either direction of mass transfer.

Drop size distributions were best described by the functions proposed by Gal-or, and then Mugele-Evans. Using data from this study and the literature, correlations were developed for dispersed phase hold-up, mean drop size in the preferred jetting regime and in the non-jetting regime, and coalescence zone height.

A method to calculate the theoretical overall mass transfer coefficient allowing for the range of drop sizes encountered in the column gave the best fit to experimental data. This applied the drop size distribution diagram to estimate the volume percentage of stagnant, circulating and oscillating drops in the drop population. The overall coefficient K_{cal} was then calculated as the fractional sum of the predicted individual single drop coefficients and their proportion in the drop population.

In a comparison between the experimental and calculated overall mass transfer coefficients for cases in which all the drops were in the oscillating regime (ie 6.35mm hole size plate), and for transfer from the dispersed(d) to continuous(c) phase, the film coefficient k_d predicted from the Rose-Kintner correlation together with k_c from that of Garner-Tayeban gave the best representation. Droplets from the 3.175mm hole size plate, were of a size to be mainly circulating and oscillating; a combination of k_d from the Kronig-Brink (circulating) and Rose-Kintner (oscillating) correlations with the respective k_c gave the best agreement.

The optimum operating conditions for the SPC were identified and a procedure proposed for design from basic single drop data.

Key Words : Liquid-Liquid Extraction. Sieve Plate Column.

ACKNOWLEDGMENTS

The author is greatly indebted to and expresses his gratitude to Professor G.V. Jeffreys and Dr. C.J. Mumford for their supervision encouragement, motivation, continual help and constructive criticism throughout the period of this research and compilation of this report. The author values highly the opportunity to have worked with such stimulating individuals.

The author also wishes to thank Mr. N.Roberts and the entire staff of the Chemical Engineering Department's workshop, analytical laboratory and stores, and also Mr. J.Holloway for his assistance with the photographic work.

Finally, thanks are due to Aston University for the award of a University Studentship.

LIST OF CONTENTS

		Page
	SUMMARY	2
	ACKNOWLEDGEMENTS	3
	LIST OF CONTENTS	4
	LIST OF FIGURES	8
	LIST OF TABLES	10
1	INTRODUCTION	13
2	EQUIPMENT FOR LIQUID-LIQUID EXTRACTION	
	2.1 Selection of Extraction Equipment	16
	2.2 Liquid-liquid Extraction Operations	20
	2.3 Design Fundamentals	20
3	THE SIEVE PLATE EXTRACTION COLUMN (SPC)	
	3.1 Column Design	25
	3.2 Distributor and Sieve Plate Design	26
	3.3 Settling/Flocculation Zone	31
	3.4 Effect of Operating Parameters	33
	3.4.1 Effect of Plate Spacing	33
	3.4.2 Effect of Hole Size and Hole Area	34
	3.4.3 Coalescence Height	34
	3.4.4 Effect of Physical Properties	35
	3.4.5 Effect of Surfactants	36
	3.5 Applications and Advantages	37

Page

4 DROPLET HYDRODYNAMICS

4.1 Droplet Phenomena 40

4.1.1 Drop Formation From Sieve Plates 40

4.1.2 Jetting 41

4.1.3 Dropsize Distribution 43

4.2 Droplet Velocity 44

4.2.1 Terminal Velocity 46

4.2.2 Characteristic/Slip Velocity 47

4.3 Droplet Coalescence 50

4.3.1 Mechanisms 50

4.3.2 Drop-Interface Coalescence 51

4.3.3 Drop-Drop Coalescence 52

4.3.4 Coalescence in Swarms 52

4.3.5 Effect of Coalescence on Mass Transfer 55

4.3.6 Coalescence Aids 55

4.4 Dispersed Phase Hold-up 56

4.5 Flooding 57

5 MASS TRANSFER CHARACTERISTICS

5.1 Introduction 61

5.2 Mass Transfer During Drop Formation 61

5.3 Mass Transfer During Travel Through The Continuous Phase 64

5.3.1 The Dispersed Phase Mass Transfer Coefficient 65

5.3.1.1 Stagnant drops 66

5.3.1.2 Circulating drops 68

5.3.1.3 Oscillating drops 70

Page

5.3.2 The Continuous Phase Mass Transfer Coefficient 71

5.3.2.1 Stagnant drops 72

5.3.2.2 Circulating drops 72

5.3.2.3 Oscillating drops 73

5.3.2.4 Swarms of drops 73

5.4 Mass Transfer During Coalescence 77

5.5 Surface Active Agents and Interfacial Effects 78

5.6 Mass Transfer Characteristics Of the Sieve Plate Column 79

5.6.1 Stage Efficiency 79

5.6.2 Effect of Flowrates on Mass Transfer 81

5.6.3 Axial Mixing 82

6 **EXPERIMENTAL INVESTIGATION**

6.1 Introduction 85

6.2 Equipment Design 85

6.3 Experimental Techniques 94

6.3.1 Selection of Liquid-Liquid Test System 94

6.3.2 Measurement of Physical Properties 95

6.3.3 Determination of Equilibrium Distribution Data 98

6.3.4 Solute Analysis 99

6.4 Experimental Procedure 102

6.4.1 Hydrodynamics 102

6.4.1.1 Flooding 103

6.4.1.2 Dropsize and Dropsize Distribution 104

6.4.1.3 Dispersed Phase Hold-up 106

6.4.1.4 Flow Distributions 106

Page

6.4.2 Mass Transfer Experiments 109

7 PRESENTATION AND DISCUSSION OF RESULTS : HYDRODYNAMICS

7.1 Modelling of the Hydrodynamic Characteristics by Dimensional Analysis 109

7.2 Experimental Hydrodynamics 111

7.2.1 Flooding 111

7.2.2 Jet Lengths From Sieve Plates 116

7.2.3 Coalescence Heights 124

7.2.4 Dropsize and Size Distribution in Column. 130

7.2.5 Characteristic/Slip Velocity and Dispersed Phase Hold-up 142

8 PRESENTATION AND DISCUSSION OF RESULTS : MASS TRANSFER 145

8.1 Effect of Mass Transfer on Jet Length 145

8.2 Experimental Mass Transfer Coefficients 147

8.3 Mass Transfer Theoretical Models 148

8.4 Volume fractions or Area fractions for Weighted Overall Mass Transfer Coefficient Calculations 152

8.5 Experimental Observations 154

8.6 Comparision of Experimental and Theoretical Results 163

9 DEVELOPMENT OF A DESIGN PROCEDURE FOR A SIEVE PLATE COLUMN

9.1 Introduction 168

9.2 Design Parameters 169

9.3 Design Recommendations 170

9.4 Pilot Scale Testing and Scale-up 172

9.5 Design of Column Internals 173

9.6 Design Flow Diagram 174

Page

10 CONCLUSIONS AND RECOMMENDATIONS

10.1 Conclusions 175

10.2 Recommendations For Further Work 177

APPENDICES 180

NOMENCLATURE 275

REFERENCES 280

LIST OF FIGURES

2.1 A selection of liquid-liquid extraction columns. 18

3.1 Sieves in vertical plates. 30

3.2 Modified sieve plate 30

3.3 Underflow weir plates. 30

3.4 Drop formation and coalescence phenomena in the sieve plate extraction column. 32

4.1 Correlation of drag coefficient C_D and Reynolds number Re for drops and rigid sphere. 50

4.2 Effect of mass transfer on interdrop coalescence. 54

5.1 Murphree stage efficiency. 79

6.1 General arrangement of the sieve plate extraction column. 86

6.2 Schematic flow diagram of the Sieve plate extraction column. 88

6.3 General arrangement of the Sieve Plate Extraction column. 90

6.4a Knitmesh Coalescer. 91

6.4b Top cover detail of the SPC. 91

6.5 Sieve plate details. 92

6.6 Variation of Interfacial Tension with Concentration of Acetone in Clairsol'350'- Deionised water. 96

6.7 Equilibrium Diagram For Clairsol-Acetone- Water System. 100

page

6.8 Concentration of Acetone in Clairsol versus Ultra-Violet Absorbance. 101

6.9 Concentration of Acetone in Water versus Ultra-Violet Absorbance. 101

7.1 Linear Regression Logic Diagram. 112

7.2 Comparison of flooding correlations. 113

7.3 Drop formation by jetting. 117

7.4 Drop formation by drip-point. 117

7.5 Experimental flood points. 113

7.6 Effect of dispersed phase flowrate on jet length. 119

7.7 Effect of continuous phase flowrate on jet length. 119

7.8 Coalescence/Floocculation height beneath the sieve plate. 125

7.9 Typical droplet dispersion. 125

7.10 Droplet swarm flow patterns. 132

7.11 Droplet swarm flow patterns (reduced circulation). 132

7.12 Experimental vs Calculated coalescence height. 133

7.13 Experimental vs Calculated hold-up. 133

7.14 Typical drop size distribution . 135

7.15 Experimental and Theoretical distribution function curves. 136

7.16 Comparison of Experimental and Calculated values of d_{32} 138

7.17 Drop size profile along the Column. 138

7.18 Experimental vs Calculated mean drop size d_{32} (jetting regime with U_c). 140

7.19 Experimental vs Calculated mean drop size d_{32} (jetting regime without U_c). 140

7.20 Experimental vs Calculated mean drop size d_{32} (Non-jetting regime with U_c). 141

7.21 Experimental vs Calculated mean drop size d_{32} (Non-jetting regime without U_c). 141

page

7.22 Variation of U_k with plate spacing. 144

7.23 Variation of U_k with plate hole size. 144

8.1 Effect of mass transfer on jet length 146

9.1 Design flow diagram. 174

10.1 Novel Sieve Plate Column 179

LIST OF TABLES

2.1 Factors Determining the Choice of an Extractor. 17

3.1 Summary of Industrial Applications of the SPC. 39

4.1 Distribution functions. 45

4.2 Factors affecting Coalescence Rate. 53

5.1 Correlations for Mass Transfer During Drop Formation. 62

5.2 Correlations for Dispersed Phase Mass Transfer Efficiency During Drop Travel. 67

5.3 Correlations for Continuous Phase Mass Transfer During Drop Travel. 74

6.1 Plate Layout Details 94

7.1 Experimental Hold-up at Flooding for the 6.35mm Hole Size Plate . 115

7.2 Experimental Flooding Velocities. 115

7.3 Jetting Velocities. 115

7.4 Experimental Jet Length. 120

7.5 Experimental Hydrodynamics Results. 126

7.6 Distribution Parameters in the SPC for the 6.35mm Hole Size Plate 134

8.1 Mass transfer coefficient models. 150

8.2 Experimental Mass Transfer Results. 155

8.3 Theoretical Mass Transfer Results. 158

8.4 Theoretical Mass Transfer Results Using Drop Size Distribution 161

LIST OF APPENDICES

		Page
1	System physical properties.	180
2	Derivation of dimensionless groups for coalescence height correlation	181
3	Computer Program Description for Multi-linear Regression	184
4	Dimensions of the Sieve Plate Column internals and Tanks	190
5	Drop size distribution table	191
6	Computer program for the calculation of drop size distribution data from photographs counted on the Carl Zeiss TG3 particle size analyser.	193
7	Computer program for the calculation of experimental mass transfer coefficients	195
8	Computer program for the calculation of theoretical mass transfer coefficients.	196
9	Calculation of the mean dropsize and distribution parameters for the Log-normal, Mugele-Evans (Upper-Limit) and Gal-or distribution functions.	198
10	Calculation of the experimental mass transfer coefficients	200
11	Calculation of the theorectical mass transfer coefficients	202
12	Calculation of the Slip velocity using Grace *et al* and Olney's equation.	207
13	Publications	208
i)	"Hydrodynamics of a Pilot Scale Sieve Plate Extraction Column" Solvent Extraction and Ion Exchange Research Meeting, Soc. of Chem. Ind. 8th May 1985 J.O.Oloidi and C.J.Mumford.	209
(ii)	"Correlation of Design Parameters for the Sieve Plate Extraction Column (SPC)" Int.Solvent Extraction Conference, Munich Vol.3,p157 1986 J.O.Oloidi, G.V.Jeffreys and C.J.Mumford.	231

Page

(iii) "Mass Transfer Characteristics of a Pilot-Scale Sieve Plate Extraction Column" 242
Extraction '87 -The Recovery of High Value Materials,Inst. of Chem.Eng. Symp. 103 Dounreay 22-25 June 1987.
J.O.Oloidi, G.V.Jeffreys and C.J.Mumford.

(IV) "Mass Transfer Characteristics of Single, and Pairs of Large Oscillating Drops" 258
Extraction '87 -The Recovery of High Value Materials,Inst. of Chem.Eng. Symp. 103 Dounreay 22-25 June 1987.
M.M Al-Faize, G.V.Jeffreys, C.J.Mumford and J.O.Oloidi.

UNBOUND MATERIAL

Table U1 Literature data of experimental coalescence height (static hold-up)
Table U2 Experimental and predicted (Equation 7.9) coalescence height
Table U3 Experimental and Theoretical (Table 4.1) distribution functions
Table U4 Literature data of experimental mean dropsize in the jetting regime.
Table U5 Experimental and predicted (Equation 7.11 &7.12) mean dropsize in the jetting regime.
Table U6 Literature data of experimental mean dropsize in the non-jetting regime
Table U7 Experimental and predicted (Equation 7.13&7.14) mean dropsize in the non-jetting regime.
Table U8 Literature data of experimental hold-up data.
Table U9 Experimental and predicted (Equation 7.15) hold-ups.

CHAPTER ONE

INTRODUCTION

Liquid-liquid extraction relies upon the unequal distribution of components between two immiscible liquid phases. Mass transfer of a solute will occur as a spontaneous process if the phases when contacted are not at equilibrium. The unit operation therefore comprises the recovery of solute(s) from a solution by admixture with a solvent. The extracting solvent used must be immiscible, or partially miscible, with the solution to be extracted. In addition, the solute should have a high affinity for the extracting solvent.

Liquid-liquid extraction is often applied to separate a mixture when it is impracticable, inconvenient, or less economical to use alternative processes such as evaporation, crystallisation and distillation. It is used when the substances to be recovered are relatively non-volatile, of close boiling point, heat sensitive, or present in relatively small amounts.

Liquid-liquid extraction involves two basic steps: (1) intimate mixing of the extracting solvent with the solution to be extracted followed by (2) separation of the mixed solution into two immiscible liquid phases. The liquid phase that contains the greater concentration of the solvent and smaller concentration of the feed is referred to as the extract . The other liquid phase, which contains a greater concentration of the feed liquid and a smaller concentration of solvent is referred to as the raffinate. Other operations are necessarily involved in the total separation process, ie separation of the solute from the extracting solvent and the subsequent recovery of the solvent for further extraction. These may be by distillation, solvent-stripping or further extraction. Whilst distillation exploits differences in volatilities of components, liquid-liquid extraction exploits differences in solute solubilities in a selected solvent. Generally, it offers some potential for energy reduction compared to other separation processes.

Liquid-liquid extraction currently plays a very important role in some areas of

chemical production [12, 97, 156, 295-6]: nuclear fuel extraction and recovery, hydrometallurgical processes, petrochemicals, agricultural (fertilizers) production and petroleum refining. In all the above cases, a rational selection of operating conditions, based on both theoretical and practical considerations, leads to a technically sound and economical extraction process.

The increased use of liquid-liquid extraction has been an incentive to research on the fundamentals of extraction processes and on design methods. Most of the fundamental work is being conducted using systems specially recommended for investigations by the European Federation of Chemical Engineering (EFCE) and other authors [9] due to (a) prospects of energy savings compared with distillation when a minor but heavy constituent of the feed mixture is to be recovered; (b) possibilities of avoiding temperature damage that might be caused by distillation or other 'thermally-driven' separation methods.

The majority of research to date has, with few exceptions, totally neglected the distribution of drop sizes that will almost inevitably be present in most liquid-liquid dispersions, and the effect this has on the hydrodynamics and (since mass transfer coefficients are dropsize related) on the mass transfer performance of an extraction column.

The present work forms part of a continuing study of the hydrodynamics and mass transfer performance of a pilot-scale sieve plate extraction column (SPC). Many SPC's are in use commercially with uncertainty as to their mode of operation and the SPC appears increasingly attractive compared to agitated columns which require some energy input. As with other extraction columns, investigations performed in laboratory columns, eg of 10 to 15 cm diameter, are unlikely to model conditions in commercial scale equipment because of difficulties in maintaining geometric and dynamic similarity, due to wall effects and interplate mixing characteristics.

The sieve plate column (SPC) used in this research was 45 cm in diameter with a working height of 2.3 m. The test system was deionised-water(continuous)

-acetone(solute)-Clairsol'350(dispersed), a paraffinic hydrocarbon, principally decane.

The hydrodynamic studies included measurements of dropsize distribution, jetting phenomena, dispersed phase (operating) hold-up, coalescence height (static hold-up), flooding and characteristic velocity. Mass transfer experiments were performed for either direction of solute transfer, with initial solute concentrations of 0-5% w/w. Both the hydrodynamics and mass transfer experiments were performed at four plate spacings: 34, 30, 26 and 20 cm with two different holesize plates: 3.175 mm (drilled) and 6.350 mm (drilled and punched) respectively. In addition to furthering understanding of how an SPC column operates and the factors affecting hydrodynamics and mass transfer characteristics, this has enabled a proposal to be made for a design procedure.

CHAPTER TWO

LIQUID-LIQUID EXTRACTION EQUIPMENT

2.1 Selection of Extraction Equipment

A wide range of extractor designs has been proposed, albeit not all with industrial applications [12, 172, 196, 199a, 223, 304]. Numerous criteria, in the form of charts or tables, have been proposed to assist in the selection of extraction equipment [96, 211, 292]. Table 2.1 is typical [172]. However, these recommendations are generally only of a qualitative nature and are, in some cases, contradictory because data upon which to base an objective comparison are not available. Furthermore, none of the selection tables or charts is complete in itself, ie they must be considered in combination and none take fully into account extractor and extraction process economics.

The selection of a particular extractor for a specific separation process is generally dictated by economics and is still largely based on experience. It is first necessary to establish the desired solute recovery for specific flowrates and to determine the physical and chemical properties of the system. Any specific problems, such as complications arising from the accummulation of solids, emulsion formation or the presence of degradable materials, must be taken into account. The location of the extractor in terms of floor area or headroom available is also an important factor. Finally, the cost of installation, maintenance and operation must be estimated for the extractor that approaches closest to all requirements.

In the intermediate range of power requirement for the interdispersion of solvents, rotary agitated columns generally represent the best choice, but their operation becomes unstable if emulsions are formed. In such situations, centrifugal extractors are the obvious choice. Unagitated columns are used, if the power requirement is low [231]. Pulsed column designs are favoured if the column must be leak-tight (ie avoiding agitator seals) and maintenance free, eg in nuclear fuel reprocessing applications.

Many different extractors are used commerically, Figure 2.1, operating in either

Table 2.1 Factors Determining the Choice of an Extractor (172)

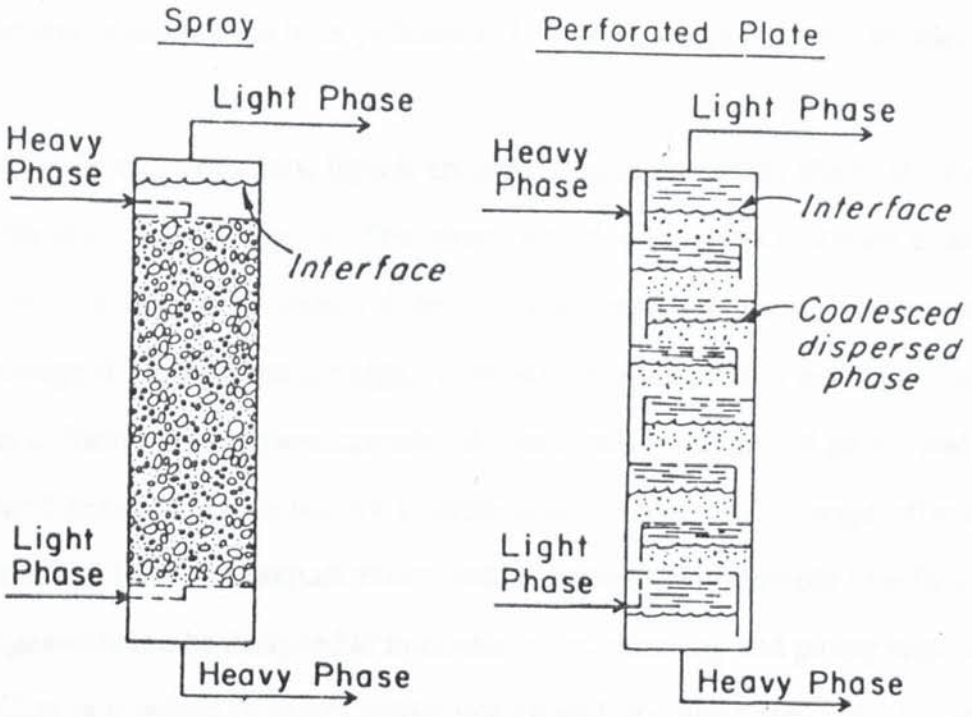

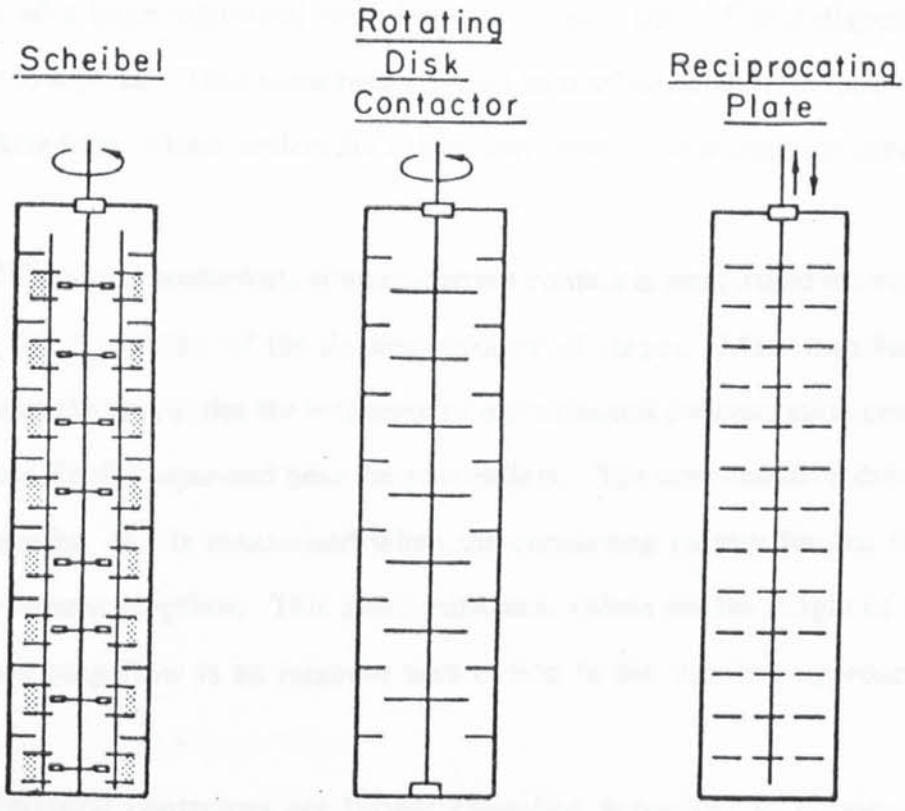

Figure 2.1 A selection of liquid-liquid extraction columns

a stagewise or differential mode. A summary of features and fields of application of various extractors has been published [117, 167], which also aids in selection.

a) In stagewise extractors, liquids are mixed, extraction takes place, and the phases are separated in discrete stages. The mixer settler is the most common example but, in general, is applied only when > 4 theoretical stages are required. The capital cost tends to be large if throughputs are high. For continuous operation, many units are placed in series to form a counterflow cascade. A considerable amount of piping and pumping is required between stages but, by suitable mixer design, 100% stage efficiency can be approached [117]. Compact mixer settler systems with simple overflow-underflow arrangements can be designed to minimise space, pumping and piping requirements.

Care is required in mixer settler design and operation since intense agitation can provide high mass transfer rates, due to turbulence in the continuous phase and the creation of a large interfacial area, but can produce liquid-liquid dispersions that are difficult to separate. Thus some balance must be reached between intensity of dispersion and settling time. Mixer settlers are extensively used in the mining industry.

(b) In differential contactors, counter-current contact is established between the phases to give the equivalent of the desired number of stages. Mass transfer takes place throughout the unit under the influence of a continuous concentration gradient and the phases are finally separated near the two outlets. The concentration driving force for mass transfer, ΔC, is maximised when the contacting pattern for the two phases is counter-current plugflow. This gives minimum values for the height of transfer unit, HTU, and plug flow is an inherent assumption in the simplest approach to column design.

Differential contactors are further classified according to gravity-driven flow, mechanical agitation or centrifugal action [12, 97, 156, 295-6].

2.2 Liquid-Liquid Extraction Operations

Commercial and pilot scale extractions may be carried out under either co-current or counter-current conditions but the latter predominates. In co-current extraction solvent is added to the feed mixture, and after phase contacting to approach equilibrium, the phases are separated. The resultant extract phase and raffinate phase are drawn-off in single contact operation. However, more often the process is repeated until a raffinate phase is obtained from which, after removal of the solvent, a solute is produced having the specified composition. Each treatment with solvent represents an extraction stage (multiple contact). Co-current operation is rarely used in a commercial process because of the large volume of solvent required and the low concentration of extract which is obtained.

In counter-current extraction the feed and solvent are introduced continuosly at opposite ends of the column or cascade. The two phases pass counter-current to each other. In differential contactors, one phase remains dispersed throughout the column until it is allowed to flocculate and coalesce at the end of the device before being discharged. In stagewise contactors intermittent, rather than continuous, contact occurs between the phases. The stages often take the form of horizontal plates of varied design, arranged vertically above each other in a column. The two phase usually flow counter-currently, mix together to allow interphase mass transfer within a given stage, and then separate and flow up or down respectively to the next stage in series.

Counter-current multiple contact operation with reflux may be used for separation of homologous substances where both the separation factor and distribution coefficient are low. The use of reflux serves to reduce the large number of theoretical stages which would be necessary to obtain the desired purity of the extract.

2.3 Design Fundamentals

Procedures for the design and analysis of the performance of extractors are still incomplete. The cause lies mainly in the complex behaviour of the dispersed phase, resulting from the generation of a distribution of drop sizes and the effects of drop

break-up and coalescence and, axial mixing phenomena. Design of any specific extractor from fundamentals is not possible without correction of these individual phenomena for the specific liquid-liquid system and operating conditions involved.

The design of a liquid-liquid extractor involves the determination of three principle parameters:

(a) Diameter or cross-sectional area, based upon the maximum permissible throughput of the phases;

(b) Total height or number of actual stages, with correction for axial dispersion (if any); and

(c) Dimensions of equipment internals, derived from design models, pilot-plant tests or general scale-up rules.

The rate of solute transfer depends mainly on the physical properties, hydrodynamic characteristics ie phase flowrates and driving force, ΔC. The rate of solute transfer, N, may be expressed as the product of the overall mass transfer coefficient ,the overall interfacial area, A, and the mean concentration driving force, ΔC,

$$N = K.A.\Delta C \qquad \text{.... 2.1}$$

Either the dispersed or continuous phase may be used as a basis for calculation. The overall mass transfer coefficient K_{od} or K_{oc} is dependent on the series resistance, inside , outside and at the interface of the drop.

$$\frac{1}{K_{od}} = \frac{1}{k_d} + \frac{m}{k_c} + \frac{1}{k_i} \qquad \text{.... 2.2}$$

or

$$\frac{1}{K_{oc}} = \frac{1}{k_c} + \frac{1}{mk_d} + \frac{1}{k_i} \qquad \text{.... 2.3}$$

for a linear equilibrium relationship,

where $m = \frac{y^*}{x}$ 2.4

k_i, the interfacial resistance is usually small and can in most cases be neglected unless a chemical reaction results in interfacial scum.

The interfacial area, A, depends on the characteristic dropsize and dispersed phase hold-up, x, which is the ratio of the volume of the dispersed phase to the total effective volume of the extractor at steady state. Assuming that the drops are spherical and can be represented by the Sauter mean (volume surface) diameter, d_{32}

$$d_{32} = \frac{\Sigma n_i d_i^3}{\Sigma n_i d_i^2} \quad \text{.... 2.5}$$

where n = total number of drops. The specific interfacial area, a (interfacial area, A, per unit volume) is defined as

$$a = \frac{6x}{d_{32}} \quad \text{.... 2.6}$$

In practice, a wide distribution of dropsize exists in extractors (section 4.1.3) because of the initial drop dispersion mechanisms and, often, subsequent coalescence and redispersion effects. The drop size is an important parameter since the internal flow patterns differ according to size and surface conditions, ie the drop may exhibit stagnant, circulating or oscillating behaviour. The mass transfer mechanisms associated with each of these modes are reviewed in Chapter 5. As discussed later in Chapter 7, the effect of dropsize distribution has been partly catered for in the present work by developing a method to calculate the theoretical overall mass transfer coefficient by applying the dropsize distribution diagram to estimate the volume percentage of stagnant, circulating and oscillating drops in the drop population. Each drop size fraction in the dispersion was assumed to contribute to the overall column performance in terms of its own

residence time and mass transfer rate. Individual mass transfer coefficients were then estimated for the corresponding drop state, using the different single-drop mass transfer models. The overall coefficient K_{cal} was then calculated as the fractional sum of the individual coefficients and their proportion in the drop population.

Any design is speculative unless the principles governing the performance of an extractor are fully understood, and taken into account, at the design stage. Essentially, the design of an extractor is based on equation 2.1. However, there are many deficiencies in this basic equation, the theoretical development of which requires many simplifications and assumptions [234], eg the assumption that the mass transfer coefficient K and the interfacial area A remain constant with position in an extraction column and that some mean ΔC can adequately express the variation of concentration driving force over the column height. In differental extractors, use is made of Simpson's rule to evaluate ΔC to give the best approximation [2].

The characteristic sizes of drops are used to predict the mass transfer coefficient K from single drop data and the interfacial area A. The value of K depends on the mass transfer resistance within each phase, interfacial turbulence, wake shedding and the system physical properties, which may vary throughout the extractor. The mean concentration driving force ΔC is a maximum when there is perfect plug flow but axial mixing may in practice cause departure from plug flow and account for additional height, especially in cases of high degrees of agitation [119] or in large diameter columns.

In a design exercise, commencing with the predicted drop size, values may be estimated for the flooding velocities and hence the operating velocities, column diameter, mass transfer coefficients and finally column height. By repeating this procedure for a range of dropsizes an acceptable combination of design and operating parameters may be established and the sensitivity of extractor design to changes in dropsize may also be demonstrated.

Dropsizes, and mass transfer resistances in both phases, vary with system

physical properties, which may change through an extractor. They also depend upon the mass transfer process itself, through the promotion of Marangoni effects or other interfacial instabilities. For this reason, pilot-scale work aimed at producing design data should be carried out with the real process streams rather than simulated ones. Furthermore the molecular diffusion coefficient used for predicting film coefficients cannot readily be estimated in multicomponent systems. Mass transfer will vary with solute concentration, hence the concept of a transfer unit is not always appropriate. There is also recent evidence, certainly in the case of large oscillating drops, that interaction between drops which approach or collide but do not coalesce enhances mass transfer (3).

The precise application of such fundamentals to the design and analysis of a column, even one as apparently simple as a sieve-plate column, is therefore extremely complex. Droplet redispersion and coalescence phenomena, droplet velocity, dispersed phase hold-up and flooding are discussed in detail in Chapter 4. A more detailed discussion of mass transfer in gravity operated columns is given in Chapter 5

CHAPTER THREE

THE SIEVE PLATE EXTRACTION COLUMN (SPC)

3.1 Column Design

The SPC in its present form was first described by Laird [158] in a patent specification in 1919. A modified version, with the sieve plates having downcomers, was proposed by Harrington [99] in 1934. Even now however, it is not possible to design such columns from first principles with confidence, ie without resorting to pilot scale tests. This is due to the complex hydrodynamic conditions in the SPC which are sensitive to flowrates and, as in all extractors, to the degree and direction of mass transfer. Moreover, no serious attempt has previously been made to apply information from the literature on the momentum, mass and energy transfer processes in swarms of drops, to conditions in the SPC.

A typical SPC comprises a vertical, cylindrical column containing a series of equi-spaced, horizontal sieve plates. Downcomers, are provided on alternate sides of consecutive sieve plates. For a heavy continuous phase, downcomers are provided on alternate sides of consecutive sieve plates. Each downcomer extends from the sieve-plate to which it is attached to a fixed height above the next sieve plate. Each downcomer is spaced about 1 to 2 cm from the inner surface of the column wall, to prevent the forming drops from colliding with the column wall. Holes are omitted from the plate area directly beneath the downcomer from above. The column also includes entrance and exit ports, to facilitate counter-current flow of immiscible liquids within the column.

Typically in operation, with the light phase dispersed, it is pumped into the column via a bottom distributor and the droplets travel as a swarm through the continuous phase. The swarm of droplets accumulates underneath the next plate, to form a dense packing and subsequently coalesces into a single phase stagnation layer until sufficient hydraulic head is built up to redisperse the liquid through the plate holes. This process is repeated at each plate in the column. The dispersed phase eventually coalesces at the

top bulk interface and leaves the column; an external settler is an alternative arrangement.

The (denser) continuous phase enters at the top of the column and flows horizontally across a sieve-plate and through the downcomer to the compartment below. The continuous phase hence flows cross-currently within the compartments, although it is counter-current between the stages. The downcomer is flush with the plate from which it carries the continuous phase and must extend well-below the flocculation layer of the dispersed phase beneath the plate to avoid re-entrainment.

It has been the practice to obtain design data from a pilot-scale column in which certain structural features are identical to those on the commercial scale [67, 188, 222]. The hole size and pitch distance must be identical so that the flowrate per unit area and the dropsize distribution can be identical on both scales. The actual area of the downcomer in relation to the cross-sectional area of the column (or sieve-plate) must be the same, so that the degree of axial dispersion of the phases flowing counter-currently remains unchanged. This requirement is fulfilled for the dispersed phase if the dropsize distribution is the same. It has been shown in a rectangular 49.5 x 14cm SPC, that with a high interfacial tension system (30 mN/m), which characteristically gives low point efficiencies, axial mixing was not an important feature in the SPC [60a]. It is difficult to maintain exact geometric similarity between pilot-scale and commercial columns. This applies to columns having inside diameters <152 mm, in which the area taken up by the downcomer represents a substantial portion of the total cross-sectional area of the column. Hence the droplet swarm tends to approach closer to the column walls than in large diameter columns. Furthermore, with smaller columns the ring support which seals each sieve plate with the column wall requires about 1.3 cm (1/2") thickness inside the column wall. This can restrict the flow capacity of the column in relation to larger diameters.

3.2 Distributor and Sieve Plate Design

The design of the distributor and sieve plates should preferably be sufficiently flexible to handle a wide range of phase flowrates and to accommodate any variations in

viscosity or density differentials anticipated in the process. An additional practical requirement may be for the column to continue to perform to design requirements even after the introduction of quantities of dirt, sludge and corrosion by-products during extended periods of operation.

The distributor and sieve plates generally have the same geometrical configuration, ie hole size, pitch, free area and downcomer area. The horizontal sieve plates with a downcomer is the simplest, and commonest form. Hole diameters are generally in the range 1.5 to 8 mm located on a square, triangular or circular pitch [156, 270, 295]. The hole size depends mainly on the system interfacial tension. The dispersed phase in low interfacial tensions systems, < 5 mN/m, tends to coalesce on the top plate surface if the pitch distance is < 3 times the holesize and only a very thin layer of dispersed phase is required under the plate, to force flow through the holes. In addition, the hole diameter must be < 2 mm to prevent continuous phase weeping. However, coalesced layers and hole diameters of such small dimensions are not suitable for commercial columns. Therefore, sieve plates with downcomers are unsuitable for systems of low interfacial tension. Dual flow plates ie plates without downcomers have proved suitable for this purpose [110].

Small hole sizes < 6 mm are preferred for systems of high interfacial tension, eg > 20 mN/m, since coalescence is likely to be relatively slow for larger dropsizes, resulting in an insufficient coalescence height for reproducible drop formation.

The sieve plate holes are either drilled or drilled and punched. Holes < 3 mm are drilled whilst larger holes are drilled and punched, to provide a sharp edged protrusion so that spreading of drops across the plate during drop formation is avoided. Holes < 2 mm are expensive to produce reproducibly; they also result in small drop sizes, which have the disadvantage of excessive entrainment which leads to flooding. The holes could also be plugged, if fine solids are present in the phases. The plate thickness should normally be > 1.5 mm to ensure rigidity for drop reformation. Nozzle plates ,ie plates incorporating nozzles protruding about 2 cm, have been found suitable for the dispersion

of the heavy phase as encountered in metal extraction [83a].

The pitch size should be approximately 3 times the hole size [67, 295] to avoid coalescence of drops on the plate at low flowrates and to avoid mutual interference between adjacent jetting streams at high flowrates. A free area of 55-60% is desirable [131, 222], but too large a free area obviously results in a reduced column capacity.

Usually the two phases in an extraction process will possess different wetting characteristics with respect to the column internals. This is defined by the contact angle, Ø, which is the angle between the tangent and solid surface (internals). Ø ranges from 0 to 180°; a low value of Ø implies wetting and a high value non-wetting. Ø is also a function of temperature and surface roughness. Generally, the contact angle decreases with increasing temperature. If $Ø < 90^{o}$, roughening the surface would decrease Ø, whereas if $Ø > 90^{o}$ roughening the surface would increase Ø [51]. Water wets stainless steel, brass and glass, and organic solvents wet p.t.f.e, perspex and polyethylene [51, 73, 200] . In the SPC, the distributor and sieve plate materials should be hydrophobic (organic wetted) when water is dispersed and hydrophilic (water wetted) when organic liquid is dispersed. This should ensure the formation of uniform drops. If a material that is wetted by the dispersed phase is used, or if preferential wettability changes due to 'ageing' or scum deposition, irregular streams without break-up into drops occur [200], unless holes are punched to form projections (nozzle holes) [295] on which drops may be formed at low flowrates.

The importance of surface wetting has been indicated for sieve plates as well as for packings [47]. When the kinetic energy of an approaching drop is less than the increase in surface energy required to deform the drop, droplets that wet the plate cannot pass through the sieve-plate holes. Conversely for a non-wetting plate, the droplets pass through the holes without change in size, even when the holesize is 0.8 times the approaching drop size. The mean droplet sizes produced by clean sieve plates were significantly larger than those obtained with aged plates in a pulsed sieve plate column

[14a], an effect which is associated with the different surface characteristics of the two types of plate.

The distributor and sieve plates may be fabricated from a wide range of materials depending upon both the process liquids. Most metals and commercial alloys can be perforated conveniently in a multiple punch process. In non-corrosive systems stainless steel is normally used and adequate bolting or welding should be provided to achieve reasonably tight contact with the downcomer.

Various modified sieve plates have been patented [196] mainly for use with a particular liquid-liquid system. However, if the system properties are outside the range applicable to the SPC, viz possessing very low ($\sigma < 5$mN/m) or very high ($\sigma > 45$ mN/m) interfacial tension, low density difference, or if it is prone to emulsification and separation problems, it would be more practicable to consider alternative extractor designs.

Some plates incorporate 'coalescence aids' [Section 4.3.6]. One proposed design has the plates arranged vertically as shown in Figure 3.1. This results in some sacrifice of height per plate but the holes are protected to some extent from any solids carried along with the continuous phase. This design is for when the continuous phase contains solid particles which would clog the orifices of a horizontally arranged sieve plate.

Another modified sieve plate, in which the disperse phase travels horizontally into a high velocity stream of the continuous phase, is shown in Figure 3.2. The drops are swept-up against, and through, a perforated vertical baffle and redispersed into a second stream of the continuous phase. This process is repeated several times across the plate.

Some plate designs have an underflow weir or cascade weir as in Figure 3.3 [29], which provides separate zones for mixing and separation. The significance of this design is the hydraulic 'lift' it gives to the dispersed phase for redispersion.

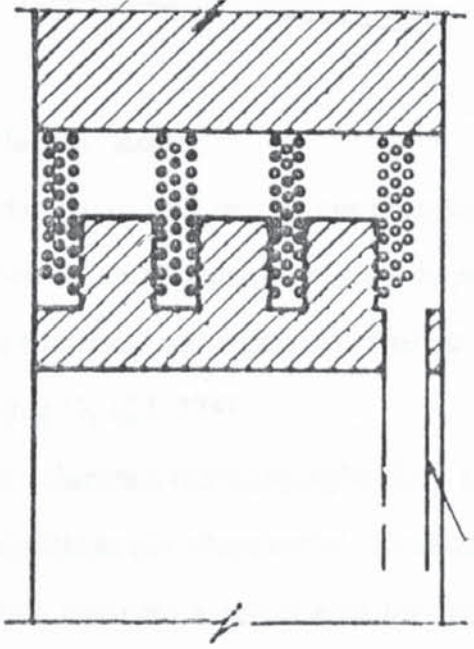

Figure 3.1 Sieves in vertical plates

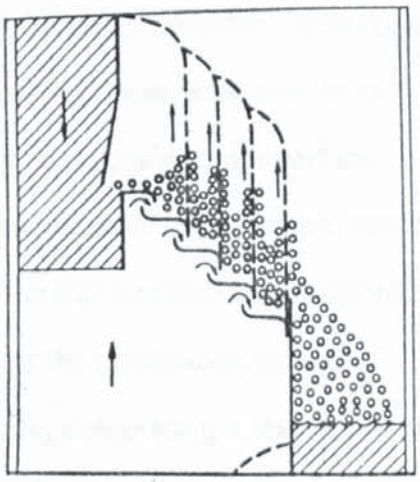

Figure 3.2 Modified sieve plate

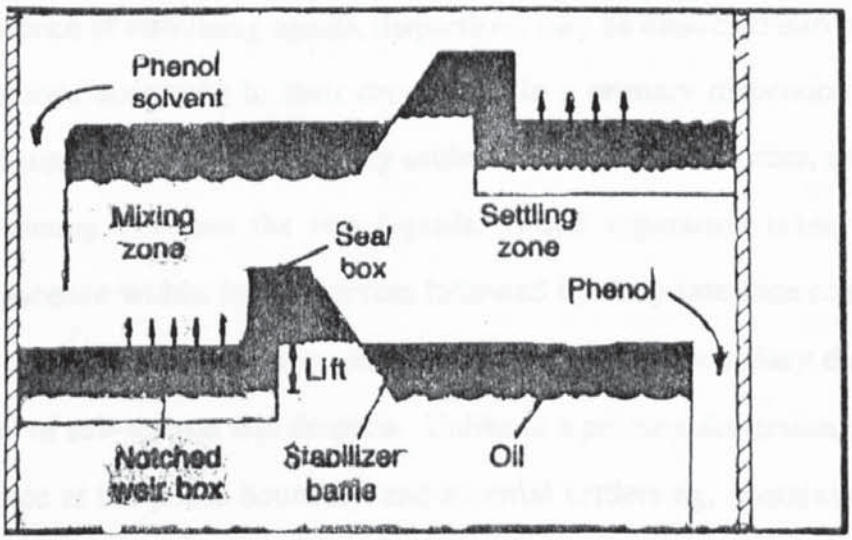

Figure 3.3 Underflow weir plates

3.3 Settling/Flocculation Zone

Coalescence fundamentals and modes are discussed in Section 4.3. Droplet dispersions within extraction columns, namely primary dispersions with drop diameter ≥ 100 μm, have finally to be coalesced and separated. Failure to achieve rapid coalescence can cause premature flooding [5, 124, 278].

In most extraction columns a disengaging/settling zone, in which an interface is formed, is provided near the dispersed phase outlet. Usually the diameter of this zone is larger than the column; this provides a larger area for drop interface interaction and prevents carry-over of the continuous phase.

Phase separation at the phase boundary involves three distinct zones [5]:

(a) the interface coalescing zone with one or two layers of dodecahedra-shaped drops just below the main coalescing interface.

(b) the main packed droplet zone within which considerable interdroplet coalescence takes place within the flat boarders of pentagonal dodecahedra drops forming the drainage network for the continuous phase.

(c) the flocculating zone, comprising a less dense packed bed of spherical droplets in which little interdroplet coalescence occurs. These zones are illustrated in Figure 3.4.

In the absence of stabilising agents, dispersions may be classified into primary or secondary dispersions according to their drop size. In a primary dispersion the drop diameter is > 100 μm and the droplets readily settle, due to buoyancy forces, and collect at the phase boundary between the two liquids. Final separation takes place by interdroplet coalescence within the dispersion followed by drop-interface coalescence. This is the type of dispersion normally generated in the SPC. Secondary dispersions comprise a myriad of sub-micron size droplets. Unlike in a primary dispersion, these will not readily coalesce at the phase boundary and external settlers eg, containing fibrous beds have to be constructed for their separation [277].

The settling zone height has to be taken into account in the design of extraction

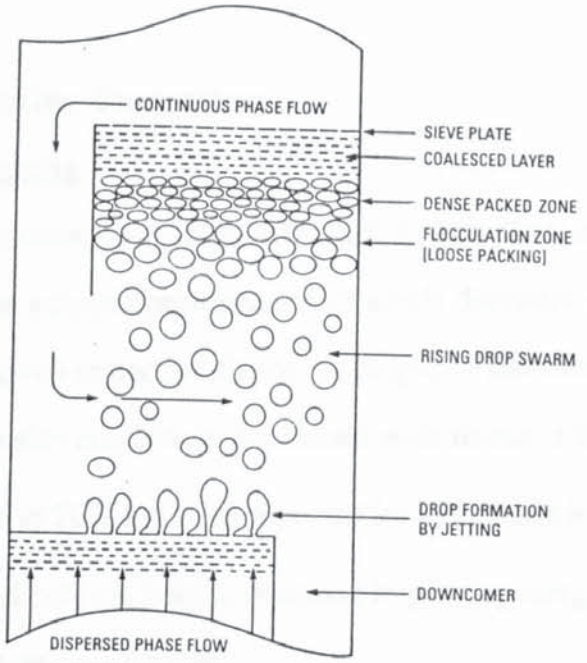

Figure 3.4 Drop formation and coalescence phenomena in the sieve plate extraction column

columns. Correlations have been proposed to predict these heights in spray columns [277-8].

$$\frac{H}{d_o} = 15.1 \times 10^{-3} \left[\frac{U_d\ \mu_c}{\sigma}\right]^{1.10} \left[\frac{d_o^2\ \Delta\rho g}{\sigma}\right]^{-1.38} \left[\frac{\mu_d}{\mu_c}\right]^{1.13} \quad \ldots. 3.1$$

Similar correlations are given by Hitit [111] albeit for specific test systems.

Attempts have been made to promote coalescence in order to increase the separation rate of the phases and hence achieve higher throughputs. If the dispersed phase volumetric capacity exceeds the coalescing capacity of the interface, a dense droplet layer is built up, which limits the continuous phase throughput. In many commercial columns, coalescence aids are installed in the coalescing zone. These are in the form of a knitmesh or packed section (Chapter 4) preferably with surfaces completely-wetted by the dispersed phase or alternatively of dual materials of different surface energies. These aids

accelerate the process of coalescence and hence reduce the height of a droplet layer [5, 124, 278].

3.4 Effect of Operating Parameters

3.4.1 Effect of Plate Spacing

Several investigations [142, 170, 197, 202-3, 228, 294] have considered the effect of plate spacing on column performance in small diameter columns (<0.15 m). Most reported that for a given extraction factor the height of transfer unit HTU increased and the overall mass transfer coefficient decreased with increase in plate spacing. An increase of K_{OC}.a by 15% to 20% has been reported for a decrease in plate spacing [170]. So for fixed flowrates and column height, decrease in plate spacing (increase in number of plates) improves the mass transfer rate.

The improvement in mass transfer rate at reduced plate spacing is due to the increase in the number of times drops are coalesced and redispersed, which results in enhancement of mass transfer through a large number of end effects (Chapter 5). However, the operational cost is increased due to increase in number of plates; an economical balance is therefore required.

Downcomer geometry is another factor which affects plate spacing. To avoid entrainment, the cross-sectional area of the downcomer is selected to ensure that the average velocity of the continuous phase within it is less than the free rise (terminal or characteristic) velocity of the smallest drops. At small dispersed phase volumetric flowrates, the downcomer length has no effect on the minimum continuous phase volumetric flowrate [188]. The downcomers should be positioned, so that hand or man holes can be provided to permit removal of dirt and interfacial 'rag' after continuous operation.

The plate spacing should be large enough for uninterupted jet break-up to occur and the resulting drop rise to be through a sufficient height that the requisite interfacial

area is provided for mass transfer. In practice, plate spacings between 15 and 60 cm are employed [131].

3.4.2 Effect of Hole Size and Hole Area

Holes are generally of 1.5 to 8 mm diameter, located on a square, triangular or circular pitch [156, 270, 295-6] depending upon the system interfacial tension. Smaller holes are preferred for systems with interfacial tensions > 20 mN/m [156]. However, for larger holes > 8 mm, there will be a tendency for heavy (continuous phase) 'dumping' through the holes even at reasonably low continous phase flowrates, possibly leading to premature flooding. Dumping also causes continuous phase short-circuiting and intermittent issue of the dispersed droplets, which reduces the capacity of the column.

The pitch between adjacent holes and the arrangement of holes to be drilled or punched, on the plate is also important. The pitch should be approximately 3 times the hole size [67, 295] to avoid interdrop coalescence on the plate at low flowrates, and to avoid mutual interference between adjacent jets at high flowrates. A free area of 55% to 60% is desirable [131, 222], but too large a free area obviously results in a reduced volumetric capacity and thereby loss of efficiency. A pitch of 12.7, 15.9 or 19 mm is generally recommended [156, 222]. The fractional free area of the holes determines the minimum throughput of the dispersed phase to achieve operation of all holes. The remaining plate area is utilised for either a downcomer or a receiving section beneath the downcomer from the previous plate.

3.4.3 Coalescence Height

Although the coalescence height is a dependent variable, it is discussed here for convenience. The coalescence height, h_t, (static hold-up) is the thickness of the dispersed phase layer beneath each plate during steady state operation. It is a measure of the flow capacity of the column, ie the greater the thickness, the closer the column is to flooding.

i.e pseudo flooding. The coalescence height should be sufficient to provide the driving force required for the flow of the dispersed phase [143, 147]. The plates should be levelled to ensure uniform coalesced layers beneath them and hence similar operation of all plate holes across the column cross section.

The coalescence height is determined by the drop formation and coalescence characteristics of the dispersed phase, and the variable effect of continuous flow as it passes from plate to plate. h_t represents the minimum theoretical height of the downcomer necessary to avoid by-passing of the dispersed phase.

The coalescence height is independent of plate spacing [147, 170]. A value of twice the coalescece height is recommended as the plate spacing for laboratory scale columns, and 10 to 12 times the coalecence height for commercial scale columns [156]. However, the latter is predominantly for flexibility, to allow the location of hand or man holes along the column.

Various workers [28, 30, 52, 67, 142-3, 147, 178, 285] have investigated the coalescence height in the SPC and most have identified 3 major factors contributing to this:

(a) the interfacial tension effect, which affects the drop formation,deformation and drainage characteristics of the dispersed phase.
(b) the orifice effect, namely friction through the plate holes.
(c) the downcomer effect, arising from the resistance offered to the flow of continuous phase from plate to plate.

3.4.4 Effect of Physical Properties

Interfacial tension and density difference are generally the most important physical properties of a system in any liquid-liquid extraction column. In an SPC interfacial tension affects drop size distribution, the pressure drop across the sieve plate, and volumetric flowrate for a steady state operation. A decrease in interfacial tension will

result in a decrease in mean drop diameter, hence the combination of volumetric flowrates decreases because of the latter [188]. The effect of interfacial tension on coalescence is covered in Section 4.3

The hydrostatic buoyancy forces depend upon the density difference. This determines rate of rise or fall of the droplet swarm, and hence the fractional dispersed phase hold-up at any specific combination of volumetric flowrates of the two phases. An increase in density difference will be accompanied by an increase in column volumetric capacity. An increase in density difference decreases the dispersed phase hold-up as a result of the increased drop swarm velocity, ie characteristic velocity [188]. This has also been established for the pulsed sieve plate column [15b]. Increase in continuous phase viscosity increases the dispersed phase hold-up[[15b].

3.4.5 Effect of Surfactants

The effect of 3 surfactants: Teepol, Sodium lauryl sulphate (SLS) and Peptone on overall mass transfer coefficitent $K_{oc}.a$ was investigated in a 4.2 cm diameter SPC, with the system: kerosene (d)-acetic acid (s)-water(c), when used at a concentration of 0.0005% w/w [1]. The surfactants were found to depress $K_{oc}.a$ by 33% for Teepol, 8% for SLS and 4% for Peptone. Using Peptone alone at concentrations of 0.0005, 0.001 and 0.005% w/w resulted in a decrease in $K_{oc}.a$ by 4, 8 and 12 % respectively.

The effect of Mannoxol-ot surfactant on mass transfer of either acetic, propionic or lactic acids from kerosene (d) to aqueous sodium hydroxide (c) was investigated using a 9 cm diameter SPC. A surfactant concentration of 0.0004% w/w in each solute resulted in a decrease in HTU of 14.1% for lactic acid, 41.7% for propionic acid and 44.4% for acetic acid respectively. The different decreases were attributed to variation in the diffusivity of each solute.

The effects of 6 different surfactant concentrations of Aerosol-ot, ranging from 0.0005 to 0.02% w/w, on mass transfer rates for the system kerosene(d) - acetic acid(s)

-water(c) were studied in a 4.1 cm diameter SPC [134]. It was observed that the mass transfer coefficient $K_{oc.}a$ decreased initially with increase in concentration form 0.0005 to 0.0015% w/w and thereafter showed an increasing trend with further increase in concentration up to 0.005% w/w. Further increases in concentration of surfactant up to 0.02% w/w were found to have no significant effect. The $K_{oc.}a$ values obtained for higher surfactant concentrations, ie 0.005% w/w and above, were found to approach those for the pure system, ie without surfactant. It has also been reported that for the extraction of benzoic acid from benzene in a packed column [40] the presence of 0.15%w/v Aerosol-ot increased $K_{oc.}a$ by 32%.

The presence of a surfactant at the interface of a liquid-liquid system has been proved to have a profound effect on changing the interfacial resistance to mass transfer [40]. No single specific mechanism could be found to satisfactorily explain the lowering or raising of the interfacial resistance to mass transfer in the presence of small amounts of surfactant. Both the barrier-layer theory as well as hydrodynamic effects jointly contribute to the occurrence of the phenomenon. While a surfactant may be found to be a 'promoter' of mass transfer rates for a particular system, it can also act as a 'inhibitor' for another system [134].

3.5 Application and Advantages

The SPC has been used in many applications especially in petroleum refining and petrochemical plants [12]. Columns range in diameter up to 7.62 m (Table 3.1)

The SPC would be expected to find application with moderate (10-40 mN/m) interfacial tension systems ie where mechanical agitation is not necessary to achieve a homogenous dispersion and rapid coalescence of the dispersion could be achieved. It is used when the number of theoretical stages required is relatively high > 5 and the density difference between the phases exceeds 100 kg/m^3 [188].

In general, industrial use of the SPC would be considered under a combination of the following conditions,

(a) Operations involving a high throughput of the phases, up to 60 m/hr

(b) Where a relatively high (>5) number of theoretical stages is required, ie 10 theoretical stages was used in a 24 m high SPC [335]

(c) Systems with a substantial density difference ie > 100 kg/m^3

(d) With moderate interfacial tension systems ie 10-40 mN/m.

(e) With a dispersion which is relatively easy to coalesce.

(f) Corrosive systems, where the absence of mechanical moving parts is advantageous, although a packed column could be cheaper.

Some industrial applications of the SPC are summarised in Table 3.1. The stage efficiency relates the performance of a real stage to that of a theoretical stage, ie the behaviour of a real extractor to that of an ideal one. (Section 5.7.1).

The main advantage of a gravity operated extractor like the SPC is the absence of moving parts. In the SPC drop formation and motion is determined largely by interfacial tension and density difference. One means of increasing the rate of mass transfer between contacting phases is to provide for frequent coalecence and redispersion of the dispersed phase; such a condition is offered in the SPC. It also offers the advantage of cross-flow with little axial mixing [60a, 180, 222, 295-6]. The vertical recirculation of the continuous phase, a common characteristic of the spray column is significantly reduced. The SPC can provide a good stage efficiency and high throughputs [29, 180, 295-6].

Table 3.1 Summary of Industrial Applications of the SPC

Process Applic.	Column dia. (m)	Column Height (m)	Sieve plate design	No of Plates	Interfacial tension (mN/m)	Density difference (kg/m^3)	Stage Efficiency (%)	Ref
Lubricating oil extraction (Fulfural as solvent)	2.4-3.7	11-20	Vertical Arrange-ment Fig 3.1	14-20	-	150	20-50	66,196
De-asphalt-ing (Propane as solvent)	3	12	Sieve plates without downcomers	16	-	250	-	66
Anthraquin-one process (water as solvent)	2.8	24	Sieve plates without downcomers	24	-	150	20-50	310
Lubricating oil Extraction	7.6	-	Cascade weir plate Fig 3.3	-	-	-	82	29
Aromatic fractions (Sulpholane as solvent)	4	-	Sieve plate with downcomer	-	11.6	300	12	212
Acetic Acid Extraction (organic solvent mix as solvent)	2	-	Sieve plate with downcomer	-	1.5-7.5	189-419	15-20	212
Acetonitrile Extraction (water as solvent)	1.2	-	Sieve plate with downcomer	-	59	294-400	15-20	212

CHAPTER FOUR

DROPLET HYDRODYNAMICS

Provided operation is below the critical flowrates leading to flooding, the mode of drop formation (preferably by jetting), the drop size distribution and the dispersed phase hold-up are the most important hydrodynamic characteristics affecting mass transfer performance. The drop size distribution and hold-up determine the interfacial area during drop travel which, when coupled with a suitable single drop mass transfer model, will permit calculation of the overall mass transfer rate.

In the SPC, many drops are formed simultaneously and rise or fall as a swarm. Whilst various studies have covered systems employing single drops or a single stream of drops, little work has been undertaken to study the effect of neighbouring drops. Moreover it has been shown in work with an RDC that it is preferable to use a combination of single drop models depending upon the fractional distribution of drop size [2].

4.1 Droplet Phenomena

4.1.1 Drop Formation From Sieve Plates

In spray, pulsed sieve plate and sieve plate columns which are commonly used industrially, drops are formed from multiple orifices. Conversely most studies have covered systems employing single drops or a single stream of drops from a submerged nozzle [39, 54, 103, 120, 132-3, 154-5, 183, 188, 207, 232, 271, 299] which are never employed commercially in extraction columns. The most common internals are sieve plates. Various correlations have been proposed to relate the size of single drops to system physical properties, nozzle dimensions and formation rates, in the drip-point, jetting and atomisation regions. These are all summarised by Kumar and Hartland [152]. Only limited work has been undertaken to study the effects of neighbouring drops on drop formation [53, 152, 219, 249], in which the single drop correlations have been proved unsatisfactory.

Drops formed from any hole in a sieve plate distributor may be affected by drops from adjacent holes. Interdrop coalescence may occur on the plate at low flowrates or there may be interference between adjacent jets at high flowrates. Only a proportion of holes function at low flowrates [53, 79, 213, 245] and correlations derived for single drops do not predict the mean drop diameters correctly, especially when a large number of holes of large diameter > 3.175 mm is used [152].

In an investigation by Ruff et al [245] using a 22 cm diameter SPC, it was confirmed that, as would be expected, each hole requires a certain minimum throughput in order to operate. This minimum throughput is that which causes drops to form by drip-point. The manner by which a liquid distributed from a sieve plate into another immiscible liquid leaves the orifice depends mainly upon the holesize, pitch size, plate material and the system physical properties. The plates should be constructed such that the surfaces are hydrophobic when water is dispersed and hydrophilic when an organic liquid is dispersed [73] (Chapter 3). If the plate material is preferentially wetted by the dispersed phase, then at low flowrates the liquid will tend to spread over a wider plate surface and non-spherical, enlarged drops detach without any reproducibility. At high flowrates the reproducibility improves due to the high nozzle velocity [219].

4.1.2 Jetting

An increase in dispersed phase hole velocity, U_n leads to drops which are formed by jet disintegration ($U_n = U_j$, jetting velocity). With a further increase the jet rapidly lengthens and a maximum length is obtained for a critical velocity ($U_n = U_{max}$). For higher injection velocities the jet length decreases and drops are less uniform. Finally the jet break-up point retreats to the holes and a non-uniform spray of drops results. The latter phenomena is not observed from sieve plates in the SPC because the column floods at much lower flowrates than are required for atomisation in single nozzles.

Jetting has been reported to enhance mass transfer rates in liquid-liquid extraction

processes [22, 65, 180]. Many investigators [52, 103, 114, 133, 219, 271] reported that for single nozzles the jet length increases with increasing dispersed phase flowrate up to a maximum and then decreases with increasing flowrate until atomisation occurs.

A reliable method for predicting the mean dropsize resulting from liquid jet break-up, and the jet length, is therefore important for the design of spray and sieve plate columns. For single drops, operation at jet velocities near the maximum length can be two or three times more efficient than when drops are formed by drip-point [22]. For the SPC drop formation by jetting is the preferred mode of operation [131, 180, 245].

Various investigators [54, 68, 183, 251] have presented correlations for the minimum jetting velocity. Meister and Scheele [183] suggested two mechanisms of jet formation upon which a prediction of jetting velocity can be based. In the first it is assumed that a jet will be formed if there is a sufficient upward force at the nozzle exit. In the second mechanism, it is considered that a jet will form when the velocity of the drop is sufficiently low that it will rise less than one diameter during the time of formation of the next drop. The merging drops then form a continuous jet.

Kitamura et al [138] confirmed that the behaviour of jets injected into quiescent liquid differs from those injected into moving liquids. The difference is caused either by the existence of a velocity distribution or the relative motion of the jets which affects the stability , eg growth rate and wave number of disturbances. Bright [22] confirmed the hypothesis that the minimum drop size produced from a liquid jet in another liquid is governed by the frequency of the fastest growing capillary wave on the jet, rather than by the wavelength, and proposed a simple expression for the minimum drop volume in liquid-liquid systems.

Various investigators [27, 59, 184, 273-4] have considered the effect of mass transfer on jet breakup, and drop formation at jetting. Most experimental and theoretical investigations have revealed that the jet length is proportional to the interfacial tension of the system. The situation is more complicated when mass transfer is taking place. For the commonest case the presence of a solute results in a reduction of interfacial tension

(which is related to solute concentration); if this occurs at a jet interface, it will affect the jet break-up mechanism. The jetting velocity was found to be lower for mass transfer in either direction compared with non-mass transfer conditions [59]. This phenomena was attributed to the lowering of interfacial tension.

4.1.3 Dropsize Distribution

The dropsize distribution under operating conditions influences both the hydrodynamic and mass transfer performance. From a knowledge of mean drop size, d_{32}, an idealised approach enables the rate of solute transfer , N, to be calculated.

$$N = K.A.\ \Delta C \qquad \ldots. 2.1$$

where $A = a.V$

In practice, a wide distribution of drop size exists in any extraction column because of drop breakage and often coalescence. Extensive investigations [37, 44, 53, 70, 81, 125, 191, 198, 213-5] on the laboratory and pilot scales have indicated the important features that size distribution will affect, viz residence time distribution of the dispersed phase, and a tendency to reduce the proportion of oscillating and circulating drops, and hence a lowering of extraction efficiency compared with predictions based on an assumed mean drop size.

Two possible extremes of droplet behaviour may be observed for most systems in the SPC. In one case where mass transfer is occuring so as to induce Marangoni instabilities, generally for mass transfer from dispersed to continuous phase, droplets are formed which may have sizes predicted by the existing single drop correlations but many of which could be much smaller or much larger. Also many satellite drops may be formed. In the other extreme, where mass transfer rates are very slow, or impurities are present as surfactant, the drop sizes differ from those predicted from single nozzle

correlations. This results in a dispersion of very small drops with high surface area for mass transfer and which approach equilibrium more rapidly than larger ones leading to a loss of performance [215]. Kumar and Hartland [152] have summarised various single nozzle correlations to predict mean drop sizes.

The dispersion in an SPC covers a wide range of drop size distribution eg between 1mm to 11mm depending on plate hole size. The larger drops pass through the column more rapidly than smaller drops. Accordingly, different drops may possess different concentrations and mass transfer coefficients even if they are at the same cross-section of the column. Thus each dropsize fraction in the dispersion contributes to the overall column performance in terms of its own residence time and mass transfer rate.

Dropsize distribution is a very important factor to consider in the design procedure. Various functions have been used to represent the types of drop size distribution generated from different types of drop formation mechanisms. The main characteristics of the distribution equations used in liquid-liquid extraction calculations are summarised in Table 4.1.

Whilst a useful summary has been published of the distribution functions applied to particles (solids or liquids) [135] only limited detailed descriptions are available of dropsize distributions in the SPC [53, 213-4]. Previous investigations have been confined to the Sauter mean diameter, d_{32}.

4.2 Droplet Velocity

In the design and operation of liquid-liquid extraction columns it is necessary to be able to predict the dispersed phase droplet velocity relative to the continuous phase. The problem is complicated by droplet interactions and distortion of the streamlines and

Table 4.1 Distribution Functions

Distribution	Function	Mean Diameter d_{32}
Log-normal	$\frac{dv}{dy} = \frac{\delta}{\sqrt{\pi}} \exp(-\delta^2 y^2)$; $y = \ln \frac{d}{d_{gm}}$ (4.1) $\delta = \frac{0.394}{\log_{10}(\frac{d_{90}}{d_{gm}})}$	$d_{32} = \exp(\ln d_{gm} + 2.5 \ln^2 S_G)$ (4.2) $S_G = d_{84.14}/d_{50}$ (4.3)
Mugele - Evans upper limit (198)	$\frac{dv}{dy} = \frac{\delta}{\sqrt{\pi}} \exp(-\delta^2 y^2)$; $y = \ln \frac{a'd}{d_m - d}$ (4.4) Skewness parameter $a' = \frac{d_m - d_{50}}{d_{50}}$ (4.5) Uniformity parameter $\delta = \frac{0.907}{\ln(\frac{d_{90}}{d_m - d_{90}} \cdot \frac{d_m - d_{50}}{d_{50}})}$ (4.6) Maximum stable drop size, d_m $d_m = d_{50} \left(\frac{d_{50}(d_{90} + d_{10}) - 2d_{90}d_{10}}{d_{50}^2 - d_{90}d_{10}}\right)$ (4.7)	$d_{32} = \frac{d_m}{1 + a' \exp^{0.25\delta^2}}$ (4.8)
Gal-or and Hoescher (70)	$\frac{dv}{dy} = 8 \left(\frac{\delta^3}{\pi}\right)^{0.5} y^2 (\exp - \delta y^2)$; $y = d$ (4.9) $\delta = \left(\frac{4}{\sqrt{\pi}} y_v^3\right)^{2/3}$; $y_v = \left(\frac{\Sigma n_i y_i}{N}\right)^{1/3}$ (4.10)	$d_{32} = 1.148\, y_v$ (4.11)
Rosin - Rammler (239)	$\frac{dv}{dy} = \frac{\delta (y)^{\delta - 1}}{(y)^{\delta}} \exp(-\frac{y}{\bar{y}})$; (4.12) $\frac{y}{\bar{y}} = d$ = value of y at 36.8% on the Rosin - Rammler graph plot	$d_{32} = \frac{\bar{y}}{\Gamma(1 - \frac{1}{\delta})}$ (4.13)

wakes. Fluid flow around a drop is hindered by other drops in the dispersion, and irrespective of their size, drops may sometimes move together. Drops also deform and oscillate unless they are very small, ≤ 1 mm so that interfacial tension forces predominate. Small amounts of surface active impurities can have a significant effect on drop velocity because they increase drop rigidity.

4.2.1 Terminal Velocity, U_t

The velocity of a drop which is free to rise, or fall , under gravity through another liquid is conveniently described by comparison with the velocity of an equivalent sphere. However, the lack of rigidity at the liquid-liquid interface renders the drop liable to both distortion and to exhibit a quasi-steady state, oscillatory motion. The initial motion caused by the transfer of tangential shear stress from the continuous phase leads to an increase in the velocity whereas distortion and oscillation reduce the velocity [60]. Reductions in velocity up to 50% have been observed [64, 76, 128, 139] compared to rigid drop motion.

When a drop is released from rest in another immiscible liquid it will accelerate to its terminal velocity and rise, or fall, through the liquid at this rate. Terminal velocity measurements for drops in a variety of liquid-liquid systems have been investigated by various workers [64, 76, 128, 251, 290-1] and various correlations have been proposed for the prediction of U_t. The terminal velocities of the drops were observed to be strongly influenced by system purity [60, 84, 115, 231, 284, 286, 291].

Grace et al [84] combined data and correlations [115, 128, 139, 201] from several sources with their own data to produce a correlation that covers a wide range of variables. The purity of the system had a large effect on the terminal velocity of a drop. Therefore they separated the data from the literature according to the care taken by the respective authors to eliminate surfactants. However, based as it was solely on published descriptions, this was bound to be only a subjective judgement. They developed the following correlation for contaminated systems;

$$J = 0.94\, H^{0.757} \quad (2 < H \leq 59.3) \qquad \ldots. 4.14$$

$$J = 3.42\, H^{0.441} \quad (H > 59.3) \qquad \ldots. 4.15$$

where H and J are parameters defined as,

$$H = \frac{4}{3} E_o M^{-0.149} \left[\frac{\mu_c}{\mu_w}\right]^{-0.14} \quad \text{.... 4.16}$$

$$J = ReM^{0.149} + 0.857 \quad \text{.... 4.17}$$

The value of 59.3 for H corresponds to the transition from non-oscillating to oscillating drops. The terminal velocity is then given by

$$U_t = \left[\frac{\mu_c}{\rho_c d}\right] M^{-0.149} (J - 0.857) \quad \text{.... 4.18}$$

The above equations are valid for $M < 10^{-3}$, $E_o > 40$ and $Re > 0.2$, but are clearly limited in value since the nature and concentration of the contaminants are variables. For pure systems, involving bubbles or drops at low Re, equation 4.18 was modified to

$$U_t, \text{pure} = U_t \left[1 + \left(\frac{1}{2 + 3\,\mu_d/\mu_c}\right)\right] \quad \text{.... 4.19}$$

U_t correlations of Hu and Kintner [115], Johnson and Braida [128], Klee and Treybal [139], Misek and Marek [190], and Murrucci et al [201] are also recommended. The equations of Grace et al (4.14-4.19) have been shown to be more accurate for the prediction of U_t, for swarms, than any other single drop correlations [275].

4.2.2 Characteristic/Slip Velocity

In order to determine the specific interfacial area, a, either the drop residence time or the hold up, x, which is the fraction of the effective column volume occupied by the dispersed phase, must be known. The work of Pratt et al [80, 163] for\ packed columns,

and extended by Thornton to spray [289], rotary annular [288], rotating disc [171] and pulsed sieve plate [288a] columns used an approach based upon the slip velocity. This is the relative velocity between the two phases of a counter-current flow,

$$U_s = \frac{U_d}{x} + \frac{U_c}{1 - x} \qquad \text{.... 4.20}$$

The slip velocity is a function of drop size and the physical properties of the liquid-liquid system. It has also been found to depend upon hold-up itself [14, 80, 151, 279]. Pratt [224] observed that the mechanism of dispersion flow in liquid-liquid systems is analogous to that in the hindered settling of suspensions. Thus, by modifying the equation of Steinour [282] for the latter process, the hold-up in a column working at low flowrates and involving no interdrop coalescence was found to be related to the phase flowrates through the equation,

$$U_s = U_K (1 - x) \qquad \text{.... 4.21}$$

U_K is the characteristic velocity of the drop , defined as the hypothetical droplet velocity when $U_c = 0$ and $U_d \rightarrow 0$. It is the mean velocity of the dispersed phase relative to that of the continuous phase. This may also be identified as the terminal velocity of a single drop having a Sauter mean diameter which represents the drop ensemble [301].

Combination of equations 4.20 and 4.21 gives

$$U_K (1 - x) = \frac{U_d}{x} + \frac{U_c}{1 - x} \qquad \text{.... 4.22}$$

This suggests that a plot of

$$U_d + U_c \frac{x}{1 - x} \text{ versus } x (1 - x)$$

should give a straight line with U_K as its slope. It has been shown to be acceptable for spray [289], rotary annular [288], rotating disc [171], packed [80, 163], pulsed sieve plate [288a] and sieve plate columns [52-3, 213, 222]. However in the case of an SPC the straight line gradually changes to a curvilinear as the plate spacing is decreased [213]. Recently [15b], equation 4.22 has been modified taking into account the average fraction of the column cross-sectional area occupied by the column internals, ε (sieve plates and supports) for pulsed sieve plate columns to give,

$$U_K (1 - x) = \frac{U_d}{(1 - \varepsilon) x} + \frac{U_c}{(1 - \varepsilon)(1 - x)} \quad \text{.... 4.23}$$

This has been shown to be a better representation than equation 4.22.

Equations 4.20-4.23 have been found useful in correlating hold-up with phase flowrate for counter-current extraction columns. The hold-up may be predicted for any given set of phase flowrates provided a suitable correlation is available for estimating U_s or U_K. Several investigators [13, 18, 151, 161, 191, 281-2, 289] have suggested correlations for various types of extraction column. These are summarised by Kumar and Hartland [152]. They illustrated the differences between the behaviour of single drop terminal velocities and multi-drop slip velocities by comparing their drag coefficients. For single drops, the drag coefficient decreases sharply with increased Reynolds number, but approaches a constant limiting value in drop swarms as for single rigid spheres, Figure 4.1. A possible explanation for drop swarms behaving like solid spheres rather than single drops is that the oscillation and distortion of individual drops may be damped out due to the presence of other drops [275]. However this is contrary to the observations of Al-Faize[3] of single large oscillating drop pairs.

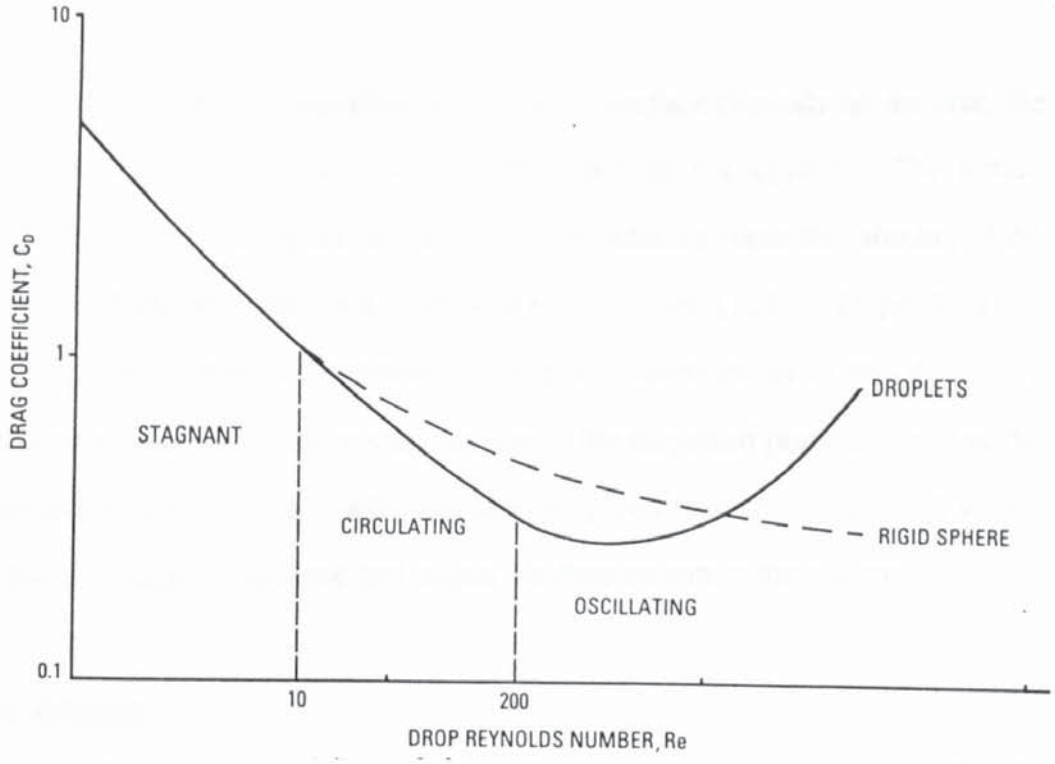

Figure 4.1 Correlation of drag coefficient C_D and Reynolds number Re for drops and rigid sphere

4.3 Droplet Coalescence

On completion of an extraction process the dispersion preferably containing drops > 100 μm has to be separated, usually under the action of gravity. The separation occurs by a sequence of settling, flocculation and coalescence which involves both drop-interface and drop-drop coalescence. However, whilst this sequence adequately describes the steps, the boundary between each step may not be clearly defined, since all occur simultaneously.

The mechanisms of coalescence and factors affecting it, have been reviewed in the literature [12, 124, 236]. Only a brief summary of aspects relevant to the SPC operation is given here and Section 3.3.

4.3.1 Mechanisms

Coalescence is associated with the decrease in free energy of the liquid-liquid interface and is aided by suppression of turbulence, which helps the droplets to aggregate to form a heterogeneous, dense-packed, zone at the main interface between the bulk

phases. The rate of migration of droplets to the bulk interface depends on the size, the physical properties, and the interfacial characteristics of the system. The actual coalescence mechanisms are complex, involving factors which govern the thinning of the continuous phase film between two coalescing interfaces [124]. Depending on conditions, coalescence may occur either at the plane interface or at the drop-drop interface. Coalescence at the plane interface occurs at the dispersed phase exit end of the extractor after mass transfer is over, whereas drop-drop coalescence occurs both within the droplet band awaiting coalescence and within the drop swarm in the column.

4.3.2 Drop-Interface

Studies of single drop behaviour at flat interfaces have helped in the understanding of coalescence without the complexities of drop-drop and multi-drop interactions. However, the time interval between the arrival of a droplet at a plane interface and its final coalescence into the bulk phase is not constant but exhibits a time distribution.

Jeffreys and Davies [124] concluded that coalescence takes place in successive stages, as follows:

(i) the drop as well as the interface are deformed as the drop approaches.

(ii) oscillation of the drop at the interface is dampened and a film of continuous phase is held between the drop and its bulk phase.

(iii) the film thins by drainage and rupture initiating the drop coalescence process.

(iv) the rupture hole expands and the drop contents flow (either completely or partially) into its main phase.

The mean coalescence time, t, also termed the rest time, comprises the mean of several observations of the total time taken for stages 1-3 above. The time taken for stage 1 is termed the predrainage time and that for stages 2 and 3, the drainage time. The coalescence time comprises the sum of the predrainage and drainage times. The coalesence of a drop at a flat interface is controlled by the various factors listed in Table

4.2. in which the effects of an increase in each variable is listed.

4.3.3 Drop-Drop Coalescence

Few experimental studies have been reported with drop pairs, since it is difficult to carry out drainage measurements between two drops that remain close to each other. However, various mathematical models have been proposed [175-6, 181-2, 225]. The significant omission in most of these models is the effect of internal circulation within the drops upon the coalescence time for the film thinning process. Neilson et al [205] measured the coalescence times of drops at a plane interface and found a progressive increase of coalescence time with surfactant concentration, since as the drop circulation is dampened by the surfactant, the film drainage rate is also reduced. Attempts have been made at modelling to include circulation within the drops [24]. Partial or stepwise interdrop coalescence have also been observed [24, 35, 48, 176] leading to the formation of a secondary droplet. In the absence of surfactants this occurs when β, the drop diameter ratio (d_2/d_1) of the drops approaching each other, is greater than about 3.5 The drop coalescense behaviour becomes identical to that of Figure 4.2b, the film becomes depleted of solute and the higher interfacial tension has the effect observed for partial coalescence at a flat interface when $\beta > 12$, at which the surface of the larger drop behaved as it if were flat [176].

4.3.4 Coalescence in Swarms

There are two main aspects of the coalescence of dispersions (i) interdroplet coalescence within the dispersion during the process of dispersion and contacting and (ii) droplet coalescence at the phase boundary to effect a separation of the phases. This will first be considered for an incomplete layer of droplets or monolayer and then extended to

Table 4.2 Factors affecting Coalescence Rate

Variable	Effect on coalescence time	Explanation
Drop size	Longer	More continuous phase in film
Length of fall	Longer	Drop 'bounces' and film is replaced
Curvature of interface towards drop		
(a) concave	Longer	More continuous phase in film
(b) convex	Shorter	Less continuous phase in film
Interfacial tension	Shorter	Less continuous phase in film. More rigid drop
Viscosity ratio $\left[\frac{\mu \text{ drop}}{\mu \text{ continuous}}\right]$	Shorter	Either less continuous phase in film or increase in drainage rate
Phase $\Delta\rho$	Longer	More defomation in drop. More continuous phase film
Temperature	Shorter	Increased rupture
Temperature gradients	Shorter	Thermal gradients weaken film
Vibrational effects	Shorter	Assist drainage and rupture
Electrostatic effects	Shorter	Increase effective gravitational force
Applied electric field	Shorter	Increase effective gravitational force
Presence of a third component:		
(a) Stabiliser	Longer	Forms skin around droplets
(b) Mass transfer into drop	Longer	Sets up interfacial tension gradients which oppose flow of film
(c) Mass transfer out of drop	Shorter	Sets up interfacial tension gradients which assist flow of film

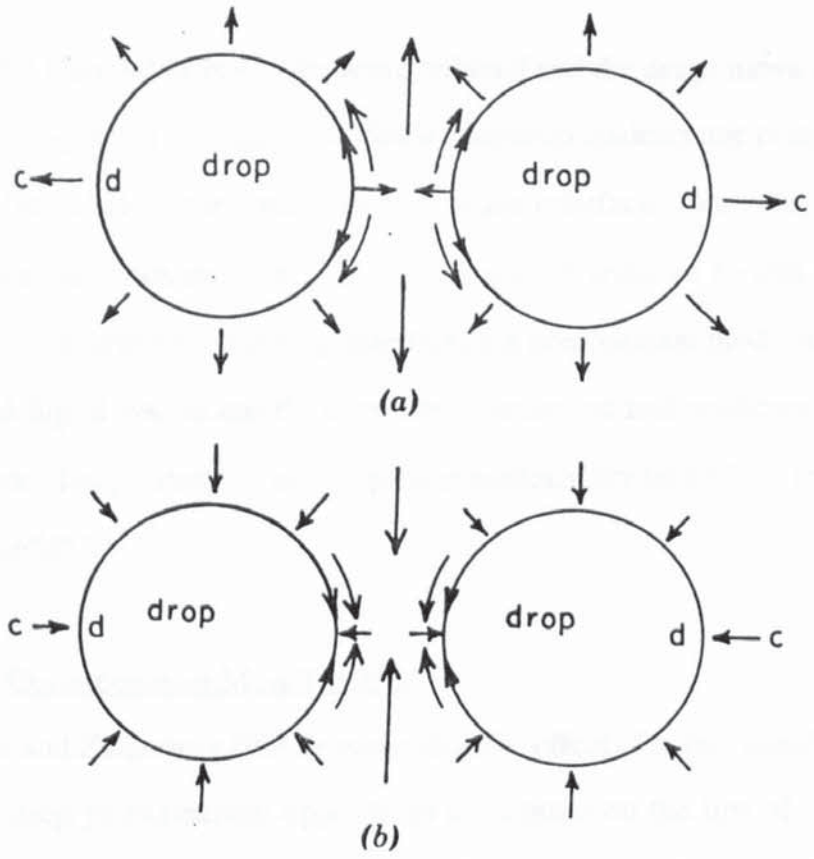

Figure 4.2 Effect of mass transfer on interdrop coalescence Direction of transfer (a) d to c (b) c to d

multilayers (swarms). The degree of coalescence in a monolayer is affected by various disturbances. However, various investigations have produced conflicting results as to the degree of variation of coalescence rates with varying degrees of disturbance. Lawson [159] studied the coalescence of drops at an interface and found that disturbance propagated from a coalesing drop did not promote coalescence in other drops. However, other workers have suggested that coalescence rates would be increased as a result of vibrations or disturbances at the interface. Disturbances at the monolayer could be caused by either the arrival or disappearance of drops. In addition, movement of neighbouring drops affects the drainage and rupture of the film between the surfaces.

Coalescence of droplets within a swarm necessitates firstly that they approach each other to form a close-packed, heterogeneous zone between the bulk liquid phases.

This results in the high initial velocities being reduced and the drops move towards the interface in a close-packed arrangement. Some interdrop coalescence occurs amongst the dense population before they reach the two phase interface where they eventually undergo drop-interface coalescence. Thus, coalescence within a swarm of droplets involves both modes: interdrop and drop-interface, the predominant mode depending on the actual liquid-liquid system and the drop size distribution and residence time in the flocculation zone. Drop-interface and drop-drop coalescence take place beneath each sieve plate in the SPC.

4.3.5 Effect of Coalescence on Mass Transfer

Groothuis and Zuiderweg [90] demonstrated the effect of solute transfer upon the coalescence of drop pairs retained opposite to each other on the tips of nozzles in a continuous phase. Coalescence was promoted by solute transfer from dispersed to continuous phase (d to c), even when only one of the drops in the pair contained the solute. However, coalescence was strongly inhibited when the solute was transferred in the opposite direction (c to d), Figure 4.2. Treybal [295] pointed out that this is due to the Marangoni effect, viz the generation of interfacial tension gradients resulting from concentration gradients along the surface in the region between the approaching drops. This phenomena has been widely-observed [121, 14, 174, 276]. The effect of mass transfer in extraction columns is discussed further in section 5.4.

4.3.6 Coalescence Aids

Attempts have been made to promote coalescence near the outlets of extractors in order to increase the separation rate of the phases and thus facilitate higher throughputs. Unwanted fine dispersions, or secondary hazes, are not uncommon in practice. Special packings or coalescence promoters to assist primary dispersion separation range from conventional ring or saddle packings of small sizes to knitted or woven wire-mesh packings [295] (Chapter 6).

Coalescence promotion is usually needed with three kinds of dispersion: (i) primary dispersions (ii) dispersions involving fine droplets (> 100 μm) and (iii) secondary dispersions (< 10 μm) comprising mircometer and submicrometer size droplets.

In the gravity settling of primary dispersions a large inflow of dispersed phase will lead to the formation of a dispersion band at the main interface between the phases. Within this band separation takes place by interdroplet coalescence. Any further increase in flowrate will cause this dispersion band to grow until it fills the available settling space. This will ultimately result in a flooding condition. The capacity of the settler can be increased by a coalescence aid.

It appears from the literature that no use has been made of coalescence aids beneath sieve plates; these could reduce flocculation zone height. However, if they consisted of packing eg Knitmesh or raschig rings, there could be problems of pressure drop and scum deposition.

The factors affecting the separation of secondary dispersions are discussed in Sections 3.3.

4.4 Dispersed Phase Hold-up

The dispersed phase hold-up is the fraction of the effective column volume occupied by the dispersed phase during steady state operation. The dispersed phase hold-up must be known for the calculation of interfacial area, a, which in the SPC is a function of both the hold-up and drop size distribution generated in each stage. (Equation 4.25)

In the operation of the SPC, three types of hold-up may be identified: static, operational and total hold-up. Static hold-up is the total volume of the dispersed phase accumulated under the sieve plates (flocculation/coalescence bands) during steady state operation. The operational hold-up is the total volume of the dispersed phase flowing through the continuous phase during steady state operation. The total hold-up is the

sum of static and operational hold-ups. A knowledge of the total hold-up is essential for inventory purposes. The operational hold-up, x, is given by,

$$x = \frac{(\text{Total hold-up} - A \sum_{1}^{n} h_t)}{(\text{Total volume} - A \sum_{1}^{n} h_t)} \quad \text{.... 4.24}$$

where n = number of plates.

The interfacial area of contact is given by

$$a = \frac{6x}{d_{32}} \quad \text{.... 4.25}$$

and

$$d_{32} = \frac{\sum nd^3}{\sum nd^2} \quad \text{.... 4.26}$$

4.5 Flooding

One of the characteristics of a liquid-liquid extraction column is that for each flowrate of one phase there is a maximum possible flowrate for the other governed by the system physical properties and column internal design. If the flowrate of either phase is increased beyond this point, steady-state operation cannot be maintained and 'flooding' occurs. The phase flowrates at flooding represent the upper limit on volumetric capacity of the column at the specific phase ratio and mass transfer conditions. Furthermore optimum operation is achieved close to the flood point [17]. This maximum condition can be estimated approximately by differentiating equation (4.22)

$$U_K (1-x) = \frac{U_d}{x} + \frac{U_c}{1-x} \quad \text{.... 4.22}$$

and setting both

$$\frac{dU_d}{dx}\bigg|_{U_c \text{ constant}} \quad \text{and} \quad \frac{dU_c}{dx}\bigg|_{U_d \text{ constant}}$$

equal to zero, which yields

$$U_{df} = 2U_K x_f^2 (1-x_f) \quad \text{.... 4.27}$$

$$U_{cf} = U_K (1-2x_f) (1-x_f)^2 \quad \text{.... 4.28}$$

These critical flowrates, which are interdependent, are termed the limiting flowrates or flooding velocities. Elimination of U_K from equations 4.27 and 4.28 yields an expression relating hold-up at flooding and the flow ratio R.

$$x_f = \frac{(R^2 + 8R)^{0.5} - 3R}{4(1-R)} \quad \text{.... 4.29}$$

$$\text{where } R = \frac{U_{df}}{U_{cf}} \quad \text{.... 4.30}$$

This approach, is popular because flooding rates can be estimated from only two parameters R and U_K, and it has been successfully applied to many types of extraction column [12].

Although equation 4.29 is a good basis for design, the method is not strictly applicable in practice because of the assumption that U_K is constant throughout the flow range up to flooding; this is only true if the drop sizes in the extractor remain fairly constant and there is no coalescence or interactions between adjacent droplets. It is reliable if for a particular column U_K can be estimated, with reasonable accuracy, for the particular operating condition. Flooding is always a combination of the dispersed and continuous flowrates in some critical ratio.

In the SPC, the coalesced height (static hold-up), (Section 3.4.3) beneath each plate increases rapidly with the dispersed phase flowrate, resulting finally in flooding. This growth of the coalesced layer with increase in dispersed phase rate is more significant at high continuous phase flowrates. At the flooding condition the column's main interface cannot be maintained(Section 3.3).

Several types of flow limiting phenomena have been observed in extraction columns. One is phase inversion, which occurs when the dynamic equilibrium between coalescence and redispersion is shifted towards coalescence. It has been observed that 'inversion flooding' occurs in the hold-up region of about 42-50% [11, 62, 189, 191, 199]. Phase ratio, physical properties, (ie density, density difference, viscosities and interfacial tension) power input - if mechanical energy is applied to assist dispersion, direction of mass transfer, the presence of any surfactants, and the order of introduction of the liquid into the extractor are all important, but their effects are not clearly understood.

Another type of flooding is characterised by the formation of a stable emulsion of the dispersed phase in the continuous phase. Attempts to predict such 'emulsion flooding' have so far been unsuccessful [191]. For systems with a tendency to emulsify the choice of 'mild' operating conditions, ie avoidance of excessive local turbulence and their verification by experiments, is imperative.

From work with a spray column, Letan and Kehat [161] reported that the maximum hold-up occurred at flowrates much above the start of coalescence and rejection from the column, and defined flooding as a combination of any of the following:

(i) the onset of swirling motion of drops in the lower part of the column.

(ii) the rejection of drops from the entry cone.

(iii) the set of flowrates at which the dispersed phase becomes continuous and vice-versa, ie phase inversion.

(iv) the formation of a dense packing of drops in the column.

Although the above combination aid in assessing flooding conditions, the way flooding is approached ie which phase flow is increased, and the drop size would be critical to which phenomena are observed.

In an SPC, in addition to the normal factors limiting flow capacity in any gravity operated column, the dispersed phase pressure drop through the holes may be a limiting parameter. Some unfavourable flow characteristics likely to be associated with high

volumetric throughputs in the SPC include excessive entrainment of droplets, overloading of the downcomers and restriction of flow through the plate holes. The flooding flowrates are difficult to determine experimentally and the 'maximum volumetric capacity' is usually synonymous with an incipient flooding condition brought about by any of the above phenomena.

Under mass transfer conditions, flooding characteristics were found to depend on the direction of mass transfer, which, due to Marangoni effects and other interfacial instabilities [295], affects the droplet coalescence characteristics, the mean drop size, hold-up and characteristic velocity within the column.

CHAPTER FIVE

MASS TRANSFER CHARACTERISTICS

5.1 Introduction

In liquid-liquid extraction the rate of mass transfer depends upon three factors, viz, the area of contact, the effective driving force and the combined resistances to solute transfer. These factors are not easily evaluated in the SPC since there are 3 stages during which mass transfer occurs between any two consecutive plates, ie during droplet formation, travel and flocculation/coalescence beneath the next plate.

Furthermore the dispersed phase tends to be present with a wide distribution of drop sizes. This may result in stagnant, circulating and oscillating drops co-existing in the dispersion during travel. Each type of drop is associated with a particular mass transfer mechanism and since the effect of being present in a swarm cannot be accounted for, the mass transfer models of single drops in the stagnant, circulating and oscillating regimes are used to model dispersions.

5.2 Mass Transfer During Drop Formation

Numerous correlations have been published for mass transfer coefficients pertaining during formation [43, 89, 106, 165, 252, 268, 306]. The most important ones are summarised in Table 5.1. Values ranging from 5 to 50% have been reported for overall mass transfer efficiency during formation. Some of these discrepancies undoubtedly arise because of the variation in the accuracy of the experimental methods. West et al [311-2] attributed some deviation to the presence of surface active impurites which form a barrier across the liquid-liquid interface, thereby setting up a resistance to diffusion so that the extraction mechanism approaches that for a rigid sphere, Figure 4.1. Numerous observations have been made of circulation within the forming drops under a variety of conditions and it is generally accepted that this makes a major contribution to the overall mass transfer efficiency during the formation period [26].

Table 5.1 Correlations for Mass Transfer During Drop Formation

Author &	Correlation	Remarks	Eqn No
Licht & Pensing (165)	$K_{df} = \frac{6}{7}\left(\frac{D_d}{\pi t_f}\right)^{0.5}$	The whole area ages according to Penetration Theory. Only area varation with time is considered.	5.1
Heertjes *et al* (106)	$K_{df} = \frac{24}{7}\left(\frac{Dd}{\pi t_f}\right)^{0.5}$	Velocity of diffusion is small compared with velocity of drop growth.	5.2
Groothuis *et al* (89)	$K_{df} = \frac{4}{3}\left(\frac{D_d}{\pi t_f}\right)^{0.5}$	With drop diameters between 0.035-0.085 cm the rate of absorption increases at Re>750.	5.3
Coulson and Skinner (43)	$K_{df} = 2\sqrt{(3/5)}\left(\frac{D_d}{\pi t_f}\right)^{0.5}$	Average time of exposure and average exposed surface are obtained by the fresh surface mechanism.	5.4
Heertjes & de Nie (104)	$K_{df} = 2\left[\frac{r_o}{a_d} + \frac{2}{3}\right]\left[\frac{D_d}{\pi t_f}\right]^{0.5}$	At slow formation rates, the fresh surface model was very successful.	5.5
Ilkovic (118)	$K_{df} = 1.31\left(\frac{D_d}{\pi t_f}\right)^{0.5}$	Based on surface stretch mechanism; proved by many workers and used	5.6
Angelo *et al* (8)	$Kdf = \frac{2}{\sqrt{\tau}}\left[\frac{D_d}{\pi t_f}\right]^{0.5}$	For the more restricted situation of Ilkovic(118).	5.7
Sawistowski (253)	$K_{df} = \frac{40}{7}\left[\frac{D_d}{\pi t_f}\right]^{0.5}$	For a sphere, whose volume is linearly related to time. successfully.	5.8

continued/...

Table 5.1 *Continued*

Author &	Correlation	Remarks	Eqn No
Johnson *et al* (129)	$E_m = \frac{C_1 - C_2}{C_1 - C^*}$ $= \frac{20.6}{d_e}\left[\frac{D_d t_f}{\pi}\right]^{0.5}$	Most practical because "the end effect criteria" still exists.	5.9

Angelo and Lightfoot [7] working with a 30.5x5.1 cm rectangular SPC,with the system Isopar H (σ=48.5 mN/m) (d)-water (c)-benzyl alcohol(s) or acetophenone(s), found no substantial mass transfer during formation ie < 3%. The application of the surface stretch model [8] to both the formation and free rise periods, neglecting any mass transfer during coalescence, overestimated the experimental extraction efficiency and predicted that 10% of the overall mass transfer occured during formation.

Reviews of the various single drop models and correlations for mass transfer during formation are available in the literature [36, 107, 268]. Since jetting is the preferred mode of operation of the SPC [131, 180, 273], only mass transfer during formation under jetting conditions is reviewed here.

When the velocity of the dispersed phase through each individual hole in the sieve plate exceeds the jetting velocity, a series of jets issues from each plate. Each jet breaks into drops at some distance from the plate. Mayfield and Church [180] found experimentally using a 5.1 cm diameter SPC with the systems: toluene(d) - benzoic acid(s) - water(c) and ethyl acetate(d) - acetic acid(s) - water(c), that extraction rates were substantially higher under jetting than non-jetting conditions.

Meister and Scheele [185] concluded that with an interfacial tension lowering solute

,mass transfer into a drop during formation tends to stabilise the interface and deter coalescence, and that mass transfer out of a drop tends to de-stabilise it and promote coalescence. Mass transfer into the jet was found to produce longer jets than when transfer was in the opposite direction.

Sawistowski [254] suggested that because of the quasi-equilibrium between a jet and its surroundings, transfer into the jet causes the solute concentration to be greater at the neck or valley of a growing interface corrugation than at the peak. Thus the interfacial tension is lower (for an interfacial tension-lowering solute) at the valley than at the peak. The interface then expands towards the peak and causes liquid transport from the valley to the peak, thus reinforcing jet breakup. This theory explains why transfer into the jet is 'destabilising'.

Burkholder and Berg [27] suggested that either stabilisation or destabilisation may occur without quasi-equilibrium of both phases. Whether the mass transfer is stabilising or destabilising depends upon which phase exhibits the stronger Marangoni convection as dictated by the system physical properties.

5.3 Mass Transfer During Travel Through The Continuous Phase

The overall resistance to mass transfer during droplet travel through the continuous phase in an extraction column is, as given in Equation 2.2 earlier, considered to be made up of three hypothetical film resistances, each expressed as the reciprocal of an individual film mass transfer coefficient. These comprise the dispersed phase coefficient, k_d, the continuous phase coefficient, k_c, and the interfacial resistance, k_i. Under normal conditions k_i, is negligible, except where there is a chemical reaction. The resistances are assumed to exist solely in the dispersed and continuous phase boundaries at the interface, and either or both of these may be rate controlling. The diffusion of mass through these films depends upon the degree of turbulence and whether the drops are stagnant, circulating or oscillating. Stagnant drop behaviour in which there is no internal mixing, results in a low mass transfer rate, whereas circulation or oscillation induce vigorous mixing inside the drops resulting in

higher mass transfer rates to, or from, the drop.

A number of theories have been developed for mass transfer through interfaces [100]: the Whitman Two-Film theory [313], the Higbie Penetration theory [109], its modification by Danckwerts [46] and the Film Penetration Theory of Toor and Marcello [293].

5.3.1 The Dispersed Phase Mass Transfer Coefficient

The mass transfer coefficient inside a drop depends upon its mode: stagnant, circulating and oscillating as shown in Figure 4.1. At low Reynolds number corresponding to small drop diameters, drops behave as rigid spheres, but as the size increases, internal circulation starts to take place. Very large drops generally oscillate and the contents are well-mixed.

The system physical properties and purity also affect the drop behaviour. Both circulation and oscillation are known to increase with an increase in the viscosity ratio of the continuous phase to dispersed phase. Levich [162] and Garner and Skelland [76] considered that the surface tension of the dispersed phase would affect the circulation rate. When the resistance to mass transfer is in the dispersed phase, the overall transfer rate will be controlled by the transfer mechanism inside the drop which is influenced by the hydrodynamics of the system. Thus, Hadamard [91] demonstrated that the liquid inside a drop would circulate at Reynolds > 1.0 and Levich [162] postulated that circulation would occur between Reynolds numbers of 1.0 and 150.

The dispersed phase mass transfer models have been presented in the form of an extraction efficiency, E_m or mass transfer coefficient, k_d. The common assumptions are that the droplet is spherical and of constant volume, and that the solute concentration is sufficiently dilute for the physical properties to be considered constant. The liquids are also assumed to be Newtonian and incompressible.

5.3.1.1 Stagnant drops

For very small droplets < 1.0 mm in diameter, with no internal circulation, mass transfer by molecular diffusion is generally considered to be the dominant mechanism. Newman [206] developed a correlation for rigid drops on the assumption that the continuous phase was of uniform concentration and offered no resistance to mass transfer. The extraction efficiency, E_m, is given by equation 5.10 [Table 5.2].

The mass transfer film coefficient could be evaluated from the efficiency, by the use of Whitman's two-film theory,

$$k_d = - \frac{d}{6t} \ln (1 - E_m) \qquad \text{.... 5.11}$$

Newman's equation may also be applicable to large drops if there is a significant concentration of surfactant impurities.

Vermeulen [302], proposed an approximation to Newman's equation 5.10 by using the first term, n=1 only, and proposed equation 5.12 [Table 5.2]. An approximate value of the film coefficient was given by

$$k_d = 6.6 \frac{D_d}{d} \quad (t \rightarrow \infty) \qquad \text{.... 5.13}$$

Grober [88] considered the case where the mass transfer resistance was also present in the continuous phase and presented equation 5.14 [Table 5.2]. The parameter constant A_n and eigen value λ_n, depend on the continuous phase mass transfer film coefficient and the eigen values have been given by Lykov and Mikhaylon [173]. This model is a limiting case, valid only for small drops or when internal motion within the drops is hindered by surface contaminants. This situation however should not be disregarded, particularly in industrial systems where impurities are invariably present and involving fairly small drops <1.0 mm.

Elzinga and Banchero [63] relaxed the assumption of no resistance to mass transfer within the continuous phase and proposed equation 5 .15 [Table 5.2]. A_n and

Table 5.2 Correlations for Dispersed Phase Mass Transfer Efficiency During Drop Travel

Author & Reference	Correlation	State of drop	Remarks	Eqn No
Newman (206)	$E_m = 1 - \frac{6}{\pi^2}\sum_{n=1}^{n=\infty} 1/n^2 \exp\left[\frac{-4n^2\pi^2 D_d t}{d^2}\right]$	Stagnant	For small drop size	5.10
Vermeulen (302)	$E_m = \left[1 - \exp\left(\frac{-\pi^2 D_d t}{d^2}\right)\right]^{1/2}$	Stagnant	No continuous phase resistance	5.12
Grober (88)	$E_m = 1 - \frac{6}{\pi^2}\sum_{n=1}^{n=\infty} A_n \exp\left[\frac{-4\lambda_n^2 D_d t}{d^2}\right]$	Stagnant	Finite continuous phase resistance	5.14
Elzinga & Banchero (63)	$E_m = 1 - \frac{3}{8}\sum_{n=1}^{n=\infty} A_n^2 \exp\left[\frac{-64\lambda_n D_d t}{d^2}\right]$	Circulating	Finite continuous phase resistance A_n and λ_n functions of Re	5.15
Kronig & Brink (150)	$E_m = 1 - \frac{3}{8}\sum_{n=1}^{n=\infty} A_n^2 \exp\left[\frac{-64\lambda_n D_d t}{d^2}\right]$	Circulating	No continuous phase resistance Re > 1	5.17
Calderbank & Korchinski (31)	$E_m = \left[1 - \exp\left(\frac{-4R\pi^2 D_d t}{d^2}\right)\right]^{1/2}$	Circulating	No continuous phase resistance	5.18
Handlos & Baron (95)	$E_m = 1 - 2\sum_{n=1}^{n=\infty} An \exp\left[\frac{-16\lambda_n D_d t Pe_d / 1 + U_d/Uc}{2048 d^2}\right]$	Circulating	No continuous phase resistance Re≥1000	5.20
Skelland & Wellek (266)	$Sh_d = 31.4\, T_m^{-1.338} Sc_d^{-0.125} We^{0.371}$	Circulating	Drops falling in a stationary continuous phase	5.22
Olander (210)	$k_d = 0.972\, k_{HB} + 0.075\ {}^{d}/_{t}$	Circulating	No continuous phase resistance short contact times Re>1, R=2.25	5.23

continued/...

Table 5.2 *Continued*

Author & Reference	Correlation	State of drops	Remarks	Eqn No
Rose & Kintner (238)	$k_d = 0.45\ (D_d\omega)^{0.5}$	Oscillating	For symmetrical spherical drops	5.25
Angelo et al (8)	$k_d = \left[\frac{4D_d\omega(1+\varepsilon+3/8\ \varepsilon^2)}{\pi}\right]$	Oscillating	For integral number of completed oscillations	5.26

λ_n, were listed as functions of k_c.

Treybal [295] proposed a correlation for k_d based on a linear concentration difference driving force,

$$k_d = \frac{2\pi^2 D_d}{3d} \qquad \text{.... 5.16}$$

This equation has been considered to be applicable to rigid spheres [295].

5.3.1.2 Circulating droplets

At a given Reynolds number the solute inside a drop commences to circulate. Experimental studies indicate that due to the mobility of the interface the rate of mass transfer is enhanced when circulation occurs in comparison with rigid spheres. Circulation leads to the drop contents becoming mixed by either laminar or turbulent circulation.

(a) Laminar circulation

Internal circulation is laminar for $Re \geq 1$. Kronig and Brink [150], used the Hadamard - Rybczynski [91, 247] flow patterns to describe this internal circulation.

Their basic assumptions were that the time of circulation is small compared to the time of solute diffusion, the solute diffusion is in a direction perpendicular to the internal streamlines, and that the continuous phase resistance is negligible. On this basis they proposed equation 5.17 [Table 5.2]. The parameter constant A_n and eigen value λ_n have been presented by Heertjes et al [106]. The assumed flow pattern is restricted to Re≥1.0, but some workers [75, 106] have suggested that it's validity could be extended to Re≥10.

Calderbank and Korchinski [31] proposed a correlation for the mass transfer efficiency of droplets experiencing laminar internal circulation of the solute. They evaluated a constant experimental effective diffusivity, R (defined by Equation 5.24) equal to 2.25, times the molecular diffusivity, proposed equation 5.18 [Table 5.2] and provided the approximate solution for the Kronig and Brink correlation

$$k_d = \frac{17.9\, D_d}{d} \quad (t \rightarrow \infty) \qquad \ldots. \ 5.19$$

(b) Turbulent circulation

When circulation is present the interior of the drop may be considered perfectly mixed at any time. At low Reynolds number the drop shape is normally spherical, and therefore the circulation is laminar. With increased Reynolds number random mixing commences inside the drop; subsequently, at still higher Re values, the drop starts to change shape and oscillates.

Handlos and Baron [95] were the first to consider the case of turbulent mixing within a drop. A model was proposed taking into account 'the vibrations of the drop as well as the circulation patterns within it. For negligible continuous phase resistance, they proposed equation 5.20 [Table 5.2] which for infinite time, t becomes

$$k_d = \frac{\lambda_1 U}{768\,(1 + [\mu_d/\mu_c])} \qquad \ldots. \ 5.21$$

$\lambda_1 = 3.75$. The conditions for application of this model are not easily defined but Re> 150 and We>3.3 are suggested for free rising drops.

Skelland and Wellek [266] extended the Handlos and Baron model with a continuous phase resistance, but retained the assumption of infinite contact time. They proposed the empirical equation 5.22 (Table 5.2).

Olander [210] was the first to consider short contact times, but assumed no mass transfer resistance in the continuous phase. The resulting equation is 5.23 (Table 5.2).

Johnson and Hamielec [129] modified the models of Handlos and Baron (equation 5.20) and of Grober (equation 5.14) for use with high Re values for both circulating and oscillating drops by the introduction of an effective diffusivity factor, R, which was defined as

$$R = \frac{Pe_d}{2048\,(\mu_d/\mu_c)} \qquad \text{.... 5.24}$$

Patel and Wellek [217] analysed the more general case, ie any contact time and continuous phase resistance, but considered a uniform continuous phase concentration. They presented a numerical solution to be used in conjuction with the Handlos and Baron model.

5.3.1.3 Oscillating drops

For systems with a low continuous phase velocity, drops begin to oscillate at approximately Re>150-200. Large oscillating drops can be completely-mixed resulting in high mass transfer coefficients, ie up to a factor of 20 higher than for rigid drops [91, 123]. Several single drop models and correlations have been presented depending upon the different concepts of drop physical phenomena. Hydrodynamic factors which affect any of the three variables in equation 1.1 will be reflected in the transfer rate. Thus the area of the drop may be in a state of dynamic renewal, the concentration gradient ($\Delta C/\Delta x$) may vary enormously over short time increments, or the value of K may be affected by

temperature, since viscosity, diffusivity and density are temperature dependent. All these factors have been considered in the single oscillating drop models.

Dispersed phase mass transfer coefficients for oscillating drops can be predicted approximately by the Handlos and Baron model [95] equation 5.20. However, Rose and Kintner [238] used an approach in which it is assumed that complete internal mixing occurs within a large drop for each oscillation. They assumed a constant value for the mass transfer zone, to account for changes in area resulting from the oscillation, and that the local mass transfer coefficient varied in proportion to the thickness of this zone. They proposed equation 5.25 with the frequency of oscillation being predicted from the Schroeder and Kintner correlation [257].

Angelo et al [8] proposed a model, based upon the stretching or shrinking of phase boundaries and complete internal mixing. Their model may be considered a generalisation of the Penetration Theory. It provided slightly lower predictions of mass transfer rates than the correlation of Rose and Kintner. They proposed equation 5.26 (Table 5.2), which has also been recommended by Yamaguchi et al [283].

Although the models of Rose-Kintner and of Angelo et al give a more accurate picture of the behaviour of oscillating drops their practical application is limited to cases where the amplitudes and frequency of oscillation are known, or can be reliably predicted. The application of the Handlos and Baron model has been recommended for both turbulent circulating and oscillating drops in agitated extraction columns [260].

5.3.2 The Continuous Phase Mass Transfer Coefficient

The main difficulty of using the available continuous mass transfer coefficient models for predicting k_c in conditions where drop swarms are present, is the estimation of contributions due to drop wakes, which cause a variation in the continuous phase concentration around the drop.

The continuous phase mass transfer coefficient may be evaluated in terms of the

resistance in the film surrounding the drop through which the transfer takes place by molecular diffusion. The continuous phase mass transfer coefficient correlations and the particular application of each are detailed in the literature [127, 226]. An assumption as to the interfacial area is implicit in all the expressions, the usual choice for the area of a deformed droplet being that of a sphere of equivalent volume. The drop size and internal solute hydrodynamic state (ie the droplet Reynolds number) and shape, lead to enormous changes in droplet characteristics depending on whether it is stagnant, or exhibits internal circulation or deforms and oscillates.

5.3.2.1 Stagnant drops

On the basis of boundary layer theory, some workers have assumed that the effect of the liquid can be represented by its bulk properties and correlated the rate of mass transfer from, or to, a solid sphere by the general equation,

$$Sh_c = a + b\, Re^m Sc^n \qquad \ldots. \ 5.27$$

m is an index of the effect of convective velocity on mass transfer and n is an index of the effect of the ratio of momentum and diffusion boundary layer thickness on mass transfer. The correlations used most often or prediction of stagnant drop mass transfer coefficients are summarised in Table 5.3.

5.3.2.2 Circulating drops

Many workers [76, 78, 129, 150] have indicated that the continuous phase mass transfer coefficient is increased when circulation occurs inside a droplet. This is explained by the reduction in the boundary layer thickness. The correlations are similar to those for stagnant drops, equation 5.27, but the constant b is usually lower; this is attributed to the existence of wakes under circulating conditions.

Hadamard [91] postulated that the drag on the surface of a liquid-drop moving in a liquid medium causes internal circulation. Thus a drop would fall more quickly than an equivalent solid sphere in the same liquid medium since there is less drag. Boussinesq

Text cut off in original

[19] modified Hadamard's theory, and suggested that two surface layers are present on the drop. The surface viscosities cause a resistance to motion of the surface and the velocity of internal circulation is also reduced. Both theories reasonably predict circulation in fluid drops. The correlations used most often for the prediction of circulating drop mass transfer coefficients are listed in Table 5.3.

5.3.2.3 Oscillating drops

In the majority of correlations for continuous phase mass transfer coefficient a sphere, or an equivalent sphere, is used to characterise the circulating liquid drop. In the calculation of mass transfer the significance of distribution is primarily that the surface area increases rapidly with increase in distortion.

Many workers [129, 266, 318] have proposed correlations for mass transfer rates for oscillating drops with turbulent internal circulation, and the effect of oscillation causes high rates of mass transfer [64, 78, 238].

The most used correlations for oscillating drops, and their limitations, are listed in Table 5.3.

5.3.2.4 Swarms of drops

A theoretical approach by Waslo and Gal-or [308] was used to correlate continuous pha: mass transfer coefficients in drop swarms assuming no dispersed phase resistance an no internal circulation. The effect of impurities was also considered. The proposed the correlations,

$$Sh_c = 1.26 \left[\frac{1-x}{N - x^{1/3} M}\right] Re^{1/3} Sc^{1/3} \text{ for } \beta \rightarrow 0 \qquad \ldots. 5.38$$

and

$$Sh_c = 0.923 \left[\frac{\beta(1-x)^{5/3}}{N - x^{1/3}}\right] Re^{1/2} Sc^{1/2} \text{ for } \beta >> o \qquad \ldots. 5.39$$

where $N = 2 + 3\beta + x^{5/3} (3 - 2\beta)$ 5.40

Table 5.3 Correlations for Continuous Phase Mass Transfer During Drop Travel

Author and Reference	Correlation	State of Drops	Remarks	Eqn No
Linton *et al* (166)	$Sh_c = 0.582\ (Re)^{0.5}(Sc)^{0.33}$	Stagnant	Ignores diffusion and wake effects	5.28
Rowe *et al* (243)	$Sh_c = 2 + 0.76\ (Re)^{0.5}(Sc)^{0.33}$	Stagnant	Accounts for diffusion process	5.29
Kinard *et al*	$Sh_c = 2 + (Sh_c)_n + 0.45\ (Re)^{0.5}(S_c)^{0.33}$	Stagnant	Includes diffusion process and wake effects	5.30
Boussinesq *et al* (19)	$Sh_c = 1.13\ (Re)^{0.5}(Sc)^{0.5}$	Circulating	Assumes no boundary layer separation	5.31
Garner and Tayeban (78)	$Sh_c = 0.6\ (Re)^{0.5}(Sc)^{0.5}$	Circulating	Not valid for Re>450	5.32
Garner *et al* (74)	$Sh_c = -126 + 1.8\ (Re)^{0.5}(Sc)^{0.42}$	Circulating	For partially miscible binary systems of low σ	5.33
Mekasut *et al* (186)	$Sh_c = 1.04\ (Ga)^{0.49}$	Circulating	$Ga = d_e^3\ \rho_c^2\ g/\mu_c^2$	5.34
Garner and Tayeban (78)	$Sh_c = 50 + 8.5 \times 10^{-3}\ (Re)(Sc)^{0.7}$	Oscillating	Successfully used by other workers (137)	5.35
Yamaguchi *et al* (317)	$Sh_c = 1.4\ (Re')^{0.5}(Sc)^{0.5}$	Oscillating	$Re' = \rho_c\ \omega d^2/\mu_c$	5.36
Mekasut *et al* (186)	$Sh_c = 6.74\ (Ga)^{0.34}$	Oscillating	Ignores the effect of frequency of oscillation	5.37

$$M = 3 + 2\beta + 2x^{5/3}(1-\beta) \qquad \text{.... 5.41}$$

β is the degree of impurity defined as,

$$\beta = \frac{\mu_c}{[\mu_d + \gamma]} \qquad \text{.... 5.42}$$

and γ is the retardation coefficient due to the presence of surfactant.

For relatively large amounts of impurity (β->o), equation 5.38 expands to,

$$k_c = 0.55 \left[\frac{1-x^{5/3}\ D^{2/3}}{3-2x^{5/3}}\right] \left[\frac{\Delta\rho g}{\mu_c}\right]^{1/3} \qquad \text{.... 5.43}$$

for relatively small drops.

Gal-or and Hoescher [70] proposed a correlation that takes into account interaction between drops, or bubbles, in a swarm as well as the effect of drop size distribution and proposed,

$$k_c = 0.379 \left[\frac{D_c\,\Delta\rho g}{2\mu_c + 3\mu_d}\right] \left[\frac{d_{32}}{2}\right]^{1/2} \qquad \text{.... 5.44}$$

Calderbank and Moo-Young [32] combined literature data for liquid-liquid and solid-gas dispersions in which the dispersed phase was free to move under the action of gravity. The data were correlated to give,

$$k_c = 0.31 \left[\frac{\Delta\rho\mu_c g}{\rho_c^{\,2}}\right]^{1/3} Sc^{-2/3} \qquad \text{.... 5.45}$$

For large liquid drops which do not behave like rigid spheres they proposed,

$$k_c = 0.42 \left[\frac{\Delta\rho\mu_c g}{\rho_c^{\,2}}\right]^{1/3} Sc^{-2/3} \qquad \text{.... 5.46}$$

If the drops are not free to move under gravity and transfer is due to turbulence in the

surrounding liquid they proposed,

$$k_c = 0.13 \left[\frac{(P/v)\,\mu_c}{\rho_c^2}\right]^{1/4} Sc^{-2/3} \quad \text{.... 5.47}$$

P/v is the power dissipation per unit volume. Although the effect of wakes is important in single drop studies, they were reported to be less significant in swarms, particularly in agitated systems, where interaction and turbulence results in destruction of the wakes.

Heertjes et al [106] proposed:

$$Sh_c = 0.8\, Re^{1/2} Sc^{1/2} \quad \text{.... 5.48}$$

for a swarm of drops undergoing internal circulation. Ruby and Elgin [244] proposed a correlation for k_c, for a swarm of circulating drops at low hold-up.

$$k_c = 0.725\, Re^{-0.43} Sc^{-0.58}\, U_s(1-x) \quad \text{.... 5.49}$$

Hughmark [116] used a correlation of k_c for drop swarms [106, 244] to analyse his experimental results and concluded that : (a) for systems with ratios of continuous to dispersed phase viscosity <1, mass transfer coefficients for the continuous phase of drop swarms are similar to those of single drops, (b) for systems with ratios of continuous to dispersed phase viscosity >1, the increase in mass transfer coefficient for the continuous phase as a result of this viscosity effect is not apparently realised in drop swarms.

Sawistowski et al [255, 316] reported that the equations of Clift et al [41] for single drops gave a good prediction of k_c for drop swarms.

$$k_c = 1.2\, [f_n D_c]^{0.5} \quad \text{.... 5.50}$$

$$\text{where } f_n = \left[\frac{48\sigma}{\pi^2 d_e^3 \rho_c [2+3(\rho_d/\rho_c)]}\right] \quad \text{.... 5.51}$$

and the equivalent k_d

$$k_d = 1.4 \left[f_n D_d \right]^{0.5} \quad \text{.... 5.52}$$

5.4 Mass Transfer During Coalescence

Whilst studies of coalescence mechanisms of drops have been extensively reported (Section 4.3), information on mass transfer during coalescence is relatively scarce. Most workers have evaluated it using the 'end effect' method, in which mass transfer coefficients are measured in different column lengths and the results compared with models which give different time allowances for mass transfer during formation and coalescence. Hence, the percentage of mass transfer during formation and coalescence can be evaluated.

Mass transfer during coalescence was modelled by Johnson and Hamielec [129] for the case where a drop coalesced immediately it reached the interface. It was assumed that the drop contents spread quickly across the interface in a uniform layer and transient mass transfer occurred until the next drop arrived at the surface. Mass transfer was regarded as occurring according to the Penetration Theory with the exposure time equal to the formation time. They obtained

$$k_{dc} = \left[\frac{D_c}{\pi t_f} \right]^{1/2} \quad \text{.... 5.53}$$

Similar results were reported by other workers [43, 164]. Some workers [81, 165, 268] reported that mass transfer during formation was many times greater than that for coalescence and the contribution during the latter could be ignored. Heertjes and De Nie [105-6] concluded that mass transfer during coalescence can be neglected for two reasons:

(a) The mechanism of coalescence is such that the drainage of a drop into the homophase does not permit entrainment of the continuous phase in the homophase.

(b) Coalescence is so rapid (0.03 secs) that no substantial mass transfer is to be expected.

Heertjes and De Nie [107] suggested that coalescence of drops in swarms causes an increase in oscillation and hence the creation of a fresh interface of very small magnitude, counteracting the reduction in surface area. The net result may be an overall decrease in the mass transfer coefficient. However in a study by Mok and Treybal [195] in agitated vessels for drops of about 0.1 mm in diameter, k_c was found to be approximately twice as large for unbaffled vessels than for baffled vessels at the same impeller speed. This was attributed to the greater coalescenceand redispersion frequency in the unbaffled vessels.

5.5 Surface Active Agents and Interfacial Effects

The presence of surfactants may have a significant effect on the system hydrodynamics [204]. Although all drops above a critical size are expected to exhibit internal fluid motion when moving through another liquid, the presence of surfactants will lead to the formation of an absorbed film at the interface.

Industrial systems are rarely pure and surfactants accumulate at drop surfaces. It is known from various experiments [64, 77, 128, 289] that the process of mass transfer to, or from, drops is very sensitive to small quantities of surface-active impurities at the interface, even when the amount is so small that there is no measurable change in the bulk physical properties. The effect of surface active agents can be summarised as:

(a) Reduction of mass transfer coefficients;

(b) Hindrance of internal circulation or of oscillation within drops;

(c) Reduction of flow velocity (slip, characteristic or terminal);

(d) Reduction of any interfacial turbulence.

The interfacial phenomena associated with mass transfer have been investigated theoretically and experimentally by Orella and Westwater [216]. Surface active agents tend to make the drop interface rigid by forming a barrier, and to supress or even eliminate interfacial turbulence, which reduces internal circulation in the dispersed phase. When appreciable mass transfer is taking place across a liquid-liquid interface, it is possible to

develop local concentration gradients along the interface which, in turn, give rise to interfacial renewal which, in turn, enhances mass transfer.

Sternling and Scriven [283] investigated these interfacial phenomena and reported that they are due to the flow driven by the interfacial tension gradient (the Marangoni effect). Effects of surfactant specifically in the SPC are reported in Section 3.4.5

5.6 Mass Transfer Characteristics Of The Sieve-Plate Column (SPC)

The SPC comprises a series of discrete stages,but each individual compartment can be treated as a differential contactor. Therefore performance data can be interpreted in terms of both stage efficiencies and overall mass transfer coefficients.

5.6.1 Stage Efficiency

For liquid-liquid extraction columns in which contacting is stagewise, mass transfer performance is generally defined by stage efficiency. The most widely used expression for stage efficiency is that of Murphree [295] applied to either the dispersed or continuous phase. It is defined as the ratio of the actual concentration change which a phase undergoes within the stage to the change which would have occured if equilibrium were reached, Figure 5.1.

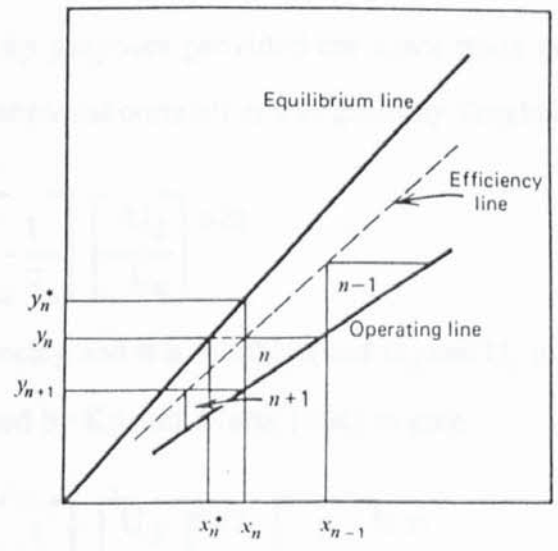

Figure 5.1 Murphree stage efficiency

$$E_m = \frac{x_{m-1} - x_m}{x_{m-1} - x_{m*}} \qquad \text{.... 5.54}$$

or

$$E_m = \frac{y_m - y_{m+1}}{y^*_m - y_{m+1}} \qquad \text{.... 5.55}$$

where x_m and y_m represent the average effluent compositions and y_{m+1} and x_{m-1} those of the streams entering the stage. x_m* and y_m* represent the equilibrium compositions. Although convenient for design purposes, Murphree efficiency is only strictly applicable if there is a linear equilibrium relationship over the concentration range considered.

Relationships between Murphree efficiencies and mass transfer coefficients are considered in Section 5.3 (Table 5.2)

The overall stage efficiency , E_o, of an extractor is simply the ratio of the number of ideal to real stages required to accomplish the same duty, ie the same concentration change at similar throughputs, thus

$$E_o = \frac{N_s, \text{ideal}}{N_s, \text{real}} \qquad \text{.... 5.56}$$

Stage efficiencies determined experimentally in a small SPC < 15 cm may be used for approximate scale-up purposes provided the same plate geometry and spacing are maintained [117]. An empirical correlation was given by Treybal [295];

$$E_o = 5.65\, H_t^{0.5} \left[\frac{1}{\sigma}\right] \left[\frac{U_d}{U_c}\right]^{0.42} \qquad \text{.... 5.57}$$

where H_t is the plate spacing and σ is in mN/m and U_d and U_c in m/hr.
This was further modified by Krishna Murty [144] to give

$$E_o = 1.58\, H_t^{0.5} \left[\frac{1}{\sigma}\right] \left[\frac{U_d}{U_c}\right]^{0.42} \left[\frac{1}{d_n}\right]^{0.35} \qquad \text{.... 5.58}$$

These available correlations were found to overpredict efficiency for high interfacial tension systems and underpredict it for low interfacial tension systems [117].

The evidence concerning the effect of direction of transfer upon stage efficiency is contradictory [73, 200] and the value of m may have a practical bearing on this effect [131]. Treybal's correlation predicts a higher E_o for m<1 if the extract phase is dispersed and for m>1 if the raffinate is dispersed. The result for when the raffinate is dispersed appears to contradict the expectation that coalescence would reduce efficiency in this case. However, the relatively short distance of drop rise between plates may mean that inter-plate coalescence is negligible.

The SPC can be operated with high throughputs, 10-60 m^3/m^2 hr [12, 29, 180, 221]. It has the advantages of repeated coalescence and redispersion of drops, and crossflow of the continuous phase which induces turbulence in the dispersed drops. Despite this it has not however found wide application compared for example with rotary agitated columns because of the low efficiencies reported by earlier workers [270],e.g efficiences as low as 3% were reported [73, 243]. However, it is not clear whether these low efficiencies are characteristic of the SPC or are related to poor design, or to operation outside the proper flow regimes.

5.6.2 Effect of Flowrates on Mass Transfer

Increase in the continuous phase flowrate has been reported to have no appreciable effect on the overall mass transfer coefficient '$K_{oc}.a$' using brass and stainless steel sieve plates in a 15 cm diameter column with the system: kerosene(d) - benzoic acid(s) - water(c), with solute transfer from d to c. With plastic (perspex) sieve plates, the continuous phase flowrate was observed to have considerable influence upon '$K_{oc}.a$' [170]. The above observations are explained by wetting effects which are discussed in detail in Section 3.2. The influence of U_c upon '$K_{oc}.a$' with plastic sieve plates, is attributed to the considerably greater diffusional resistance offered by the continuous (water) film, in view of the hydrophobic nature of the plastic material of the plate [170].

Mass transfer efficiency was found to decrease as the ratio of continuous to dispersed phase flowrates was increased [170]. This decrease in efficiency was believed to be due to the greater effect of the continuous phase film resistance at higher values of U_c/U_d. These observations are in agreement with the findings of Pyle et al [228] using the system: ethyl ether(d) - acetic acid(s) - water(c) in a 22 cm diameter SPC with stainless steel sieve plates,with solute transfer from d to c.

Murty and Rao [144] working with a 12 cm SPC, with stainless steel sieve plates using the system: MIBK(d) - butyric acid(s) - water (c), with solute transfer from d to c, reported that 'K_{oc}.a' increased markedly with increase in the dispersed phase flowrate. This was attributable to the increase in the number of drops, which resulted in both increased interfacial area of contact and vigorous turbulence inside the column. At a particular dispersed phase flowrate 'K_{oc}.a' remained almost constant with an increase in the continuous phase flowrate, indicating little dependency on the continuous phase flowrate. The number of drops did not increase greatly with increase in the continuous phase flowrate. Hence, there was little increase in contact area and little change in 'K_{oc}.a'.

5.6.3 Axial Mixing

Axial mixing phenomena, ie the non-ideal flow of the phases, may seriously affect the performance of an extractor and can, in extreme cases, account for most of the installed height [119]. An extractor design may be based initially on the assumption that the flow pattern is countercurrent with perfect plugflow of each phase. In practice, this assumption is rarely true because of axial mixing effects. Axial mixing results in a reduction in the concentration driving force for interphase mass transfer below that assumed in the standard design procedure, and consequently a variation in the HTU or HETS values.

The plugflow assumption is characterised by the orderly flow of individual fluid elements without overtaking or mixing with any other element ahead, or behind, ie there

must be no mixing or diffusion along the flow path. Perfectly mixed flow is such that each phase in a contactor is well-mixed, is uniform in properties and is of a similar composition as the outlet stream.

In practice, the flow patterns in extractors range in mixing intensity between plugflow and perfect mixing depending on equipment design and operation [281]. The main components of the mixing processes are: (a) molecular diffusion (b) eddy diffusion (c) convective mixing (d) channelling and (e) recirculation. The contribution from molecular diffusion is negligible when compared to gross mixing induced convectively. Convective mixing results from shear forces setting-up a velocity profile in the flowing phase, which will create a distribution of residence times of the liquid elements. Channelling is the forward transfer of a flowing phase beyond the mean position of elements. Such a maldistribution of flow results from uneven pressure distribution.

The recirculation of any fraction of a phase will affect the residence time distribution. Another generally observed flow imperfection is the presence of 'dead spaces', ie fractions of the phase which appear to be stagnant. Such spaces may follow from the arrangement of internals , eg redistributor or baffles or packing supports.

Axial mixing occurs, to some extent, in all types of extractor but differential are generally more prone to it. If allowance for the effect of axial mixing is not made in the design, the resultant plant could be seriously underdesigned. The effects of axial mixing in various commercial extractors have been reviewed by Ingham [119]. Mathematical methods for evaluation of axial mixing, and methods for the calculation of extractor efficiency which take into account axial mixing, have been reviewed by Misek and Rod [172].

In conclusion modern extractors are developed with the aim of achieving a high volumetric capacity, high mass transfer rates and low axial mixing. In the SPC, there is little or no axial mixing [60a, 180, 222, 295-6]. Any such mixing is restricted to the space between two adjacent plates, which serve to eliminate the vertical recirculation of the continuous phase. Axial mixing is probably low in the dispersed phase [7, 60a] and

the degree of mixing in the continuous phase must be between certain limits [131], that is between plug flow across the plate and through backmixing with uniform concentration. However, the continuous phase on the plate can be considered as completely mixed [270, 296].

CHAPTER SIX

EXPERIMENTAL INVESTIGATION

6.1 Introduction

Although as described in Chapters 3 and 5 there have been some studies of the performance of the SPC, these were mainly with small diameter columns and no reliable design or scale-up procedure has been published. The main objective of this work was to develop a design procedure for the SPC based upon pilot scale data following investigation of the effects of the major operating parameters, eg plate and distributor design, downcomer area, plate spacing and plate hole size, upon column performance.

6.2 Equipment Design

The pilot-scale equipment used comprised a 450 mm diameter, 2305 mm high industrial glass sieve plate extraction column (SPC) Figure 6.1. The column itself was constructed from one 2000 mm and one 305 mm long, flanged glass section. The effective height depended upon the plate spacing but was within the range 1800-2000 mm. The remainder of the column served as a disengaging section. The process lines, feed and effluent tanks were arranged so that the column was accessible from all sides to facilitate sampling and photography. All the valves were within easy reach. Six side-arms of 25 mm diameter and 60 mm long were provided, at a spacing of 300 mm, the first one being 200 mm from the bottom of the column. It was through these that sampling head probes were set in position. Each sample point comprised a 3 mm diameter stainless steel tube, extending to the middle of the column, with a stainless steel, quick-acting toggle value at the end. When the plate spacing was changed, at least one sample point remained in each compartment.

The column internals were fabricated entirely from 18/8 stainless steel. The sieve plates with downcomers in position were supported by four 6.35 mm diameter stainless steel tie rods running the entire length of the column. The rods were threaded at

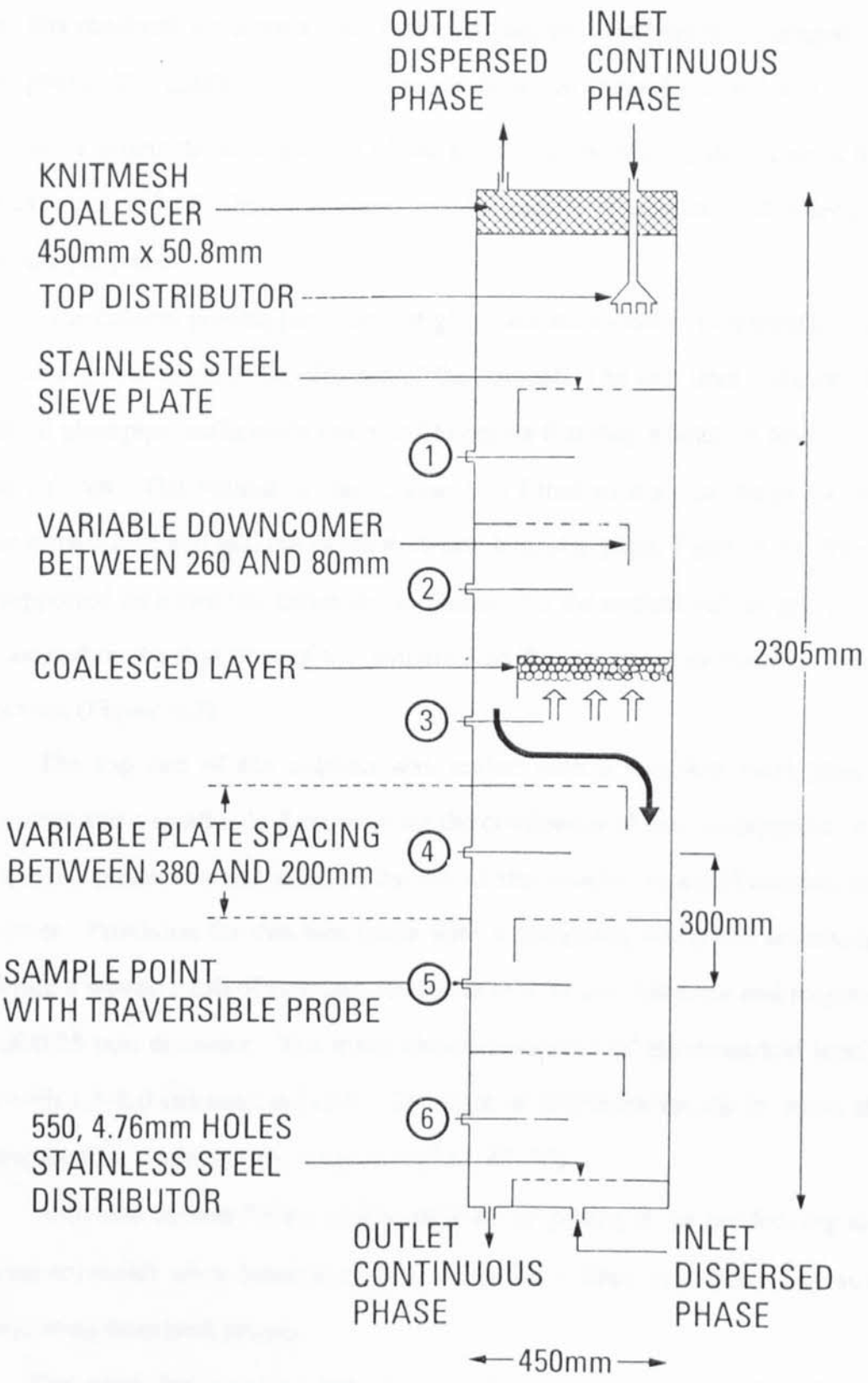

Figure 6.1 General arrangement of the sieve plate extraction column (SPC)

one end to permit fastening to the top end of the column. The plates were held in position by screwed locking collars. A 1.59 mm thick Viton rubber skirt was fitted around each plate; this rendered the plate a tight fit in the column, and prevented irregular flow of either phase. The details of construction are shown in Figures 6.1, 6.2 and 6.3. Figure 6.2 shows a schematic arrangement of the apparatus comprising the column, four 1 m^3 stainless steel tanks for liquid storage, transfer pumps, rotameters and, inlet and outlet phase sample points.

The column process parts were of glass, stainless steel or polytetraflouroethylene (ptfe), in order to avoid contamination of the solvent. The exit lines were of 38.10 mm industrial glass pipe, sufficiently oversized to ensure that they would not limit the capacity of the column. The bottom of the column was fitted with a distributor (with similar orifice dimensions and spacing as the 4.76 mm hole size plate, Figure 6.5). The column was supported on a two tier handy-angle frame. All the contral valves and instruments were located on the first floor of this structure, so that the extractor could be operated by one person (Figure 6.3).

The top end of the column was sealed with a stainless steel plate with a downcomer and a small side distributor for the continuous phase. Complete coalescence of dispersed phase was desirable at the top of the column to avoid continuous phase carry-over. Provision for this was made with a composite Knitmesh coalescer which comprised a woven mesh of stainless steel wire of 0.15 mm diameter and polypropylene wire of 0.25 mm diameter. The mesh chosen consisted of asymmetrical interlocking loops with 1.5-2.0 stitches/cm [124]. This type of Knitmesh results in more effective coalescence than a one component packing [47, 49, 50].

Activated carbon filters, which could be by-passed if not needed, (eg in newly prepared solvents) were incorporated in the process lines to remove any surfactant contamination from both phases.

The plate layouts used are shown in Figure 6.5 and Table 6.1. These were

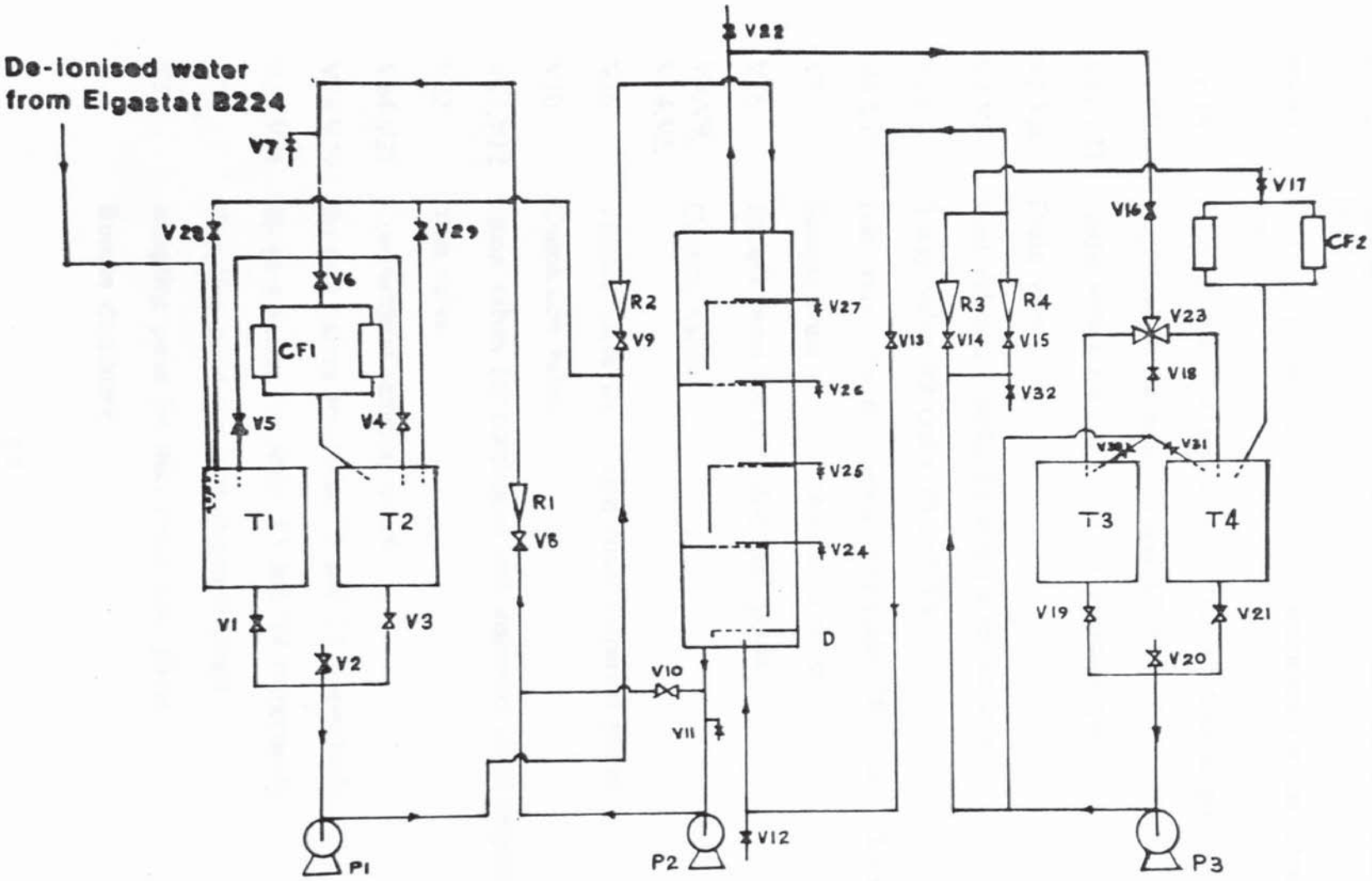

Figure 6.2 Schematic flow diagram of the Sieve plate extraction column (SPC)

LIST OF SYMBOLS FOR FIGURE 6.2

CF1,CF2	Activated carbon filters for continuous and dispersed phase.
P1,P2	Inlet and outlet pumps for continuous phase.
P3	Inlet pump for dispersed phase.
R1,R2	Inlet and outlet flow measuring rotameters for the continuous phase.
R3,R4	Inlet and outlet flow measuring rotameters for the dispersed phase.
T1-T4	Holding tanks for the dispersed and continuous phase.
V1,V3	Outlet valves for tanks T1 and T2 respectively.
V19,V21	Outlet valves for tanks T3 and T4 respectively.
V2,V20	Drain valves.
V4,V5	Inlet valves for tanks T1 and T2 respectively.
V23	3-way valve for tanks T3 and T4.
V6,V17	Inlet valves for the carbon filter tanks CF1 and CF2 respectively.
V7	Sample point for inlet continuous phase.
V18	Sample point for inlet dispersed phase.
V8,V9, V14,V5	Control valves
V16	Throttle valve for column outlet dispersed phase.
V10	Connection valve.
V11,V12	Drain valves for continuous and dispersed phase respectively.
V22	Vent valve.
V24-V27	Compartment sampling point.
V28,V29	By-pass valves for tanks T3 and T4 respectively.
V30,V31	By-pass valves for tanks T3 and T4 respectively.
V32	Sampling point for inlet dispersed phase.
V33	Sampling point for inlet continuous phase.
D	Bottom distributor.

Figure 6.3 General Arrangement of the Sieve Plate Extraction Column

Lower access platform at 108 cm elevation with reservoirs in background

Upper access platform at 208 cm coincides with top of column section

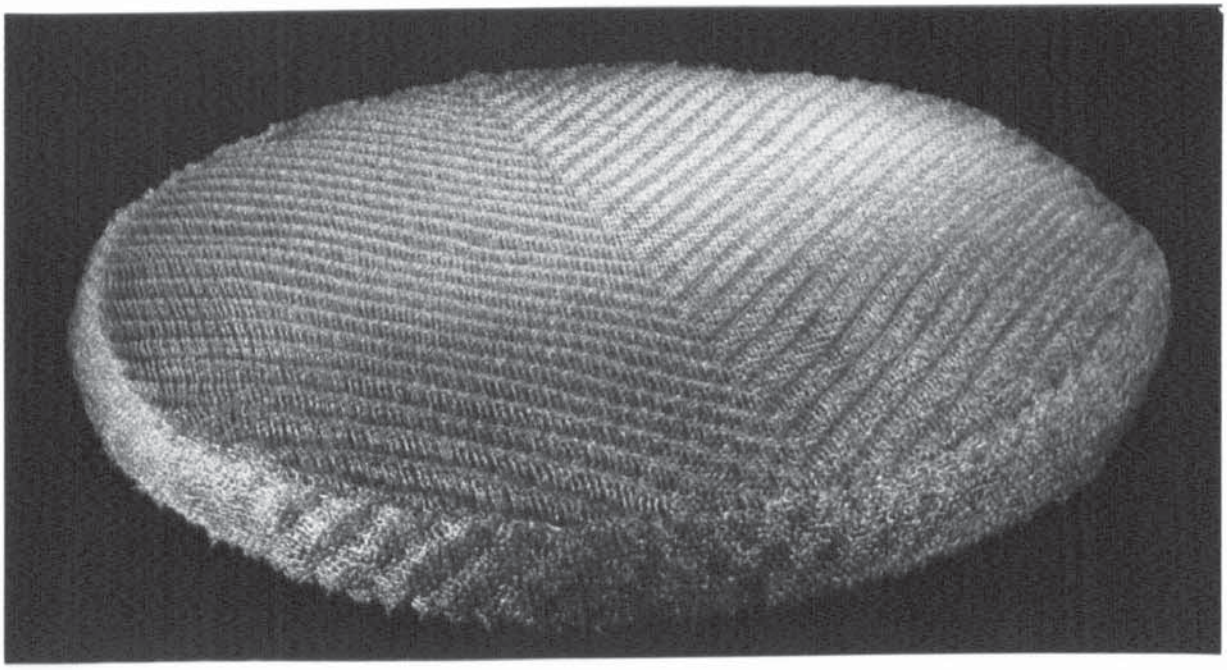

Figure 6.4a — Knitmesh Coalescer
Stainless Steel and Polypropylene D.C. packing
457.2 mm diam x 50.8 mm thick

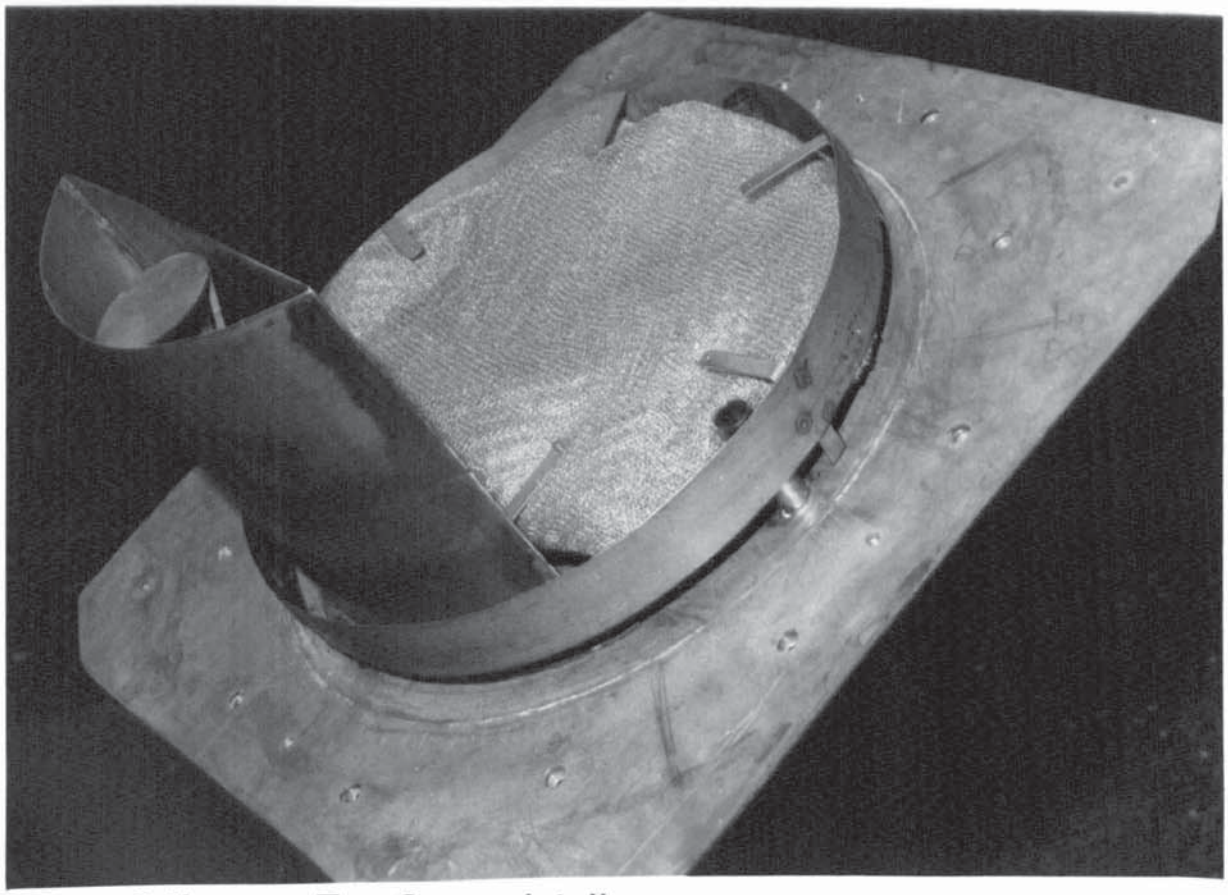

Figure 6.4b — Top Cover detail
Knitmesh pad in position for coalescence of outlet dispersion and top distributor in place

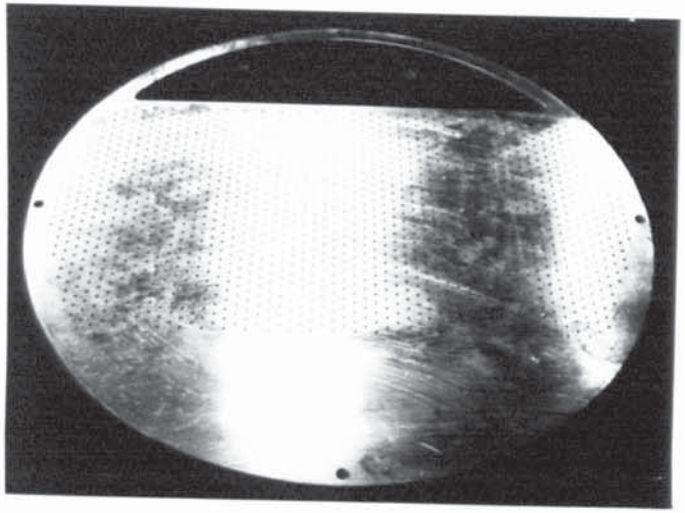

1.588 mm dia. 1517 holes
8.00 mm pitch, drilled only

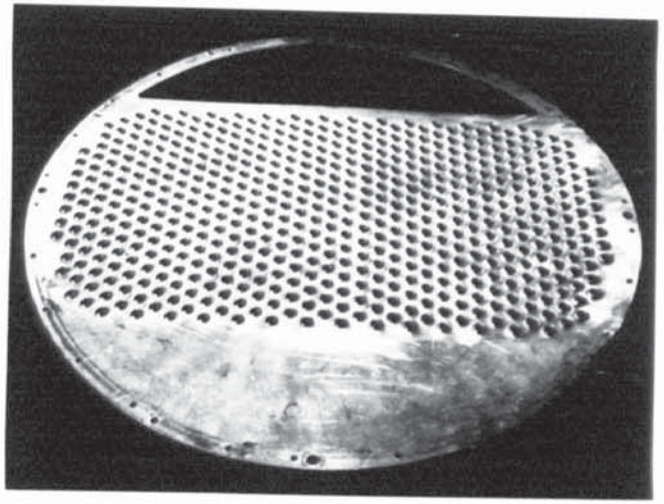

4.763 mm dia. 550 holes
13.0 mm pitch, drilled and punched

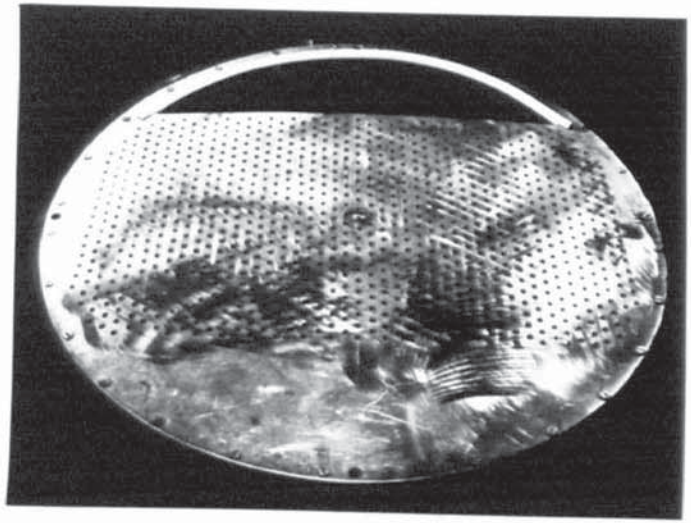

3.175 mm dia. 985 holes
10.0 mm pitch, drilled only

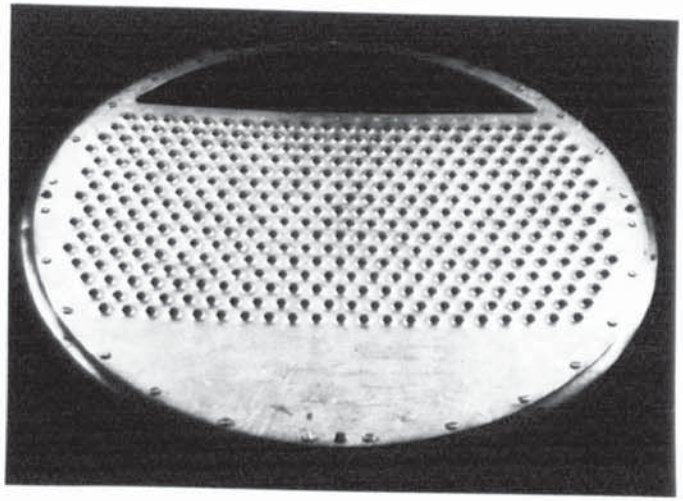

6.350 mm dia. 380 holes
16.0 mm pitch, drilled and punched

Figure 6.5 Sieve plate details

chosen because industrial columns are based on hole sizes between 1.588 and 8 mm [295]. The plate spacing was adjusted between 380 and 200 mm in decrements of 40 mm using a corresponding downcomer length between 240 mm and 60 mm, so that there was always a gap of 140 mm between the end of the downcomer and the plate beneath, ie the same flow area for the continuous phase above the plate. Between 4 to 6 plates were used in the column depending on the plate spacing, ie 4 plates at 240 mm and 6 plates at 260 mm and 200 mm.

Two holding tanks were provided for each phase. Each pair of tanks was interconnected such that one of the two tanks could be used separately or both could be used simultaneously. A recycle line was provided for each phase, for use during feed preparation and for mutual saturation of the phases by recirculation within a closed loop.

Two flameproof pumps (Newman 3 phase, 0.75 HP, 2850 rpm of 1.67 l/s capacity) were used for the continuous phase. One served to feed the column; the other served to transfer the continuous phase from the bottom of the column into the receiver tank, and also for recycle of the continuous phase to give a well-mixed solution when solute was added for mass transfer experiments. A flameproof pump (Beresford PV71, 3 phase, 0.75 HP, 2900 rpm of 2.5 l/s capacity) was also used to transfer the dispersed phase from the tank into the column via the bottom distributor. Flowrates were indicated on directly-calibrated, GEC Elliot metric rotameters with stainless steel floats of type 47F and 65 F for the dispersed phase and 47F for the continuous phase. The range of the dispersed phase flowrates was 0-3.83 l/s and of the continuous phase flowrates 0-1.67 l/s.

De-ionised water was used as the continuous phase. This was obtained by passing tap water through an Elgstat B224 de-ioniser, since filtered tap water was previously found to form a scum with the dispersed Clairsol '350' [2].

The equipment was located in a flameproof laboratory in which the atmosphere was changed 30 times per hour by forced ventilation. The entering air

temperature was controlled to 18.5 -20 °C and therefore no provision was made to control the temperature of the liquids processed, although the temperature of each stream was measured frequently during the course of an experiment.

Table 6.1 Plate Layout Details

Hole type	Plate Thickness (mm)	Hole Size (mm)	No of Holes Per Plate
Drilled	3.175	1.587	1517
Drilled	3.175	3.175	985
Drilled then punched	1.587	4.763	550
Drilled then punched	1.597	6.350	380

6.3 Experimental Techniques

6.3.1 Selection of Liquid-Liquid Test System

The chemical systems for liquid-liquid extraction recommended for test work by the European Federation of Chemical Engineering (EFCE) Working Party on Distillation, Absorption and Extraction [193] are:

a) Water - Succinnic Acid - n-Butanol

b) Water - Acetone - Toluene

c) Water - Acetone - Butyl acetate

but all of these have low flash points below 32 °C and therefore require strict precautions in storage and handling set by UK legislation.(ie The Highly Flammable Liquids and Liquified Petroleum Gases Regulations 1972)

In this work, and in previous liquid-liquid extraction studies (2, 52) the system used was water - acetone - Clairsol '350' (principally decane). The physical properties of this system are given in Appendix 1. It has the desirable features of a test system [9] and was available at reasonable cost to a fixed specification and could be handled safely under laboratory conditions. This was based mainly on the following considerations:

(1) low volatility of Clairsol '350', low toxicity and a high flash point of 71°C.

(2) the physical properties of Clairsol '350' (Appendix 1) are very close to those of kerosene . Therefore comparison was possible with results from other studies. The system does not exhibit sufficient interfacial turbulence and it is thus ideal for use in gravity operated columns.

A disadvantage with the use of Clairsol '350' was that interfacial scum accumulated with ordinary filtered tap water [2]. Therefore de-ionised water was used in this work.

6.3.2 Measurement of Physical Properties

Physical property measurements were made on mutually-saturated phases. Interfacial tension measurements were perfomed both with and without solute (acetone) to approximate to the column operating conditions. All the measurements were carried out at approximately 20°C.

Interfacial tension

The interfacial tension and surface tension were measured on a White torsion balance equipped with a 4 cm diameter ring. Temperature control at 20±1°C was applied by a Townson and Mercer temperature control system . An average was taken of the eight observations which gave the highest interfacial tension. Lower values were considered unreliable because the film could be ruptured by external disturbances before the maximum tension could be applied to the ring.

Interfacial tension measurements were also carried out for different solute concentrations in the phases, Figure 6.6.

Viscosity and Density

A Canon Fenske capillary tube viscometer type BS/1P/CF number 50 was used to measure the viscosity. Using a constant temperature control, the viscometer was

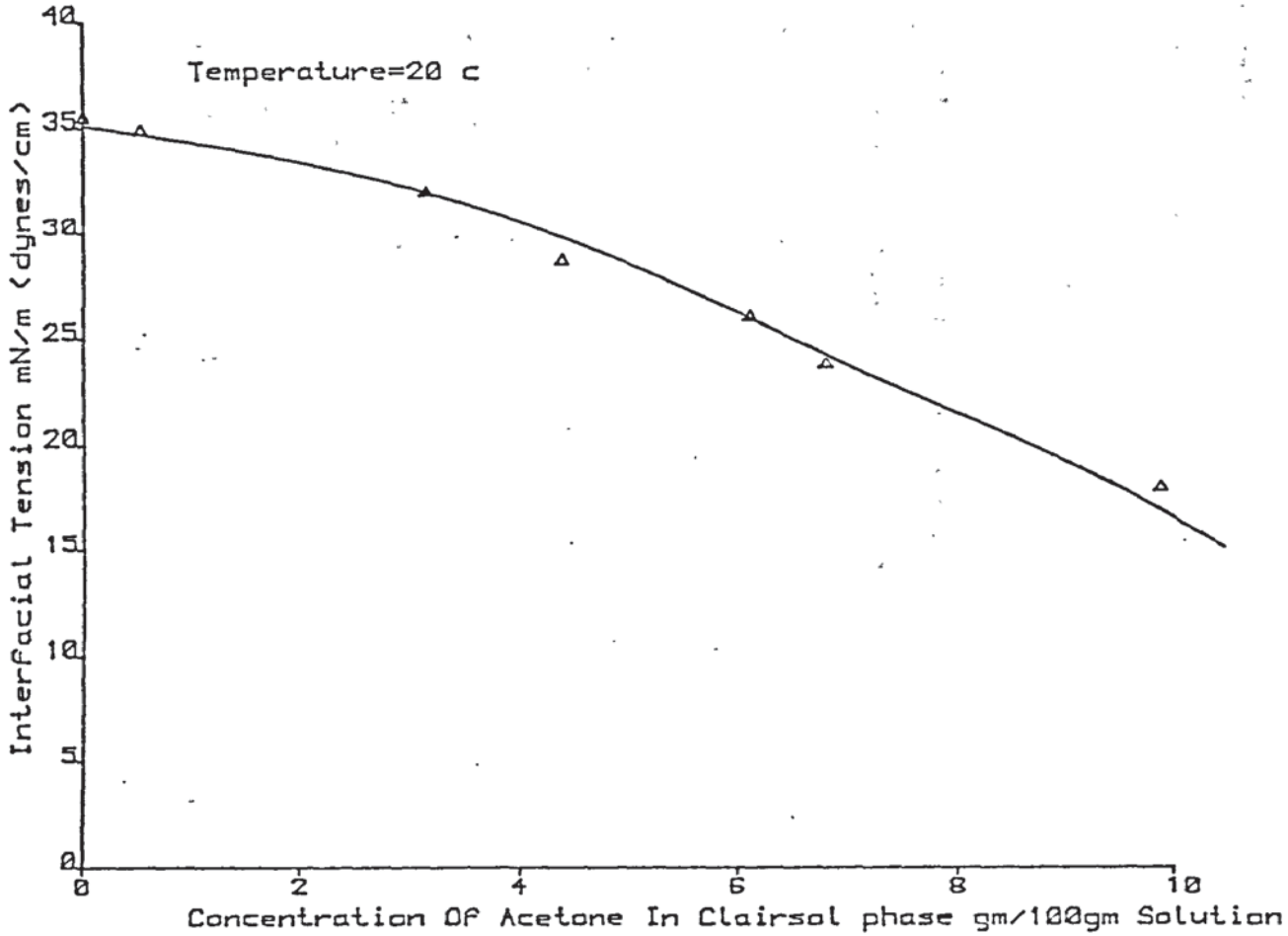

Fig.6.6 Variation Of Interfacial Tension With Concentration Of Acetone In Clairsol phase

calibrated with de-ionised water at a temperature of 20 ± 1°C, assuming a linear relation between kinematic viscosity and the time needed for the liquid levels to fall from one mark to another while the liquid flowed through the capillary tube into another leg.

The viscometer was then filled with Clairsol '350' which had previously been saturated with water. The time taken for the Clairsol '350' to fall a known distance on the viscometer was timed. Viscosities were calculated using the relationship

$$\frac{\mu_1}{\mu_2} = \frac{\rho_1 t_1}{\rho_2 t_2} \qquad \text{.... 6.1}$$

$\frac{\mu_1}{\rho_1 t_1}$ = the viscometer constant, was given for the viscometer used.

Here, 1 = de-ionised water and 2 = Clairsol '350.

Since the viscometer constant was known, the Clairsol '350' viscosity was calculated (Appendix 1).

Density measurements were made using a DMA 60 parr Digital Density Meter (Appendix 1).

Diffusion Coefficient

Diffusion coefficient is an important variable in the general treatment of mass transfer in liquid-liquid systems. Several correlations [137, 209, 233, 256, 287, 305, 314] are available, but the most widely-used are those of Wilke and Chang [314], Wagner [305] and King et al [137]. The standard deviation of these correlations from the experimental results on which they were based were for Wilke and Chang 18.5%, for Wagner 24.3% and for King et al 21.5%. The correlation of Wilke and Chang can be quite useful in cases where information on the physical properties needed by the other two correlations is not easily available. This correlation was therefore used to estimate the diffusion coefficient for the present test system. The diffusion coefficient, D_d of acetone in Clairsol '350' was 1.37×10^{-5} cm^2/s and acetone in water D_c was 1.10×10^{-5} cm^2/s at

20°C.

6.3.3 Determination of Equilibrium Distribution Data

Equilibrium distribution data were determined by making-up mixtures on a weight basis to represent points below the mutual solubility curve [264]. A study was made of the effect of solute concentration upon the equilibrium distribution, since the ratio of the concentrations of a component (solute) in the two liquid phases varies in general with concentration. Various distribution laws have been proposed but are frequently empirical [61, 265] and no general rule is obeyed in practice over wide concentrations. Graphical representation of experimental distribution data is therefore generally necessary.

The apparatus used was a Smith-Bonner equilibrium cell of 100 ml capacity surrounded by a glass jacket through which water was circulated to maintain the contents of the vessel at the desired temperature. The water jacket was connected to a Tecam C-400 thermostatic system containing a circulating pump. Experiments were conducted at 20 °C ± 0.5 °C. The cell was provided with a stirrer with variable speed control and a top side-arm for charging the liquid contents while the bottom was provided with a screw type, ptfe stop-cock for emptying the contents. Three cells were connected to the thermostatic system in series.

A heterogenous ternary mixture of deionised water, acetone and Clairsol '350' was made up in each cell and stirred continuously for eight hours to bring the mixture to equilibrium. The three cells were run simultaneously and contained an identical mixture. The mixture was then allowed to settle into two distinct clear layers with a sharp interface; the average settling time was about one hour. A sample of the top Clairsol-rich layer was withdrawn for analysis using a pipette, care being taken to prevent the pipette tip from reaching the interface. A sample of the water layer was taken for analysis by opening the stop cock and letting the water run directly into a sample bottle. A small volume was run-off initially to remove the small stagnant layer that might be present.

Each determination was repeated three times to ensure reliability; any result outside ±5% was disregarded. The mean result was then used.

An ultra-violet spectrophotometer (SP1800) was used for analysis (Section 7.6). The results were then combined with those of previous workers with the same system [2, 52], to give more points on the equilibrium diagram. The equilibrium diagram is shown in Figure 6.7.

6.6 Solute Analysis

Acetone concentration in the continuous phase (deionised water) or dispersed phase (Clairsol '350') was determined by measurement of the relative absorbance of ultra-violet radiation.

A Pye Unicam ultra-violet spectrophotometer (SP1800) was used for the measurement of the relative absorbance of the sample placed in a 2 mm cell size and a liquid blank (without solute) in another 2 mm cell. The apparatus was zeroed for calibration by inserting liquid blanks in both cells. The calibration for acetone in the range of 0-14% w/w was found to be at a band width of 3.0 nm for both phases, and a wave length of 310 nm for the Clairsol phase and 300 nm for the water phase.

Calibration charts were prepared for relative absorbance of solutions of known acetone concentrations between 0-14% w/w as shown in Figures 6.8 and 6.9.

Only about 10 mls of solution was required for analysis by this method. The calibration was linear within the concentration range measured. Hence very accurate measurements of the solute concentration could be obtained.

The above method was chosen in preference to the refractive index method used by Dawodu [52], which presented difficulties in obtaining reproducible results because different batches of Clairsol tended to have different refractive indices [33]. A major advantage of the ultra-violet method was that different batches of Clairsol absorbed at the

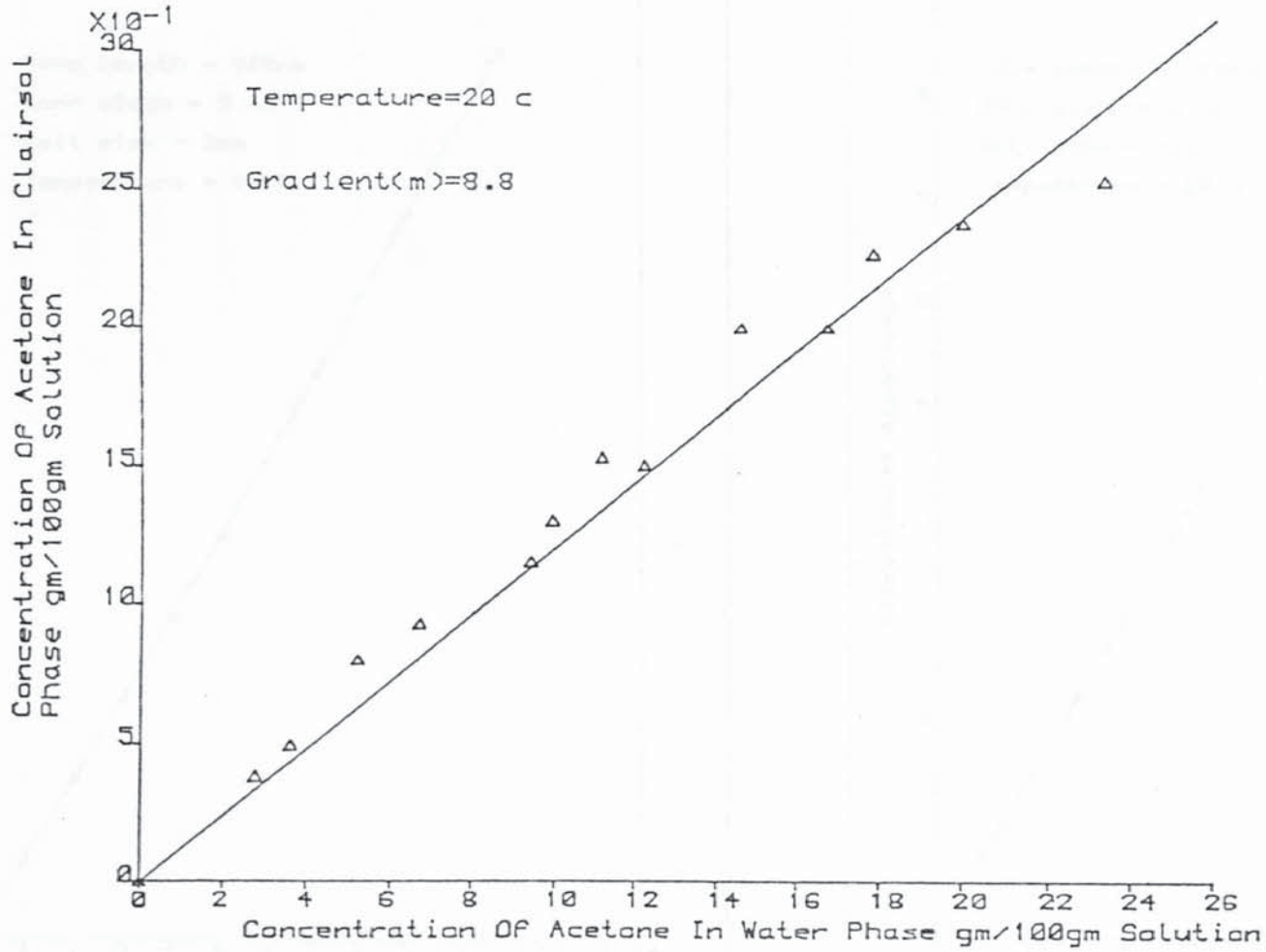

Fig.6.7 Equilibrium Diagram For Clairsol-Acetone-Water System

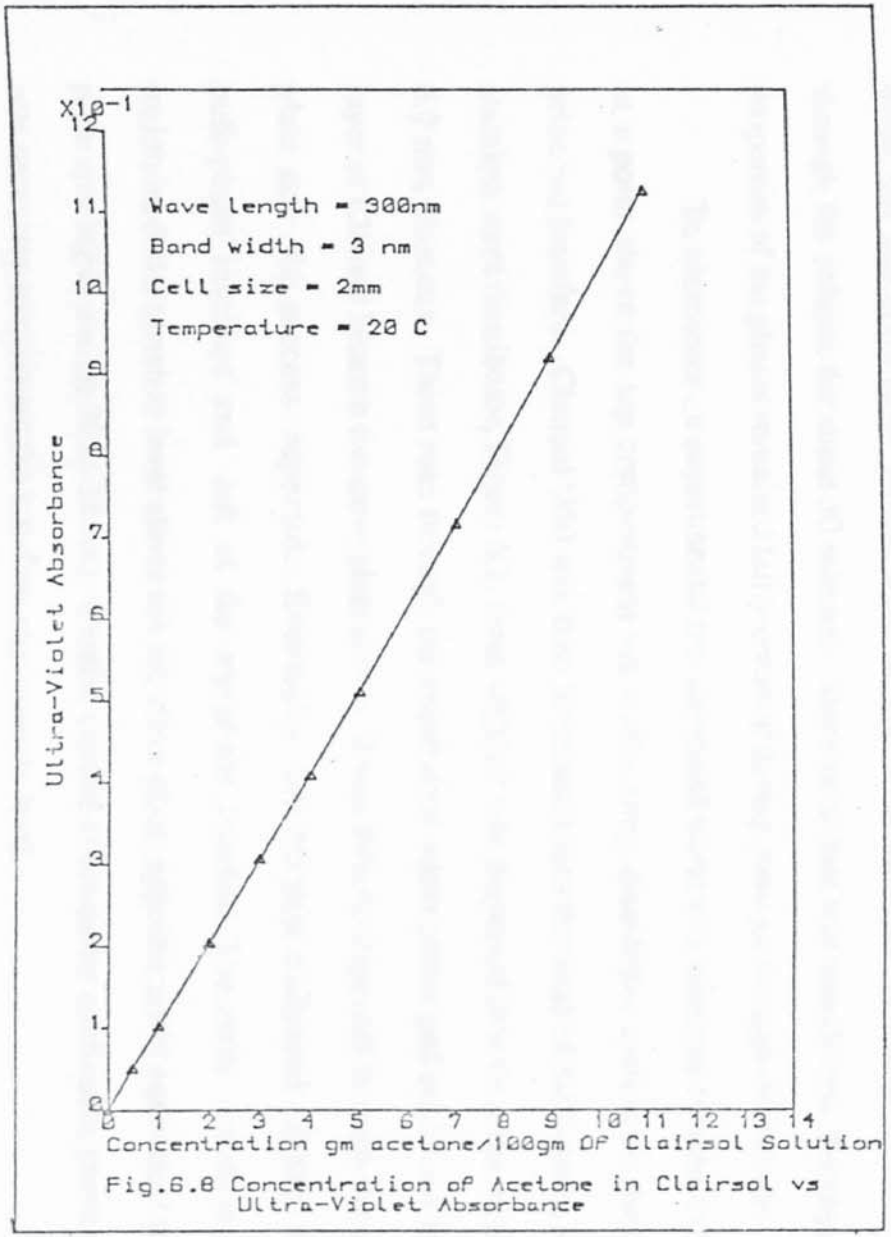

Fig.6.8 Concentration of Acetone in Clairsol vs Ultra-Violet Absorbance

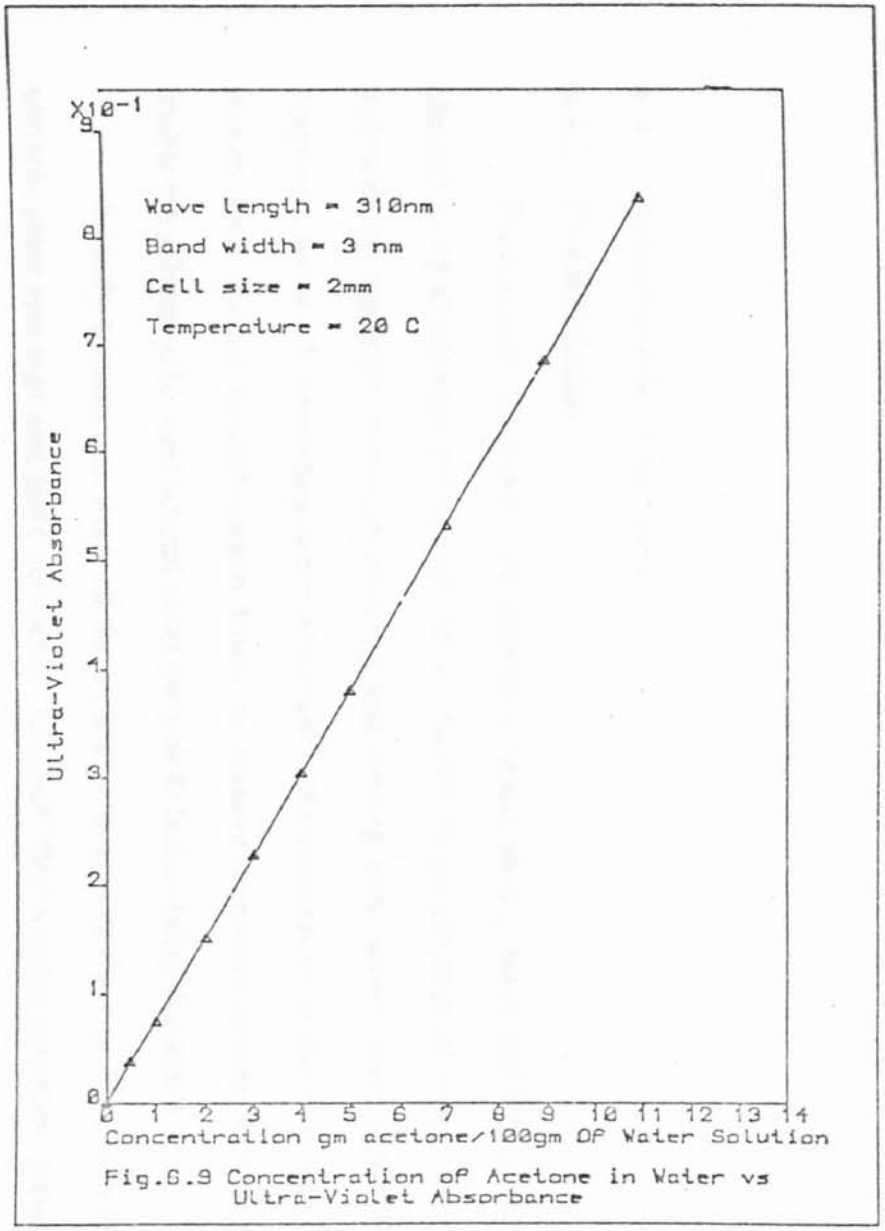

Fig.6.9 Concentration of Acetone in Water vs Ultra-Violet Absorbance

same wavelength.

6.4 Experimental Procedure

6.4.1 Hydrodynamics

Prior to each experiment, the column internals, storage tanks and flow lines were cleaned using an aqueous solution of 100 ml, Decon 90 per 20 litres of water. This was followed by repeated, thorough draining and rinsing with warm water followed by deionised water. If impurities were observed in the column or at the interface, both phases were passed through carbon filters to remove impurities or interfacial scum to enable the solvent to be used several times (recycled) before being discarded.

Initially a study was made of the hydrodynamic behaviour of the column with variable plate spacings and plate geometry. Clairsol '350' was the dispersed phase and deionised water the continuous phase throughout this experimental investigation. The dispersed and continuous phases were mutually-saturated by extended recirculation through the column for about 30 minutes. Since no solute was transferred, the physical properties of the phases remained fairly constant during passage through the column.

To commence an experimental run, deionised water was admitted into the column at a point above the top compartment via a side entry distributor until it reached the principal interface. Clairsol '350 was then introduced into the base of the column via a stainless steel distributor, Figure 6.1, from which it was dispersed into droplets of 4.2 to 6.7 mm diameter. These rose through the continuous water phase and coalesced into a layer of Clairsol beneath the sieve plate above. It was then re-dispersed through the sieve plate and the process repeated. Eventually the droplets coalesced at the main bulk-phase interface and left at the top of the column. The main interface was maintained at a constant level above the top sieve plate, approximately equivalent to the plate spacing in use (ie 20 to 34 cm). Careful control of the outlet continuous phase flow was necessary to maintain the interface at a constant level.

The remainder of the column functioned as a disengaging section, to prevent

carry-over of the water with the Clairsol leaving the column.

A steady principal interface, indicative of a constant arrival rate of drops within a given distribution was usually attained within 5 to 10 minutes after any change in the operating conditions. The dispersed and continuous phase pumps were purged at regular intervals to avoid haze formation. Under steady state operation, dispersed phase flowrates corresponding to 70%, 65%, 60% and 55% of the flooding velocities (Section 6.7.1.1) were used in the hydrodynamic investigation. To alter the plate spacing, or to insert a different set of sieve plates, the column was dismantled at the top and the sample points at the side of the column taken out. The complete column internals were then lifted out with the aid of a 50 kg hoist.

6.4.1.1 Flooding

As discussed in Chapter 5, the combination of 'flooding' flowrates represents the upper limit on volumetric capacity of the column under a given set of conditions and is governed by the system physical properties and column internal design.

To determine the flooding flowrates the flowrate of one phase was increased incrementally whilst the other was held constant, and vice-versa. A period of about 6 mins was allowed following incremental adjustment to allow steady state to be re-attained.

Flooding was characterised by a rapid increase in the flocculation zone heights beneath the plates, commencing at the top of the column, indicative of unsteady state operation.

Both phase flowrates were recorded at the flood point. An attempt was also made to measure the hold-up at flooding by the shut-off method [Section 6.4.1.3]; this proved quite difficult because of the increased flocculation layer heights and only approximate values were obtained ie unsteady state operation. As a check on the accuracy of the flood point determination, the flow being varied was decreased by about 10%, to allow the column to revert to normal operation and then increased until flooding re-occurred.

6.4.1.2 Dropsize and Dropsize distribution

Drop size distributions at various dispersed and continuous phase flowrates were studied using high speed still photography, since it is the most recommended technique [45]. High speed cine photography and a colour video camera were also used. These allowed droplet motion to be stopped and images recorded for subsequent analysis. Results analysed by the different methods for the same experimental conditions, were of similar magnitude. Therefore the results from the still photographic technique employed can be treated with confidence. This was an important factor, since different results have previously been obtained using several of the acceptable techniques [115].

The method used was the simple photographic technique suggested by Damon et al [45] together with additional lighting provided by a Flectalus fan-cooled, 1000 Watt quartz iodine floodlight positioned behind the column. A Asahi Pentax SP II 35 mm still camera with a 100 mm macro Takumar Telephoto lens and Ilford 400 ASA films were employed to photograph the dispersion. The aperture opening, shutter speed and focal length were adjusted according to the lensometer reading. In most cases a shutter speed of 0.002 seconds was sufficient. This produced sharp droplet outlines at all flowrates.

A correlation factor, to allow for the effect of the different refractive indices of the field liquid and the glass column walls, and for magnification due to the curvature of the column, was determined by standardising with a glass marble of known size inside the column filled with water at the field of focus with respect to the fixed position of the camera. However this factorwas close to unity in most cases and could be neglected.

A JVC GXN70E colour video camera with a 9.8-80mm zoom lens with maximum aperture of f1.4 was subsequently used at a distance of 1.6 m to reduce parralax errors. A frame rate of 25 f/s was used for drop size measurement.

A Hadland high-speed, cine camera was also used to photograph the motion of the droplets as they moved up the column. This was operated at 100 frames per second with a 75 mm lens using Ilford HP5 400 black and white film. The lighting was provided

by a Flectalus fan cooled 1000 watt quartz iodine floodlight.

Dropsize measurements were made from photographic prints with an enlargement of about 2 to 3 times. These gave sufficient magnification and contrast for counting the drops on a Carl Zeiss TG3 Particle Size Analyser. The number of drops initially measured for each run and compartment was between 350 to 900. This was subsequently reduced to 200 to 500, which is justifiable in contactors involving primary dispersions [2, 70, 81, 125, 213]. The second compartment was taken as the representative one to be photographed after initially taking photographs of all the compartments and analysing the drop size distributions [Chapter 7]. Drop counts were made from two to three replicate photographs for most runs. Typical photographs are reproduced in Figure 7.9 [Chapter 7]. Only drops with $d_1/d_2 < 2$ were included in the counts, where d_1 and d_2 are the true diameters of the major and minor drop axes respectively.

The Sauter mean diameter was evaluated from equation 2.5

$$d_{32} = \frac{\sum n_i d_i^3}{\sum n_i d_i^2} \qquad \text{.... 2.5}$$

where n = total number of drops.

The jet length, L_j, was measured for two different sieve plates: 6.35 and 3.175 mm, within the normal operating range of the column. At high dispersed phase flowrates > U_j, jetting occured from the sieve plates rather than the formation of discrete drops. The jet length was measured from the tip of each hole to the furthest point from the hole to which the jet reached as a continuous stream. The jet length tended to vary, eg by 10 to 30% because of the regular pulsation exhibitied especially at high dispersed phase flowrates, ie > U_d = 0.48 cm/s. Therefore it was necessary to obtain a representative jet length averaged over the fluctuations. A minimum of 6 jets were measured from two or three replicate photographs. A correction was allowed for non-jetting holes by counting their average number and introducing a correction factor to obtain the actual jetting velocity.

6.4.1.3 Dispersed Phase Hold-up

The fractional dispersed phase hold-up was determined by the simultaneous shut-off method [2, 562, 125, 171], which involved rapidly closing the inlet and outlet phase valves when the column was operating under steady-state conditions. This allowed the dispersion to settle under gravity and hence displace the interface. The total hold-up was then determined by dividing the shift in position of the interface by the effective column height. The static hold-up was measured by noting the height of the coalesced dispersion layer beneath each plate after the dispersed phase was allowed to settle completely. The operational hold-up, x, was then calculated according to equation 5.32.

Local hold-ups were also measured by rapidly removing about 250 ml of dispersion from the sample point in the centre of each compartment during steady-state operation

After settling the dispersed phase content of each sample was found volumetrically.

6.4.1.4 Flow Distributions

In a separate series of experiments the continuous phase flow distribution was followed by injecting pink potassium permanganate solution into the top sample point. The movement of pink colouration through the continuous phase was recorded using a JVC GXN70E Colour video camera (Section 7.7.1.2).

6.4.2 Mass Transfer Experiments

Experiments, involving the transfer of acetone from either phase, were performed at acetone concentrations of < 5% w/w in order to avoid formation of emulsions at higher acetone concentrations [2]. Dispersed phase flowrates were set at approximately similar values to those used in the hydrodynamic experiments. Flooding phenomena were not studied under mass transfer conditions since it was considered to

be too expensive in terms of the solute (acetone) recovery and also time consuming for settling of the resulting dispersion.

Prior to each experiment, the phases were mutually saturated. This was to ensure that only transfer of the solute (acetone) was investigated under mass transfer conditions. The dispersed, or continuous, phase containing the desired solute concentration was thoroughly mixed until a uniform concentration was attained, which required about 20 minutes; samples from different sections of the tank were analysed to confirm this. (Each phase was circulated through a closed loop back into its storage tank.) The desired solute concentration was achieved by adding a calculated weight of acetone to the particular phase; this was followed by analysis after through-mixing to determine the precise concentration. In all cases of solute transfer from the dispersed phase to continuous phase the initial acetone concentration in the continuous phase was always zero. However, when the organic phase was the extract the initial concentration was in most cases between 0-0.5%. The organic phase was back extracted (stripping) with fresh de-ionised water to reduce its concentration.

In all experiments, the column was filled with the continuous phase to the principal interface. The dispersed phase was then introduced into the column, after setting the desired flowrate for the experiment. A steady principal interface was maintained at the top of the column by controlling the outlet flow of continuous phase. Samples of the inlet and outlet streams were taken after the column had been operating for about 15 mins and then again after another 15 mins to ascertain whether steady-state had been established. An initial experiment was performed to determine the time to reach steady state, by taking 20 ml samples from the outlet streams at 3 min intervals until an identical acetone concentration was obtained for consecutive samples. This was found to be about 15 mins corresponding to approximately 2-3 complete changes of the column volume.

Generally, when steady-state had been established, 20 ml samples were taken from the inlet and outlet sample points. The acetone content was determined using an

ultra-violet spectrophotometer (section 6.6). The flowrates of both phase were recorded. The hold-up measurements (Section 7.1.3) and droplet photographs were taken as described earlier (Section 6.7.1.2) to determine the interfacial area.

Due to the scale of the equipment and its operation some changes in system physical properties were unavoidable. The system purity was therefore checked at intervals during experiments by measuring the relevant system physical properties, ie density, viscosity and interfacial tension. Whenever a significant discrepancy (ie > 5%) was observed in the values of these properties, the liquids were discarded.

CHAPTER SEVEN

PRESENTATION AND DISCUSSION OF RESULTS: HYDRODYNAMICS

7.1 Modelling of the Hydrodynamic Characteristics by Dimensional Analysis

Experimental investigations have been conducted to assist the formulation of mathematical relationships to characterise the hydrodynamics of the SPC based upon similarity theory. Similarity theory and physical modelling are methods which generalise experimental results from small scale tests in order to predict the performance of industrial scale equipment. They provide a means of economically evaluating important process parameters, thereby limiting costly industrial-scale tests.

Use of similarity theory and physical modelling cannot provide a complete theoretical understanding of physicochemical phenomena in terms of fundamental equations. They only provide integral solutions of the theoretical equations which define the process, by generalising the experimental data by dimensional analysis.

Dimensional analysis establishes the relationship between factors involved in a physical process. Application involves the logical selection of measurable system properties to form a dimensionless group; a positive result is obtained only if the initial set of all the factors governing the process is properly selected.

Difficulties may arise in establishing the precise quantitative relationships, because the existing conditions, or the manner in which the various factors interact, cannot be specified. Simplifying assumptions are therefore necessary. A qualitative solution to the problem can sometimes be obtained by structured reasoning based on a preliminary dimensional analysis. Subsequent experimental investigation based on this analysis frequently leads to the complete solution of the real problem. The Buckingham Pi theorem, is used to determine the number of independent dimensionless groups that exist, derived from the dimensional equation governing the physical process.

Dimensional Analysis

Although dimensional analysis does not provide specific information about the nature of a function, it facilitates identification of pertinent parameters that can be studied to reduce experimental effort.

The predominant hydrodynamic design parameters of the SPC: namely hold-up, x, coalescence height beneath a plate, h_t, and Sauter mean diameter, d_{32} have been characterised by their dependency upon column internal geometry, phase flowrates and the system physical properties.

The system physical properties were all measured by standard methods (Section 6.3.2) and the phase flowrates from independently calibrated rotameters.

The design parameters were correlated using experimental and literature data in conjunction with the Buckingham Pi theorem to give an equation of the form;

$$Y = A_o [F_1]^{A_1} [F_2]^{A_2} ..... [F_n]^{A_n} \quad .... 7.1$$

The constant A_o and exponents A_1-A_n were obtained by multiple regression analysis. The values of the unknown parameters in Equation 7.1 were evaluated by satisfying the least square objective function

$$S = \sum_{i=1}^{N} (Y_i - \hat{Y}_i)^2 \quad .... 7.2$$

$\hat{Y}_i$ = Predicted value of the dependent variable for the i^{th} observation.

Y_i = Experimental value of the dependent variable for the i^{th} observation.

N = Number of experimental points.

(Using this approach, the best values of the model parameters are obtained when the objective function is minimised).

A Fortran 4 computer program [150a] was redeveloped and modified into Fortran 77 (Appendix 3). The program solves for the coefficients in a multivariable, linear regression equation of the form

$$Y = A_0 + A_1F_1(x) + A_2F_2(x) + ... A_nF_n(x) \quad .... 7.3$$

Y = the model dependent variable.

A_j = the unknown coefficient, j = 0,1, 2 ... n

F_j = functions of the independent variables x_i, i = 1, 2, 3 ...k; j = 1, 2 ....m

Equation 7.1 is linearised by taking the logarithms and rearrangement in the form of Equation 7.3. The constant A_0 is found at the end of the program by taking the exponential of its linearised result. The method of the program consists of minimising a 'lease square' objective function, Equation 7.2. The algorithm is detailed in Figure 7.1.

Two tests are performed to determine the validity of the model. Firstly, the least square objective function is evaluated. This value is zero for a perfect fit. Secondly, the multiple correlation coefficient, R^2, which has a value between 0 and 1 is calculated, with $R^2 = 1$ corresponding to a perfect fit.

The computer program and description are given in Appendix 3 and the derivation of the dimensionless groups for coalescence height beneath a plate is given in Appendix 2.

7.2 Experimental Hydrodynamics

7.2.1 Flooding

Flooding was characterised by an increase in the coalescence/flocculation zone height beneath each plate. The dispersed phase hold-up in the column increased rapidly

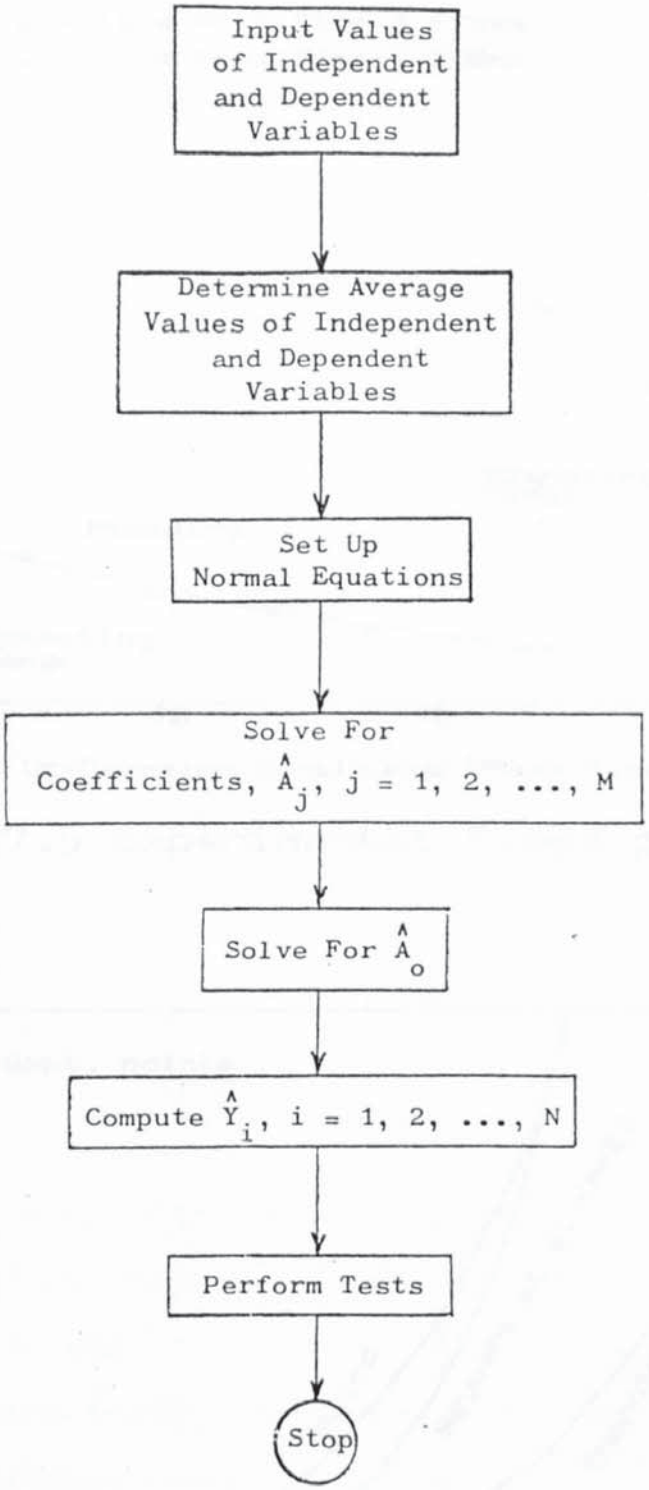

Figure 7.1 Linear Regression (LINREG ALGORITHM) Logic Diagram

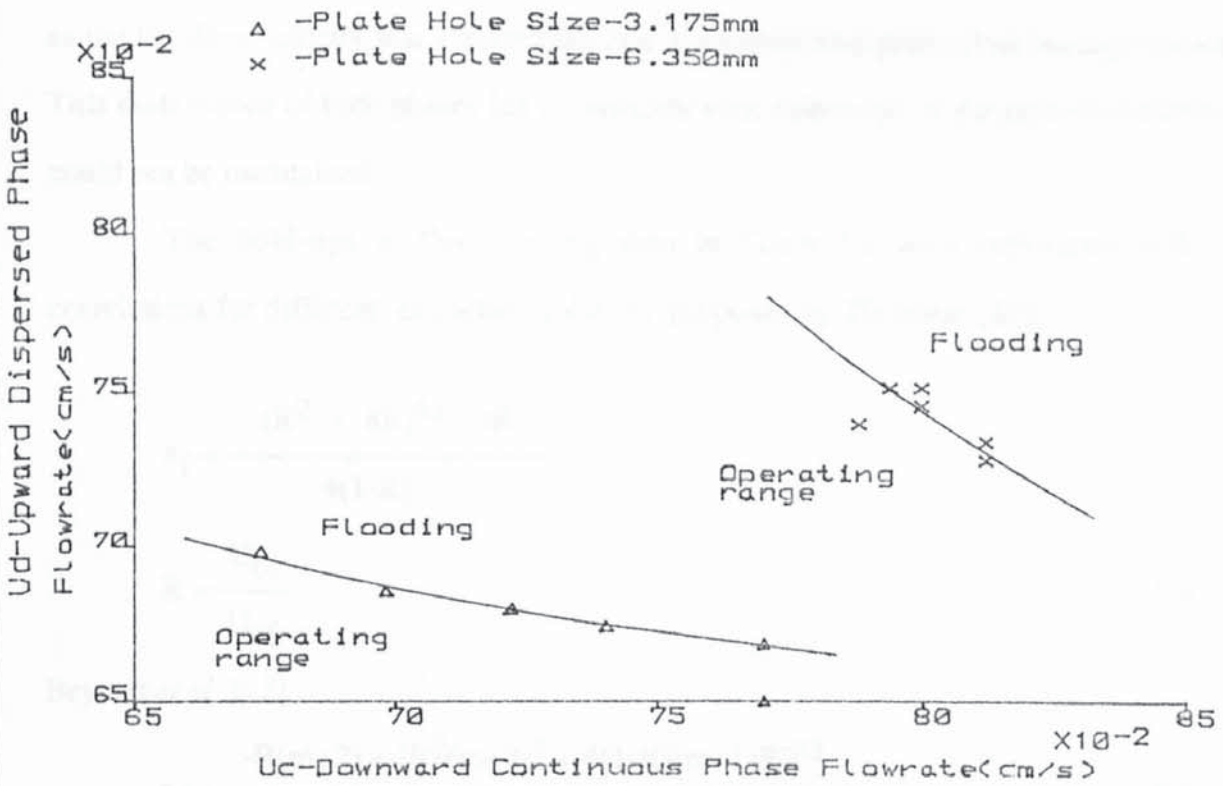

Fig.7.5 Experimental Flood points

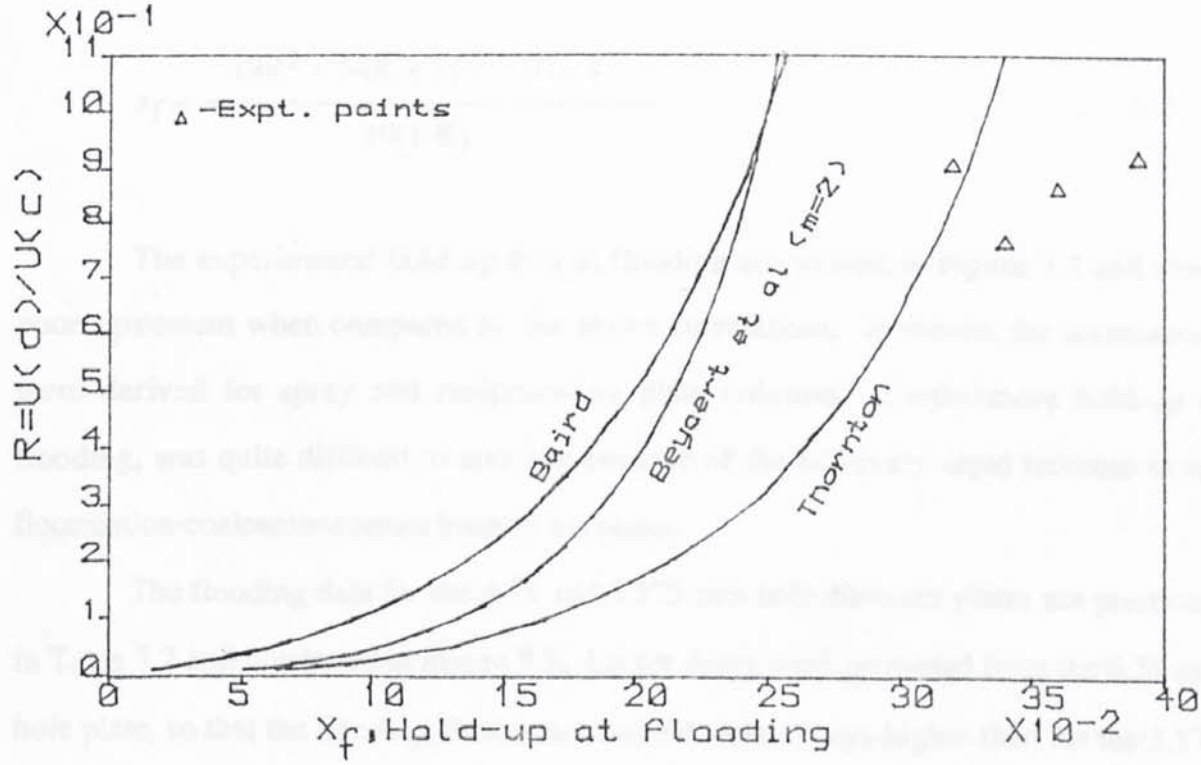

Fig.7.2 Comparison of Flooding correlations

as the flooding velocity was approached, and the continuous phase flow became uneven. This disturbance of both phases led to unsteady state operation, ie the principal interface could not be maintained.

The hold-ups at flooding, x_f, data in Table 7.1 were compared with the correlations for different extraction columns proposed by Thornton [289],

$$x_f = \frac{(R^2 + 8R)^{0.5} - 3R}{4(1-R)} \quad \text{.... 7.4}$$

$$R = \frac{U_{df}}{U_{cf}} \quad \text{.... 7.5}$$

Beyaert *et al* [18]

$$x_f = \frac{-R(m+2) + [R^2(m+2)^2 + 4(1-R)(m+1)R]^{0.5}}{2(1-R)(m+1)} \quad \text{.... 7.6}$$

and Baird and Shen [13]

$$x_f = \frac{(9R^2 + 54R + 1)^{0.5} - 7R - 1}{10(1-R)} \quad \text{.... 7.7}$$

The experimental hold-up data at flooding are plotted in Figure 7.2 and show poor agreement when compared to the above correlations. However, the correlations were derived for spray and reciprocating plate columns. Furthermore hold-up at flooding, was quite difficult to measure because of the relatively rapid increase in the flocculation-coalescence zones beneath the plates.

The flooding data for the 6.35 and 3.175 mm hole diameter plates are presented in Table 7.2 and illustrated in Figure 7.5. Larger drops were generated from the 6.35 mm hole plate, so that the flooding flowrates obtained were always higher than for the 3.175 mm hole plate. In each case operation with a high dispersed phase flowrate ie>0.82cm/s,

Table 7.1 Hold-up at Flooding for the 6.350 cm Hole Size Plate

U_c	U_d	R	x_f
0.94	0.73	0.77	0.34
0.89	0.77	0.87	0.36
0.85	0.77	0.91	0.32
0.89	0.82	0.92	0.39

Table 7.2 Experimental Flooding Velocities

Plate hole size (cm)	U_c cm/s	U_d cm/s
0.6350	0.89	0.82
	0.90	0.82
	0.92	0.78
	0.90	0.81
	0.79	0.81
	0.92	0.79
0.3175	0.73	0.71
	0.77	0.70
	0.69	0.73
	0.80	0.69
	0.85	0.68
	0.85	0.65

Table 7.3 Jetting Velocities

Plate hole size (cm)	Observed initial jetting velocity U_j(cm/s)	Calculated initial jetting velocity U_j(cm/s)
0.3175	8.8	16.9
0.6350	6.3	11.4

resulted in flooding conditions in the column.

Unfavourable flow characteristics which may be associated with high volumetric throughput in the SPC are excessive entrainment of the dispersed phase drops, overloading of the downcomers and restriction of flow through the plate holes which could cause the dispersed phase coalesced layer to backup into the downcomer.

The results confirm that SPC throughput is restricted by the plate geometry and downcomer geometry, its upper limit being the flood point. The higher the required loading capacity, the larger must be the free cross-sectional area of the column. However, this reduces the back mixing via a downcomer, and the separation efficiency of the column will therefore be reduced.

The superficial velocities of the phases at flooding are a decisive factor in the calculation of column diameter for design. The flooding limit is not an operational limit which can be identified precisely from theory. Therefore flooding data are required with various variables; plate hole size, free area, physical properties, (ie various test systems and column diameters) to give a range of graphical or empirical correlations. Figure 7.5 identifies the operating range of the SPC studied here with one system, but as recommended in Section 10.2 this investigation should be extended.

7.2.2 Jet Length From Sieve Plates

The jet length, L_j, was measured for two different sieve plates with hole sizes of: 6.35 and 3.175 mm, within the normal operating range of the column. At high dispersed phase flowrates > U_j, jetting occured from the sieve plate holes rather than the formation of discrete drops. The flowrates ranged from those at which jetting was initiated to the formation of turbulent jets. (Section 4.1.2)

The jet length was measured from the tip of each hole to the furthest point from the hole to which the jet reached as a continuous stream, as exemplified in Figure 7.3. The jet length tended to vary, eg by 10 to 30% because of the regular pulsation exhibited especially at high dispersed phase flowrates, ie > U_d = 0.48 cm/s corresponding to > U_n

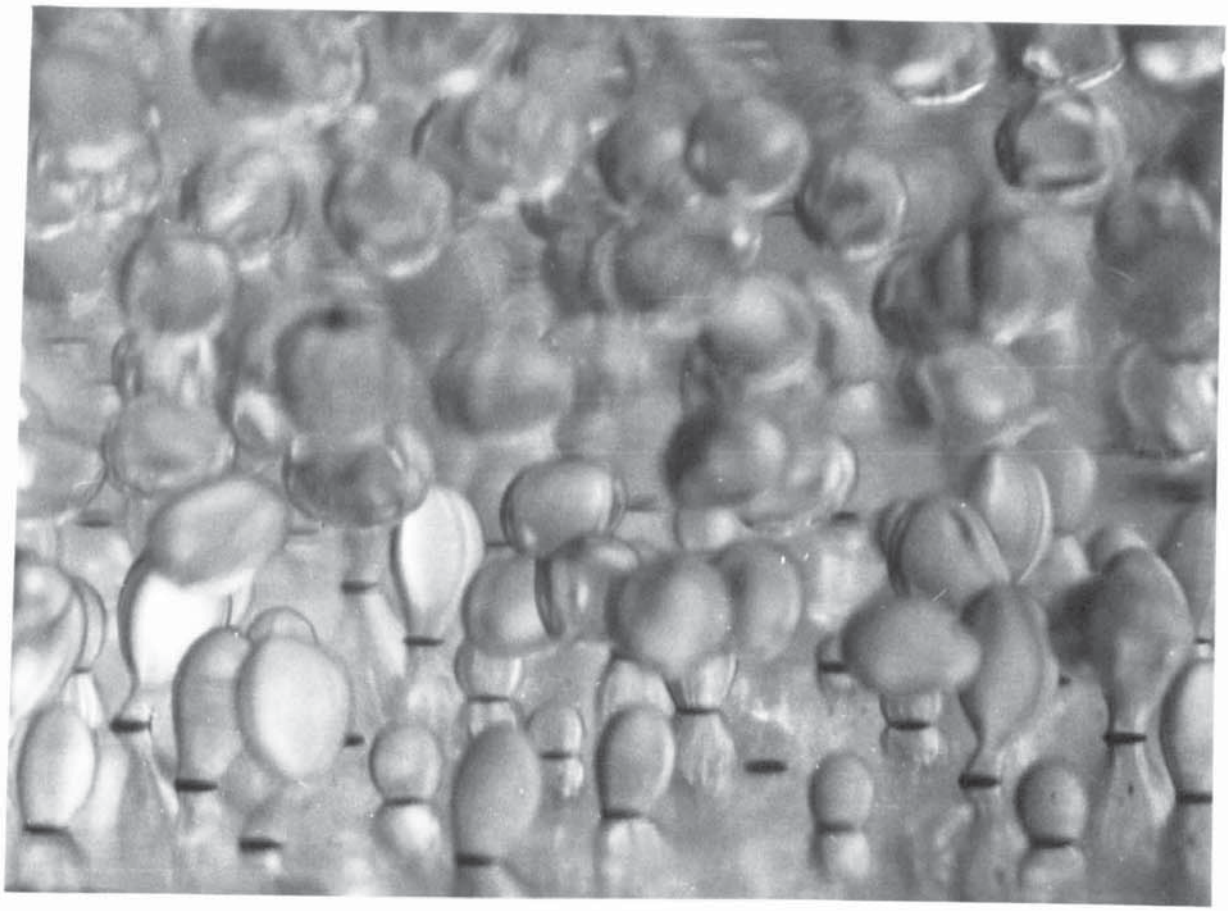

Figure 7.4 **Drop formation by drip-point**

U_c = 0.30 cm/s U_d = 0.31 cm/s
U_n = 6.45 cm/s d_n = 3.175 mm

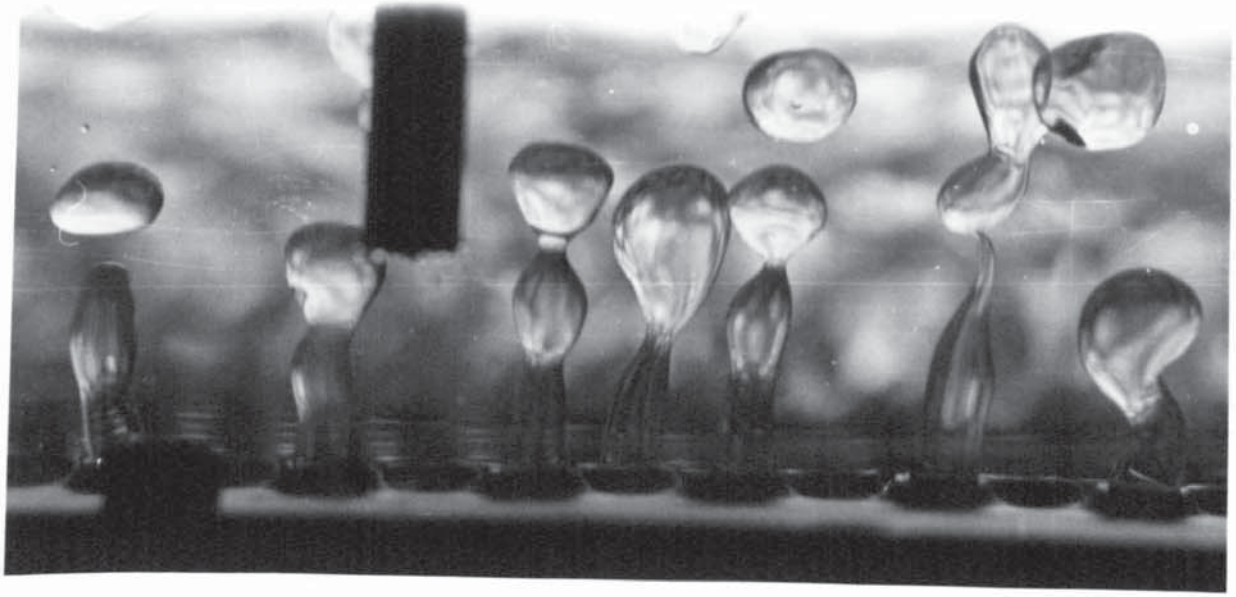

Figure 7.3 **Drop formation by jetting**

U_c = 0.55 cm/s U_d = 0.48 cm/s
U_n = 9.97 cm/s d_n = 3.175 mm

values of 9.79cm/s and 7.30cm/s for the 3.175mm and 6.35mm plate hole size respectively. Therefore it was necessary to obtain a representative jet length averaged over the fluctuations.

A minimum of 6 jets were measured from two or three replicate photographs. A correction was allowed for non-jetting holes by counting their average number and introducing a correction factor to obtain the actual jetting velocity.

The jet diameter tapered by approximately 10-20% towards the end of the jet and there was no perfectly cylindrical section of the jet; this is shown in Figure 7.3. Jet symmetry improved at high dispersed phase flowrates ie U_d>0.52cm/s. The dropsize in the jetting regime was also investigated as discussed in section 7.1.4. The distributor had punched holes of 4.763 mm plate diameter, and a similar geometry to the 4.763 mm hole sieve plate. Some holes tended to be preferred and others to be 'starved' at low throughputs, ie < U_d=0.43 cm/s. However after drops had left the distributor, the majority of the holes (ie > 90%) on consecutive sieve plates functioned properly. Generally, the jet length from the distributor was similar to those from sieve plates. The jet length results are tabulated in Table 7.4. and Figure 7.6 demonstrates that, as would be expected, jet length increased with an increase in dispersed phase superficial velocity. At low hole velocities, U_n < 6.3 cm/s for the 6.35mm hole size plate and U_n < 8.8 cm/s for the 3.175 mm hole size plate, uniform drops were formed and released by a drip-point mechanism. At increased dispersed flowrates the mechanism changed from discrete drop release to jet formation. The velocity at this transition point is termed the initial jetting velocity. The equation of Ruff *et al* [218a] for predicting the initial jetting velocity at a single nozzle is;

$$U_j = \sqrt{\frac{2\sigma}{\rho d_n}} \qquad \text{.... 7.8}$$

However, although this correlation is recommended by Kumar and Hartland for drop swarms [152], it lacks the important physical properties of $\Delta\rho$,μ_c or μ_d. The initial

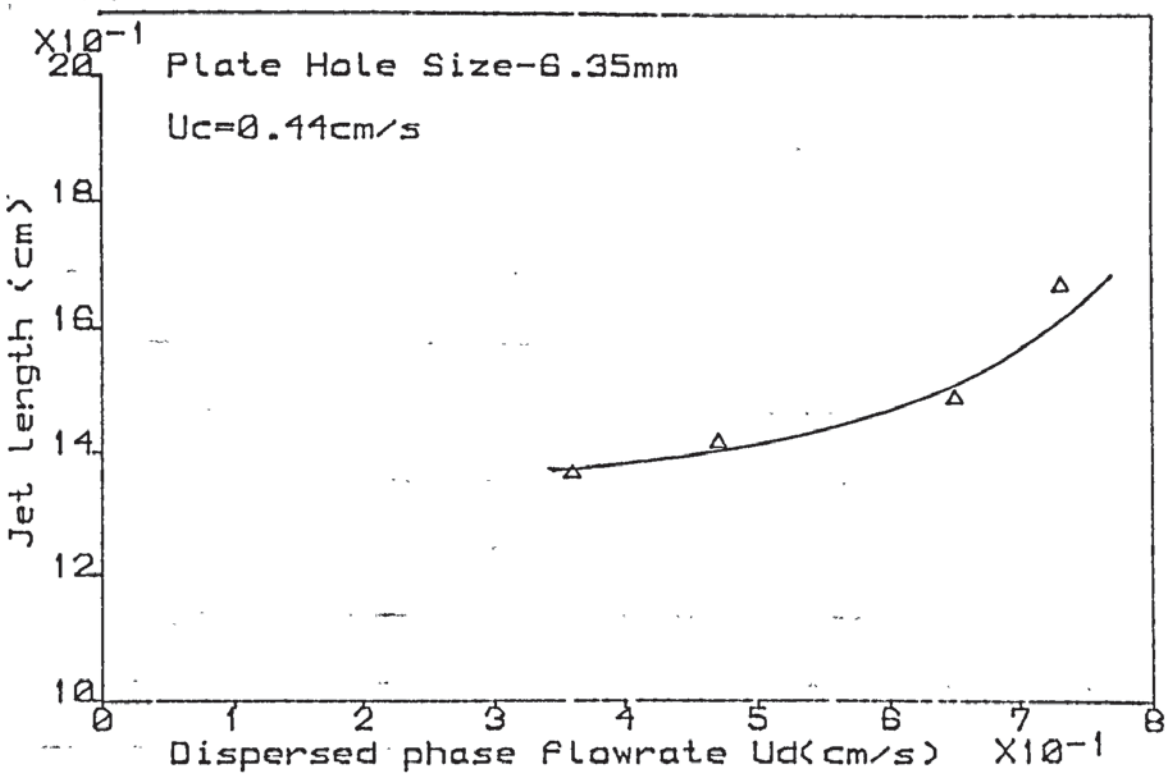

Fig.7.6 Effect of Dispersed Phase Flowrate On Jet Length

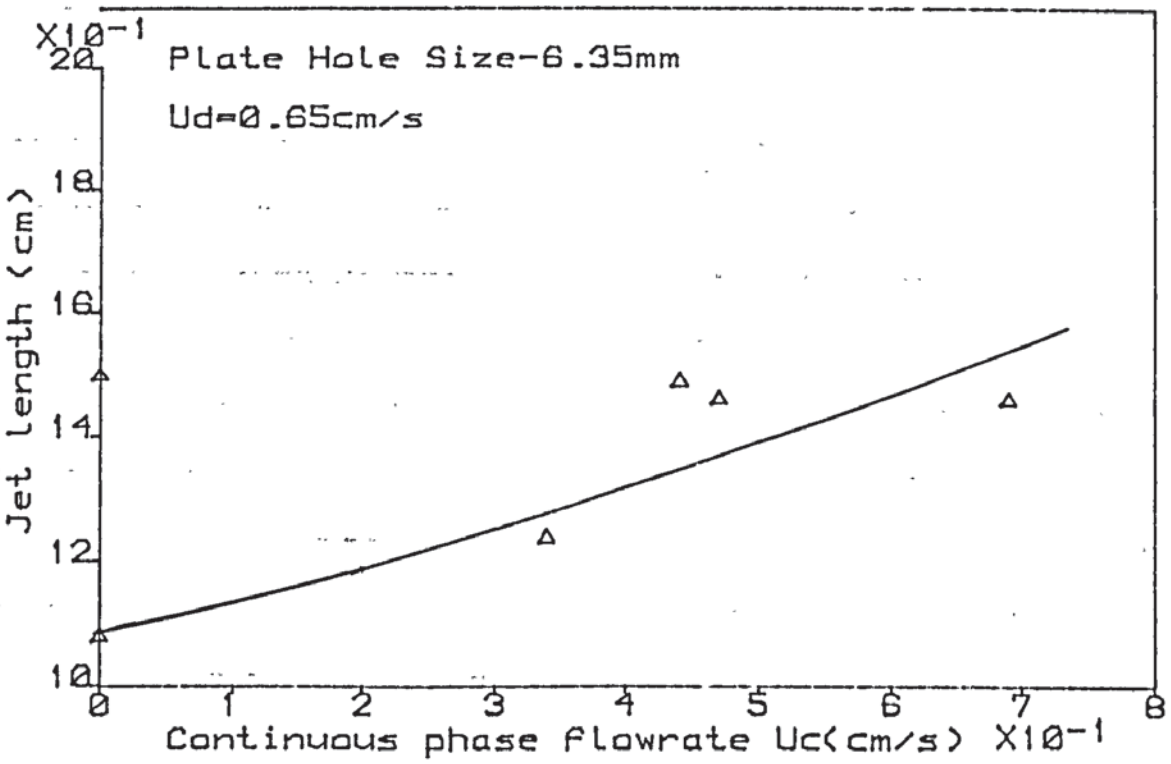

Fig.7.7 Effect of Continuous Phase Flowrate On Jet Length

Table 7.4 - Experimental Jet Lengths

Jet Len. Expt. Run No.	Plate Hole Size (cm)	U_c (cm/s)	U_d (cm/s)	U_n (cm/s)	Ave. Jet Length (cm)	Direction of mass Transfer
*1	0.1588	0.27	0.27	15.68	0.70	- --
*2	0.1588	0.27	0.36	18.32	1.80	---
*3	0.1588	0.27	0.43	22.09	2.30	---
*4	0.1588	0.27	0.56	29.00	1.90	- --
*5	0.3175	0.27	0.27	5.94	1.48	---
*6	0.3175	0.27	0.36	6.98	2.47	- --
*7	0.3175	0.27	0.43	8.67	3.29	---
*8	0.3175	0.27	0.56	11.21	2.58	- --
9	0.3175	0.30	0.43	8.67	1.75	---
10	0.3175	0.30	0.48	9.79	1.83	--
11	0.3175	0.30	0.52	10.60	1.91	---
12	0.3175	0.30	0.65	13.25	2.32	---
13	0.3175	0.30	0.73	14.88	2.66	---
14	0.3175	0.55	0.43	8.67	1.69	---
15	0.3175	0.55	0.48	9.79	1.79	---
16	0.3175	0.55	0.52	10.60	1.87	---
17	0.3175	0.55	0.65	13.25	2.20	---
18	0.3175	0.55	0.73	14.88	2.63	---
19	0.3175	0.30	0.43	8.67	1.82	D to C
20	0.3175	0.30	0.48	9.79	1.89	D to C

/continued

Table 7.4 cont.

Jet Len. Expt. Run No.	Plate Hole Size (cm)	U_c (cm/s)	U_d (cm/s)	U_n (cm/s)	Ave. Jet Length (cm)	Direction of mass Transfer
21	0.3175	0.30	0.52	10.60	1.94	D to C
22	0.3175	0.30	0.65	13.25	2.49	D to C
23	0.3175	0.30	0.73	14.88	2.82	D to C
24	0.3175	0.55	0.43	8.67	1.74	D to C
25	0.3175	0.55	0.43	8.67	1.80	D to C
26	0.3175	0.55	0.48	9.79	1.89	D to C
27	0.3175	0.55	0.52	10.60	1.96	D to C
28	0.3175	0.55	0.65	13.25	2.39	D to C
29	0.3175	0.55	0.73	14.88	2.76	D to C
30	0.3175	0.55	0.43	8.67	1.87	C to D
31	0.3175	0.55	0.48	9.79	1.94	C to D
32	0.3175	0.55	0.52	10.60	2.02	C to D
33	0.3175	0.55	0.65	13.25	2.38	C to D
34	0.3175	0.55	0.73	14.88	2.84	C to D
*35	0.4763	0.27	0.23	3.68	1.73	---
*36	0.4763	0.27	0.31	5.11	2.52	---
*37	0.4763	0.27	0.40	6.20	3.03	---
*38	0.4763	0.27	0.48	7.30	3.78	---
*39	0.4763	0.27	0.52	8.42	2.59	---
*40	0.6350	0.27	0.27	3.92	1.65	---

/continued

Table 7.4 cont.

Jet Len. Expt. Run No.	Plate Hole Size (cm)	U_c (cm/s)	U_d (cm/s)	U_n (cm/s)	Ave. Jet Length (cm)	Direction of mass Transfer
*41	0.6350	0.27	0.36	4.62	2.91	---
*42	0.6350	0.27	0.40	5.11	4.26	---
*43	0.6350	0.27	0.43	5.92	4.87	---
*44	0.6350	0.27	0.56	7.81	3.18	---
45	0.6350	0.0	0.65	8.56	1.08	---
46	0.6350	0.34	0.65	8.56	1.24	---
47	0.6350	0.47	0.65	8.56	1.37	---
48	0.6350	0.69	0.65	8.56	1.49	---
49	0.6350	0.44	0.48	6.63	1.42	---
50	0.6350	0.44	0.36	5.58	1.46	---
51	0.6350	0.44	0.48	6.63	1.49	---
52	0.6350	0.44	0.69	9.14	1.54	---
53	0.6350	0.44	0.73	9.64	1.67	---
54	0.6350	0.34	0.52	6.81	1.77	D to C
55	0.6350	0.34	0.65	8.56	1.78	D to C

* Dawodu's data (52)

--- No mass transfer

D Dispersed phase

C Continuous phase

jetting velocities calculated from this equation were compared with those observed experimentally in the absence of mass transfer. The equation predicted a velocity about twice the minimum observed in the present study, as illustrated in Table 7.3. This could be due to its lack of important physical properties.

At increased dispersed phase flowrates U_n> 13.25cm/s for the 3.175mm hole size plate, the jets rapidly lengthened until they were indistinguishable because of interactions with adjacent jets as they oscillated from side to side.

The effect of countercurrent and crossflow of the continuous flow on jet length is shown in Figure 7.7. Little change was detectable, even at high U_c ie>0.55cm/s. However, the crossflow aided interaction between adjacent jets. The effects ranged from distortion of the jet by displacement from the vertical axis at relatively low U_c values to a jet bending almost 60° at high U_c, as exemplified by Figure 7.3. In a separate series of experiments, potassium permanganate solution was injected through a sample point into the continuous phase at the top of the column, and the flow pattern recorded with a video camera [Section 6.4] . It was observed that the flow was not simply horizontal across each sieve plate, but tended to spread out ie it was slightly backmixed before flowing out through the downcomer. The tendency for drops to swarm via a central core of the column was observed at high (> 0.43 cm/s) dispersed phase flowrates. This is illustrated in Figures 7.10 and 7.11 [Chapter7]. The effect was found to decrease as the plate spacing was reduced from 38 to 20 cm. This phenomena was also recorded using the Hadland high speed cine camera.

The plot of jet length versus U_d under normal operating conditions of the column, is shown in Figure 7.6; it does not exhibit a peak as reported for single nozzles. With single nozzles, since flooding is not a limiting parameter, U_d could be increased to very high flowrates. Such high flowrates, ie U_n> 30 cm/s, cannot be attained for a conventional SPC without flooding.

Dawodu [52] used the single nozzle correlations of previous workers to predict the jet lengths and compared them to those observed experimentally. Most of the predicted lengths deviated widely from those actually observed with sieve plates.

There was a wide variation in jet length from the same holes ie up to 20%, at a particular dispersed phase flowrate. This might be expected due to variations in (a) holesize about the design value [the tolerance on a 6.35mm diameter hole was about 3%] (b) edge smoothness of holes (c) flatness of the sieve plates (d) different wetting properties of the plates, e.g variation in wettability of different areas of the underside of the plate, and its change with time [Chapter 3] (e) not all the holes functioning, which led to a slight variation in the hole velocity (f) differences in pressure drops across the holes due to the uneven coalescence/flocculation layers under the sieve plate. With references to (d) and (f) the phenomenon of local collapse of coalescence zones is well known [111]. Most of the above properties could be controlled for single nozzles.

Due to the considerable scatter of the results no reliable correlations could be proposed for jet length as a function of physical properties, phase flowrates and plate geometry.

7.2.3 Coalescence Heights

The coalescence height, h_t (static hold-up) was measured under normal operating conditions, as shown in Figure 7.8. The data subsequently correlated comprised :

(i) 61 data points from this study [Table 7.5]

(ii) 9 data points of Prabhu *et al* [222] Table U1, from a 5 cm diameter column with 42, 0.16 cm hole size plates with water as the continuous phase and isoamyl alcohol as the dispersed phase.

(iii) 11 data points of Fujita *et al* [69], Table U1, from a 5.6 cm diameter column with 36 ,0.2 cm hole size plates using an oil of viscosity 0.00037 kg/ms, density 890 kg/m^3 and interfacial tension 25.3 mN/m, and water as the continuous phase.

The 81 data points were correlated to give,

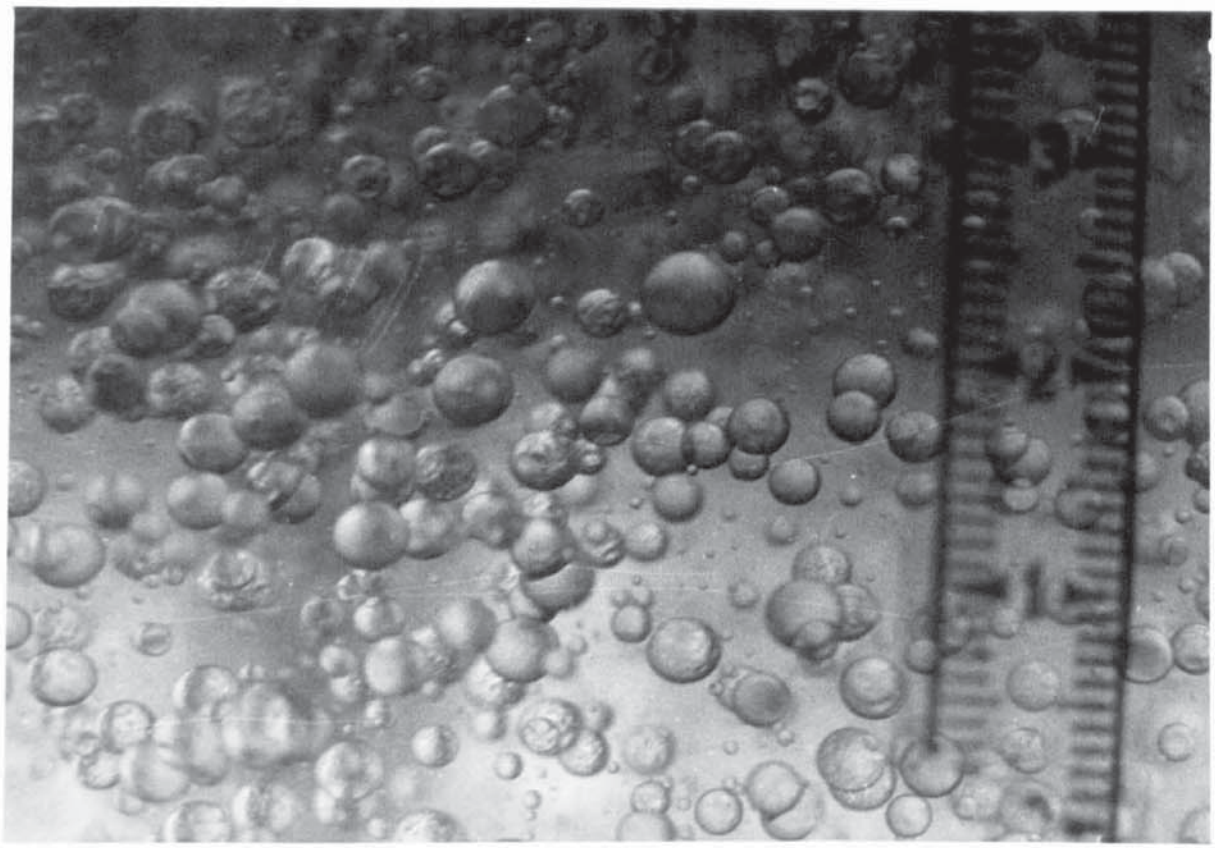

Figure 7.9 Typical droplet dispersion

U_c = 0.30 cm/s U_d = 0.48 cm/s d_n = 3.175 mm

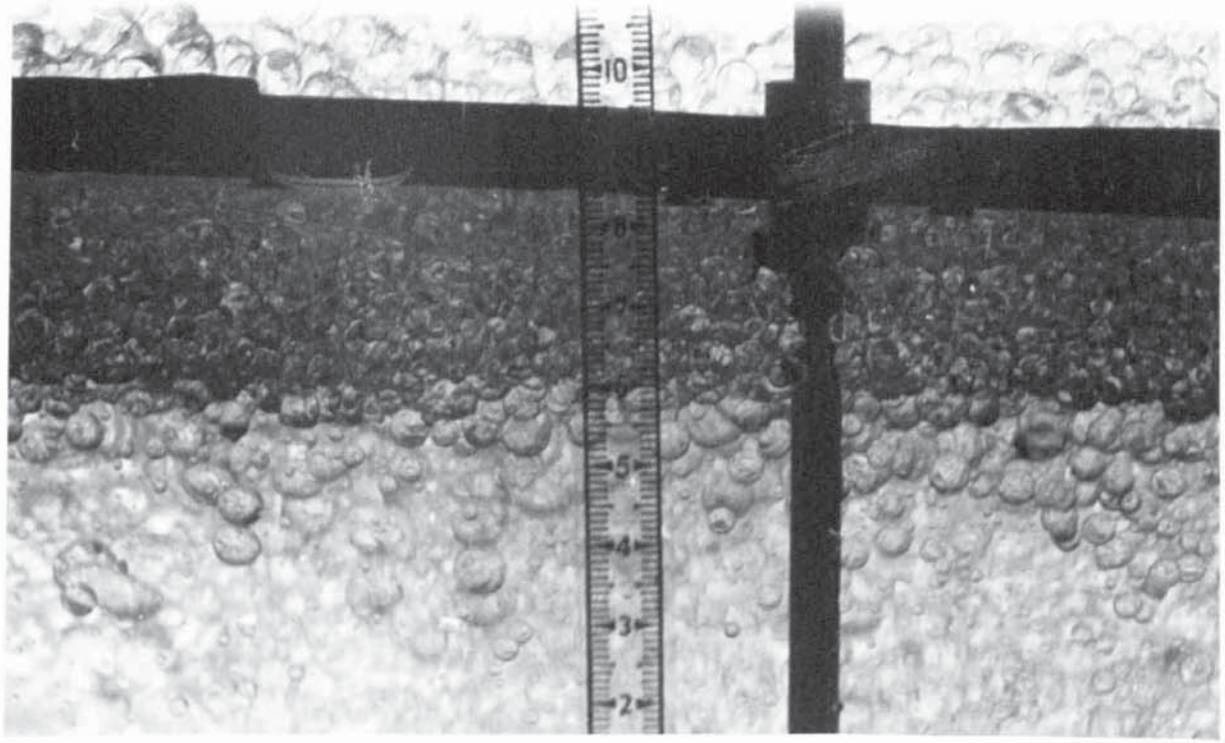

Figure 7.8 Coalsecence /flocculation height beneath the sieve plate

U_c = 0.30 cm/s U_d = 0.48 d_n = 3.175 mm

Table 7.5 Hydrodynamic Results

RUN No	d_n (cm)	U_c (cm/s)	U_d (cm/s)	U_n (cm/s)	H_c (cm)	x%	h_t (cm)	d_{32} (cm)
11	0.6350	0.34	0.36	5.58	34	0.71	1.50	0.464
12	0.6350	0.34	0.43	6.30	34	1.10	1.63	0.534
13	0.6350	0.34	0.52	6.81	34	1.40	2.13	0.423
14	0.6350	0.34	0.65	8.56	34	1.70	2.50	0.491
15	0.6350	0.58	0.36	5.58	34	0.80	2.05	0.537
16	0.6350	0.58	0.43	6.30	34	1.00	2.15	0.438
17	0.6350	0.58	0.52	6.81	34	1.50	2.50	0.441
18	0.6350	0.58	0.65	8.56	34	2.10	2.63	0.425
25	0.6350	0.34	0.36	5.58	30	0.55	1.39	0.512
26	0.6350	0.34	0.43	6.30	30	0.83	1.763	0.543
27	0.6350	0.34	0.52	6.81	30	1.10	1.78	0.491
28	0.6350	0.58	0.65	8.56	30	1.45	1.98	0.478
29	0.6350	0.58	0.36	5.58	30	0.61	1.41	0.425
30	0.6350	0.58	0.43	6.30	30	0.92	1.67	0.429
31	0.6350	0.58	0.52	6.81	30	1.21	1.96	0.459
32	0.6350	0.58	0.65	8.56	30	1.64	1.92	0.415
E1	0.6350	0.34	0.13	1.66	30	0.21	0.52	-
E2	0.6350	0.34	0.27	3.49	30	0.60	1.10	-
40	0.6350	0.34	0.27	5.58	30	0.60	1.24	0.579
41	0.6350	0.34	0.43	6.30	26	1.96	1.69	0.524
42	0.6350	0.34	0.52	6.81	26	2.51	1.85	0.561
43	0.6350	0.47	0.27	4.54	26	1.29	1.37	0.542
44	0.6350	0.47	0.36	5.58	26	1.34	1.61	0.578
45	0.6350	0.47	0.43	6.30	26	2.39	1.65	0.575

Table 7.5 Continued/...

RUN No	d_n (cm)	U_c (cm/s)	U_d (cm/s)	U_n (cm/s)	H_c (cm)	x%	h_t (cm)	d_{32} (cm)
46	0.6350	0.47	0.52	6.81	26	2.94	1.90	0.518
47	0.6350	0.58	0.27	4.54	26	1.33	1.30	0.630
48	0.6350	0.58	0.36	5.58	26	1.46	1.52	0.605
49	0.6350	0.58	0.43	6.30	26	2.63	1.88	0.527
50	0.6350	0.58	0.52	6.81	26	3.08	1.88	0.501
59	0.3175	0.30	0.31	6.45	34	2.54	2.27	0.601
60	0.3175	0.30	0.36	8.07	34	3.18	2.40	0.551
61	0.3175	0.30	0.43	8.77	34	5.71	2.62	0.488
62	0.3175	0.30	0.48	9.79	34	6.66	2.83	0.611
63	0.3175	0.55	0.31	6.45	34	1.90	2.67	0.599
64	0.3175	0.55	0.36	8.07	34	2.86	2.68	0.670
65	0.3175	0.55	0.43	8.77	34	6.03	2.96	0.587
66	0.3175	0.55	0.48	9.79	34	7.12	3.13	0.497
73	0.3175	0.30	0.31	6.45	30	3.12	2.31	0.591
74	0.3175	0.30	0.36	8.07	30	4.23	2.33	0.588
75	0.3175	0.30	0.43	8.77	30	5.40	2.45	0.548
76	0.3175	0.30	0.48	9.79	30	6.57	2.81	0.502
77	0.3175	0.55	0.31	6.45	30	3.64	2.46	0.601
78	0.3175	0.55	0.36	8.07	30	4.96	2.53	0.538
79	0.3175	0.55	0.43	9.79	30	6.07	2.91	0.543
80	0.3175	0.55	0.48	8.79	30	7.62	3.18	0.520
85	0.3175	0.30	0.31	6.45	26	2.49	2.16	0.583
86	0.3175	0.30	0.36	8.07	26	3.06	2.32	0.504

Table 7.5 Continued/...

RUN No	d_n (cm)	U_c (cm/s)	U_d (cm/s)	U_n (cm/s)	H_c (cm)	x%	h_t (cm)	d_{32} (cm)
87	0.3175	0.30	0.43	8.77	26	5.43	2.68	0.493
88	0.3175	0.30	0.48	9.79	26	6.53	2.80	0.583
89	0.3175	0.55	0.31	6.45	26	2.03	2.55	0.526
90	0.3175	0.55	0.36	8.07	26	2.74	2.62	0.543
91	0.3175	0.55	0.43	8.77	26	5.89	2.98	0.593
92	0.3175	0.55	0.48	9.79	20	7.04	3.04	0.572
97	0.3175	0.30	0.31	6.45	20	2.86	2.07	0.408
98	0.3175	0.30	0.36	8.07	20	3.97	2.28	0.635
99	0.3175	0.30	0.43	8.77	20	5.43	2.48	0.437
100	0.3175	0.30	0.48	9.79	20	6.76	2.62	0.465
101	0.3175	0.55	0.31	6.45	20	2.77	2.59	0.465
102	0.3175	0.55	0.36	8.07	20	4.86	2.70	0.572
103	0.3175	0.55	0.43	8.77	20	5.92	2.87	0.469
104	0.3175	0.55	0.48	9.79	20	7.54	2.92	0.555

$$\frac{h_t}{d_n} = 1.86 \times 10^5 \left[\frac{U_n^2 \rho_c d_n}{\sigma}\right]^{0.45} \left[\frac{U_c^2 \rho_c d_n}{\sigma}\right]^{0.14} \left[\frac{g \rho_c d_n^2}{\sigma}\right]^{-0.83} \left[\frac{\Delta\rho}{\rho_c}\right]^{2.64} \left[\frac{\mu_d^2}{\rho_c d_n \sigma}\right]^{0.28} \quad \text{.... 7.9}$$

The derivation of this dimensionless relationship is given in Appendix 2. Equation 7.9 correlated the results with an average error of ± 9.9%. (The average % error $\gamma = 100/N \sum$ (pred-Expt)/Expt) and a correlation coefficient of $R^2 = 0.9$, $R^2 = 1$ being the perfect fit (Section 7.1). The experimental and predicted results are given in Table U2, and the results are plotted in Figure 7.12. The range of physical properties from which equation 7.9 was derived are: ρ_c 998.2 - 1000 kg/m^3; ρ_d 783 - 890 kg/m^3; μ_c 0.0011 - 0.0136 kg/ms; μ_d 0.0018 - 0.0037 kg/ms; σ 25.3 - 35.5 mN/m; Δ_ρ 110-217 kg/m^3 and clearly its use is restricted to within these ranges. However, this correlation is Weighted by small column data where h_t/D_n is small, and omits μ_c from which the range was small anyway.

The value of the coefficient on each dimensionless group (a combination of variables) shows how significant it is,ie the higher the coefficient the more influence it has. The ratio of $\Delta\rho/\rho_c$, which is the ratio of the buoyant forces, which depends upon the density difference of the phases is the most significant group in equation 7.9.

The coalescence height, h_t, represents the minimum theoretical height of the downcomer necessary to avoid by-passing of the dispersed phase. Experimental h_t values did not exceed 2.6 cm for the 6.35 hole size plate and 3.04 cm for the 3.175 mm plate hole size. However as is clear from equation 7.9, different values would be expected for other systems, since it is determined by the drop formation and coalescence characteristics of the dispersed phase and hence the physical properties in equation 7.5. h_t can also be used to assess the static hold-up and hence the minimum amount of solvent required to operate an SPC. Naturally h_t increases rapidly as the flooding velocities are approached.

7.2.4 Dropsize and Size Distribution in Column.

Various statistical distribution functions have been proposed to represent the dropsize data in extractors [135]. Four functions were considered most likely to represent those in the SPC because of the way in which drops form from the sieve plates. These were the Log-normal, Mugele-Evans or Upper Limit Function, Gal-or and Rosin-Rammler (Table 4.1). To fit these functions to the experimental data normally involves the estimation of 2 parameters which define them, but 3 parameters are required to be estimated for the Mugele-Evans function.

The existence of a maximum dropsize in extraction columns led to the modification of the Log-normal distribution function by Mugele and Evans [198], whose distribution function is specified with the three parameters , d_m, σ and a'. The parameter d_m can be considered as the maximum dropsize in the dispersion, but is normally adjusted to improve the accuracy of the representation of the data. The index σ determines the spread of the distribution, a smaller value indicating a wider range of drops sizes. a' is the skewness parameter; a value of a' greater than unity indicates a wider range of drop sizes larger than d_{50}.

The general procedure to derive the functions was to determine the parameters such as d_{10}, d_{50}, $d_{84.14}$, d_{90}, a', σ, d_m, y_v directly from the data or from the plot of drop sizes against the cumulative percentage on a probability scale,as demonstrated in Appendix 5 and illustrated on the log-probability paper in Appendix 5. y_v and σ (Rosin-Rammler) were determined from a plot on Rosin-Rammler paper. A sample calculation of drop distribution parameters is given in Appendix 9 and a computer program for the calculation of drop distribution data from photographs counted on the Carl Zeiss TG3 particle size analyser is given in Appendix 6. Figure 7.15 illustrates the fitting of typical experimental data to these drop size distribution functions. The Rosin-Rammler function was out of range and was disregarded. The parameters for the 4 distribution functions for 108 experimental data points are given in Table U3.

Droplets ranging from 0.7 to 9.5 mm were observed in the absence of mass

transfer, as exemplified in Figure 7.9. Larger drops in the range 1.52 to 12.6 mm were subsequently observed with mass transfer (d to c), but only about 3-8% of the drops in any particular population were stagnant.< 1mm . These were satellite drops caused by the breakage of larger drops due to collision with each other or from jet disruption at high dispersed phase flowrates. Coalescence of the drops also occurred, leading to larger drops. These larger drops ie>10mm, although small in number, ie < 5% of the population, contributed substantially to the experimental mean diameter.

An undesirable feature of operation was the swarming of drops via a central core of the column resulting in poorly-contacted, continuous phase passage around the periphery, and recirculation of this swarm , ie dispersed phase . This feature illustrated in Figure 7.10 and 7.11 was found to decrease as the plate spacing was reduced in the range 38 cm to 20 cm. At 20 cm this recirculation pattern was completely eliminated.

The drop size spectrum tended to widen with an increase in dispersed phase flowrate, with the generation of smaller drops, as exemplified in Figure 7.15. The ratio of d_{32}/d_{50} (Table 7.6) ranged from 0.91 -0.98, which is within the range to be expected for primary dispersions [198].

Several different mean drop diameters can be defined, on the basis of direct measurement or on the basis of an average volume, mass, or surface area. The one commonly used is the mean-volume surface diameter (Sauter mean diameter) d_{32}. This relates the total surface area of the drops to the total volume, and is expressed mathematically by

$$d_{32} = \frac{\Sigma n_i d_i^3}{\Sigma n_i d_i^2} \qquad \ldots. 2.5$$

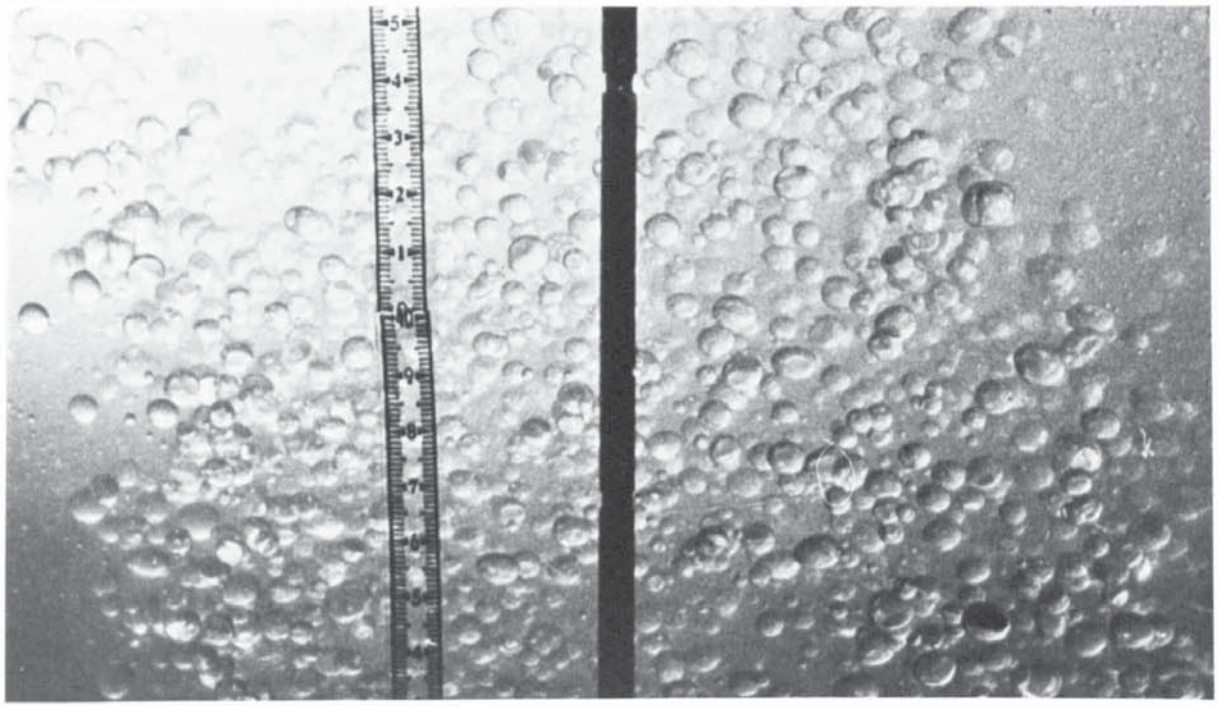

Figure 7.11 **Droplet Swarm Flow patterns**

(b) plate spacing 300 mm - reduce d circulation

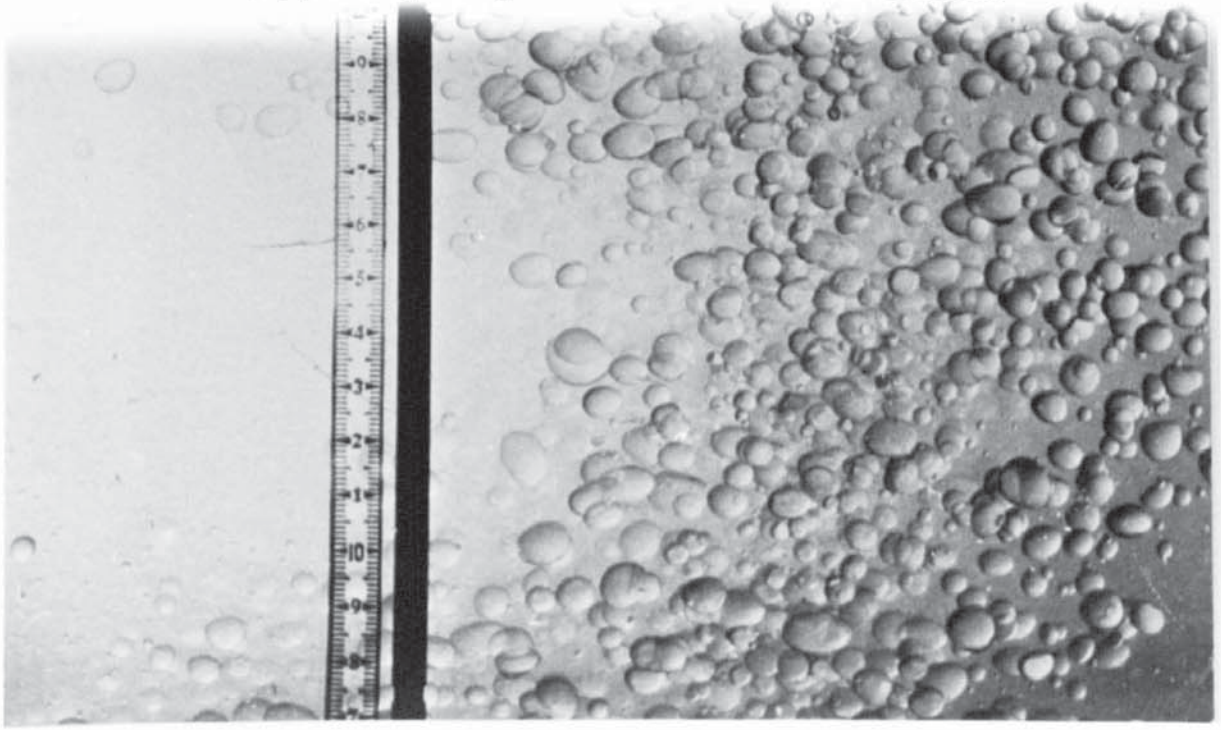

Figure 7.10 **Droplet Swarm Flow Patterns**

(a) plate spacing = 380 m - showing swarm recirculation

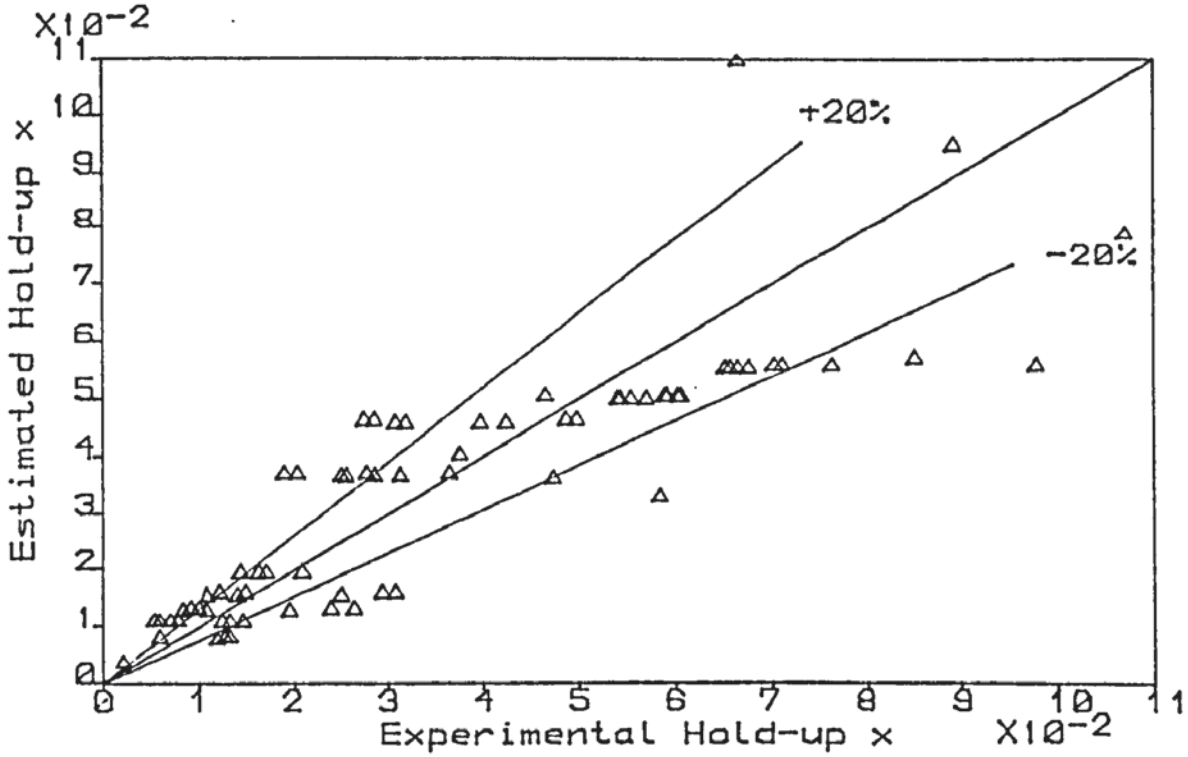

Fig.7.13 Comparison Of Experimental and Calculated Values Of Hold-up

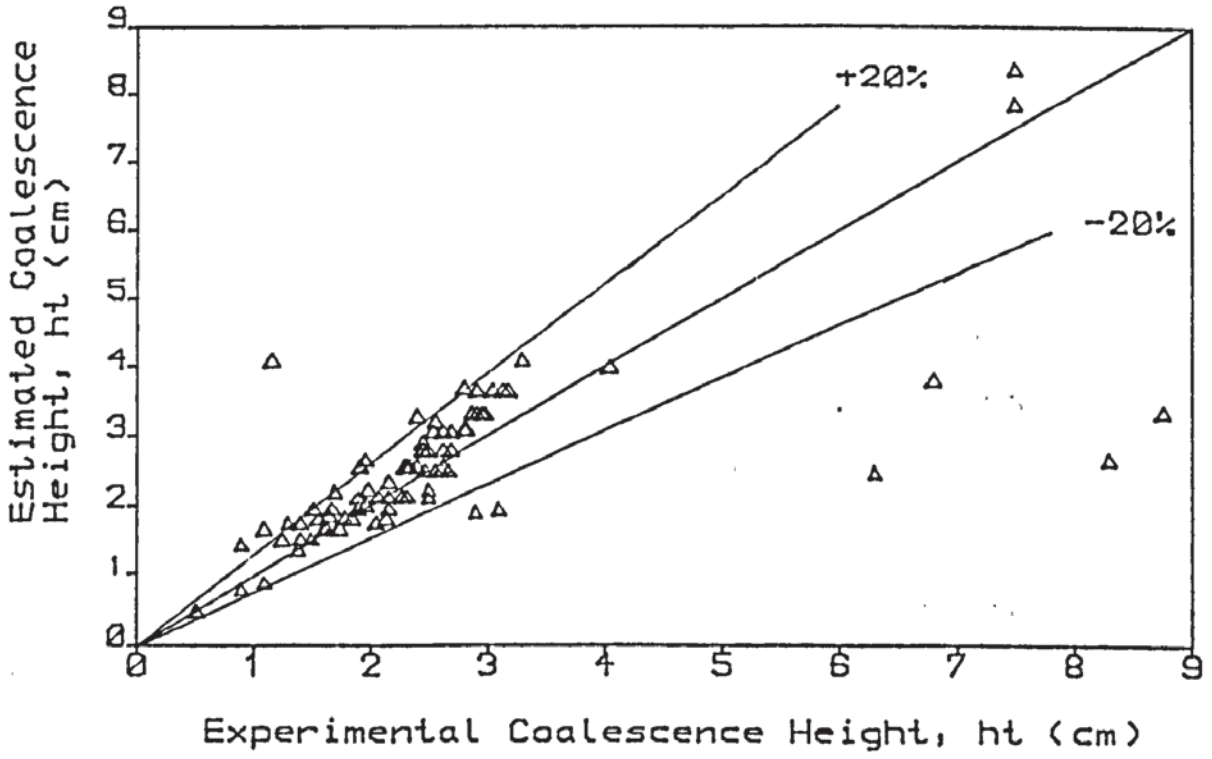

Fig.7.12 Comparison Of Experimental and Calculated Values Of Coalescence Height, ht(cm)

Table 7.6 Distribution Parameters in the SPC for the 6.35mm Hole Size Plate

Function	Distribution parameters			
Log-normal	d_{gm}	δ		
	4.4–7.2	2.9–3.5		
Mugele- Evans (198)	δ	a'	d_m	d_{32}/d_{50}
	1.01-2.76	0.8-8.0	9.1-96.0	0.91-0.98
Gal-or and Hoescher (70)	δ			
	0.04 - 0.12			
Rosin-Rammler (239)	δ	y_v		
	4.0-7.2	5.0-7.8		

$$a = \frac{6x}{d_{32}} \qquad \text{.... 2.6}$$

Moreover, it is appropriate because mass transfer is interfacial area controlled. The interfacial area calculated from equation 2.6 is the specific interfacial area, ie the total contact area per unit volume of the extractor, m^2/m^3.

The Sauter mean diameters calculated by each of the distribution functions given earlier were compared to those obtained experimentally. The results are shown in Table U3 and illustrated in Figure 7.16. The Log-normal shows a deviation of ±25%, Mugele-Evans ±15.6% and Gal-or ±2.8%. The inadequacy of the Log-normal distribution function, and the deviation of its d_{32} from experimental values, are clearly demonstrated in Figure 7.16. The Mugele-Evans and Gal-or functions give a reasonable representation of the experimental data.

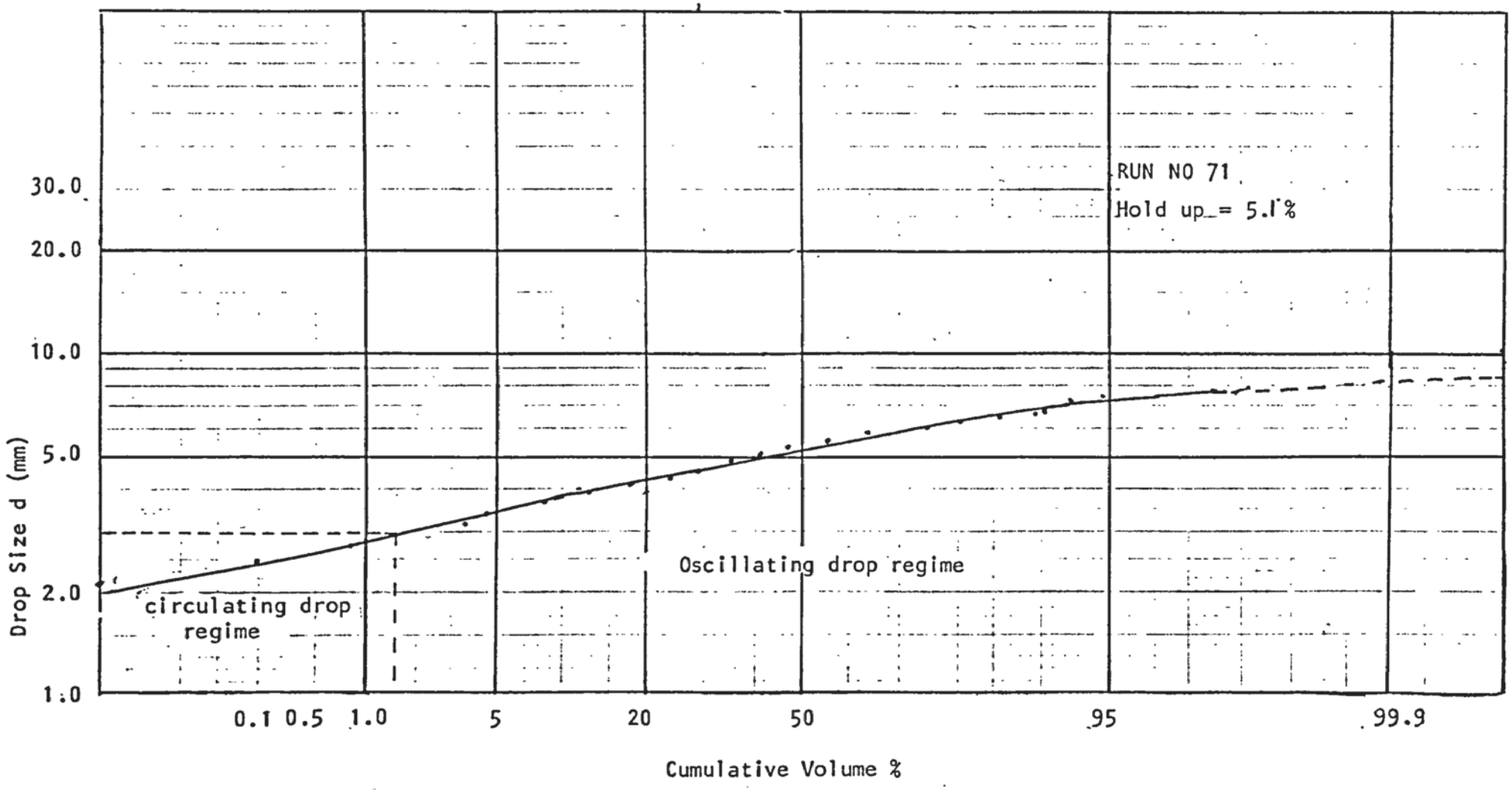

Fig 7.14 Typical drop size distribution

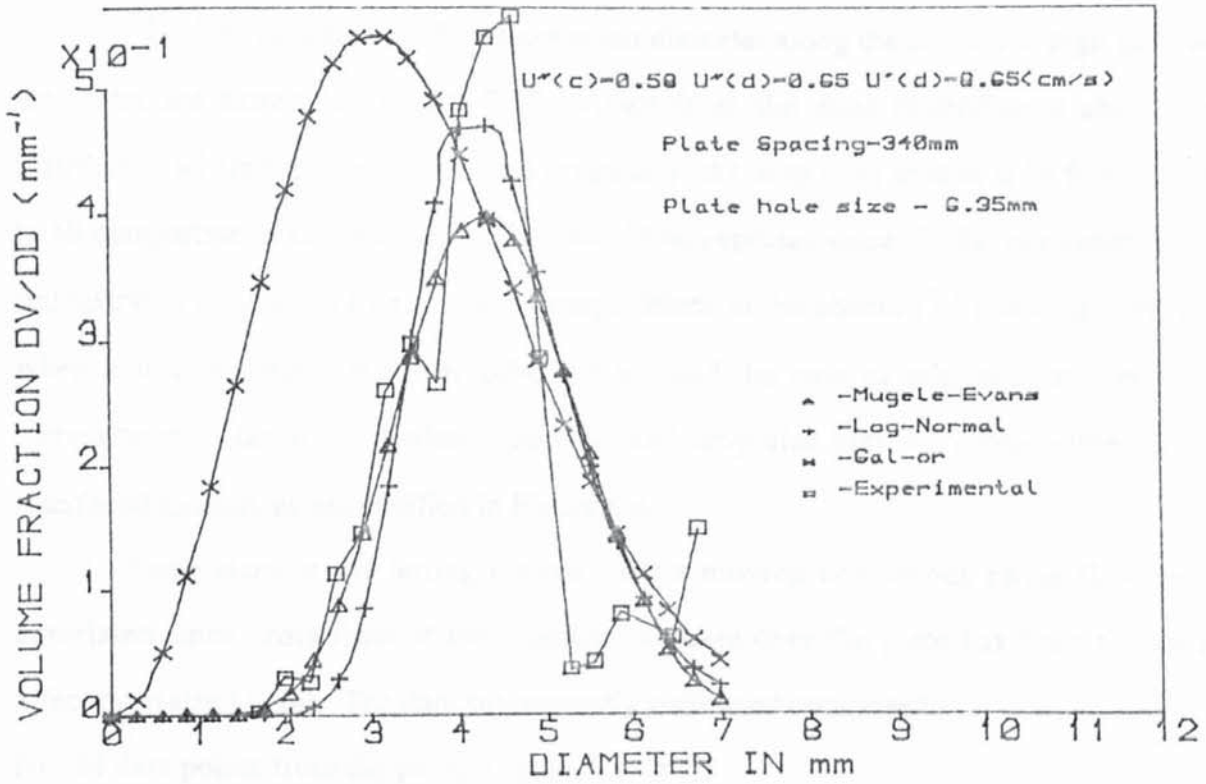

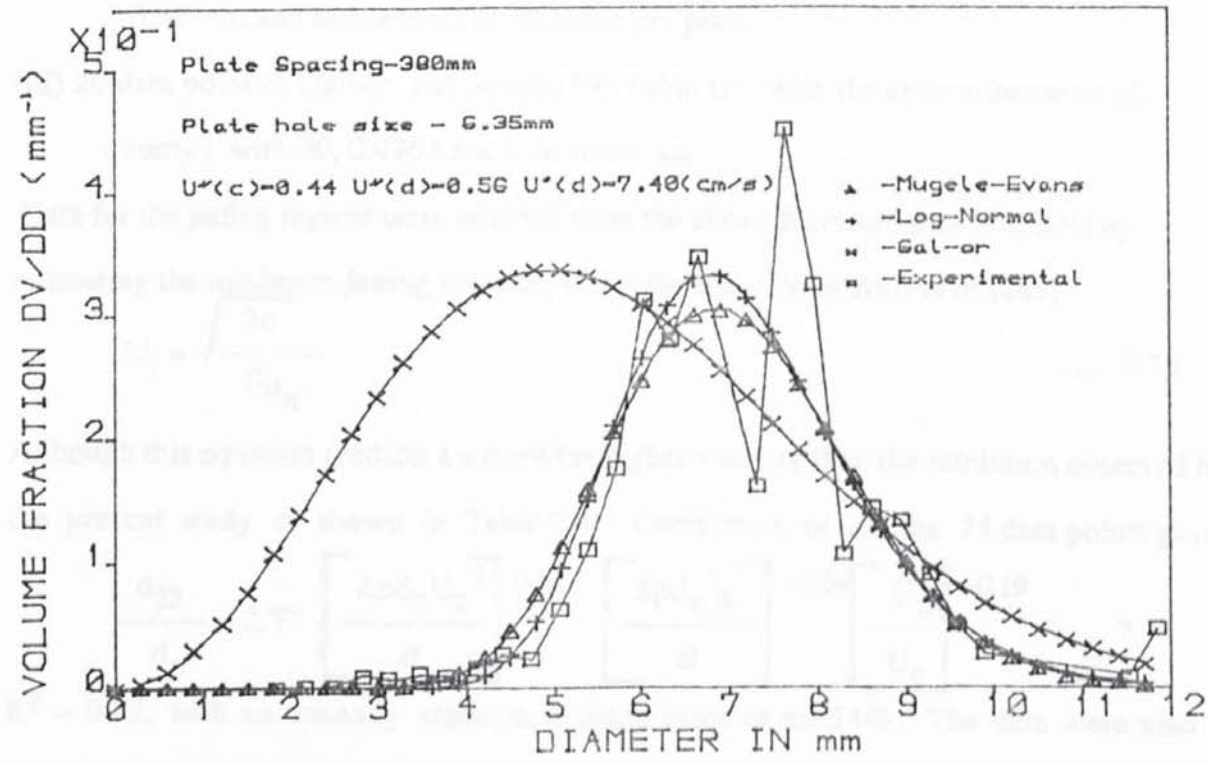

Fig.7.15 Experimental and Theoretical distribution functions curves

Typical variations of the Sauter mean diameter along the column at high and low flowrates are shown in Figure 7.17. Apart from the zone immediately above the distributor, where the holes functioned irregularly, the drop sizes tended to be fairly stable in all compartments of the column. This would be expected since similar coalescence and redispersion conditions exist in each compartment in the absence of mass transfer, but when solute is present the interfacial tension and the ease of coalescence vary with compartment. Hence the coalescence zone and drop size may vary depending on the interfacial tension, as exemplified in Figure 6.6

Drop sizes in the jetting regime with a moving continuous phase flow were correlated since cross-flow of the continuous phase over the plate has been shown to affect drop size [132a]. The data subsequently correlated comprised:

(i) 34 data points from the present study, Table 7.5.

(ii) 20 data points of Vedaiyan *et al* [301] Table U4, with the system: benzene (d) - water (c), Mibk (d) - water(c) and water(d) - CCl_4(c), plate hole sizes between 0.20 and 0.37 cm and between 12 to 20 holes per plate.

(iii) 20 data point of Garwin and Smith [79] Table U4, with the system benzene (d) - water(c) with 20, 0.4763 cm hole size plate.

Data for the jetting regime were selected from the above literature data [79, 301] by estimating the minimum jetting velocity, U_j by the equation of Ruff *et al* [245]

$$U_j = \sqrt{\frac{2\sigma}{\rho d_n}} \qquad \text{.... 7.10}$$

Although this equation predicts a somewhat higher velocity than the minimum observed in the present study as shown in Table 7.4. Correlation of all the 74 data points gave

$$\frac{d_{32}}{d_n} = 2.77 \left[\frac{\Delta\rho d_n U_n^2}{\sigma}\right]^{0.19} \left[\frac{\Delta\rho d_n^2 g}{\sigma}\right]^{-0.34} \left[\frac{U_n}{U_c}\right]^{-0.19} \qquad \text{.... 7.11}$$

$R^2 = 0.82$, with an unsually accurate average error of ±0.54%. The data were also correlated in the form proposed by Kumar and Hartland [152], omitting U_c (ie without the effect of crossflow) to give;

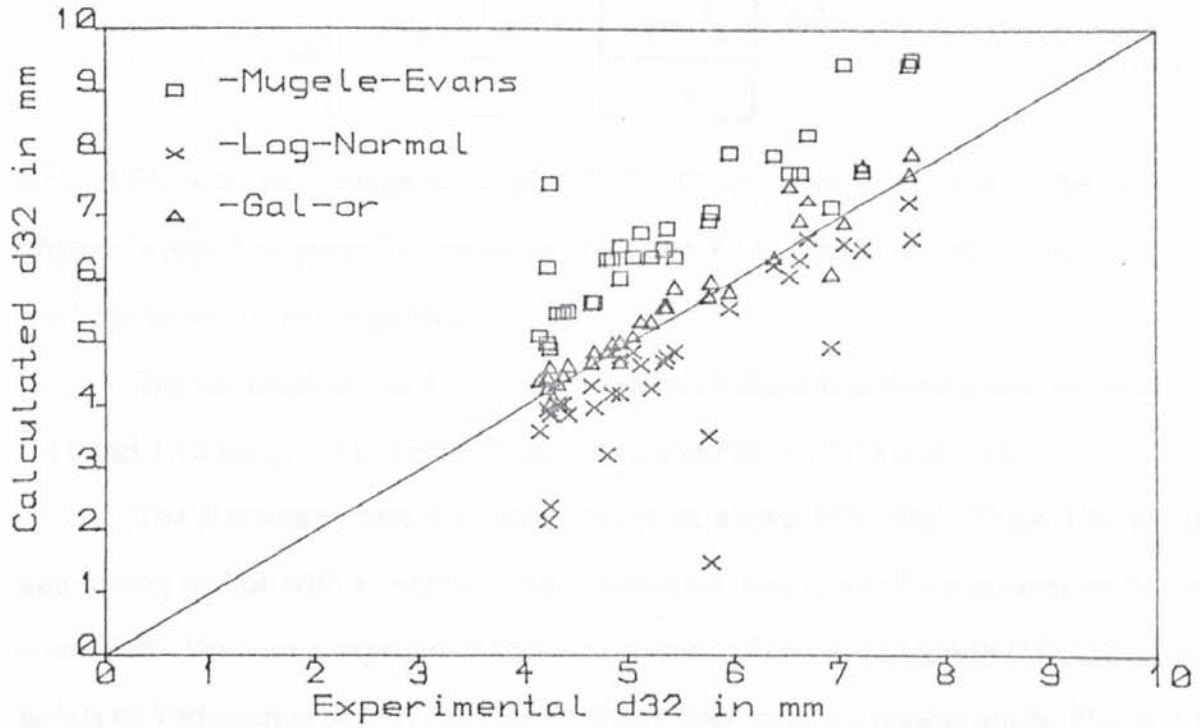

Fig.7.16 Comparison of experimental and calculated values of d32

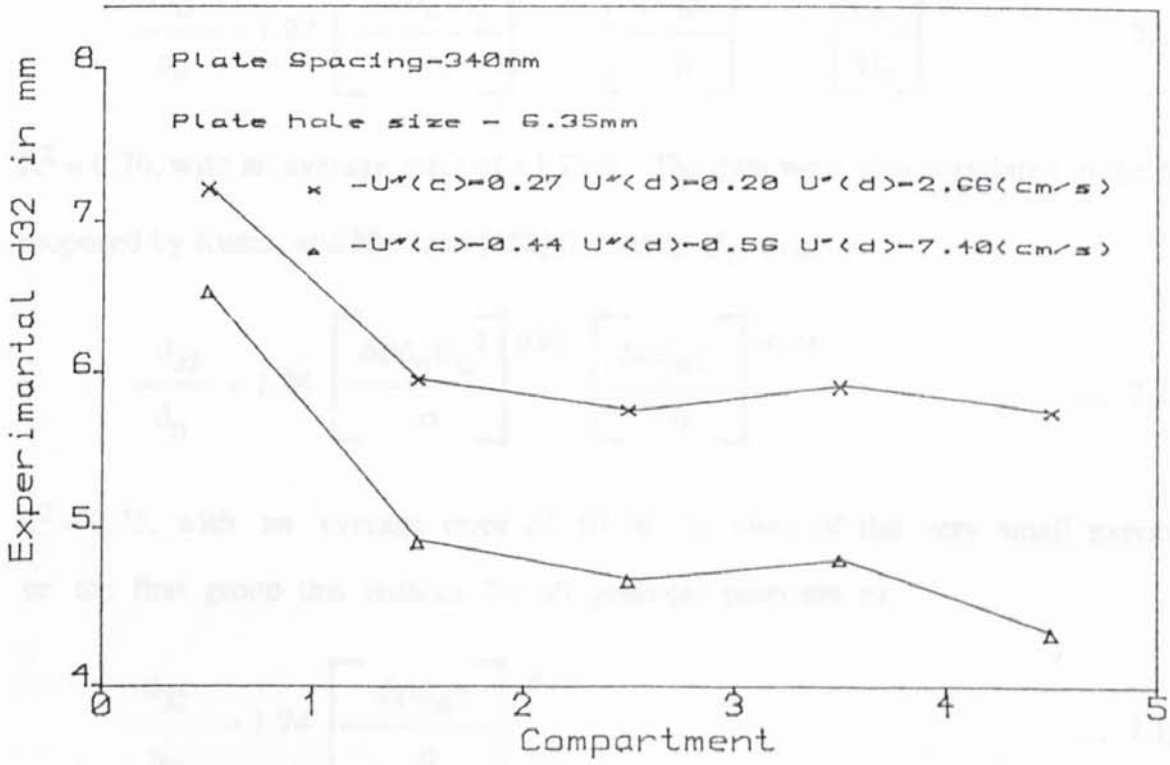

Fig.7.17 Drop size profile along the column

$$\frac{d_{32}}{d_n} = 1.46 \left[\frac{\Delta\rho d_n U_n^2}{\sigma}\right]^{0.11} \left[\frac{\Delta\rho d_n^2 g}{\sigma}\right]^{-0.31} \quad \text{.... 7.12}$$

$R^2 = 0.74$, with an average error of 2.52%. Clearly this is limited to the range of physical properties given for equations 7.13 and 7.14 The effect of μ_d and μ_c on d_{32} has been proved to be insignificant [132].

The experimental and calculated values of the correlations given by equations 7.11 and 7.12 are given in Table U5 and shown in Figures 7.18 and 7.19.

The literature from the same source as above [79, 301], Table U6, for the non-jetting regime with a moving continuous phase, and those of the present study were combined. The data comprised the 45 data points of Garwin and Smith [79], the 10 data points of Vedaiyan *et al* [301] and the 21 data points from the present study, [Table 7.5] These were subsequently correlated to give;

$$\frac{d_{32}}{d_n} = 1.97 \left[\frac{\Delta\rho d_n U_n^2}{\sigma}\right]^{0.08} \left[\frac{\Delta\rho d_n g}{\sigma}\right]^{-0.43} \left[\frac{U_n}{U_c}\right]^{-0.04} \quad \text{.... 7.13}$$

$R^2 = 0.76$, with an average error of ±1.22%. The data were also correlated in the form proposed by Kumar and Hartland [152] (omitting U_c) to give;

$$\frac{d_{32}}{d_n} = 1.74 \left[\frac{\Delta\rho d_n U_n^2}{\sigma}\right]^{0.07} \left[\frac{\Delta\rho d_n g}{\sigma}\right]^{-0.44} \quad \text{.... 7.14}$$

$R^2 = 0.75$, with an average error of ±0.58. In view of the very small exponent on the first group this reduces for all practical purposes to

$$\frac{d_{32}}{d_n} = 1.74 \left[\frac{\Delta\rho d_n g}{\sigma}\right]^{-0.44} \quad \text{.... 7.15}$$

The range of physical properties from which equations 7.11 to 7.14 were derived were:

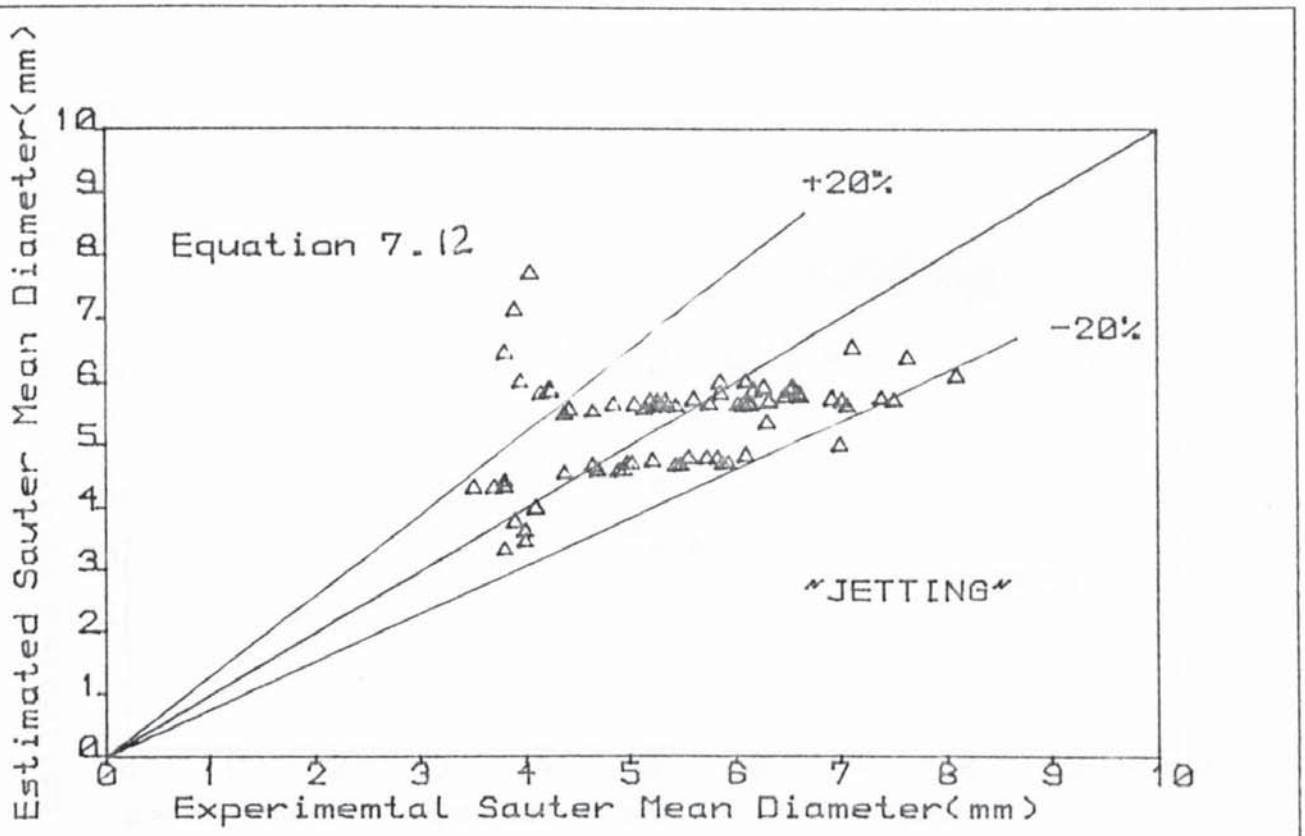

Fig.7.19 Comparison Of Experimental and Calculated Values of Sauter Mean Diameter

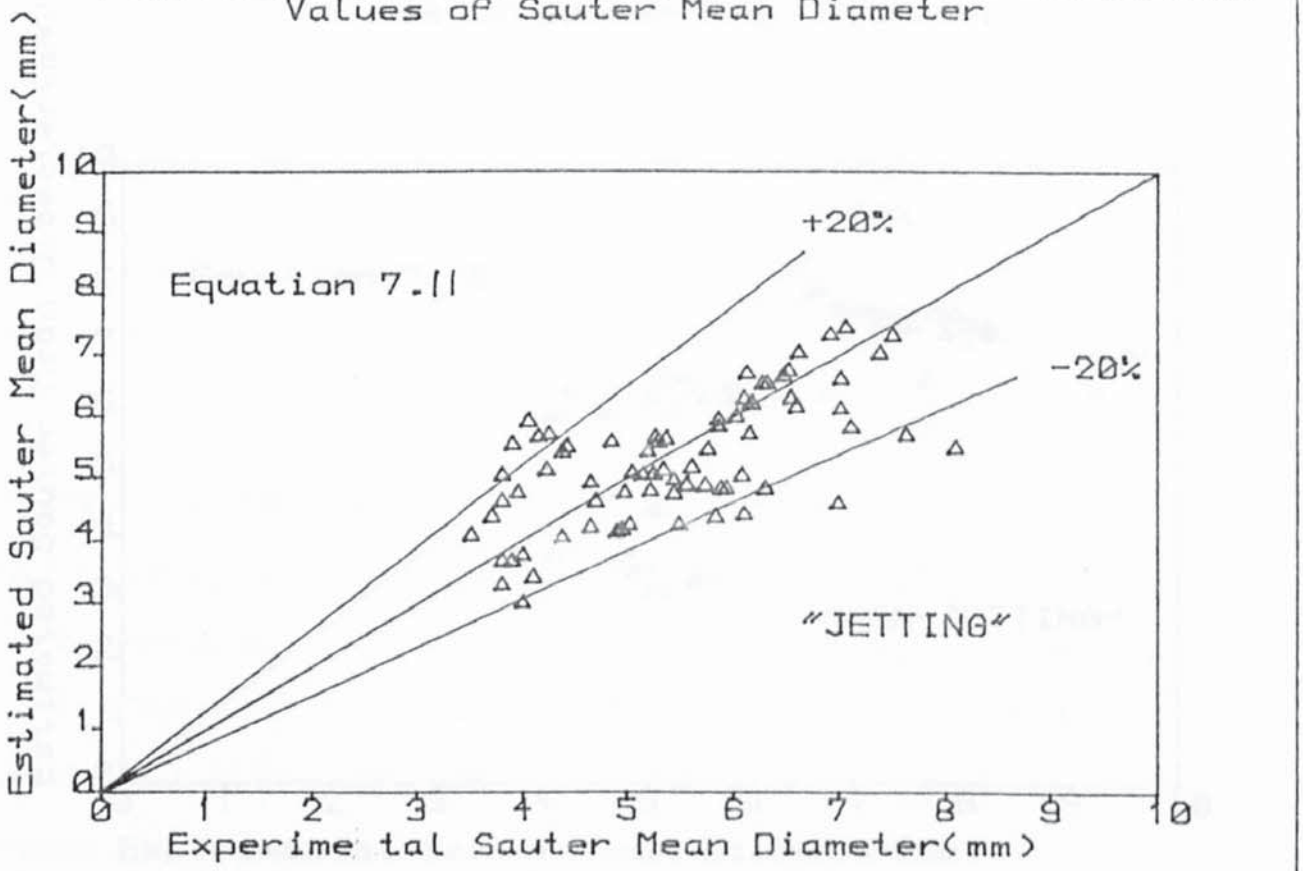

Fig.7.18 Comparison Of Experimental and Calculated Values of Sauter Mean Diameter

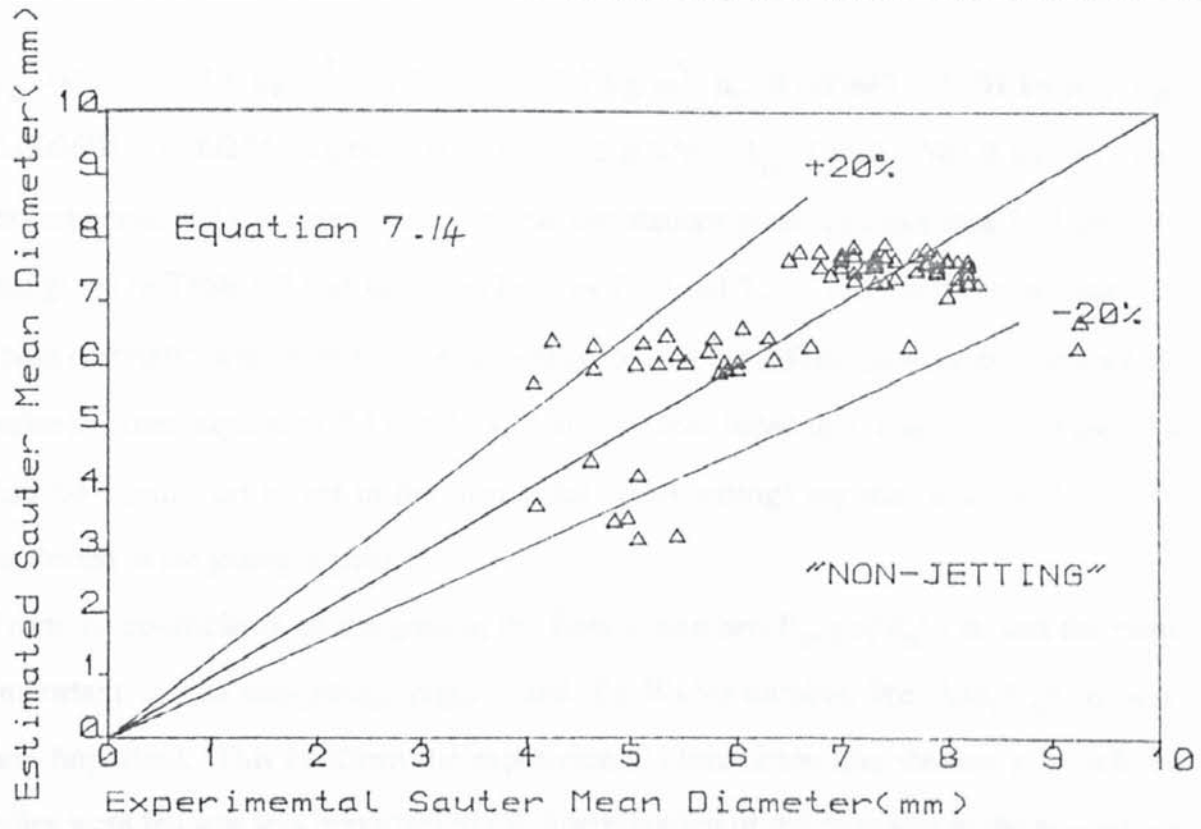

Fig.7.21 Comparison Of Experimental and Calculated Values of Sauter Mean Diameter

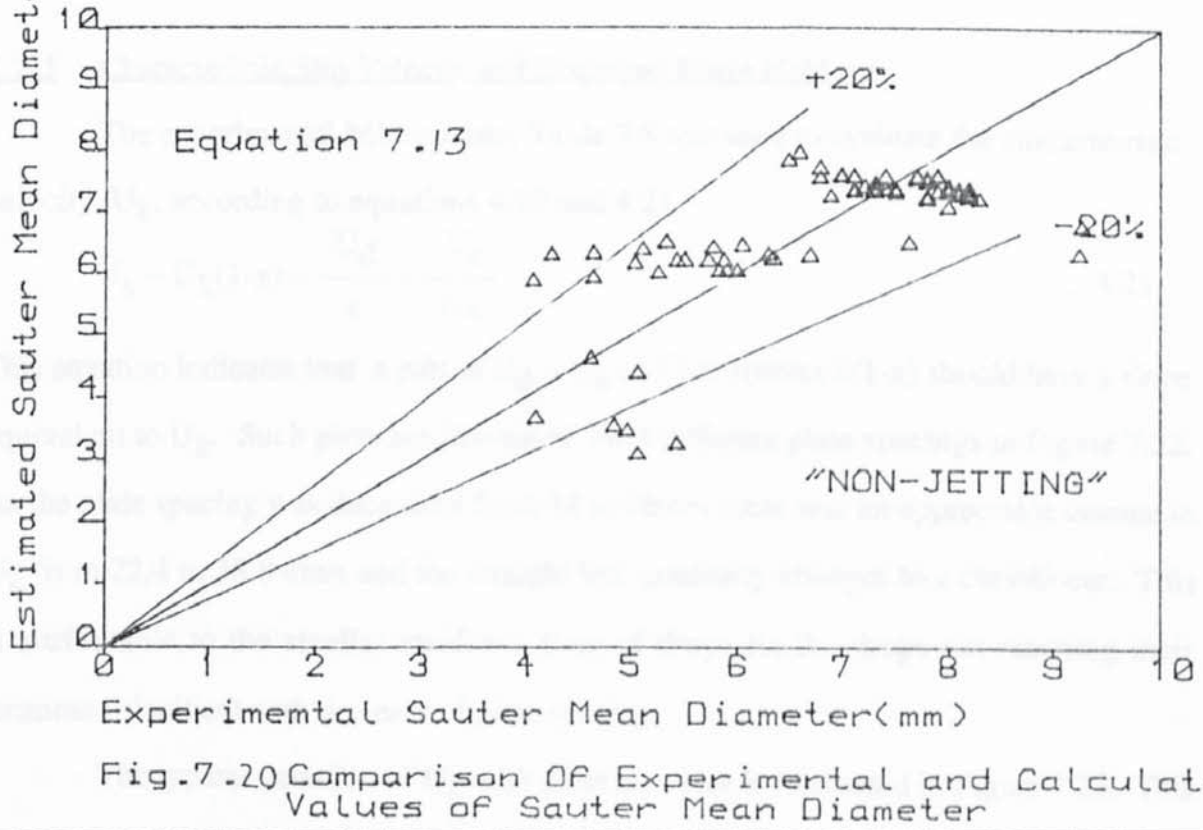

Fig.7.20 Comparison Of Experimental and Calculated Values of Sauter Mean Diameter

ρ_c 995.6 - 1582.6 kg/m^3; ρ_d 795.4 - 997.7 kg/m^3; μ_c 0.000849 - 0.001 kg/ms; μ_d 0.000605 - 0.002746 kg/ms; σ 4.9 - 42.2 mN/m; Δ_ρ 196.2 - 584.9 kg/m^3. The experimental and calculated values of the correlations given by Equations 7.13 and 7.14 are given in Table U7 and shown in Figures 7.20 and 7.21. (The apparent accuracy of these correlations is unusual since, generally, only some 300 drops were counted per d_{32} value). From equations 7.11 to 7.14, it may be concluded that continuous phase flow had no significant effect in the drip-point (non-jetting) regime but should not be neglected in the jetting regime.

From the coefficients on the groups, the Eotvos number, E_o, $g\Delta\rho d_n^2 / \sigma$, was the most important in the non-jetting regime and the Weber number, We, $\Delta\rho d_n U_n^2 / \sigma$, was less important. This confirms the experimental observation that the rate at which the holes were fed was less important in the determination of the drop size in the non-jetting regime ie the rate at which a drop grew at a hole had no great bearing on the size attained before drip-point release.

7.2.5 Characteristic/Slip Velocity and Dispersed Phase Hold-up

The experimental hold-up data, Table 7.5 was used to evaluate the characteristic velocity, U_k, according to equations 4.20 and 4.21

$$U_s = U_k(1-x) = \frac{U_d}{x} + \frac{U_c}{1-x} \qquad \text{.... 4.21}$$

This equation indicates that a plot of $U_d + U_c$ (x / 1-x)versus x(1-x) should have a slope equivalent to U_k. Such plots are illustrated for 4 different plate spacings in Figure 7.22. As the plate spacing was decreased from 38 to 26 cm there was an appreciable change in U_k from 22.4 to 38.8 cm/s and the straight line gradually changes to a curvilinear. This is attributable to the smaller residence time of drops (ie the drops not reaching their terminal velocities) with decrease of plate spacing.

The typical variation of U_k with plate hole size is illustrated in Figure 7.23. This shows an increase in U_k with increased plate hole size, since U_k is affected by dropsize,

varies with the plate hole size and dispersed phase hole velocity, U_n. As the hole size increases, so does the mean drop size, resulting in higher rise velocity and reduced residence time of the drops.

The 61 hold-up data points of this study, Table 7.5 were combined with the 9 data points of Prabhu *et al* [222], Table U8, obtained from a 5 cm diameter column with 42, 0.16 cm hole size plates using the systems: water (c) and kerosene, toluene and isoamyl alcohol (d). The 70 data points were correlated by multiple regression analysis, to give;

$$x = 3.66 \times 10^{-2} \left[\frac{\Delta\rho}{\rho_c}\right]^{-0.15} \left[\frac{U_d}{U_c}\right]^{-0.02} \left[\frac{U_n^2 \rho_c d_n}{\sigma}\right]^{0.77} \left[\frac{U_n^2}{d_n g}\right]^{-0.27} \quad \ldots. 7.16$$

$R^2 = 0.81$, and with an average error of ±9%. The range of physical properties for which equation 7.15 was derived are: ρ_c 992.9 - 1000 kg/m^3; ρ_d 781.4 - 862 kg/m^3; μ_c 0.0008067 - 0.0011 kg/ms; μ_d 0.000657 - 0.0031 kg/ms; σ 5.20 - 35.5 mN/m; $\Delta\rho$ 138 - 214.2 kg/m^3.

The experimental and predicted values using equation 7.15 are given in Table U9 and shown in Figure 7.13. All the data were in the absence of mass transfer since any specific solute will affect the system physical properties differently. In real systems, allowance has to be made for the presence of solutes, by using the appropriate physical property for the solute concentration range. e.g. the variation of interfacial tension with solute concentration in this work is illustrated in Figure 6.6.

The Weber number, $U_n^2 \rho_c d_n / \sigma$, which is the ratio of inertia to interfacial forces is the most important dimensionless group in equation 7.15, followed by the Froude number, $U_n^2 / d_n g$, which is the measure of the inertia to gravitational forces. The group U_d/U_c can be neglected for all practical purposes.

Equal credence was given to data from small diameter columns, but wall effects and inter-plate flow pattern would in fact differ from those in larger columns. Therefore the experimental data from the 0.45 m column should be more reliable.

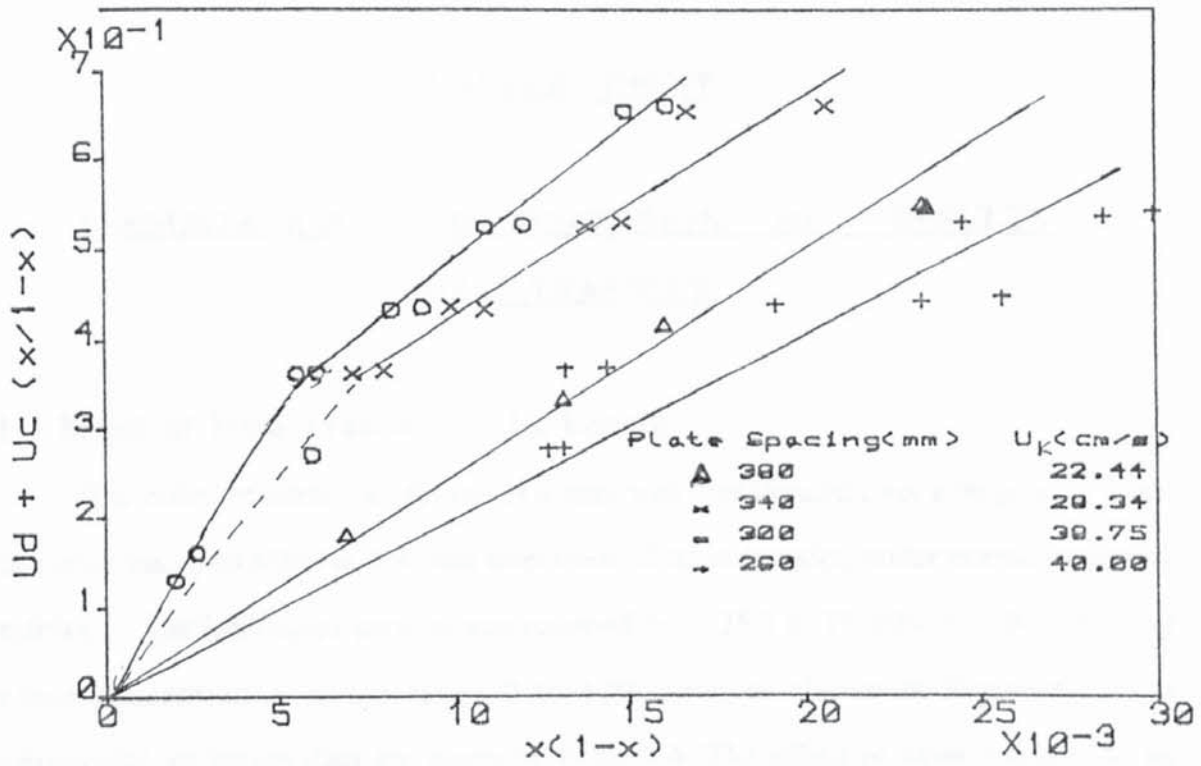

Fig.7.22 Variation of U_K with plate-spacing

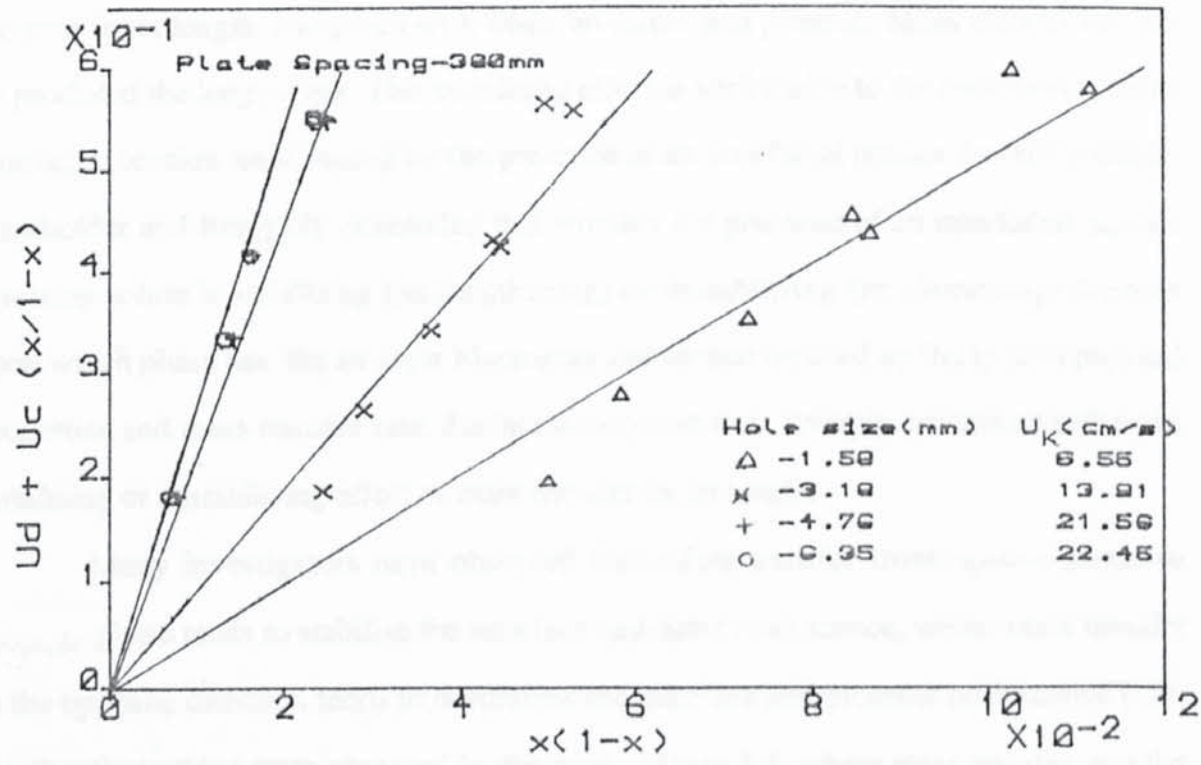

Fig.7.23 Variation of U_K with plate hole-size

CHAPTER EIGHT

PRESENTATION AND DISCUSSION OF RESULTS : MASS TRANSFER

8.1 Effect of Mass Transfer on Jet Length

The effect of mass transfer on jet length was investigated over a range of acetone concentrations up to 8%w/w, for both directions of mass transfer, under normal operating conditions. The interfacial tension was reduced from 35.5 to 18 mN/m with increasing acetone concentration in the range 0 to 10% w/w, as shown in Figure 6.6. The experimental jet length data are given in Table 7.4. The effect of mass transfer on jet length is shown in Figure 8.1.

Mass transfer in either direction tended to stabilise the jets and result in an overall increase in jet length compared with when no solute was present. Mass transfer into the jet produced the longest jets. This stabilising effect is attributable to the reduction in mean interfacial tension level caused by the presence of an interfacial tension lowering solute. Burkholder and Berg[27] concluded that whether the presence of an interfacial tension lowering solute is stabilising (jet lengthening) or destabilising (jet shortening) depends upon which phase has the stronger Marangoni convection dictated by the system physical properties and mass transfer rate. Surface adsorption may strongly counteract either the stabilising or destabilising effect of mass transfer on jet length.

Many investigators have observed that solute transfer from aqueous phase to organic phase tends to stabilise the interface and deter coalescence, whilst mass transfer in the opposite direction tends to destabilise the interface and promote coalescence [12]. Similar phenomena were observed in this work, Figure 8.1, where mass transfer into the jet resulted in greater jet lengths than the corresponding system with mass transfer out of the jet. The initial concentration of solute was <5% in each case so that, given the

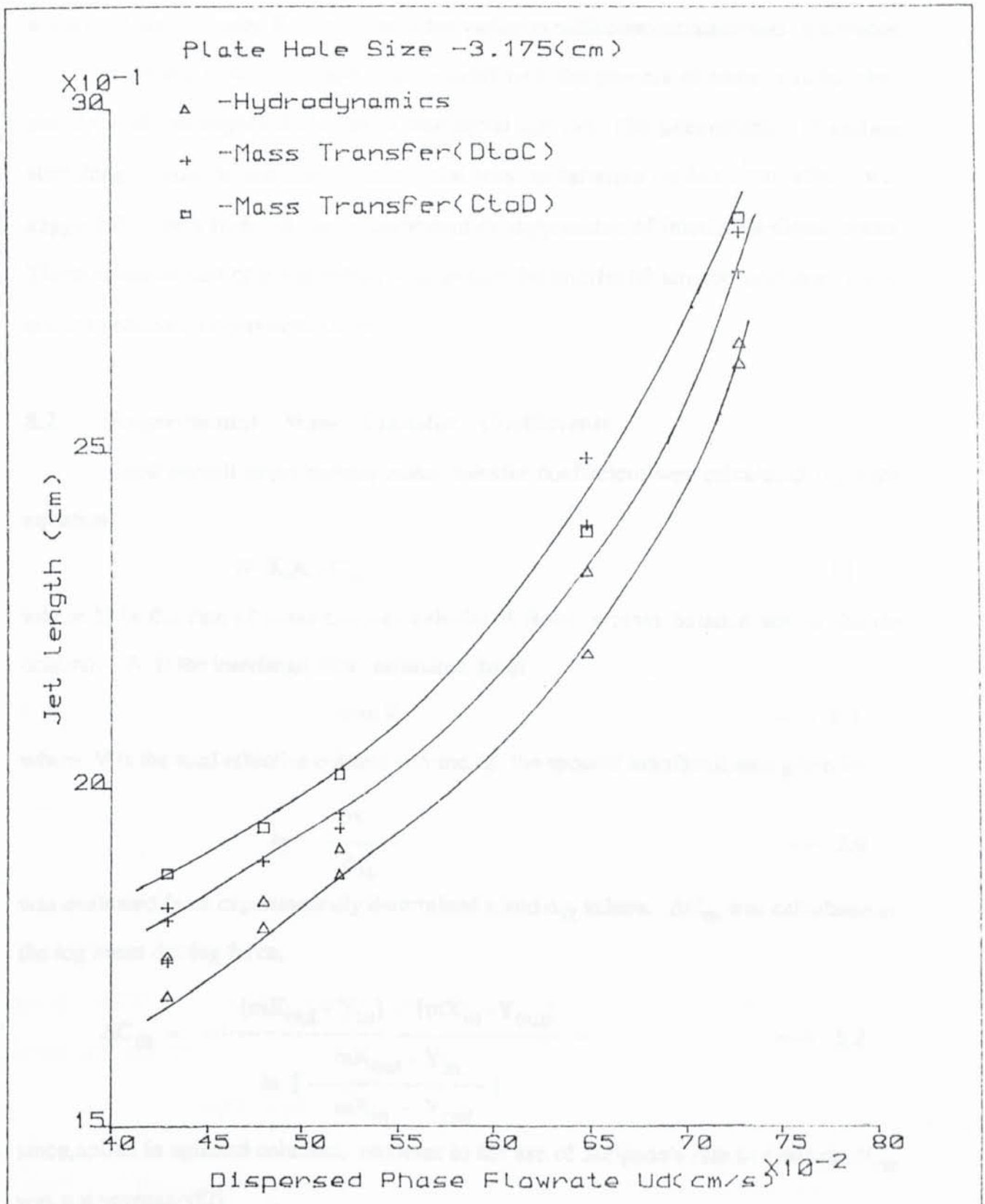

Fig.8.1 Effect Of Mass Transfer On Jet Length

associated small change in σ, no significant variation with concentration was observable.

Increase in the jet length is associated with the process of transfer rather than simply with the expected change in interfacial tension. The phenomenon of surface stretching or contraction through interfacial tension variation (ie Marangoni effect) was suggested to be a factor in the enhancement or suppression of interfacial disturbances. There is movement of the interface to alleviate the interfacial tension gradients which occur to enhance or suppress the jet.

8.2 Experimental Mass Transfer Coefficients

Each overall experimental mass transfer coefficient was calculated from the equation

$$N=K.A.\Delta C_m \qquad \text{----- 2.1}$$

where N is the rate of mass transfer calculated from a mass balance across the the column. A is the interfacial area estimated from

$$A=a.V \qquad \text{----- 8.1}$$

where V is the total effective column volume. 'a' the specific interfacial area given by

$$a=\frac{6x}{d_{32}} \qquad \text{----- 2.6}$$

was evaluated from experimentally determined x and d_{32} values. ΔC_m was calculated as the log mean driving force,

$$\Delta C_m = \frac{[mX_{out} - Y_{in}] - [mX_{in} - Y_{out}]}{\ln\left[\frac{mX_{out} - Y_{in}}{mX_{in} - Y_{out}}\right]} \qquad \text{----- 8.2}$$

since,unlike in agitated columns, recourse to the use of Simpson's rule to evaluate ΔC_m was not necessary[2]

Since the hold-up and mean dropsize were experimentally determined, results are reported as '$K_{expt.}$' rather than '$K_{expt.}a$'. However, because the drop size distribution

was very similar in each compartment, as a result of coalescence and redispersion at each plate, the trends in '$K_{expt.}$' and '$K_{expt.}a$' were found to be almost identical. Conversely in differential agitated columns, the use of '$K_{expt.}a$' instead of '$K_{expt.}$' may be significant. '$K_{expt.}a$' is based upon the mean specific interfacial area 'a' and takes no account of drop size distribution. If the intensity of agitation is increased, smaller drops are generated so 'a' also increases; '$K_{expt.}$' will decrease due to the increased proportions of stagnant/circulating drops generated but a similar '$K_{expt.}a$' value can be obtained.

Overall experimental mass transfer coefficients were determined at four different plate spacings: 34,30,26 and 20cm with two different holesize plates: 3.175 and 6.35mm. The results are tabulated in Table 8.2 A sample calculation is shown in Appendix 10 and a computer program for the calculation is given in Appendix 7

8.3 Mass Transfer Theoretical Models

No attempt was made to correlate the experimental mass transfer results, since these would be system specific. Results are reported in terms of overall mass transfer coefficients rather than the column efficiency, since different test systems gives different efficiencies[60a].

A fairly-wide range of drop sizes existed within the SPC under mass transfer conditions e.g from about 2.5 to 10mm, so that more than one single-drop mass transfer mechanism occurred simultaneously. The mass transfer coefficient within each phase is greatly-affected by the fluid conditions inside the drop, as characterised by the drop Reynolds number

$$Re = \frac{d\rho_c U_s}{\mu_c} \qquad \text{----- 8.3}$$

where U_s is the slip velocity ie the mean relative velocity between the phases, determined by

$$U_s = \frac{U_d}{x} + \frac{U_c}{1-x} \qquad \text{----- 4.20}$$

Hence, it is necessary to ascertain the drop size and size distribution in the dispersion passing through the SPC to assess its mass transfer performance. The droplet Reynolds number is used as a measure of the drop state[91,257,271] ie stagnant,circulating or oscillating. The most reliable single drop models for estimating the dispersed phase and continuous phase mass transfer film coefficients, verified by various workers [127,129,217,255,283,316], depending whether a drop is stagnant, circulating or oscillating are summarised in Table 8.1

The theoretical mass transfer coefficient, K_{cal} was evaluated by using the dropsize distribution diagram, Figure 8.2, to estimate the volume percentage of stagnant, circulating and oscillating drops in the drop population. Individual mass transfer coefficients were then evaluated for the corresponding drop state, using the single drop models. The maximum drop size for each regime was estimated, the mean drop size found, and the mean overall mass transfer coefficient for the particular regime calculated from the appropriate single drop correlations. The overall mass transfer coefficient was then calculated as the fractional sum of the individual overall mass transfer coefficient of each regime in proportion to the volume fraction [2] of that regime in the drop population. Thus based upon volume fraction,

$$K_{cal}=K_sP_s + K_cP_c + K_oP_o \qquad \text{------ 8.4}$$

where P_s,P_c and P_o are the volume fraction of drops in the stagnant, circulating and oscillating drop regimes respectively and, K_s,K_c and K_o are the overall mass transfer coefficients relating to each regime. The basis for preferring volume fraction is discussed in Section 8.4

(i) Stagnant drop regime

The correlations for k_d of Treybal[295], equation 8.5 and k_c of Rowe *et al* [243], equation 8.6 were used to calculate the film coefficients for this regime.

The Reynolds number was set equal to 10 to find the maximum diameter of stagnant drops in the whole population. As shown in Table 8.2, d_s was too small to be

Table 8.1 Mass Transfer Coefficient Models

State of droplet	Reynolds Number	Dispersed Phase Coefficient		Continuous Phase Coefficient	
		Model	Eqn No	Model	Eqn No
Stagnant	Re<10	$k_{d.s} = \frac{2\pi^2 D_d}{3d_s}$	8.5	$Sh_{c.s} = 2.076\ (Re)^{0.5}(Sc)^{0.3}$	8.6
		Treybal (295)		Rowe (243)	
Circu-lating	10<Re< 200	$k_{d.c} = \frac{17.9 D_d}{d_c}$	8.7	$Sh_{c.c} = -126+1.8(Re)^{0.5}(Sc)^{0.42}$	
		Kronig and Brink (150)		Garner-Foord Tayeban (74)	8.8
		$k_{d.c} = \frac{0.00375 U_s}{1 + \mu_d/\mu_c}$		$k_{c.c} = \left[\frac{4 D_c U_s}{\pi d_c}\right]^{0.5}$	
		Handlos and Baron (95)	8.9	Higbie (109)	
8.10					
Oscill-ating	Re≥200	$k_{d.o} = 0.45(\omega D_d)^{0.5}$	8.11		
		Rose-Kintner (238)		$Sc_{c.o} = 50+0.0085\ (Re)(Sc)^{0.7}$	
8.13					
				Garner-Tayeban (78)	
		$k_{d.o} = \sqrt{\left(\frac{4\omega D_d[1+\varepsilon_o]}{\pi}\right)}$	8.12		
		Where $\varepsilon_o = \varepsilon + 3/8\varepsilon^2$			
		Angelo-Lightfoot (8)			

accurately analysed by the photographic technique used in this study but stagnant drops comprised only about 1-3% by volume, mainly satellite drops caused by the breakage of larger drops.

(ii) Circulating drop regime

The correlations for k_d's of Kronig and Brink[150], equation 8.7 and of Handlos and Baron [95], equation 8.9 and for k_c 'of Garner *et al* [74], equation 8.8 and Higbie[109], equation 8.10 were used to calculate the film coefficients for this regime.

The overall mass transfer coefficient of the circulating drops $K_{o.c}$ was calculated as

$$\frac{1}{K_{o.c}} = \frac{1}{k_{d.c}} + \frac{m}{k_{c.c}} \qquad \text{----- 8.14}$$

To find the maximum diameter of circulating drop in the whole population, the Reynolds number was set equal to 200.

(iii) Oscillating drop regime

The remainder of the drop population was considered to correspond to the oscillating drop regime. The correlations for k_d of Rose and Kintner, equation 8.11 and of Angelo-Lightfoot, equation 8.12. were used to calculate the dispersed phase film coefficient for this regime. The frequency of oscillation ,ω, in equation 8.11 was evaluated by,

$$\omega^2 = \frac{\sigma b}{r^3}\left[\frac{n(n-1)(n+1)(n+2)}{(n+1)\rho_d + n\rho_c}\right] \qquad \text{-----8.15}$$

r=drop radius

n=2

b=Constant depending on drop size, $b=d_o^{0.225}/1.242$

ε, which is the eccentricity in equation 8.12, was estimated by Al-Hassan's correlation[4] as,

$$\varepsilon = 0.434\left[\frac{\omega \bar{d}_o}{U_s}\right]^{-0.46}\left[\frac{\bar{d}_o U_s^2 \rho_c}{\sigma}\right]^{-0.53}\left[\frac{\mu_c U_s}{\sigma}\right]^{-0.11} \qquad \text{-----8.16}$$

where $\bar{d}_o$ is the oscillating drop mid-sector diameter.

k_c values predicted from Garner and Tayeban's equation 8.13 were used to calculate the continuous phase film coefficient.

The overall mass transfer coefficient was calculated as

$$\frac{1}{K_{o.o}} = \frac{1}{k_{d.o}} + \frac{m}{k_{c.o}} \qquad \text{----- 8.17}$$

For the case of Angelo-Lightfoot [7], the overall mass transfer coefficient was calculated by

$$K_{o.o} = k_{d.o}\left[\frac{1}{1 + m\sqrt{D_d/D_c}}\right] \qquad \text{-----8.18}$$

Assuming that the stagnant drop population is negligible, equation 8.4 for the calculation of the entire drop population reduces to

$$K_{cal} = K_c P_c + K_o(1-P_c) \qquad \text{----8.19}$$

The values predicted using the models in Table 8.1, are reported in Table 8.2, together with corresponding experimental overall mass transfer coefficients. A sample calculation for the theoretical mass transfer coefficient is given in Appendix 11 and a computer program in Appendix 8.

8.4 Volume fractions or Area fractions for Weighted Overall Mass Transfer Coefficient Calculations

In any extractor in which all the drops are not oscillating the reason for preferring calculation on a volume basis to that on an area basis, for use in equation 8.4, can be explained as follows. The calculated overall mass transfer coefficient for an extractor on an incremental area basis is

$$(K_{cal})_a = K_s a_s + K_c a_c + K_o a_o \qquad \text{------ 8.20}$$

where a_s, a_c, a_o are the interfacial area fractions of drops in the stagnant, circulating, and oscillating drop regimes respectively and K_s, K_c, K_o are the overall mass transfer coefficients corresponding to each regime.

Examination of the drop size distribution Table 8.2 shows that the Reynolds number of the great majority of drops was >10. Therefore only circulating and oscillating

drop fractions are considered.

The area fractions of both regimes are:

$$a_c = \frac{6P_c}{d_c} \qquad \text{------ 8.21}$$

$$a_o = \frac{6P_o}{d_o} \qquad \text{-------8.22}$$

The average drop diameter for the circulating regime is approximately half those in the oscillating regime [Figure7.14]

$$a_o = \frac{6P_o}{d_o} = \frac{6P_o}{2d_c} \qquad \text{------ 8.23}$$

Dividing equation 8.21 by equation 8.23 gives

$$\frac{a_c}{a_o} = \frac{6P_c/d_c}{6P_o/2d_c} = \frac{2P_c}{P_o} \qquad \text{------ 8.24}$$

The rate of mass transfer corresponding to each regime is:

$$N_{Ac} = K_c a_c (\Delta C)_c \qquad \text{------8.25}$$

$$N_{Ao} = K_o a_o (\Delta C)_o \qquad \text{------ 8.26}$$

From earlier studies the mass transfer coefficient of an oscillating drop is of the order of five-fold greater than that of a circulating drop [2,3] and the solute concentration in the oscillating drop will become considerably greater than that in the circulating drops.

$$K_o \sim 5K_c \qquad \text{----- 8.27}$$

Hence, it can be shown that the ratio between the rates of mass transfer to, or from, the circulating drops and that of the oscillating drops is

$$\frac{N_{Ac}}{N_{Ao}} = \frac{K_c a_c (\Delta C)_c}{5 K_o a_o (\Delta C)_o} = \frac{2}{5}\left[\frac{P_c}{P_o}\right]\left[\frac{(\Delta C)_c}{(\Delta C)_o}\right] = \frac{P_c}{P_o}\left[\frac{2\,\Delta C_o}{5\,\Delta C_o}\right] \qquad \text{----- 8.28}$$

Since it is impracticable to estimate the ratio of the driving forces; it was considered preferable to base the fractional mass transfer coefficients on the volume fractions of the drops in each regime.

However, in the situation where very many small, theoretically stagnant, drops may be present and the turbulence does not cause them to oscillate (eg low interfacial tension systems subjected to only moderate turbulence) the area fraction would be preferable.

8.5 Experimental Observations

The effect of various operating variables: viz phase flowrates, plate geometry, plate spacing, and direction of solute transfer upon the overall mass transfer coefficient, K_{od} were investigated using analytical and photographic (drop size determination) methods [Chapter 6].

The overall mass transfer coefficient K_{od} increased when the plate spacing was reduced from 34 to 26cm. Further decrease in plate spacing to 20cm, in the case of the 3.175mm hole size plate, resulted in no significant difference in the K_{od} values compared to the 26cm plate spacing, Table 8.2 . The reason for this was that at plate spacing <26cm, there was insufficient drop-rise distance before re-coalescence occurred beneath the plate above. However, high values of K_{od} at reduced plate spacing are attributable mainly to an increase in the number of plates per net height of column resulting in an increase in the frequency of drop coalescence and redispersion, ie an increase in end effects, enhancing mass transfer. In any industrial application the operating cost would increase due to the increase in the number of plates with decrease in the plate spacing. Hence, the optimum operating plate spacing is based on economics.

At the lowest plate spacing, 20cm, the dispersed phase recirculation between adjacent plates was completely eliminated.

Table 8.2 - Experimental Mass Transfer Results

Run No	Direction of Transfer	Plate hole Size (mm)	Plate Spacing (mm)	U_c (cm/s)	U_d (cm/s)	U_s (cm/s)	X_{in}	X_{out}	Y_{in}	Y_{out}
19	D -->C	6.35	340	0.34	0.36	17.49	3.50	2.00	0.00	1.26
20	"	"	"	0.34	0.43	18.27	2.00	1.25	1.26	1.98
21	"	"	"	0.34	0.52	18.28	4.20	3.10	0.00	1.31
22	"	"	"	0.34	0.65	21.32	3.10	2.60	1.31	2.04
23	"	"	"	0.58	0.36	19.64	5.15	3.96	0.00	0.60
24	"	"	"	0.58	0.43	16.18	3.96	3.12	0.60	1.09
33	"	"	300	0.58	0.52	23.20	1.24	0.35	0.630	1.18
34	"	"	"	0.34	0.52	27.72	0.35	0.18	0.761	1.01
35	"	"	"	0.34	0.36	40.34	3.174	1.88	0.00	1.34
36	"	"	"	0.58	0.36	33.31	1.88	0.78	1.34	1.79
37	C -->D	"	"	0.34	0.65	44.56	0.80	1.13	4.30	3.71
38	"	"	"	0.34	0.36	33.07	1.13	1.72	3.71	3.14
39	"	"	"	0.58	0.36	26.30	1.72	2.98	3.14	2.21

Table 8.2 - Experimental Mass Transfer Results

Run No	Direction of Transfer	Plate hole Size (mm)	Plate Spacing (mm)	U_c (cm/s)	U_d (cm/s)	U_s (cm/s)	X_{in}	X_{out}	Y_{in}	Y_{out}
51	D -->C	6.35	260	0.34	0.27	21.44	2.85	1.05	0.00	1.65
52	"	"	"	0.34	0.43	22.74	1.05	0.41	1.65	2.33
53	"	"	"	0.34	0.52	16.55	3.20	1.67	0.00	1.55
54	"	"	"	0.58	0.27	20.14	1.67	0.58	1.55	1.93
55	"	"	"	0.58	0.43	21.94	2.50	1.72	0.00	0.65
56	C -->D	"	"	0.34	0.27	16.11	0.50	1.29	4.80	4.23
57	"	"	"	0.34	0.52	24.48	0.124	0.248	3.03	1.67
58	"	"	"	0.58	0.43	24.48	0.068	0.123	1.67	0.83
67	D -->C	3.175	340	0.30	0.31	10.99	4.20	3.18	0.00	1.07
68	"	"	"	0.30	0.43	7.04	3.18	2.53	1.21	1.96
69	"	"	"	0.55	0.31	8.73	5.20	4.06	0.00	0.63
70	"	"	"	0.55	0.43	6.65	4.06	3.32	0.63	1.14
71	C --> D	"	"	0.30	0.43	8.80	0.40	1.13	3.21	2.57
72	"	"	"	0.55	0.48	7.64	1.13	1.97	2.59	1.92

Table 8.2 - Experimental Mass Transfer Results

Run No	Direction of Transfer	Plate hole Size (mm)	Plate Spacing (mm)	U_c (cm/s)	U_d (cm/s)	U_s (cm/s)	X_{in}	X_{out}	Y_{in}	Y_{out}
81	D--> C	3.175	300	0.30	0.31	10.00	3.86	1.67	0.0	1.73
82	"	"	"	0.30	0.43	7.61	1.67	0.24	1.73	2.46
83	"	"	"	0.55	0.31	8.14	2.50	0.99	0.00	1.26
84	"	"	"	0.55	0.43	7.20	3.01	1.12	0.00	1.34
93	"	"	260	0.30	0.31	10.0	2.01	0.52	0.00	1.64
94	"	"	"	0.30	0.43	10.09	2.56	0.21	0.00	1.87
95	"	"	"	0.55	0.31	8.52	3.51	1.07	0.00	1.83
96	"	"	"	0.55	0.43	9.01	4.26	1.52	0.00	2.11
105	"	"	200	0.30	0.31	9.16	3.76	0.72	0.00	2.36
106	"	"	"	0.30	0.43	8.59	5.72	1.04	0.00	4.16
107	"	"	"	0.55	0.31	7.17	4.29	0.82	0.00	2.19
108	"	"	"	0.55	0.43	7.75	6.87	1.69	0.00	4.56

Table 8.3 - Theoretical Mass Transfer Results

Run No	Hold-up %	d_{32} cm	Effective Column Height (cm)	N gm/sec	ΔC gm/cm^3 x10^{-2}	K_{exp} cm/s x10^{-3}	$Kcal_1$ cm/s x10^{-3}	$Kcal_2$ cm/s x10^{-3}	$\frac{K_{expt}}{Kcal_1}$	$\frac{K_{expt}}{Kcal_2}$
19	2.10	0.769	170	6.81	23	0.732	1.86	3.04	0.39	0.24
20	2.40	0.704	"	3.89	12.4	0.621	1.95	3.23	0.32	0.19
21	2.90	0.636	"	7.07	31.3	0.336	1.98	3.48	0.17	0.10
22	3.10	0.765	"	3.94	23.3	0.282	2.19	3.01	0.13	0.09
23	1.89	0.697	"	5.52	39.7	0.349	2.08	3.24	0.17	0.11
24	2.76	0.661	"	4.51	30.2	0.243	1.79	3.41	0.14	0.03
33	2.30	0.850	194.5	5.06	5.29	2.07	2.30	2.78	0.90	0.75
34	1.90	0.728	"	1.34	1.33	2.27	2.70	3.08	0.84	0.74
35	0.90	0.751	"	7.23	0.212	1.63	3.53	2.96	0.46	0.55
36	1.10	0.813	"	4.14	9.41	1.91	3.04	2.82	0.63	0.68
37	1.47	0.725	"	3.18	4.39	2.09	3.82	3.03	0.55	0.69
38	1.10	0.628	"	3.07	8.93	1.15	3.17	3.39	0.36	0.34
39	1.40	0.620	"	8.56	17.6	1.27	2.67	3.46	0.48	0.37

Table 8.3 - Theoretical Mass Transfer Results

Run No	Hold-up %	d_{32} cm	Effective Column Height (cm)	N gm/sec	ΔC gm/cm^3 x10^{-2}	K_{exp} cm/s x10^{-3}	$Kcal_1$ cm/s x10^{-3}	$Kcal_2$ cm/s x10^{-3}	$\frac{K_{expt}}{Kcal_1}$	$\frac{K_{expt}}{Kcal_2}$
51	1.28	0.841	182	8.90	15.2	2.39	2.16	2.81	1.11	0.85
52	1.92	0.783	"	3.67	3.93	2.37	2.29	2.95	1.03	0.80
53	3.21	0.798	"	8.36	20.1	6.46	1.77	2.97	3.65	2.18
54	1.60	0.722	"	3.50	7.22	1.37	2.11	3.16	0.65	0.43
55	2.20	0.658	"	5.99	18.1	6.18	2.29	3.35	2.69	1.85
56	1.25	0.548	"	3.07	1.75	4.8	1.82	3.91	2.64	1.23
57	3.30	0.469	"	7.33	0.71	9.17	2.63	4.25	3.48	2.16
58	1.80	0.512	"	7.72	0.38	35.6	2.59	3.99	1.37	0.89
67	2.90	0.624	170	5.09	31.8	23.4	1.30	3.67	0.18	0.06
68	6.40	0.740	"	3.57	23.5	11.9	0.87	3.39	0.14	0.04
69	3.80	0.582	"	5.50	0.404	13.9	1.08	3.96	0.13	0.04
70	7.10	0.597	"	4.45	0.315	0.08	0.86	4.02	0.09	0.02
71	5.60	0.514	"	3.05	0.029	0.6.0	1.11	4.35	0.57	0.15
72	6.10	0.561	"	5.67	0.110	0.32	0.972	4.14	0.33	0.08

Table 8.3 - Theoretical Mass Transfer Results

Run No	Hold-up %	d_{32} cm	Effective Column Height (cm)	N gm/sec	ΔC gm/cm^3	K_{exp} cm/s	$Kcal_1$ cm/s	$Kcal_2$ cm/s	$\frac{K_{expt}}{Kcal_1}$	$\frac{K_{expt}}{Kcal_2}$
				x10^{-2}	x10^{-3}	x10^{-3}	x10^{-3}			
81	3.20	0.500	150	8.24	0.223	0.44	1.24	4.37	0.35	0.10
82	5.90	0.544	"	3.47	0.034	0.71	0.97	4.24	0.73	0.17
83	4.10	0.468	"	11.02	0.138	0.95	1.05	4.71	0.91	0.20
84	6.50	0.404	"	11.70	0.163	3.39	0.98	5.35	0.35	0.06
93	3.20	0.629	182	7.81	0.092	1.05	1.20	3.69	0.88	0.29
94	4.40	0.682	"	8.90	0.078	1.1	1.20	3.47	0.92	0.32
95	3.9	0.693	"	15.90	0.176	1.01	1.04	3.49	0.97	0.29
96	5.1	0.646	"	18.42	0.226	6.43	1.10	3.65	0.59	0.18
105	3.5	0.624	140	11.24	0.155	1.02	1.12	3.74	0.91	0.27
106	5.2	0.597	"	19.81	0.229	0.78	1.06	3.90	0.74	0.20
107	4.7	0.596	"	19.12	0.178	1.07	0.91	3.88	1.17	0.27
108	6.0	0.609	"	39.8	0.310	1.02	9.73	3.33	1.05	0.26

Table 8.4 - Theoretical Mass Transfer Results Using Dropsize Distribution

Run No	P_c	d_s (cm)	d_o (cm)	$\frac{K_{expt}}{K_{cal\ 3}}$	$\frac{K_{expt}}{K_{cal\ 4}}$	$\frac{K_{expt}}{K_{cal\ 5}}$	$\frac{K_{expt}}{Kcal\ 6}$
67	0.001	0.23	0.640	0.18	0.07	0.18	0.07
68	0.026	0.30	0.808	0.13	0.04	0.11	0.04
69	0.006	0.291	0.600	0.13	0.04	0.13	0.04
70	0.039	0.318	0.584	0.09	0.02	0.09	0.02
71	0.044	0.296	0.599	0.61	0.17	0.64	0.17
72	0.04	0.292	0.637	0.32	0.09	0.34	0.09
81	0.01	0.240	0.528	0.35	0.11	0.36	0.11
82	0.018	0.274	0.554	0.72	0.17	0.74	0.17
83	0.08	0.260	0.508	0.86	0.23	0.95	0.23
84	0.339	0.262	0.530	0.25	0.10	0.42	0.11
93	0.02	0.243	0.599	0.83	0.28	0.83	0.28
94	0.04	0.221	0.614	0.87	0.30	0.92	0.30
95	0.09	0.296	0.653	0.90	0.28	0.99	0.30
96	0.07	0.263	0.632	0.55	0.18	0.60	0.18
105	0.001	0.284	0.700	0.93	0.30	0.93	0.30
106	0 .001	0.30	0.621	0.74	0.21	0.74	0.21
107	0.01	0.352	0.622	1.12	0.28	1.19	0.30
108	0.008	0.350	0.642	1.05	0.28	1.06	0.28

$K_{cal\ 1}$ - based on Rose-Kintner
$K_{cal\ 2}$ - based on Angelo-Lightfoot
$K_{cal\ 3}$ - based on Handlos-Baron and Rose-Kintner
$K_{cal\ 4}$ - based on Handlos-Baron andAngelo-Lightfoot
$K_{cal\ 5}$ - based on Handlos-Baron and Rose-Kintner
$K_{cal\ 6}$ - based on Kronig-Brink and Angelo-Lightfoot

(The data are as calculated, or predicted and the number of significant figures is not meant to imply a higher degree of accuracy than for the experimentally measured variables)

The mean drop sizes with mass transfer in the d to c direction were greater than those in the absence of mass transfer; the latter were similar to those with mass transfer in the c to d direction. The data indicates that the reduction in interfacial tension due to solute produced interfacial gradients leading to rapid coalescence (Marangoni effects) as it was transferred from d to c. For c to d transfer, the droplet behaviour was not significantly different from that under non-mass transfer conditions because of the relatively low acetone concentrations in the continuous phase. Due to the larger drop sizes, the value of the slip/characteristic velocity was larger when transfer was from d to c direction than for c to d, or in the absence of mass transfer.

No direct comparison could be made for the dispersed phase hold-up for different directions of solute transfer, since the solute concentration was unequal for each run. Generally, the dispersed phase hold-up was greater under mass transfer conditions.

At a particular continuous flowrate U_c, K_{od} increased with increase in the dispersed phase flowrate U_d, as shown in Table 8.2. This is attributable to the increase in the number of drops ie hold-up, which enhances the mass transfer as a result of the greater crowding of the drops per unit volume of the column. The increased proximity of the drops promotes interaction, which has been shown to enhance mass transfer for drop pairs[3] and triple drops[275]. There was a slight dependence of K_{od} on the continuous phase flowrate,U_c, but this was only appreciable at high U_c>0.5cm/s which could increase the tendency of drops to oscillate due to cross-flow effects. High U_c values could also lead to the break up of larger drops resulting in surface renewal, which also enhances mass transfer.

The experimentally-determined drop sizes and distributions were compared for the 3.175 and 6.35mm hole size plates. The larger hole size naturally produced the larger drops, Table 8.2, but the proportion of satellite drops < 1mm were greater from the 6.35mm plate. This was due to the break-up of larger drops due to collision and the turbulent effects of the continuous phase at high U_c. The 3.175mm hole size plate

generated a more uniform distribution and the smaller drops provided a larger total contact interfacial area in the column. However, the drop population produced by the 3.175mm hole size plates included both circulating and oscillating drops whereas the 6.35mm hole size plate produced mainly oscillating drops resulting in an increased mass transfer efficiency. The slightly higher mass transfer coefficients obtained with the 6.35mm hole size plate might also be attributable to all the drops being in the oscillating drop regime. However, K_{od} values were, for all practical purposes, generally similar for both plates, due to a balance between these factors.

8.6 Comparision of Experimental and Theorectical Mass Transfer Coefficients

Two types of theoretical calculations were performed:

(i) Using the mean drop diameter to characterise the mode of transfer for drops from the 6.35mm and 3.175mm hole size plates.

(ii) Using the drop size distribution and equation 8.19 for the 3.175mm hole plate. (all the drops from the 6.35mm hole plate were in the oscillating regime, Table 8.3)

The mass transfer models detailed in Section 8.3 and Table 8.1 were used to calculate the theoretical mass transfer coefficients,given in Table 8.3. In a comparision between the experimental and calculated overall mass transfer coefficients for cases in which all the drops were in the oscillating regime, ie for the 6.35mm hole size plate , for the direction of transfer from d to c, better agreement was obtained when the k_d of Rose-Kintner, equation 8.11 was applied in combination with the respective k_c than when the Angelo *et al* equation 8.12 was used. This is emphasised in Table 8.3, where the ratios of the respective experimental coefficient to each of the calculated values are presented. These ratios were evaluated to assess the extent of oscillations induced through droplet collisions and additional turbulence generated by the continuous cross-flow.

The better agreement with the Rose-Kintner, equation 8.11 implies that mild oscillation, rather than turbulent oscillation as is the case of Angelo *et al* 's equation 8.12, existed in the droplet swarm. This suggests that the presence of adjacent drops has no great effect at low hold-up's of < 10% in this study.

Ratios of experimental to calculated mass transfer coefficients <1.0 imply that not all the drops oscillate, ie incipient oscillation, and ratios >1.0 imply that a large proportion of the drops in the dispersion oscillate. As the plate spacing was decreased from 34 to 30cm, the ratio of the experimental overall mass transfer coefficients to those calculated from the Rose-Kintner correlations approaches unity. Below a plate spacing of 30cm it exceeds unity; implying that the degree of oscillation increases or a large proportion of the drops oscillate. Cross-flow effects of the continuous phase at a relatively high flowrate increased the tendency for oscillation (Runs 23-4,55-6). Poorer agreement with theory was observed with data for the c to d direction of transfer. This is probably due to the very low rates of mass transferred (ie low driving force, ΔC) associated with these experiments where small errors in the estimation of the concentrations could have a significant effect on the mass transfer rate and coefficients. (The ultilisation of higher concentrations of acetone in the continuous phase was prohibited by the cost). Nevertheless the limited results are generally supportive of those obtained when the direction of mass transfer was d to c.

The droplets from the 3.175mm hole size plate were of a size to be mainly circulating and oscillating, Table 8.4. The proportion of drops in each regime, Figure 7.14, was used to calculate the theoretical mass transfer coefficient as described earlier, using Equation 8.19. Better agreement was obtained with the combination of k_d predicted from Kronig-Brink (c) and Rose-Kintner (o) with the respective predicted k_c values. This was followed by the combination of Handlos-Baron (c) and Rose-Kintner(o) for k_d. The combination of k_d's from Kronig-Brink(c) and Angelo-Lightfoot (o),and those of Handlos-Baron(c) and Angelo-Lightfoot(o) with the respective k_c gave poor results.

For the 3.175mm plate, the mean drop diameter, d_{32} was also used, instead of the fractional sum, using the correlation for the corresponding regime [Table 8.4]. using the k_d values from Angelo-Lightfoot and Rose-Kintner with the respective k_c. Application of the dropsize distribution was shown to give a better representation and this is important for design purposes.

The same K_{od} trend with plate spacing was observed for both the 6.35 and 3.175mm plates, but with the 3.175mm plate, the ratio of experimental to calculated mass transfer coefficients approaches unity gradually with decrease in plate spacing from 34 to 20cm. This could be explained by the column approaching a better operating condition as the plate spacing was decreased, ie recirculation of the dispersed phase was gradually eliminated. This approaches the condition for which the single drop models were derived.

The greatest deviations between experimental and calculated overall mass transfer coefficients corresponded to high hold-ups, ie at high phase flowrates, when conditions were furthest from the single drop situations. Moreover, higher experimental mass transfer coefficients compared with those calculated would be expected for the following reasons:

(i) The difference between local velocities experienced by different drop sizes compared with the calculated slip velocity. For example the drop velocity might be much smaller locally due to the recirculation at higher plate spacings, ie>34cm. The cross flow at higher continuous phase flowrate would also induce circulatory or oscillatory effects giving rise to an uneven velocity distribution. The slip velocity of the drops is reduced due to the crossflow effect, which in turn reduces the Reynolds number which is an important factor determining the drop mass transfer mode.

(ii) The calculated mass transfer coefficients are based upon correlations of single drop data for conditions under which the drops neither collide nor coalesce, and the

streamlines around individual drops are not disturbed. This is not analogous to conditions in the pilot - scale SPC, with relatively high hold-ups.

(iii) The models are based upon drip-point release and not jetting with crossflow, the situation in the majority of runs in the present study.

(iv) The model derivations include probable errors of 15-20% [8,95,238].

The limitations of these models may be summarised as follows,

The Rose-Kintner model[238] depended upon the amplitude of oscillation calculated by measuring only one axis of the drop neglecting the change in the other two dimensions. The model also assumes that a symmetrical spheroid shape is applicable for large oscillating drops. For the Angelo *et al* model[8], the area changes are more complex than described and the model neglects the effects of the wake, assuming that the mechanism of solute transfer at the front and rear are similar. However, drops with a Reynolds number less than 200 may be induced to circulate through collision with another drop, or through resonance by an oscillating drop in close proximity in the turbulent regime. For example three parallel streams of drops formed at the corners of a 0.019m equilateral triangle, under conditions to give stagnant drops were found to yield incipient oscillation [275]. However it appears that these oscillations will be rapidly damped out because of increased interdrop distances when the dispersion passes out of the cross-flow region of the continuous phase.

The Handlos and Baron model [95] has been shown to be very unreliable, Brunson and Wellek [25] compared the performance of different models using a selection of experimental data and among 12 models, the exact solution of the Handlos and Baron model as given by Olander [210] was found to be the least accurate. The original Handlos and Baron model describes the limiting case of mass transfer resistance in the droplet phase alone, while subsequent modifications have extended the model to finite continuous phase Sherwood numbers, either through the estimation of Eigen values [44,309] or by numerical solution of the governing differential equations [217,309]. The

Handlos and Baron model was derived for a turbulent circulating drop, with circular streamlines; random and complete mixing was assumed at the end of the circulation time. Such conditions could only be achieved in vigorously agitated columns.

Analysis with individual mass transfer coefficients related to the respective dropsize fraction, provides the best method of predicting the overall mass transfer coefficients from existing single drop models. Although this method does not involve coalescence and redispersion, prediction of the individual drop film coefficients k_c or k_d based upon Reynolds number with the velocity represented by the slip velocity appears to be reliable at lower plate spacings and U_c ie no recirculation. However, over the distribution of drop size, the slip velocity varies for each individual drop.

A more reliable method for prediction of mass transfer coefficients would be a theoretical analysis which accounts for local velocity distributions. Therefore the slip velocity correlation of Olney [215], $U_s=U_t(1-x)$, where U_t was predicted by the Grace *et al* correlation [84] [Section 4.2.1] was also used. For Run 67, the experimental U_s was 10.99cm/s and the calculated U_s was 13.6cm/s. A sample calculation is shown in Appendix 12. This predicted somewhat different values for the drop velocities with operating conditions but, for the specific condition involved, no significant influence on predicted mass transfer rates.

CHAPTER NINE

DEVELOPMENT OF A DESIGN PROCEDURE FOR A SIEVE PLATE COLUMN

9.1 Introduction

The sieve plate column merits consideration under the following conditions:

(a) Operations involving high throughput of the phases, up to 0.017m/s (U_c+U_d), with typical phase ratios, U_d/U_c between 0.1 to 10.

(b) When a large number of theoretical stages is required >5.

(c) If the dispersed and continuous phase have a substantial density difference >100kg/m^3.

(d) If the system has a moderate interfacial tension, 10-40mN/m, so that mechanical energy is not essential for a homogeneous dispersion.

(e) When the dispersion is relatively easy to coalesce, so that excessive flocculation/coalescence heights are avoided.

(f) For corrosive systems, where the absence of moving parts is advantageous.[Packed columns may be preferred for highly-corrosive systems]

(g) When particulate solids are not present in either phase, although designs are available to cope with solids [196].

The performance of the SPC is characterised by the limits of operating range and separation efficiency which can be achieved. The operating point is described by the sum of both phase throughtputs, based on the column cross-section. The separation efficiency is commonly expressed in terms of the number of theoretical stages per unit height or reciprocal of the height equivalent of a theoretical plate, HETS. The HETS values for a given column design will be system specific and also depend upon relative flowrates, (since these affect the hydrodynamics), the solute concentrations and the total volumetric throughput. Any HETS values presented can only therefore refer to specific column dimensions and geometry and a narrow range of operating parameters.

As discussed in Chapter 3, the SPC is strictly a hybrid extractor since, although contacting is stagewise ie involving intermittent coalescence and redispersion, contacting within each stage is differential-continuous with some cross-flow of the continuous phase.

9.2 Design Parameters

The design of a sieve plate column involves the determination of three main parameters:

(a) Diameter or cross-sectional area, based upon the maximum permissible throughtput of the phases.

(b) Total height or number of actual stages (with a specified plate spacing)

(c) Dimensions and geometries of plates (and downcomers) and their spacing derived from design models, pilot plant tests or general scale-up rules.

Design of the SPC from basic principles would require knowledge of at least the following variables:

(i) Flooding velocities or range.

(ii) Mean drop size or drop size distribution.

(iii) Dispersed phase hold-up.

(iv) Coalescence height (static hold-up) beneath each plate.

(v) Dispersed phase film coefficient, k_d based upon mean drop size or drop size distribution.

(vi) Continuous phase film coefficient, k_c based upon mean drop size or drop size distribution.

Emperical correlations or models may be used for the estimation of i-vi, when available and reliable (Chapter 10), ie to cross check with pilot-scale data. Each of the above variables depends upon :

(a) System physical properties.

(b) Design and arrangement of internals.

(c) Direction of solute transfer.

(d) Phase ratio.

(e) Which phase is dispersed.

The aim in design will be to attain the maximum possible mass transfer rate per unit volume commensurate with reasonable volumetric throughputs, i.e

$$N=K.A.\Delta C \qquad \text{------ 2.1}$$

As already described, K depends upon the physical properties of the system, and A, and ΔC are influenced by the construction and operating parameters of the column.

$$A=a.V \qquad \text{----- 8.1}$$

$$a=\frac{6x}{d_{32}} \qquad \text{----2.6}$$

Consequently, the specific interfacial area can be increased by reduction of d_{32} ie selection of a smaller plate hole size or a higher velocity. This decrease in d_{32} will be accompanied by a simultaneous increase in the dispersed phase hold-up, x, hence further enhancing 'a'. For a given set of feed and solvent compositions, ΔC is mainly influenced by the macroscopic flow of both phases in the column. The largest possible value is reached under ideal flow conditions, ie no axial mixing. An approach to ideal flow conditions, would be associated with division of the column into many sections by the sieve plates to reduce axial mixing. This would also improve performance by the re-generation of new interface at each sieve plate.

9.3 Design Recommendations

The following should be aimed for in the design of the SPC,

(a) Provision for reasonably-homogeneous distribution of each phase across any cross-section. This requires the maximum number of holes to be functional in the distributor and in each plate

(b) Generation of a large interfacial area per unit volume i.e 0.164m^2/m^3 (Appendix 10).

(c) The maximum height of the coalesced layer beneath the sieve plates must be less than the downcomer length (the minimum downcomer length recommended is twice the coalescence height [295]).

(d) Operation in the jetting regime ie operation above the minimum jetting velocity, to ensure a minimum head of coalesced layer under any plate and the functioning of the majority of holes. For this purpose the minimum jetting velocity can be predicted from Equation 7.8.

(e) Any number of plates can be used provided the continuous phase inlet is on the opposite side to the downcomer on the next plate, and the outlet is preferably positioned to allow cross-flow over the inlet distributor.

(f) Avoidance of erratic operation, which restricts phase flowrates to 50-70% of those at flooding. The flooding condition could be predicted from Equation 7.4.

(g) The plate material and column walls should be preferentially wetted by the continuous phase.(Section 9.5)

(h) The sieve plates should be as flat as praticable when inserted into the column. Any cross-stubs inserted into larger columns to achieve this should be of similar material to the plates, to avoid the creation of high and low surface energy junctions which could promote coalescence and lead to a distortion in the flocculation zone height . They should be spaced 10mm from the nearest row of sieve plate holes. Materials of construction should obviously be corrosion resistant.

(i) Provision of man, or hand, holes between each pairs of plates along the column for cleaning and maintenance.

9.4 Pilot-Scale Testing and Scale-Up

The recommended procedure for the design of the sieve plate column is as follows,

(1) Calculate the flooding or maximum operating phase velocities corresponding to the required phase ratio, hence select a practical operating value ie 50-70% of flooding and determine the column cross-section.

(2) A mass transfer calculation fundamental procedure can be used involving equations 2.1, 8.1 and 2.6. This involves prediction of x and hence, knowing d_{32}, A_i for each stage. The appropriate K, be calculated as already outlined, can be used to calculate N_{Ai} for each stage. Calculate the rate of mass transfer achievable in each individual stage N_{Ai} using the appropriate values of K_i, A_i, ΔC_i. Sum N_{Ai} ---->N_A and hence find the numbe of stages of known height, to give the total column height.

(3) The design of the column internals should be such that similar dispersion can be maintained in the pilot and full scale ie hole size, free area and plate spacing. When these cannot be met simultaneously a compromise is necessary.

Scale-up of the SPC is on the assumption that the stage efficiency is independent of diameter. This is normally satisfactory provided that the plates are accurately aligned and plate holes completely sealed by the layer of coalesced dispersed phase beneath the plate.

The SPC when properly designed and operated is not subject to axial mixing. For a simple cross-flow sieve plate, with the relatively large ratios of column diameter to plate spacing on an industrial scale, plate efficiency may be expected to increase on scale-up, owing to the longer flow path of the continuous phase.

The mass transfer efficiency in the SPC is slightly dependent on the cross-flow of the continuous phase and mainly on the distance the drop swarms have to travel before coalescence . The ratio of plate spacing to column diameter incorporates both these factors and hence constitutes an important scale-up factor.

Once the above calculation (1-3) has been performed using pilot-scale data, the following factors should be maintained constant on the industrial scale:

(a) Flow ratio or extraction factor.

(b) The total throughput per m^2 of column. ie total flowrate per m^2 of the dispersed phase and continuous phase through the column.

(c) Drop size distribution ie similar plate hole size, and probably the same fractional free area or ratio of plate spacing to column diameter. The continuous phase flowrate per m^2 in the downcomer should remain constant.

9.5 Design of Column Internals

(a) The sieve plates upper surfaces should probably be hydrophobic when water is dispersed and hydrophilic when organic liquid is dispersed. [Alternatively,based upon single nozzle observations, more even utilisation of available holes may be achieved if the undersides of the plates were treated to render them dispersed phase wetted.]

(b) The sieve plate hole diameters should be in the range 1.2 to 8mm, located on square, triangular or circular pitch. The pitch size should be at least three times the hole diameter.

(c) A free area of 55-60% is desirable and the sieve plate thickness should normally be > 1.5mm, to ensure rigidity.

(d) In industrial columns the distributor should be divided into four or more equal quadrants which are individually fed. Alternatively, the volume beneath the distributor plate may be packed with knitted -mesh or raschig rings which are preferentially wetted by the dispersed phase, so that a coalesced layer is maintained and evenly spread beneath the distributor.

(e) The downcomer length must be greater than the the coalescence height, h_t. A minimum of twice h_t is recommended but for flexibility in operation (e.g in cases where the column may be used with alternative liquid-liquid systems.) five times h_t is appropriate.

(f) The plate spacing has to be optimised to maximise throughput and extraction efficiency. A plate spacing equal 10 to 12 times the coalescence height, h_t is recommended for industrial columns.

9.6 DESIGN FLOW DIAGRAM

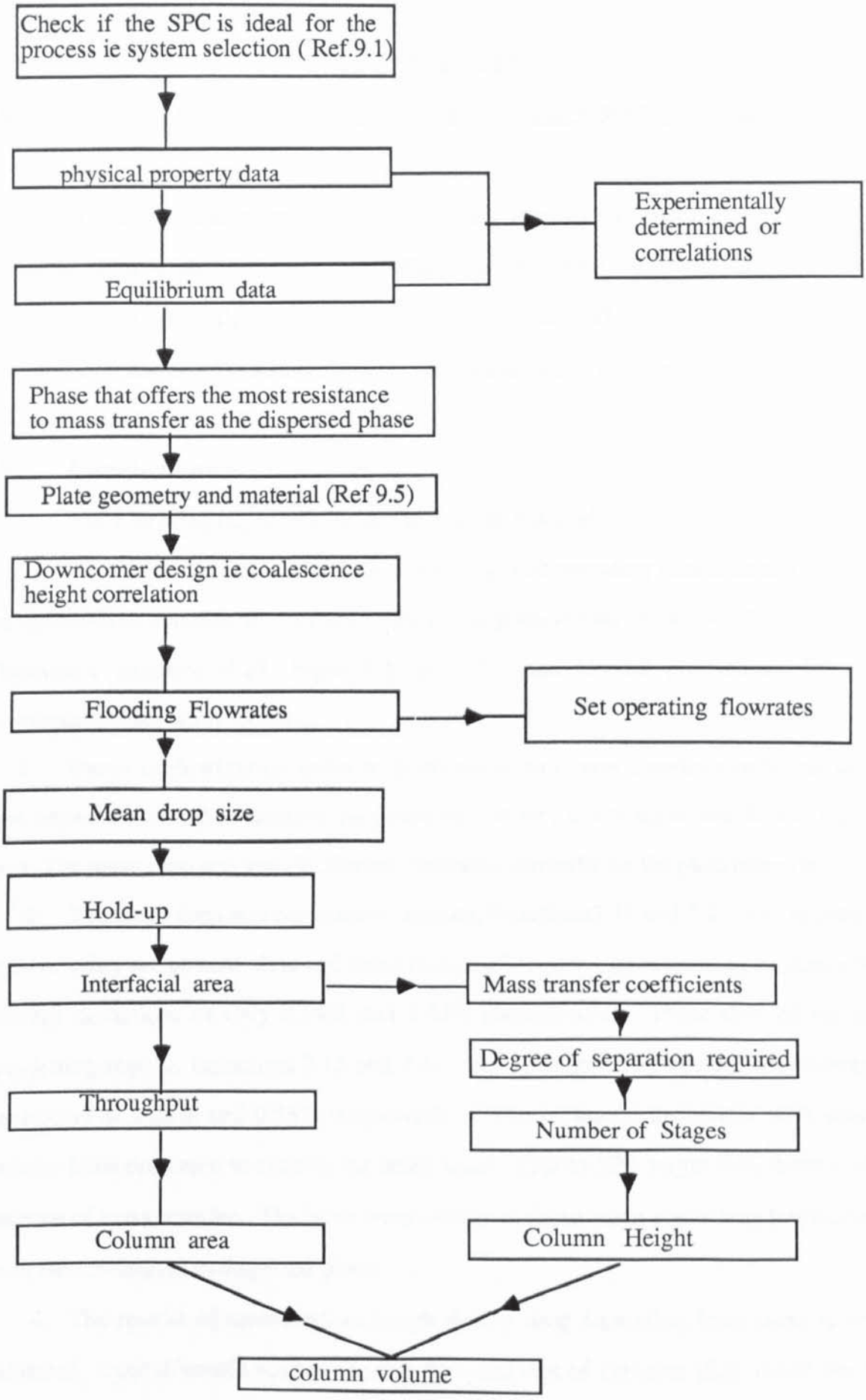

CHAPTER TEN

10 CONCLUSIONS AND RECOMMENDATION

A study of the hydrodynamics and mass transfer characteristics of a 0.45m diameter, 2.3m high pilot scale Sieve Plate Column(SPC), with variable geometry, stainless steel internals was satisfactorily concluded. The test system used was Clairsol'350' (dispersed) - acetone(solute) - deionised water (continuous).

10.1 Conclusions

The following major conclusions arise from this study:

1. Operation just below flooding point is the best operating condition and ensures the operation of majority of the plate holes. It also gives the best mass transfer efficiency. Thornton's equation 4.29, Figure7.2, provided the closest predictions for the experimental hold-up at flooding.

2. Dropsize distribution under hydrodynamic and mass transfer conditions were best represented by the functions proposed by Gal-or , and Mugele and Evans Upper limit. The mean drop size and distribution depended markedly on the plate hole size.

3. The mean drop size correlations derived, Equations7.11 and 7.12 for the jetting regime, using the present data and those from the literature, gave good agreement with average deviations of only 0.54% and 2.52% respectively. Those derived for the non-jetting regime, Equations 7.13 and 7.14, also gave good agreement with average deviations of 1.22% and 0.58% respectively. The measured drop sizes with solute transfer from dispersed to continuous phase were 20% to 30% larger than those in the absence of mass transfer. The latter were similar to those when solute was transferring from the continuous to dispersed phase.

4. The results of measured jet length during drop formation from sieve plates, exhibited a considerable scatter. Present data and that of Dawodu [52] could not be

correlated. However, in this jetting regime a majority of the plate holes functioned satisfactorily.

5. The hold-up correlation Equation 7.15 derived using the present data and those in the literature correlated the data with an average deviation of $\pm$ 9%. It offers a more direct procedure for the prediction of hold-up, than via the characteristic velocity approach. The characteristic velocity increased with either an increase in plate hole size or a decrease in plate spacing. The dispersed phase hold-up was generally greater, by an order of 20-30% , under mass transfer conditions.

6. Dispersed phase recirculation was completely eliminated at a plate spacing of 20cm. An increase in mass transfer coefficient was achievable as the plate spacing was reduced from 34 to 20cm; further reductions showed no improvement. Typical plate spacings used in commercial columns are 15-60cm.

7. The coalescence height, h_t correlation Equation 7.9 derived using the present data and those from the literature fitted the results with an average deviation of $\pm$ 10%. As would be expected h_t decreased with an increase in plate hole size, but increased with increase in the superficial velocity of either phase.

8. Comparison between the experimentally determined dropsizes and dropsize distributions from the 3.175 and 6.35mm hole size plates, indicated that the 3.175 plate generated a more uniform distribution. Virtually all the drops from the 6.35mm plates were in the oscillating regime. However, the experimentally determined overall mass transfer coefficient values were, for all practical purposes, generally similar for both plates.

9. A comparison was made between the experimental and calculated overall mass transfer coefficients for cases in which all the drops were in the oscillating regime, and with solute transfer from the dispersed to continuous phase. Better agreement was generally obtained when the overall coefficient was based upon the dispersed phase film coefficient of Rose-Kintner[238] in combination with the continuous phase film

coefficient of Garner-Tayeban[78].

10. The droplets from the 3.175mm hole size plate were of a size to include both the circulating and oscillating regimes. In using the proportion of drops in each regime with the respective single drop correlations to calculate the theoretical overall mass transfer coefficients, better agreement was obtained with the combination of the dispersed phase film coefficients from Kronig-Brink (circulating)[150] and Angelo-Lightfoot (oscillating)[7], and continuous phase film coefficients from Garner-Foord- Tayeban (circulating)[74] and Angelo-Lightfoot (oscillating)[7].

Application of the dropsize distribution was shown to give a better representation of mass transfer than the mean drop size, d_{32} for the 3.175mm hole size plate. Analysis with the individual mass transfer coefficients related to the respective dropsize fraction, is recommended as the best method of calculating the overall mass transfer coefficients from existing single drop models. However, numerous limitations are applicable to these models as outlined in Chapter 8.

10.2 Recommendations For Further Work

The following areas could usefully be studied;

1. To extend the investigation with the existing SPC, covering a plate spacing of 34 to 20cm and using only the 3.175 and 6.35mm hole size plates, to cover a range of interfacial tension systems. [A study has therefore been initiated using a medium interfacial tension system ie xylene (dispersed) - acetone (solute) - deionised water (continuous) σ=26.5mN/m.]

2. To study the performance of the SPC with the organic solvent as the continuous phase and deionised water as the dispersed phase and inverting the plates and downcomers ie downcomers become risers(upcomers),with a polypropylene (i.e organic wetted) distributor plate located at the top of the column.

3. To obtain more flooding data, with various plate geometries in order to establish

a graphical flooding correlation, indicating the flooding range and preferred operating range for the SPC.

4. The inlet bottom distributor should be divided into four or more equal quadrants which are individually fed. Alternatively the volume beneath the distributor plate may be packed with knitted-mesh or raschig rings which are preferentially wetted by the dispersed phase, so that a coalesced layer is maintained and evenly spread beneath the distributor

5. To investigate the advantages likely to result from the use of novel sieve plate designs of the type illustrated in Figure 10.1. In this design more homogeneous mixing of the phases would be accomplished by the continuous phase assisting lateral distribution of the dispersed phase. The concentration driving force within any stage should be more even.

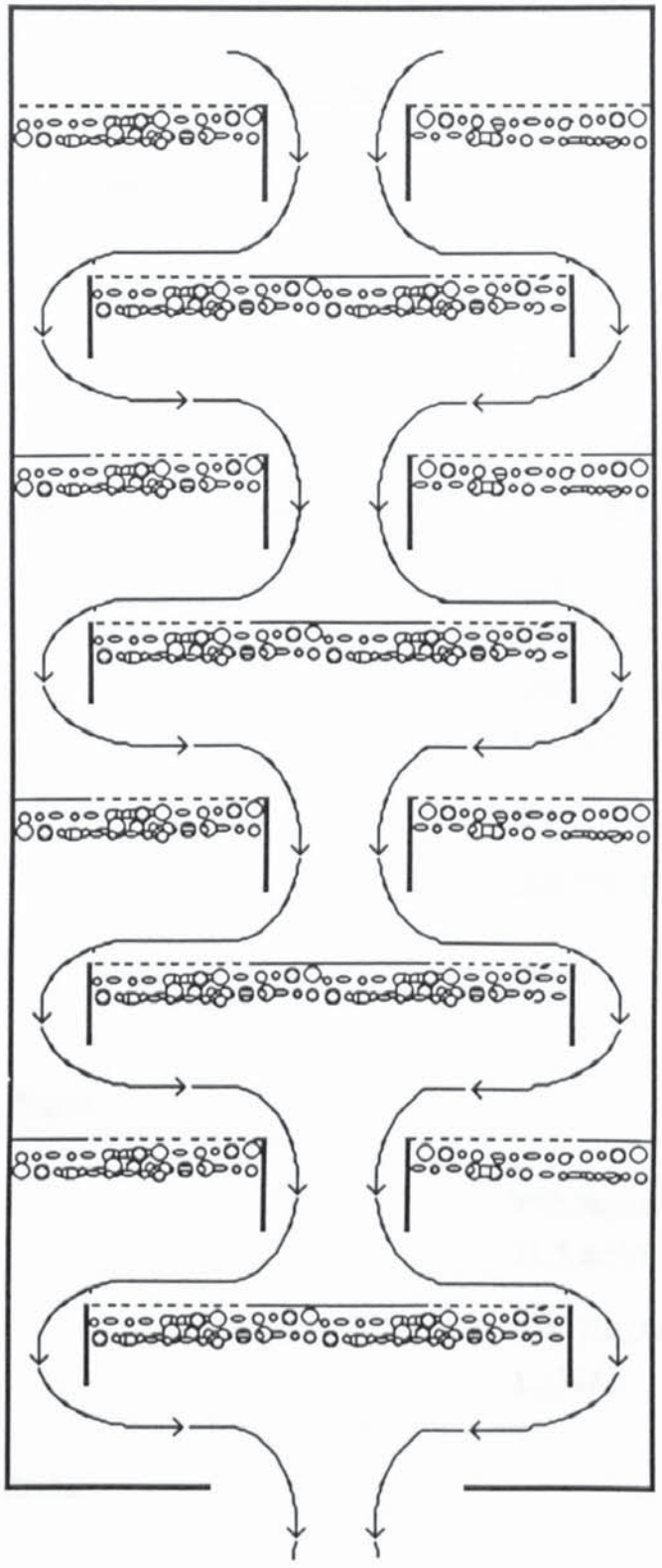

Figure 10.1 Novel Sieve Plate Column
(Constant Downcomer Flow Area)

APPENDIX 1

System physical properties

1 Clairsol-350 (industrial grade)

Density	783kg/m^3 at 20°C
Surface Tension	26.7mN/m at 20°C
Interfacial Tension with de-ionised water	35.5mN/m at 20°C
Kinematic viscosity	0.00023kg/ms at 20°C
Refractive Index	1.43920
Average Molecular Weight	160-170 kg/kg mole
Aromatic content	0.1(% w/w)
Flash Point	71°C
Boiling Range	205-230°C

2 De-ionised Water

Density	998.3kg/m^3
Surface Tension	71.5 mN/m
Kinematic Viscosity	0.0001kg/ms at 20°C
Refractive Index	1.3326

3 Acetone - Analar

Density	789-791kg/m^3 at 20°C
Boiling Range(95%)	56.0-56.6°C

APPENDIX 2

Derivation of the dimensionless groups for coalescence height, h_t

$$h_t = f(u_n, u_c, d_n, \sigma, g, \Delta\rho, \mu_c, \mu_d)$$

Applying Buckingham pi theorem and taking μ_c, σ and d_n as the three primary parameters i.e recurring sets

$$\mu_c \equiv M L^{-1} T^{-1}$$

$$\sigma \equiv M T^{-2}$$

$$d_n \equiv L$$

Each of the dimensions M,L,T are then obtained explicitly in terms of the variables:

$$L = d_n$$

$$M = \rho_c d_n^{3}$$

$$T = \rho_c^{1/2} d_n^{3/2} \sigma^{-1/2}$$

$$\Pi_1 = \frac{h_t}{\mu_c^{a1} \sigma^{b1} d_n^{c1}}$$

$$h_t = L$$

$\therefore h_t (L^{-1})$ is therefore dimensionless

$$\Pi_1 = h_t d_n^{-1}$$

$$\therefore \Pi_1 = \frac{h_t}{d_n}$$

$$\Pi_2 = \frac{U_n}{\mu_c^{a2} \sigma^{b2} d_n^{c2}}$$

$$U_n = L T^{-1}$$

$\therefore U_n (L^{-1}T)$ is therefore dimensionless

$$\Pi_2 = U_n d_n^{-1} \rho_c^{1/2} d_n^{3/2} \sigma^{-1/2}$$

$$\therefore \Pi_2 = \frac{U_n^{2} \rho_c d_n}{\sigma}$$

$$\Pi_3 = \frac{U_c}{\mu_c^{a3}\sigma^{b3}d_n^{c3}}$$

$$u_c = LT^{-1}$$

$\therefore u_c(L^{-1}T)$ is therefore dimensionless

$$\Pi_3 = U_c d_n^{-1}\rho_c^{1/2}d_n^{3/2}\sigma^{-1/2}$$

$$\therefore \Pi_3 = \frac{U_c\rho_c d_n}{\sigma}$$

$$\Pi_4 = \frac{g}{\mu_c^{a4}\sigma^{b4}d_n^{c4}}$$

$$g = LT^{-2}$$

$\therefore g\ (L^{-1}T^{-2})$ is therefore dimensionless

$$\Pi_4 = g d_n^{-1}\rho_c d_n^{3}\sigma^{-1}$$

$$\therefore \Pi_4 = \frac{g\rho_c d_n^2}{\sigma}$$

$$\Pi_5 = \frac{\Delta\rho}{\mu_c^{a5}\sigma^{b5}d_n^{c5}}$$

$$\Delta\rho = ML^{-3}$$

$\therefore \Delta\rho\ (M^{-1}L^{3})$ is therefore dimensionless

$$\Pi_5 = \Delta\rho\rho_c^{-1}d_n^{-3}d_n^{3}$$

$$\therefore \Pi_5 = \frac{\Delta\rho}{\rho_c}$$

$$\Pi_6 = \frac{\mu_d}{\mu_c^{a6}\sigma^{b6}d_n^{c6}}$$

$$\mu_d = ML^{-1}T^{-1}$$

$\therefore \mu_d(M^{-1}LT)$ is therefore dimensionless

$$\Pi_6 = \mu_d \rho_c^{-1} d_n^{-3} d_n \rho_c^{-1/2} d_n^{3/2} \sigma^{1/2}$$

$$\therefore \Pi_6 = \frac{\mu_d^2}{\rho_c d_n \sigma}$$

$$\therefore \frac{h_t}{d_n} = \left[\frac{U_n^2 \rho_c d}{\sigma}\right]^a \left[\frac{U_c^2 \rho_c d_n}{\sigma}\right]^b \left[\frac{g \rho_c d_n^2}{\sigma}\right]^c \left[\frac{\Delta\rho}{\rho}\right]^d \left[\frac{\mu_d^2}{\rho_c d_n \sigma}\right]^e$$

Using this theorem, as a result of the selection of recurring sets, this would be inapplicable to a wide variation in μ_c.

APPENDIX3

Program Description For Multilinear Regression

The program used for the multiple linear regression consists of a short MAIN program,the subroutine LINREG, and the subroutine SIMQ. All the data are supplied through the MAIN program and functions of X are set up (equation 7.3 chapter 7)

Subroutine LINREG sets up the normal equations and prints out the results.Subroutine SIMQ solves the normal (linear algebraic) equations.

Subroutines required

Subroutine LINREG [X,Y,N,M,A,B,XBAR,YHAT,AA,N2]
called from the main program ,sets up normal equations and performs test.
subroutine SIMQ [A,B,N,KS,NS]
called from LINREG,solves for the `A` vector of the coefficient.

Description of parameters

NA- Number of unknown coefficients minus one,also number of functions of X(NA≥2)
NX- Number of independent variables
M - Number of data points
X - Matrix of independent variables
Y - Vector of dependent variables

Dimension requirements

The dimension statement in the MAIN program should be modified according to the requirements of each particular problem.The parameters included in the following dimension statement conform to the input parameter

DIMENSION X(M,NA),Y(M),A[(NA)^2],B(NA),XBAR(NA),YHAT(M),AA(NA,NA)

APPENDIX 3

```
C ***************************************************************
C *          PROGRAM FOR MULTI-LINEAR REGRESSION ANALYSIS       *
C ***************************************************************
```

```
 1: C      PROGRAM FOR MULTIPLE LINREG ANALYSIS
 2:        DIMENSION X(M,N),Y(M),A(N2),B(N),XBAR(N),YHAT(M),AA(N,N)
 3:        OPEN(2,FILE= 'REGA')
 4:        OPEN(4,FILE= 'REGA1')
 5: C      10=INPUT  FILE
 6: C      2=OUTPUT  FILE (ALL PARAMETERS)
 7: C      4=OUTPUT  FILE  (EXPERIMENTAL AND REGRESSION VALUES)
 8:
 9: C      NA=NUMBER OF UNKNOWN COEFFICIENTS MINUS ONE;ALSO NUMBER OF
10: C         FUNCTIONS OF X (NA GREATER OR EQUAL TO 2)
11: C      NX=NUMBER OF INDEPENDENT VARIABLES
12: C      M=NUMBER OF DATA POINTS
13:        NN=NA*NA
14:        IF (NA) 999,999,20
15:  20    DO 100 I=1,M
16:        READ(10,*) Y(I),(X(I,J),J=1,NX)
17:  100   CONTINUE
18: C      10=RESU
19:
20:
21: C           SECTION1*****SET UP FUNCTIONS****
22:
23:
24: C       LINEARISE DATA BY TAKING LOGS.
25:
26:
27:       DO 200 J=1,M
28:       Y(J)=ALOG(Y(J))
29:       X(J,1)=ALOG(X(J,1))
30:        X(J,2)=ALOG(X(J,2))
31:        X(J,3)=ALOG(X(J,3))
32:        X(J,4)=ALOG(X(J,4))
33:        X(J,5)=ALOG(X(J,5))
34:        X(J,6)=ALOG(X(J,6))
35:  200   CONTINUE
36:        CALL LINREG(X,Y,NA,M,A,B,XBAR,YHAT,AA,NN)
37:  999   STOP
38:        END
39:        SUBROUTINE LINREG(X,Y,N,M,A,B,XBAR,YHAT,AA,N2)
40:
41:        DIMENSION X(M,N),Y(M),A(N2),B(N),XBAR(N),YHAT(M),AA(N,N)
42:        WRITE(2,16)
43:  16    FORMAT(1H1,10X,36HMULTIPLE LINEAR REGRESSION ALGORITHM )
44:
45:
```

```
46: C            CALCULATE AVERAGE X AND Y VALUES
47:
48:          DO 205 I=1,N
49:          SUMX=0.0
50:          DO 206 J=1,M
51:   206    SUMX=SUMX+X(J,I)
52:   205    XBAR(I)=SUMX/FLOAT(M)
53:          SUMY=0.0
54:          DO 207 K=1,M
55:   207    SUMY=SUMY+Y(K)
56:          YBAR=SUMY/FLOAT(M)
57:          WRITE(2,17)
58:   17     FORMAT(//,2X,23HVARIABLE AVERAGE VALUES )
59:          WRITE(2,18) (II,XBAR(II),II=1,N)
60:   18     FORMAT(/,3(2X,5HXBAR(,I2,4H) = ,1PE14.7))
61:          WRITE(2,19) YBAR
62:   19     FORMAT(/,2X,7HYBAR= ,1PE14.7)
63:
64:
65: C            CALCULATE REGRESSION MATRICES
66:
67:
68:          KK=1
69:          DO 208 I=1,N
70:          DO 209 J=1,N
71:          SUMA=0.0
72:          SUMB=0.0
73:          DO 210 K=1,M
74:          SUMA=SUMA+(X(K,I)-XBAR(I))*(X(K,J)-XBAR(J))
75:   210    SUMB=SUMB+(Y(K)-YBAR)*(X(K,I)-XBAR(I))
76:          AA(I,J)=SUMA
77:          A(KK)=SUMA
78:          KK=KK+1
79:   209    B(I)=SUMB
80:   208    CONTINUE
81:          WRITE(2,191)
82:   191    FORMAT(//,10X,8HA MATRIX )
83:          DO 211 II=1,N
84:   211    WRITE (2,20) (AA(II,JJ),JJ=1,N)
85:   20     FORMAT(/,8(2X,E10.4))
86:          WRITE(2,21)
87:   21     FORMAT(//,10X,8HB MATRIX )
88:          WRITE(2,22) (B(KK),KK=1,N)
89:   22     FORMAT(/,8(2X,E10.4))
90: C            SOLVE REGRESSION MATRICES FOR COEFFICIENTS
91:
92:
94:          CALL SIMQ(A,B,N,KS,N2)
95:          SUMX=0.0
96:          DO 212 I=1,N
97:   212    SUMX=SUMX+B(I)*XBAR(I)
98:          AZERO=YBAR-SUMX
99:           WRITE(2,23)
100:  23      FORMAT(10X,37HVALUES OF THE REGRESSION COEFFICIENTS )
```

```
101:          WRITE(2,24)(JJ,B(JJ),JJ=1,N)
102:   24     FORMAT(/,2(2X,5HAHAT(,I2,4H) = ,1PE16.8,8X))
103:          WRITE(2,25)AZERO
104:   25     FORMAT(/,2X,8HAZERO= ,1PE16.8)
105:
106:
107: C        TAKE EXPONENTIAL OF THE CONSTANT
108:
109:          AHATO=EXP(AZERO)
110:          WRITE(2,26) AHATO
111:   26     FORMAT(/,2X,10HAHAT(0) = ,1PE16.8)
112:
113:
114: C              CALCULATE S AND R TEST
115:
116:
117:          STEST=0.0
118:          DO 213 J=1,M
119:          SUMS1=0.0
120:          DO 214 K=1,N
121:   214    SUMS1=SUMS1+B(K)*X(J,K)
122:          YHAT(J)=AZERO+SUMS1
123:          DIFF=(Y(J)-YHAT(J))**2
124:   213    STEST=STEST+DIFF
125:          SUMST=0.0
126:          DO 215 I=1,M
127:   215    SUMST=SUMST+(Y(I)-YBAR)**2
128:          SUMSR=SUMST-STEST
129:          RTEST=SUMSR/SUMST
130:          WRITE(2,27)
131:   27     FORMAT(////,5X,19HEXPERIMENTAL VALUES,18X
132:        *                ,17HREGRESSION VALUES )
133:          DO 516 KK=1,M
134:   516    WRITE(2,28)KK,Y(KK),KK,YHAT(KK)
135:   28      FORMAT(/,2X,2HY(,I3,4H)= ,1PE16.8,10X
136:        *              ,5HYHAT(,I3,4H)= ,1PE16.8)
137:         DO 517 KK=1,M
138:    517  WRITE(4,4) Y(KK),YHAT(KK)
139:   4     FORMAT(2X,1PE16.8,5X,1PE16.8)
140:          WRITE(2,29)SUMST,STEST,RTEST
141:   29     FORMAT(///,2X,8HSUMST= ,1PE16.8,/,2X,4HS= ,
142:        *             1PE16.8,10X,7HR**2= ,1PE16.8 )
143:          RETURN
144:          END
145:
146:
147:          SUBROUTINE SIMQ(A,B,N,KS,NS)
148: C
149:          DIMENSION A(NS),B(N)
150: C
151: C              FORWARD SOLUTION
152: C
153:          TOL=0.0
154:          KS=0
```

```
155:          JJ=-N
156:          DO 217 J=1,N
157:          JY=J+1
158:          JJ=JJ+N+1
159:          BIGA=0.0
160:          II=JJ-J
161:          DO 218 I=J,N
162:
163: C              SEARCH FOR MAXIMUM COEFFICIENT IN COLUMN
164:
165:
166:          IJ=II+I
167:          IF(ABS(BIGA)-ABS(A(IJ))) 20,218,218
168:   20     BIGA=A(IJ)
169:          IMAX=I
170:   218    CONTINUE
171:
172: C           TEST FOR PIVOT LESS THAN TOLERANCE (SING.MATRIX)
173:
174:          IF (ABS(BIGA)-TOL) 35,35,40
175:   35     KS=1
176:          RETURN
177: C
178: C                INTERCHANGE ROWS IF NECESSARY
179:
180:   40      II=J+N*(J-2)
181:           II=IMAX-J
182:           DO 50 K=J,N
183:           II=II+N
184:           I2=II+II
185:           SAVE=A(I1)
186:           A(I1)=A(I2)
187:           A(I2)=SAVE
188:
189: C              DIVIDE BY LEADING COEFFICIENT
190:   50      A(I1)=A(I1)/BIGA
191:           SAVE=B(IMAX)
192:           B(IMAX)=B(J)
193:           B(J)=SAVE/BIGA
194:
195: C              ELIMINATE NEXT VARIABLE
196:           IF(J-N) 57,70,57
197:   57      IQS=N*(J-1)
198:           DO 217 IX=JY,N
199:           IXJ=IQS+IX
200:           II=J-IX
201:           DO 60 JX=JY,N
202:           IXJX=N*(JX-1)+IX
203:           JJX=IXJX+II
204:   60      A(IXJX)=A(IXJX)-(A(IXJ)*A(JJX))
205:   217     B(IX)=B(IX)-(B(J)*A(IXJ))
206:
207: C              BACK SOLUTION
208:
```

```
209:   70     NY=N-1
210:          II=N*N
211:           DO 219 J=1,NY
212:           IA=II-J
213:           IB=N-J
214:           IC=N
215:          DO 219 K=1,J
216:          B(IB)=B(IB)-A(IA)*B(IC)
217:          IA=IA-N
218:  219     IC=IC-1
219:          RETURN
220:          END
```

APPENDIX 4

Dimensions of Sieve Plate Column internals and Tanks

Downcomer

Material of construction:	Stainless steel
Diameter:	318mm
Arc radius:	78mm
Thickness:	10mm
Height:	6-24mm

Tie Rod

Material of construction:	Stainless steel
No of rods:	4
Diameter:	6.35mm
Length:	2350mm

Tanks

Material of construction:	Stainless steel
Length:	913mm
Width:	913mm
Height:	1223mm
Thickness:	12mm
Volume:	$1.02m^3$

APPENDIX 5

DROP SIZE DISTRIBUTION TABLE (RUN NO. 12)

HYDRODYNAMICS

U_c = 0.34cm/s U_d = 0.43cm/s U_n = 6.81cm/s m=0.61

DO(mm)	DA(mm)	N	V	[V	[%V	DV/DD(1/mm)
0.86	1.41	2	3.0	3.0	0.0	0.001
1.05	1.72	2	5.4	8.4	0.0	0.005
1.23	2.02	9	39.3	47.7	0.2	0.013
1.42	2.33	16	107.4	155.0	0.6	0.026
1.60	2.62	22	211.2	366.2	1.3	0.036
1.78	2.92	22	290.8	657.0	2.4	0.067
1.97	3.23	32	573.4	1230.5	4.5	0.110
2.15	3.52	38	885.2	2115.6	7.7	0.099
2.34	3.84	28	840.9	2956.5	10.8	0.139
2.52	4.13	30	1125.2	4081.7	14.9	0.177
2.70	4.43	31	1430.1	5511.9	20.1	0.266
2.89	4.74	40	2263.0	7774.8	28.4	0.361
3.07	5.03	43	2916.1	10690.9	39.1	0.295
3.26	5.34	31	2517.3	13208.2	48.3	0.284
3.44	5.64	24	2289.9	15498.1	56.6	0.289
3.62	5.93	21	2334.9	17833.0	65.2	0.213
3.81	6.25	14	1814.8	19647.8	71.8	0.124
4.18	6.85	12	2054.2	21701.9	79.3	0.168
4.36	7.15	7	1359.8	23061.7	84.3	0.109
4.54	7.44	4	877.3	23939.1	87.5	0.087
4.73	7.75	3	744.1	24683.1	90.2	0.069
4.91	8.05	2	554.9	25238.0	92.2	0.109
5.10	8.36	3	932.7	26170.7	95.6	0.043
5.28	8.66	1	345.0	26515.8	96.9	0.047
5.46	8.95	1	381.5	26897.3	98.3	0.028
5.83	9.56	1	464.4	27361.7	100.0	0.105

Sauter mean diameter d_{32} = 5.3357

Total number of drops counted= 439

DO – Observed drop size

DA – Actual drop size

N – Number of drops

[V – Cummulative drop volume

m – Magnification

PAGE MISSING IN ORIGINAL

APPENDIX 6

```
C ***********************************************************************
C *PROGRAM TO CALCULATE DROP SIZE DISTRIBUTION DATA FROM PHOTOGRAPHS    *
C *COUNTED ON THE ZEISS TG3 PARTICLE SIZE ANALYSER                      *
C ***********************************************************************

 1: C      PROGRAM FOR DROPSIZE DISTRIBUTION
 2: C      M-MAGNIFICATION OF PHOTOGRAPH
 3: C      MN-NUMBER OF DIFFERENT DROP SIZES FROM PARTICLE ANALYSER
 4: C      Uc-CONTINUOUS PHASE(WATER) VELOCITY IN CM/S
 5: C      Ud-DISPERSED PHASE(CLAIRSOL) VELOCITY IN CM/S
 6: C      Un-DISPERSED PHASE VELOCITY BASED ON CORRECTED PLATE AREA
    C         IN CM/S
 7: C      DO-DROP DIAMETER FROM PATICLE ANALYSER IN MM
 8: C      DA-ACTUAL DROP DIAMETER IN MM
 9: C      V-DROP VOLUME(MM**3)
10: C      VT-CUMMULATIVE DROP VOLUME
11: C      VP-CUMMULATIVE DROP VOLUME %
12: C      DVD-VOLUME FRACTION (1/MM)
13:        REAL M,MGAL
14:        DIMENSION V(60),DV(60),DVD(60)
15:        DIMENSION DO(60),DA(60),N(60),VT(60),VP(60),D2(60),D3(60)0)
16:        OPEN(UNIT=5,FILE='DATA')
17:        OPEN(UNIT=20,FILE='RESULT')
18:        READ*,MN,M,Uc,Ud,Un
19:        READ (5,*)(DO(I),N(I),I=1,MN)
20:        FOR I = 1,MN
21:        DA(I)=DO(I)/M
22:        V(I)=0.532*N(I)*(DA(I)**3)
23: C      0.532=3.14/6
24:        VT(I)=VT(I-1)+V(I)
25:        END FOR
26:        VTOTAL = VT(MN)
27:        DO  20 I=1,MN
28:        VP(I)=(VT(I)/VTOTAL)*100.00
29:  20    CONTINUE
30:        DO 30 I=1,MN
31:        DVD(0)=0.0
32:        DVD(I)=((VP(I)/100.0)-(VP(I-1)/100.0))/(DA(I)-DA(I-1))
33:  30    CONTINUE
34:        DO 40 I=1,MN
35:        D2(I)=N(I)*DA(I)*DA(I)
36:        D2T=D2T+D2(I)
37:        D3(I)=N(I)*DA(I)*DA(I)*DA(I)
38:        D3T=D3T+D3(I)
39:  40    CONTINUE
40:        D32 = D3T/D2T
41:        DO 60 I=1,MN
42:        DV(I)=((N(I)*DA(I)**3))
43:        DVTOTAL=DVTOTAL+DV(I)
44:  60    CONTINUE
```

```
45:         DO 70 I=1,MN
46:         NTOTAL=NTOTAL+N(I)
47:   70    CONTINUE
48:         DVGAL =(DVTOTAL/NTOTAL)**(1.0/3)
49:         MGAL=1.148*DVGAL
50:         ALGAL=(4/(1.7725*DVGAL**3))**(2./3)
51:         WRITE(20,120)
52:   120   FORMAT(10X,'DROP SIZE DISTRIBUTION TABLE (RUN NO. 32)'    //
53:      +           15X,'HYDRODYNAMICS'///
54:      +           15X,'PLATE SPACING--340MM'//)
55:         WRITE(20,150)Uc,Ud,Un
56:   150   FORMAT(15X,'Uc=',F4.2,'CM/S',10X,'Ud=',F4.2,'CM/S',10X
57:      *,'Un=',F4.2,'CM/S'//)
58:         WRITE(*,130)
59:         WRITE(20,130)
60:   130   FORMAT(3X,'DO(MM)',3X,'DA(MM)',5X,'N',6X,'V',7X,'{V',8X'{%V'
61:      + 4X,'DV/DD(1/MM)')
62:         WRITE(*,140)
63:         WRITE(20,140)
64:   140   FORMAT(3X,'------',3X,'------',5X,'-',6X,'-',7X,'--',8X,'---
65:      + '----------')
66:         DO 50 I=1,MN
67:        WRITE(*,100) DO(I),DA(I),N(I),V(I),VT(I),VP(I),DVD(I)
68:        WRITE(20,100) DO(I),DA(I),N(I),V(I),VT(I),VP(I),DVD(I)
69:   50    CONTINUE
70:   100  FORMAT (3X,F5.2,4X,F5.2,5X,I2,2(2X,F7.1),2X,F7.1,7X,F5.3/)
71:         WRITE(*,200) D32
72:         WRITE(20,200) D32
73:   200   FORMAT (12X,'SAUTER MEAN DIAMETER (D32)=',F6.4/)
74:         WRITE(20,250) NTOTAL
76:   250   FORMAT(12X,'TOTAL NUMBER OF DROPS COUNTED=',I4/)
77:         REWIND(5)
78:         CLOSE(5)
79:         STOP
80:         END
```

APPENDIX 7

```
C ***************************************************************************
C     PROGRAM TO CALCULATE EXPERIMENTAL MASS TRANSFER COEFFICIENT
C ***************************************************************************

C     PROGRAM TO CALCULATE THE EXPERIMENTAL MASS TRANSFER COEFFICIENT
C     X-DISPERSED PHASE CONCENTRATION
C     Y-CONTINOUS PHASE CONCENTRATION
C     Y* -EQUILIBRIUM CONCENTRATION
C     Y*=8.8
C     XH-DISPERSED PHASE HOLD-UP
C     H-EFFECTIVE HEIGHT OF COLUMN
C     DL-HEIGHT OF DOWNCOMER
C     N-NUMBER OF DOWNCOMERS
C     D32-SAUTER MEAN DIAMETER
C     DELY-MEAN DRIVING FORCE
C     DELC-MEAN CONCENTRATION DRIVING FORCE
C     AC-AREA OF COLUMN
C     AD-AREA OF DOWNCOMER
C     A3-THE SPECIFIC INTERFACIAL AREA
C     A-TOTAL INTERFACIAL AREA
C     VD-VOLUMN OF DOWNCOMER
C     VC-VOLUMN OF COLUMN
C     VE-EFFECTIVE VOLUMN OF COLUMN
C     RHOC-DENSITY OF CONTINUS PHASE
C     N-RATE OF MASS TRANSFER
C     KOA-MASS TRANSFER COEFFICIENT BASED ON AREA
C     KOV-MASS TRANSFER COEFFICIENT BASED ON VOLUMN
      REAL KOA,KOV,Nc,Nd
      RHOC=0.9982
      RHOD=0.783
      AC=1590.43
      AD=312.65
      READ*,XN,XO,YN,YO,UC,UD,XH,D32,H,DL,N
      A1=(8.8*XN)-YO
      A2=(8.8*XO)-YN
      DELY=(A1-A2)/LOG(A1/A2)
      DELC=(DELY/100.0)/RHOC
      VC=AC*H
      VD=AD*DL*N
      VE=VC-VD
      A3=(6*XH)/D32
      A=A3*VE
      Nc=UC*AC*RHOC*((YO-YN)/100.0)
       Nd=UD*AC*RHOD*((XN-XO)/100.0)
      KOA=Nc/(A*DELC)
      KOV=Nc/(VE*DELC)
      PRINT*,"KOA= ",KOA
      PRINT*,"KOV= ",KOV
       PRINT*,"DELC= ",DELC
       PRINT*,"Nc= ",Nc
       PRINT*,"Nd= ",Nd
      STOP
      END
```

APPENDIX 8

```
C     ************************************************************************
C     *     PROGRAM TO CALCULATE THEORETICAL MASS TRANSFER COEFFICIENT
C     ************************************************************************


C       PROGRAM TO CAL THEO MASS TRAN COEFF
        REAL M,KDC,KCC,KCC1,KCC,KDCR,KDCA,KCO,KCCR1
        REAL KCCR,KCCA,KDCH,KCCH1,KCCH,KCH
        READ*,DCC,DO,US
        M=8.8
        DD=1.37E-5
        DC=1.10E-5
        VISC=0.011
        VISD=0.018
        DEND=0.783
        DENC=0.998
        GA=35.5
        N=2
        R=DO/2.0
        B=(DO**0.225)/1.242
        PI=3.14
        RE1=(DCC*US*DENC)/VISC
        RE2=(DO*US*DENC)/VISC
        SC=VISC/(DENC*DC)
        W=(((GA*B)/R**3.0)*(N*(N-1)*(N+1)*(N+2))/(((N+1)*DEND)+(N*DENC)
       + **0.5
        E=(0.434)*(((W*DO)/US)**(-0.46))*(((DO*(US**2.0)*DENC)/GA)
       + **(-0.53))*(((VISC*US)/GA)**(-0.11))
C
C
C       KDC-----KRONIG AND BRINKS
C
        KDC=(17.9*DD)/DCC
C
C
C       KDCH----HANDLOS AND BARON
C
C
        KDCH=(0.00375*US)/(1+(VISD/VISC))
C
C       KCC--KD FOR THE CIRCULATING DROP REGIME FOR THE
C            GARNER-FOORD TAYEBAN(1959)
C       KCH--KC FOR THE HANDLOS AND BARON CORRELATION
C
        KCH=((4*DC*US)/(PI*DCC))**0.5
        KCC=(DC*(-126.0+(1.8*(RE1**0.5)*(SC**0.42))))/DCC
        KCC1=(1.0/KDC)+(M/KCC)
C
C       KCC---OVERALL M.T.C FOR THE CIRCULATING DROP REGIME FOR THE
C             KRONIG-BRINK AND GARNER-FOORD-TAYEBAN
C
C
```

```
      KOC=1.0/KOC1
C
C
C     KOCH---OVERALL M.T.C FOR THE CIRCULATING DROP REGIME FOR THE
C             HANDLOS-BARON AND GARNER-FOORD-TAYEBAN
C
C
      KOCH1=(1.0/KDCH)+(M/KCH)
      KOCH=1.0/KOCH1
C
C
C     OSCILLATING DROP REGIME
C     KDOR---ROSE AND KINTER
C
C
C     KDOA---ANGELO ET AL
C
C
      KDOR=0.45*((DD*W)**0.5)
      KDOA=(4*DD*W*(1+E+((3.0/8.0)*E*E))/PI)**0.5
C
C     KCO-----KD FOR THE OSCILLATING DROP REGIME FOR THE
C             GARNER AND TAYEBAN(1960) CORRERELATION
C
      KCO=(DC/DO)*(50+(0.0085*RE2*(SC**0.7)))
      KOOR1=(1/KDOR)+(M/KCO)
C
C     KOOR--OVERALL M.T.C FOR THE OSCILLATING DROP REGIME FOR THE
C           ROSE AND KINTNER,AND GARNER AND TAYEBAN
C
      KOOR=(1.0/KOOR1)
C
C
C     KOOA--OVERALL M.T.C FOR THE OSCILLATING DROP REGIME FOR THE
C           ANGELO AND LIGHTFOOT, AND GARNER AND TAYEBAN
C
C
      KOOA=KDOA*(1/(1+(M*((DD/DC)**0.5))))
      PRINT*,"W= ",W
      PRINT*,"E= ",E
      PRINT*,"KDC= ",KDC
      PRINT*,"KCC= ",KCC
      PRINT*,"KCH= ",KCH
      PRINT*,"KOCH= ",KOCH
      PRINT*,"KOC= ",KOC
      PRINT*,"KDOR= ",KDOR
      PRINT*,"KDOA= ",KDOA
      PRINT*,"KCO= ",KCO
      PRINT*,"KOOR= ",KOOR
      PRINT*,"KOOA= ",KOOA
      STOP
      END
```

APPENDIX 9

Calculation of the mean drop sizes and distribution parameters for the Log-normal, Mugele-Evans (Upper-Limit) and Gal-or distribution functions.

Log-normal

Example based on Run 12. From graph (Appendix 5)

d_{10}=3.75mm d_{50}=5.5mm $d_{84.14}$=7.1mm d_{90}=7.6mm

Geometric standard deviation, $S_G = \frac{d_{84.14}}{d_{50}} = \frac{7.1}{5.5} = 1.291$

Volume-Surface (Sauter) mean diameter is given as

$$\ln d_{32} = \ln d_{gm} + 2.5 \ln^2 S_G$$

$$\ln d_{32} = \ln (5.5) + 2.5 \ln^2 (1.291)$$

$$\therefore d_{32} = 6.47\text{mm}$$

$$\sigma = \frac{0.394}{\log_{10} (d_{90}/d_{50})}$$

$$\sigma = \frac{0.394}{\log_{10} (7.6/5.5)}$$

$$\therefore \sigma = 2.81$$

Mugele-Evans (Upper-Limit)

Example based on Run 12. From graph (Appendix 5)

d_{10}=3.75mm d_{50}=5.5mm d_{90}=7.6mm

maximum stable dropsize, d_m

$$\frac{d_m}{d_{50}} = \frac{d_{50} (d^{90} + d_{10}) - 2 d_{90} d_{10}}{d^2_{50} - d_{90} d_{10}}$$

$$\frac{d_m}{5.5} = \frac{5.5 (7.6 + 3.75) - 2 \times 7.6 \times 3.75}{(5.5)^2 - 7.6 \times 3.75}$$

$\therefore d_m = 17.06$

Skewness parameter, $a' = \dfrac{d_m - d_{50}}{d_{50}}$

$$a' = \frac{17.06 - 5.5}{5.5}$$

$$a' = 2.1$$

Uniformity parameter, σ

$$\sigma = \frac{0.907}{\ln [(d_{90}/d_m - d_{90}).(d_m - d_{50}/d_{50})]}$$

$$\sigma = \frac{0.907}{\ln [(7.6/17.06 - 7.6).(17.06 - 5.5/5.5)]}$$

$\therefore \sigma = 1.73$

$$d_{32} = \frac{d_m}{1 + a' \exp^{(1/4\sigma.\sigma)}}$$

$$d_{32} = \frac{17.06}{1 + 2.1 \exp^{(0.0835)}}$$

$\therefore d_{32} = 5.2mm$

Gal-or

Using the cummulative distribution, example based on Run 12, tabulated in Appendix5

$$y_V = \frac{(\Sigma y_i n_i)}{N} = \frac{(\Sigma N_i \times D_A)}{439}$$

$y_V = 4.08$

$d_{32} = 1.148 \times 4.08$

$d_{32} = 4.68mm$

APPENDIX 10

Calculation of experimental mass transfer coefficient

Example based on Run 19 (Computer program in Appendix 7)

U_c=0.34cm/s U_d=0.36cm/s hold-up, x =0.021 H_e=170cm d_{32}=0.769cm

$y^*=8.8x$, where 8.8 is the slope of the equilibrium line (figure6.7)

The mean concentration driving force, ΔC_m was estimated from Equation 8.2

$$\Delta C_m = \frac{[mX_{out} - Y_{in}] - [mX_{in} - Y_{out}]}{\ln\left[\frac{mX_{out} - Y_{in}}{mX_{in} - Y_{out}}\right]} \qquad \text{----- 8.2}$$

x_{in} =3.5 x_{out}= 2.0 y_{in} =0.0 y_{out} =1.26 (gm/100gm Sol.)

$$\Delta C_m = \frac{[(8.8 \times 2.0) - 0.0] - [(8.8 \times 3.5) - 1.26]}{\ln\left[\frac{[(8.8 \times 2.0) - 0.0]}{[(8.8 \times 3.5) - 1.26]}\right]}$$

ΔC_m=23.057 (gm Acetone/100gm aqu. Sol.)

or

ΔC_m=0.23057 (gm/gm Sol.)

Density of aqueous phase =0.9982gm/cm^3

ΔC_m=0.23057 /0.9982 gm Acetone/cm^3 Sol.

ΔC_m=0.23 gm Acetone/ cm^3 Sol.

Effective volume of the column =H_e x A_c

$$=170 \times (\pi/4) \times (45)^2$$

$$=270373.3\text{cm}^3$$

where A_c= cross-sectional area of the column.

Total downcomer volume, V_D= AD x DL x N

AD=Area of downcomer

DL=Length of downcomer

N = Number of downcomers

V_D= 312.65 x 20 x 4

V_D=25012 cm^3

Actual effective volume of column = 270373.3 - 25012

=243361.3cm^3

The specific interfacial area a= $6x/d_{32}$

$\therefore$ a= 6 x 0.021/ 0.769

a=0.164cm^2/cm^3

Total interfacial area A= a.V

A= 245361.3 x 0.164

A= 40202.24cm^2

Rate of mass transfer, $N=Q_c\rho_c(y_{out} - y_{in}) = Q_d\rho_d(x_{in} - x_{out})$

or

$$N=U_cA_c\rho_c(y_{out} - y_{in}) = U_dA_c\rho_d(x_{in} - x_{out})$$

N=0.34 x 1590.43 x 0.9882 [(1.26-0.0)/100]

N=6.81gm/s

$K_{expt} = N/A(\Delta C_m)$

K_{expt} = 6.81/40202.24 x 0.23 cm/s

K_{expt} =7.32 x 10^{-4} cm/s

APPENDIX 11

CALCULATION OF THEORETICAL MASS TRANSFER COEFFICIENT

Computer Program in Appendix 8

Example based on Run 71

The slip velocity was estimated by applying equation 4.20

$$U_s = \frac{U_d}{x} + \frac{U_c}{1-x} \qquad \text{----4.20}$$

$$U_s = \frac{0.43}{0.051} + \frac{0.30}{1-0.051}$$

$\therefore U_s = 8.8 cm/s$

The maximum diameter of stagnant drops d_s, in the whole drop population was found by setting Re=10

$$Re = \frac{d_s U_s \rho_c}{\mu_c} = 10$$

$$\therefore d_s = \frac{10 \times 0.01}{0.783 \times 8.8}$$

$d_s = 0.15 cm$

The maximum diameter of oscillating drops d_o, in the whole drop population was found by setting Re=200

$$\therefore d_s = \frac{200 \times 0.01}{0.783 \times 8.8}$$

$d_o = 0.29 cm$

From the cummulative drop size diagram, Figure 7.14, the drop size for the stagnant drop d_s was found to be too small to be included in the calculation. Hence, the drop population is considered to contain only circulating and oscillating drop regimes. From Figure 7.14, the fractional proportion of circulating and oscillating drop regimes is

$P_c = 0.044$ $\qquad$ $P_o = 1-0.044 = 0.956$

Circulating drop regime

(a) Dispersed phase mass transfer coefficient was estimated from the Handlos and Baron model (95)

$$k_{d.c} = \frac{0.00375U_s}{1 + \mu_c/\mu_d}$$

$$k_{d.c} = \frac{0.00375 \times 8.8}{1 + 0.18/0.11}$$

$$k_{d.c} = 0.0125 \text{ cm/s}$$

(b) Dispersed phase mass transfer coefficient was estimated by Kronig and Brink (150)

$$k_{d.c} = \frac{17.9 \times D_d}{d_c}$$

$\bar{d}_c = 0.26$ from the distribution diagram, Figure 7.14

$$k_{d.c} = \frac{17.9 \times 1.375 \times 10^{-5}}{0.26}$$

$$k_{d.c} = 9.45 \times 10^{-4} \text{ cm/s}$$

Continuous phase mass transfer coefficient was estimated by Garner *et al* (74)

$$Sh = -126 + 1.8Re^{0.5}Sc^{0.42}$$

where $$Re = \frac{d_s U_s \rho_c}{\mu_c}$$

$$Sh = \frac{k_{c.c}\,\bar{d}}{D_c}$$

$$Sc = \frac{\mu_c}{\rho_c D_c}$$

$$\frac{k_{c.c} \times 0.26}{1.1 \times 10^{-5}} = -126 + 1.8\left[\frac{(0.998 \times 8.8 \times 0.26)}{0.01}\right]^{0.5}\left[\frac{0.001}{0.988 \times 1.1 \times 10^{-5}}\right]^{0.42}$$

$k_{c.c}$= 3.44 x 10^{-4} cm/s.

overall mass transfer coefficient

$$\frac{1}{K_{o.c}} = \frac{1}{k_{d.c}} + \frac{m}{k_{c.c}}$$

Handlos and Baron , $K_{o.c}$ =3.89 x 10^{-5} cm/s

Kronig and Brink , $K_{o.c}$ = 3.75 x 10^{-5} cm/s

Oscillating drop regime

(a) Dispersed phase coefficient was firstly estimated by Rose and Kintner(238)

$$k_{d.o} = 0.45(D_d\omega)^{0.5}$$

$$\omega = \frac{\sigma b}{r^3}\left[\frac{n(n-1)(n+1)(n+2)}{(n+1)\rho_d + n\rho_c}\right] \qquad \text{------8.15}$$

r=drop radius

n=2

b=Constant depending on drop size, $b=\bar{d}_o^{0.225}/1.242$

From Figure 7.14 d_o=0.6cm

$\therefore b=(0.6)^{0.225}/1.242$

$\therefore b=0.717$

$r^3=(0.6/2)^3=0.27$

$$\omega^2 = \frac{35.5 \times 0.717}{0.027}\left[\frac{2(1)(3)(4)}{(3 \times 0.783) + (2 \times 0.998)}\right]$$

$\omega = 72.16\ s^{-1}$

$k_{d.o} = 0.45\ (1.37 \times 10^{-5})$

$k_{d.o}$=1.42 x 10^{-2} cm/s

continuous phase mass transfer film coefficient was estimated by Garner and Tayeban (78)

$Sh=50 + 0.0085\ Re(Sc)^{0.7}$

$$\frac{k_{c.o} \times 0.6}{1.1 \times 10^{-5}} = 50 + 0.0085\left[\frac{0.998 \times 8.8 \times 0.6}{0.01}\right]\left[\frac{0.01}{0.998 \times 1.1 \times 10^{-5}}\right]$$

$$\therefore k_{c.o} = 1.06 \times 10^{-2} \text{ cm/s}$$

overall mass transfer coefficient

$$\frac{1}{K_{o.o}} = \frac{1}{k_{d.o}} + \frac{m}{k_{c.o}}$$

$$\frac{1}{K_{o.o}} = \frac{1}{0.0142} + \frac{8.8}{0.016}$$

$$K_{o.o} = 1.1 \times 10^{-3} \text{ cm/s}$$

(b) Angelo *et al* (8)

$$k_{d.o} = K_{o.o}\ K_{o.o}\sqrt{(4 \times D_d (1+\varepsilon_o))/\pi}$$

where $\varepsilon_o = \varepsilon + 3/8\ \varepsilon^2$

ε, the eccentricity , is estimated by Al-Hassan's correlation[4] as,

$$\varepsilon = 0.434\left[\frac{\omega\ \bar{\bar{d}}_o}{U_s}\right]^{-0.46}\left[\frac{\bar{\bar{d}}_o U_s^2 \rho_c}{\sigma}\right]^{-0.53}\left[\frac{\mu_c\ U_s}{\sigma}\right]^{-0.11} \qquad \text{-----8.16}$$

$$\varepsilon = 0.434\left[\frac{72.16 \times 0.6}{8.8}\right]^{-0.46}\left[\frac{0.6 \times (8.8)^2 \times 0.998}{35.5}\right]^{-0.53}\left[\frac{0.01 \times 8.8}{35.5}\right]^{-0.11}$$

$\varepsilon = 0.349$

$\varepsilon_o = 0.35 + 3/8\ (0.35)^2$

$\varepsilon_o = 0.395$

$$k_{d.o} = (4 \times 72.16 \times 1.37 \times 10^{-5}(1 + 0.395))/3.14$$

$k_{d.o} = 1.76 \times 10^{-3}$ cm/s

Overall mass transfer coefficient,

$K_{o.o} = k_{d.o}[\ 1/1 + m\sqrt{(D_d/D_c)}]$

$K_{o.o} = 1.76 \times 10^{-3}[\ 1/1 + 8.8\sqrt{(1.37 \times 10^{-5}/1.1 \times 10^{-5})}]$

$K_{o.o} = 1.47 \times 10^{-4}$ cm/s

Hence, the theoretical overall mass transfer coefficients for the whole drop population on the basis of volume fraction

$$K_{cal} = K_{oc}P_c + K_{oc}P_o$$

$$K_{cal} = K_{oc}P_c + K_{oc}(1-P_c)$$

(1) For Handlos and Baron, Rose and Kintner, and Garner *et al*

$$K_{cal} = (6.45 \times 10^{-4} \times 0.044) + (0.956 \times 1.1 \times 10^{-3})$$

$$K_{cal} = 1.078 \times 10^{-3} \text{ cm/s}$$

(2) For Kronig and Brink, Rose and Kintner, and Garner *et al*

$$K_{cal} = (4.71 \times 10^{-4} \times 0.044) + (0.956 \times 1.1 \times 10^{-3})$$

$$K_{cal} = 1.076 \times 10^{-3} \text{ cm/s}$$

(3) For Handlos and Baron,and Angelo *et al*

$$K_{cal} = (6.45 \times 10^{-4} \times 0.044) + (0.956 \times 1.47 \times 10^{-4})$$

$$K_{cal} = 1.689 \times 10^{-4} \text{ cm/s}$$

(4) For Kronig and Brink, and Angelo *et al*

$$K_{cal} = (4.71 \times 10^{-4} \times 0.044) + (0.956 \times 1.47 \times 10^{-4})$$

$$K_{cal} = 3.477 \times 10^{-5} \text{ cm/s}$$

APPENDIX 12

Calculation of the Slip-velocity using Olney's and Grace *et al*'s Correlations

Grace *et al*"s (84) correlation for the terminal velocity is

$$J = 0.94\, H^{0.757} \quad (2 < H \leq 59.3) \qquad \text{.... 4.14}$$

$$J = 3.42\, H^{0.441} \quad (H > 59.3) \qquad \text{.... 4.15}$$

where

$$H = \frac{4}{3} E_o M^{-0.149} \left[\frac{\mu_c}{\mu_w}\right]^{-0.14} \qquad \text{.... 4.16}$$

$$J = ReM^{0.149} + 0.857 \qquad \text{.... 4.17}$$

The terminal velocity is then given by

$$U_t = \left[\frac{\mu_c}{\rho_c d}\right] M^{-0.149} (J - 0.857) \qquad \text{.... 4.18}$$

Olney's[215] correlation for Slip velocity is;

$$U_s = U_t(1-x)$$

Example based on Run 67, x=0.029 and μ_w =0.0009 kg/ms

E_o is the Eotvos number, $\Delta\rho d^2 g/\sigma$

M is the Morton number, $\dfrac{g\mu^4 \Delta\rho}{\rho^2\sigma^3}$

$$H = 4/3 \left[\frac{9.81 \times (0.62 \times 10^{-2})^2 \times 215.2}{0.0355}\right]\left[\frac{9.81 \times (0.0011)^4 \times 215.2}{(998.2)^2 \times (0.0355)^3}\right]^{-0.149} \left[\frac{0.0011}{0.0009}\right]^{-0.14}$$

$\therefore H = 97.96$

$J = 3.42 \times (97.96)^{0.441} = 25.8$

$\therefore U_t = 13.98$cm/s

$\therefore U_s = U_t(1-x) = 13.98(1-0.029)$

U_s=13.6 cm/s (Experimental U_s=10.99cm/s)

PAPER PRESENTED AT RESEARCH MEETING OF THE SOCIETY OF CHEMICAL INDUSTRY, SOLVENT EXTRACTION AND ION-EXCHANGE GROUP, ASTON UNIVERSITY 5th. MAY 1985

THE HYDRODYNAMICS OF A PILOT SCALE SIEVE PLATE EXTRACTION COLUMN (SPC)

Oloidi, J.O. and Mumford, C.J.

Department of Chemical Engineering
Aston University
Birmingham B4 7ET
U.K.

Drop size distributions, hold-up, flooding phenomena and the effects of variation of plate spacing have been investigated in a 0.45m variable geometry sieve plate column.

Dispersed phase backmixing was reduced with decreased plate spacing in the range 38cm to 30cm. The characteristic velocity increased with increase in plate hole size or with decrease in plate spacing.

Droplet size distribution was best represented by the functions proposed by Gal-or and Mugele-Evans. A new correlation was derived for characteristic velocity, to enable the operating hold-up to be predicted.

INTRODUCTION

The sieve plate extraction column (SPC) is unique in providing repeated coalescence and redispersion of drops and offering advantages of crossflow of the continuous phase with little axial mixing (1), all of which are beneficial for mass transfer performance. However despite these features, relatively low efficiencies have been reported (2) and scale-up from laboratory data is unreliable.

In a study using a 450mm diameter, 2.3m high column with different plate designs Dawodu reported undesirable operating phenomena involving recirculation of drop swarms between adjacent plates, and a variation in droplet discharge mechanisms between different holes on the same plate [2,20]. Further drop-size distribution data, some effects of reduced plate spacing, and a new correlation for characteristic velocity - to enable hold-up prediction - are reported here.

Hold-up and characteristic/slip velocity

The interfacial area in an SPC is a function of both the hold-up and drop size distribution generated in each stage. The latter also determines the mode of mass transfer (3). The hold-up comprises the static hold-up (the volume of the dispersed phase coalesced under the plates); and the operating hold-up (the volume of the dispersed drops suspended in the continuous phase).

The static hold-up is one of the measures of the flow capacity of the column. The greater the static hold-up, the nearer the column is to the flooding condition. It also affects mass transfer in determining the distance the drops travel before coalescing beneath the next plate.

The interfacial area of contact is given by,

$$a = \frac{6x}{d_{32}}, \text{ where } x = \text{operational hold-up} \quad (1)$$

$$d_{32} = \frac{\Sigma\, nd^3}{\Sigma\, nd^2}, \text{ where } n = \text{number of drops} \quad (2)$$

The operational hold-up, x, is the ratio of the volume of the dispersed phase droplets to the effective volume of the column.

$$x = \frac{(\text{Total hold-up} - A \sum_{1}^{n} h)}{(\text{Total Volume} - A \sum_{1}^{n} h)} \quad (3)$$

where n = number of plates.

Thornton (4) correlated the hold-up and the superficial velocities of the two phases in a spray column by the equation.

$$U_s = \frac{U_d}{x} + \frac{U_c}{1-x} \quad (4)$$

and several equations have been used to correlate hold-up data:

$U_s = U_o (1-x)$ Thornton (5) (5)

$U_s = U_o \exp(-bx_1)$ Letan and Kehat (6) (6)

$U_s = U_o(1-x)\exp(-(4.19-Z)x)$ Misek (7) (7)

$U_s = U_o(1-x)^m(1+cx)$ Slater (8) (8)

$U_s = U_o(1-x)^m$ Beyaert et al (9) (9)

where m is defined by the system physical properties and column geometry and U_s, the slip velocity, is the relative velocity between the two phases. U_o is the characteristic velocity defined as the hypothetical velocity of the drops when the continuous phase flowrate tends to zero. This may also be identified with the terminal velocity of a single drop having a mean diameter representing the drop ensemble (10).

Various empirical correlations have been proposed for U_s:

$$U_s = \frac{1-x}{K^{2/3} x^{1/3}} \, d_{32} \left[\frac{g^2 \Delta\rho}{\rho_c \mu_c}\right]^{1/3} \quad (12) \quad (10)$$

K = 15 for circulating drops
K = 30 for rigid drops

$$U_s = [2.725 \times g \, d_{32} \frac{\Delta\rho}{\rho_c} \left(\frac{1-x}{1+x^{1/3}}\right)^{1.834}]^{0.5} \qquad (22) \qquad (11)$$

Combination of equation 4 with equations 5-9, has been useful in correlating hold-up with phase flowrates, provided a suitable correlation for estimating U_o is available for the counter-current extraction column (11).

Flooding

For each flowrate of one of the phases in a gravity operated extraction column there is a maximum possible flowrate for the other, governed by the system physical properties and column internal design. If the flowrate of either phase is increased beyond this point, it would be rejected by the column; this is termed flooding. Thornton (4) correlated this maximum operating condition by combining equations 4 and 5, to give.

$$U_o(1-x) = \frac{U_d}{x} + \frac{U_c}{1-x} \qquad (12)$$

which on differentiation gives,

$$U_{df} = 2U_o x_f^2 (1-x_f) \qquad (13)$$

$$U_{cf} = U_o(1-x_f)(1-x_f)^2 \qquad (14)$$

Combining equation 13 and 14,

$$x_f = \frac{(R^2 + 8R)^{0.5} - 3R}{4(1-R)} \qquad (15)$$

$$R = \frac{U_{df}}{U_{cf}} \qquad (16)$$

By combining equation 4 and 9,

$$x_f = \frac{-R\,(m+2) + (R^2(m+2)^2 + 4\,(1-R)(m+1)R)^{0.5}}{2\,(1-R)\,(m+1)} \qquad (17)$$

Recently, Baird and Shen (12) proposed

$$x_f = \frac{(9R^2 + 54R + 1)^{0.5} - 7R - 1}{10(1-R)} \qquad (18)$$

Some unfavourable flow characteristics likely to be associated with high volumetric throughputs include excessive entrainment of liquid drops, overloading of the downcomers and restriction of flow through the plate holes.

Drop Size Distribution

The drop size distribution under operating conditions influences both the hydrodynamics and mass transfer performance. From a knowledge of the mean drop size d_{32} an idealised approach enables the rate of solute transfer N to be calculated.

$$N = K.A.\ \Delta\ C. \qquad (19)$$

where $A = a.V.$

In practice a wide distribution of dropsize exists in extraction columns, because of breakage and coalescence of drops. Extensive investigations (3,7,13-20) on the laboratory and pilot scales have indicated the important features that size distribution will affect, viz residence time distribution of the dispersed phase, and a tendency to reduce the proportion of oscillating and circulating drops - and hence a lowering of extraction efficiency compared with predictions based on an assumed mean drop size.

Various functions have been used to represent drop size distributions produced from different types of drop generating equipment. The main characteristics of the distribution equations used in liquid-liquid extraction calculations are summarised in Table 1. Whilst a useful summary has been published of the distribution functions applied to particles (solids or liquid), (18) only one detailed description is available of dropsize distribution in the SPC (20). Previous investigations have been confined to d_{32}.

The validity of the distribution function can be tested by comparing the volume fraction predicted by the distribution function to the experimental volume fraction for the same size range over the entire distribution range, or by comparing the experimental d_{32}, equation 2, with that calculated from each distribution function in Table 1.

EXPERIMENTAL INVESTIGATION

The extractor comprised a 450mm diameter, 2305mm high industrial glass-column. The flow diagram is shown in Figure 1. The complete pilot plant comprised the column, four $1.0m^3$ stainless steel tanks, transfer pumps, flow controls and instruments. Process contact parts were of glass, stainless steel or p.t.f.e.

The plate layouts selected are summarised in Table 2 and one arrangement is shown in Figure 2.

Table 1 DISTRIBUTION FUNCTIONS

Distribution	Function	Mean Diameter d_{32}
Log-normal	$\frac{dv}{dy} = \frac{\delta}{\sqrt{\pi}} \exp(-\delta^2 y^2)$; $y = \ln \frac{d}{d_{gm}}$ (20) $\delta = \frac{0.394}{\log 10(\frac{d_{90}}{d_{gm}})}$	$d_{32} = \exp(\ln d_{gm} + 2.5 \ln^2 S_G)$ (21) $S_G = d_{84.14}/d_{50}$ (22)
Mugele - Evans upper limit (15)	$\frac{dv}{dy} = \frac{\delta}{\sqrt{\pi}} \exp(-\delta^2 y^2)$; $y = \ln \frac{a'd}{d_m - d}$ (23) Skewness parameter $a' = \frac{d_m - d_{50}}{d_{50}}$ (24) Uniformity parameter $\delta = \frac{0.907}{\ln(\frac{d_{90}}{d_m - d_{90}} \frac{d_m - d_{50}}{d_{50}})}$ (25) Maximum stable drop size, d_m $d_m = d_{50} (\frac{d_{50}(d_{90} + d_{10}) - 2d_{90}d_{10}}{d_{50}^2 - d_{90}d_{10}})$ (26)	$d_{32} = \frac{d_m}{1 + a' \exp^{0.25} \delta^2}$ (27)
Gal-or and Hoescher (14)	$\frac{dv}{dy} = 8 (\frac{\delta}{\pi})^3 y^2 (\exp - \delta y^2)^{0.5}$; $y = d$ (28) $\delta = (\frac{4}{\sqrt{\pi}} y_v^3)^{2/3}$; $y_v = (\frac{\Sigma n_i y_i}{N})^{1/3}$ (29)	$d_{32} = 1.148\, y_v$ (30)
Rosin - Rammler (23)	$\frac{dv}{dy} = \frac{\delta (y)^{\delta - 1}}{(y)^{\delta}} \exp(-\frac{y}{\bar{y}})$; (31) $\frac{y}{\bar{y}} = d$ = value of y at 36.8% on the Rosin - Rammler graph plot	$d_{32} = \frac{\bar{y}}{\Gamma(1 - \frac{1}{\delta})}$ (32)

Table 2 Plate Layout Details

Hole Type	Plate Thickness (mm)	Hole Size (mm)	Numer of Holes Per Plate
Drilled	3.175	1.587	1517
Drilled	3.175	3.175	985
Drilled then punched	1.587	4.763	550
Drilled then punched	1.587	6.350	380

These were chosen because industrial columns are based on hole sizes between 1.588 and 6.350mm (1). For the 6.350mm plate, with plate spacing of 380,340 and 300mm, the dispersed phase superficial velocity based on corrected plate hole area was in the range 2.66 to 8.56cm/s.

De-ionised water constituted the continuous phase. This was obtained by passing mains water through an Elgastat B224 de-ioniser. The de-ionised water had a density of 998.2 kg/m^3 and a viscosity of 0.0011 kg/ms. The dispersed phase was Clairsol '350', a parafinic hydrocarbon solvent with a distillation range of 205 to 230^{o}C. The physical properties were: density 783 kg/m^3, viscosity 0.0018 kg/ms and interfacial tension 35.5mN/m (dyne/cm).

Activated carbon filters were used to remove any surfactant contamination from each phase.

Experimental method

Prior to each experiment, the column internals, storage tanks and flow lines were cleaned using an aqueous solution of 100ml Decon 90 per 20 litres of water; this was followed by repeated thorough draining and rinsing with warm water followed by de-ionised water. Frequent checks were made to ensure freedom from impurities or residual cleansing agent.

The phases were mutually saturated by extended recirculation through the equipment for about 30 minutes. The temperature of the Flameproof Pilot Plant in which the SPC was located remained fairly constant at 20^{o}C $\pm$ 0.5^{o}C.

Droplet hydrodynamics were studied over a range of phase throughputs corresponding to U_c = 0 to 0.82 cm/s and U_d = 0 to 0.65cm/s at plate hole size 6.35mm.

Measurements were made of (i) mean drop size and the distribution from each compartment at high and low phases flowrates, and subsequently in a 'representative' compartment (ii) flooding points at each plate spacing (iii) operating and local hold-up, and (iv) flocculation zone height beneath each plate. Only work with a mutually saturated system (ie in the absence of mass transfer) is reported in detail here, although passing reference is made to later observations in experiments in which acetone was transferred from the dispersed to continuous phase.

To determine the flooding point the flow rate of one phase was increased incrementally whilst the other was held constant. A period of 5 minutes was allowed after each adjustment to allow steady-state to be attained. Flooding was characterised, in the type of column studied in this work, by a rapid increse in the flocculating layer beneath the top interface causing it to move down the column. (ie the interface cannot be maintained).

Under steady-state operation (at flowrates corresponding to 70%, 65%, 60% and 55% of the U_d flooding point) the static hold-up was measured by noting the heights of the coalesced dispersion layer beneath each plate. The total hold-up was measured by simultaneously cutting off the phase flows to and from the column by rapidly closing the appropriate values.

The Clairsol was then allowed to settle completely, and the heights of coalesced layer under each plate noted. Equation 3 was then applied to calculate the operational hold-up x.

Measurements were also made of local hold-up by rapidly removing about 250ml of the dispersion from the sampling point in each compartment after steady state had been reached. After settling the dispersed phase content of each sample was found volumetrically.

Dropsize measurement and photographic analysis

The photographic study of dropsize distribution involved the simple photographic technique suggested by Damon et al (21) together with additional frontal lighting. Photographs were taken of the droplet swarm using a Nikkormat FTN 35mm camera with a 55mm Micro-Nikkor lens and exposures of approximately 0.02 sec. Appropriate correction factors were applied for distortion and magnification effects (20). A Carl-Zeiss particle analyser was used to analyse the photographs; d_{32} was calculated from equation 2. The number of drops measured for each flowrate and compartment varied from 350 to 900, but this was reduced to 200 to 500 taking the second compartment as the representative to be photographed. Drop counts were made from two or three replicate photographs for most of the runs. Typical photographs are reproduced as Fig. 3. Only drops with $d_1/d_2 < 2$ were included in the counts, where d_1 and d_2 are the true diameters of the major and minor axes respectively.

DISCUSSION OF RESULTS

Experimental Observations

All the holes in the distributor and plates, did not function at low flowrates but an acceptable dropsize distribution was produced. However since the phenomena of starved holes resulted in higher nozzle velocities than calculated, a correction was applied based on experimental observation of the number of holes working. As in previous work [20] it was convenient to define several 'superficial velocities',

U_C'' - continuous phase superficial velocity based on downcorner area.

U_D'' - Dispersed phase superficial velocity based on total plate hole area.

U_D' - Dispersed phase superficial velocity based on corrected plate hole area.

U_C - Continuous phase superficial velocity based on column cross sectional area.

U_D - Dispersed phase superficial velocity based on column cross sectional area.

Jetting occurred from the majority of active holes over the whole range of U_D values with longer jet lengths corresponding to mass transfer

conditions. Thus practical column operation will always be in the 'jetting' regime.

An undesirable feature of operation was the swarming of drops via a central core of the column [20] resulting in poorly contacted continuous phase passage around the periphery, and recirculation of this swarm, ie dispersed phase back-mixing. This feature illustrated in Figure 3, was found to decrease as the plate spacing was reduced in the range 38cm to 30cm.

Hold-up and Characteristic/Slip Velocity

The experimental hold-up data, Table 3, was used to calculate the characteristic velocity, U_o according to equation 12. This equation indicates that a plot of $(U_d + U_c \frac{x}{1-x})$ versus $x(1-x)$ should have a slope equivalent to U_o. This plot is illustrated for 3 different plate spacings in figure 4. As the spacing decreases from 38 to 30cm there is an appreciable change in U_o from 22.44 to 38.75cm/s and the straight line gradually changes to a curvilinear. This is attributable to the smaller residence time of the drops with decrease of plate spacing.

The variation of U_o with plate hole size is shown in Figure 5. This demonstrates an increase of U_o with increase in plate hole size, since U_o is influenced by dropsize which varies with the velocity of the dispersed phase at the nozzle outlet. As the hole size increases , the mean drop size also increases resulting in higher rise velocity and reduced residence time of the drops.

In view of the variations shown in Figures 4 and 5, a general correlation was derived between characteristic velocity U_o and plate spacing, plate hole diameter, velocity through the plate holes and the system physical properties. Assuming that

$$f(U_o, U_D', d_n, \sigma, \Delta\rho, \mu_c, \rho_c, g, H_c) = 0$$

Using the Buckingham's II - theorem, gives,

$$\frac{U_o \rho_c d_n}{\mu_c} = K \left(\frac{\sigma \rho_c d_n}{\mu_c^2}\right)^a \left(\frac{g \rho_c^2 d_n^3}{\mu_c^2}\right)^b \left(\frac{\Delta\rho}{\rho_c}\right)^c \left(\frac{H_c}{d_n}\right)^d \left(\frac{U_D' \rho_c d_n}{\mu_c}\right)^e \left(\frac{D_c}{d_N}\right)^f \quad (33)$$

Exponents a to f and constant K were determined by multiple regression analysis using the experimental data (Table 3) to give,

$$\frac{U_o \rho_c d_n}{\mu_c} = 1.73 \times 10^{-23} \left(\frac{\sigma \rho_c d_n}{\mu_c^2}\right)^{2.104} \left(\frac{g \rho_c^2 d_n^3}{\mu_c}\right)^{2.173 \times 10^{-9}}$$

$$\left(\frac{\Delta\rho}{\rho_c}\right)^{-15.98} \left(\frac{H_c}{d_n}\right)^{0.386} \left(\frac{U_D' \rho_c d_n}{\mu_c}\right)^{1.41} \left(\frac{D_c}{d_n}\right)^{2.1 \times 10^{-6}} \qquad (34)$$

The exponents on the composite groups $\left(\frac{g \rho_c^2 d_n^3}{\mu_c^2}\right)$ and $\left(\frac{D_c}{d_n}\right)$ are low and can therefore be discarded to give,

$$\frac{U_o \rho_c d_n}{\mu_c} = 1.73 \times 10^{-23} \left(\frac{\sigma\rho_c d_n}{\mu_c^2}\right)^{2.1} \left(\frac{\Delta\rho}{\rho_c}\right)^{-1.59} \left(\frac{H_c}{d_n}\right)^{0.4} \left(\frac{U_D' \rho_c d_n}{\mu_c}\right)^{1.4} \qquad (35)$$

A comparison between the experimental and regression values of U_o is shown in Figure 7 and shows an average percent error of $\pm$ 7%. 83% of the data were correlated within $\pm$ 20%.

Drop Size Distribution

Droplets ranging from 0.7mm to 9.5mm diameter were observed. Larger drops in the range 1.52mm to 12.60mm were subsequently observed with mass transfer (dispersed to continuous phase). The existence of a maximum dropsize in extraction columns led to the modification of the log-normal distribution function (equation 20, table 1) by Mugele and Evans (15), whose distribution function is specified with three parameters d_m, δ and a'. The parameter d_m can be considered as the maximum dropsize in the dispersion, but is normally adjusted to improve the accuracy of the representation of the experimental data. The index δ determines the spread of the distribution, a smaller value indicating a wider range of drop sizes. a' is the skewness parameter; a value of a' greater than unity indicates a wider range of drops of sizes larger than d_{50}. The ratio of d_{32}/d_{50} (Table 4) ranges from 0.91-0.98 and is within the range to be expected for dispersions [15]

Table 4 Distribution parameters in the SPC for Plate Hole Size 0.635cm

Function	Distribution Parameters			
log-normal	d_{gm}	δ		
	4.4-7.2	2.9-3.5		
Mugele - Evans (15)	δ	a'	d_m	d_{32}/d_{50}
	1.01-2.76	0.8-8.0	9.1-96.0	0.91-0.98
Gal-or and Hoescher (14)	δ			
	0.04-0.12			
Rosin-Rammler (23)	δ	$\bar{y}$		
	4.00-7.2	5.0-7.8		

The general procedure to derive the functions was to determine the parameters such as d_{10}, d_{50}, $d_{84.14}$, d_{90}, a', δ , d_m, y_v directly from the data or plot on a log-probability paper, and y and δ (Rosin-Rammler) from plot on Rosin-Rammler paper. Figure 8 shows the plot of the drop size distribution functions. [The Rosin-Rammler was out of range and was disregarded].

The experimental d_{32} values were compared to those calculated by the distribution functions as shown in Figure 9. The log-normal shows a deviation of 25 $\pm$ %, Mugele - Evans a deviation of $\pm$ 15.6% and Gal-or a deviation of $\pm$ 2.8%.

Typical experimental results of the variation of mean dropsize (equation 2) along the column at high and low flowrates are shown in Figure 10. These demonstrate a gradual reduction in drop size with height and the approach to a stable drop size. [This is under further study down to a plate spacing of 26cm). As expected drop size decreased with dispersed phase flowrate.

The inadequacy of the log-normal distribution function and the deviation of its d_{32} was clearly demonstrated in other plots of the data. The Mugele-Evans and Gal-or functions gave a reasonable representation of the experimental data.

There were a large number of small diameter droplets (<2.5mm) but these accounted for a relatively small proportion (3-8 volume %) of the drop size distribution. However these could account for a large interfacial area and their contribution to mass transfer should not be neglected.

Flooding

The different flooding equations 15-18 are compared and plotted in Figure 6 and the present experimental points indicated. Clearly the agreement is poor and a unique flooding correlation is to be developed for the SPC.

CONCLUSIONS

Analysis of the hold-up data indicates that the characteristic velocity U_o increased with an increase in plate hole size or a decrease in plate spacing. The correlation

$$\frac{U_o \rho_c d_n}{\mu_c} = 1.73 \times 10^{-23} \left(\frac{\rho_c d_n}{\mu_c^2}\right)^{2.1} \left(\frac{\Delta\rho}{\rho_c}\right)^{-1.59} \left(\frac{H_c}{d_n}\right)^{0.4} \left(\frac{U_D' \rho_c d_n}{\mu_c}\right)^{1.4}$$

shows an average percent error of $\pm$ 7% between the experimental and predicted results.

Reduction of plate spacing from 38cm to 30cm significantly reduced the dispersed phase back-mixing. Any advantage of further reduction in spacing and the corresponding improvements in extraction efficiency are being investigated.

The drop size distributions were found to fit the Mugele-Evans upper limit and Gal-or function better than the log-normal. The Gal-or Sauter mean diameter equations predicted the experimental d_{32} better within $\pm$ 2.8%.

Acknowledgements

The authors wish to express appreciation to Professor G. V. Jeffreys under whose direction this work was undertaken. One of them (J.O.O.) would like to thank Aston University for support in the form of a studentship.

CJM/wgo/Papers Disc

REFERENCES

1. Treybal, R.E.
   Liquid Extraction, McGraw-Hill, 2nd Ed. (1963)

2. Dawodu, F.A.,
   Ph.D. Thesis, University of Aston, 1983

3. Jeffreys, G.V., Al-Asward, K.K.M. and Mumford, C.J.,
   Separation Science and Technology 16(9), 1217, (1981).

4. Thornton, J.D.
   Chem. Eng. Sci., 5, 201, (1956).

5. Thornton, J.D.
   Trans. Inst. Chem. Engrs. 31, 290 (1953).

6. Letan, R. and Kehat, E.
   A. I. Ch. E. J. 13(3), 445 (1967).

7. Misek, T. and Marek, J.,
   Brit. Chem. Eng. 15, 202 (1970).

8. Slater, M.J.
   Chemie Ing. Technik, 46(15), 663, 1974.

9. Beyaert, B.O., Lapidus, L. and Elgins, J.C.
   A. I. Ch. E. J. 7(1), 46, 1961.

10. Vedaiyan, S., Dagellesan, C.E. and Laddha, G.S.
    Ind. JL. Tech. 12(4), 135, (1974).

11. Logsdail, D.H., Thornton, J.D. and Pratt, H.R.C.
    Tran. Inst. Chem. Eng., 35, 305, (1957).

12. Baird, M.H.I. and Shen, Z.J.
    Can. JL. Chem. Eng. 62(2), 218 (1984).

13. Chartes, R.H. and Korchinsky, W.J.
    Trans. Inst. Chem. Eng. 56,91 (1978)

14. Gal-or, B and Hoescher H.E.
    A. I. Ch. E. J. 12, 499 (1966).

15. Mugele, R.A. and Evans, H.D.
    Ind. Eng. Chem. 43(6), 1317, (1951).

16. Olney, R.B.
    A. I. Ch. E. J. 10, 827 (1964).

17. Cruz-Pinto, J.J.C. and Korchinsky, W.J.
    Chem. Eng. Sci. 35, 2213, (1980)

18. Khemangkorn, V., Muratet, G. and Angelino, H.
Proc. ISEC 1971 (Hague).

19. Giles, J.G., Hanson, C. and Marsland, J.
Proc. ISEC 1971 (Hague).

20. Dawodu, F.A., Mumford, C.J. and Jeffreys, G.V.
I. Chem. Eng. Sym. 88, 153 (1984).

21. Damon, K.G., Angelo, J.B. and Dark, R.W.
Chem. Eng. Sci. 21, 813 (1966).

22. Kumar, A, Votira, D.K., Hartland, S.
Can. JL. Chem. Eng. 58, 154, (1980).

23. Rosin, P. and Rammler, E.
JL. Inst. of Fuel 7, 29, (1933).

NOMENCLATURE

A	Interfacial area, m^2.
a	Surface area per unit volume, m^2/m^3.
ΔC	Concentration difference, $Kmol/m^3$.
b,c	Constants.
d_{gm}	geometric mean diameter, m.
d_{32}	Volume-surface of sauter, mean diameter, m.
d_n	Plate hole diameter, m.
g	Acceleration due to gravity, m/s^2.
K	Overall mass transfer coefficient, m/s.
H_c	Compartment height or plate spacing, m.
N	Rate of solute transfer, Kmol/s.
u_c	Continuous phase superficial velocity, m/s.
u_D	Dispersed phase superficial velocity, m/s.
u_o	Characteristic velocity, m/s.
u_s	Slip velocity, m/s.
V^s	Volume, m^3
x	Fractional hold-up of dispersed phase.
x_f	Fractional hold-up of dispersed phase at flooding.
Z	Coalescence factor.

Greek Letters

μ	Viscosity, Kg/ms.
ρ	Density, Kg/m^3.
σ	Interfacial tension, mN/m (dyne/cm).

Subscripts

C	Continuous
d	Dispersed
N	Nozzle

Table 3 Experimental Hold-up Data

Run No.	Plate Hole Size (cm)	U c (cm/s)	U D (cm/s)	U'D (cm/s)	Hold-up %	Hc (cm)
1	0.1588	0.27	0.18	11.12	5.28	38
2	0.1588	0.27	0.33	16.41	7.91	38
3	0.1588	0.27	0.41	22.76	9.60	38
4	0.1588	0.27	0.54	29.64	12.81	38
5	0.1588	0.44	0.25	14.29	6.22	38
6	0.1588	0.44	0.41	22.76	9.35	38
7	0.1588	0.44	0.54	29.64	11.65	38
8	0.3175	0.27	0.18	4.49	2.50	38
9	0.3175	0.27	0.33	6.45	3.81	38
10	0.3175	0.27	0.41	8.77	4.70	38
11	0.3175	0.27	0.54	11.42	5.60	38
12	0.3175	0.44	0.25	5.79	3.00	38
13	0.3175	0.44	0.41	8.77	4.60	38
14	0.3175	0.44	0.54	11.42	5.26	38
15	0.4763	0.27	0.18	3.90	0.78	38
16	0.4763	0.27	0.33	5.28	1.45	38
17	0.4763	0.27	0.54	9.08	2.57	38
18	0.4763	0.44	0.41	6.98	1.65	38
19	0.4763	0.44	0.54	9.08	2.51	38
20	0.6350	0.27	0.18	3.72	0.69	38
21	0.6350	0.27	0.33	5.20	1.33	38
22	0.6350	0.27	0.54	7.40	2.41	38
23	0.6350	0.44	0.41	6.30	1.63	38
24	0.6350	0.44	0.54	7.40	2.39	38
25	0.6350	0.34	0.36	5.58	0.71	34
26	0.6350	0.34	0.43	6.30	1.1	34
27	0.6350	0.34	0.52	6.81	1.4	34
28	0.6350	0.34	0.65	8.56	1.7	34
29	0.6350	0.58	0.36	5.58	0.8	34
30	0.6350	0.58	0.43	6.30	0.10	34
31	0.6350	0.58	0.52	6.81	1.5	34
32	0.6350	0.58	0.65	8.56	2.1	34
33	0.6350	0.34	0.36	5.58	0.55	30
34	0.6350	0.34	0.43	6.30	0.83	30
35	0.6350	0.34	0.52	6.81	1.10	30
36	0.6350	0.34	0.65	8.56	1.45	30
37	0.6350	0.58	0.36	5.58	0.61	30
38	0.6350	0.58	0.43	6.30	0.92	30
39	0.6350	0.58	0.52	6.81	1.21	30
40	0.6350	0.58	0.65	8.56	1.64	30
41	0.6350	0.34	0.13	1.66	0.21	30
42	0.6350	0.34	0.27	3.49	0.60	30

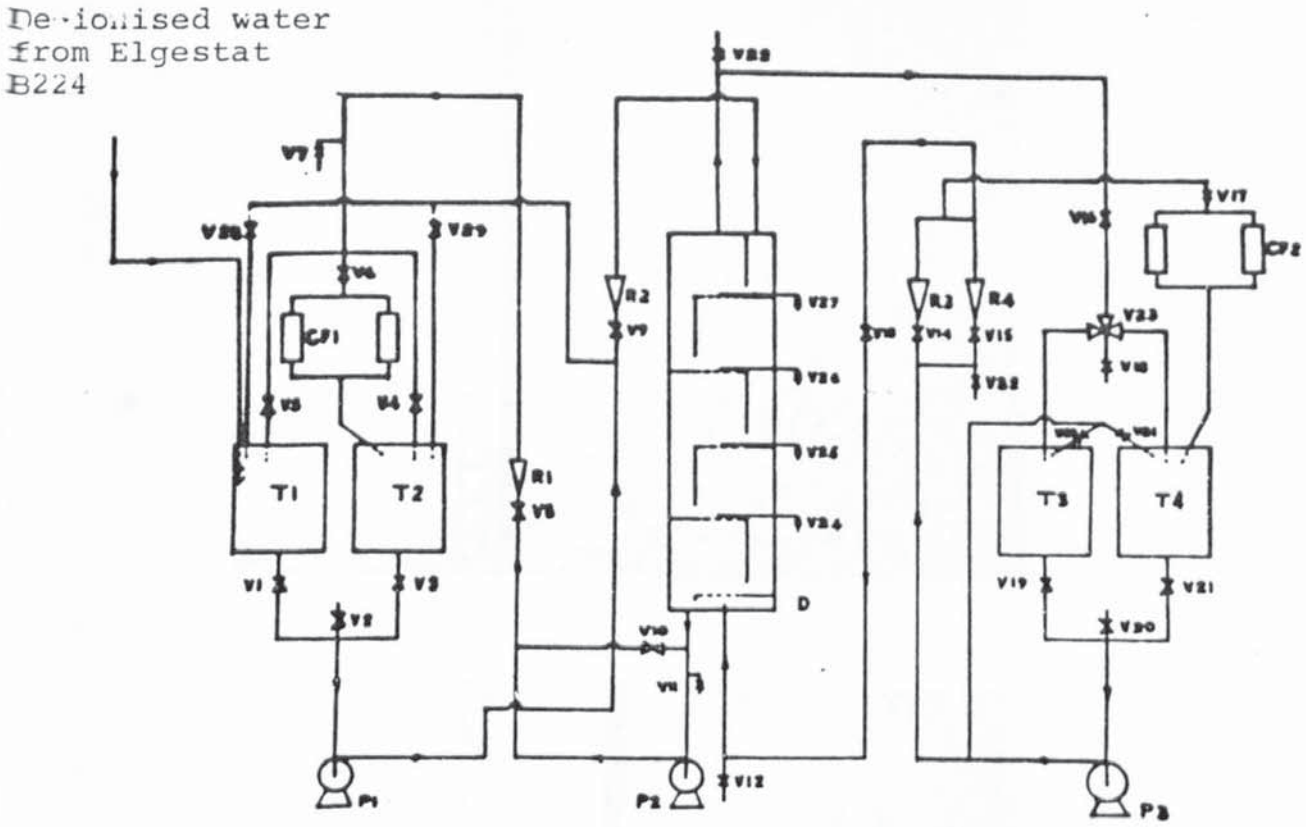

Figure 1 Flow diagram of pilot-scale, Sieve Plate Column

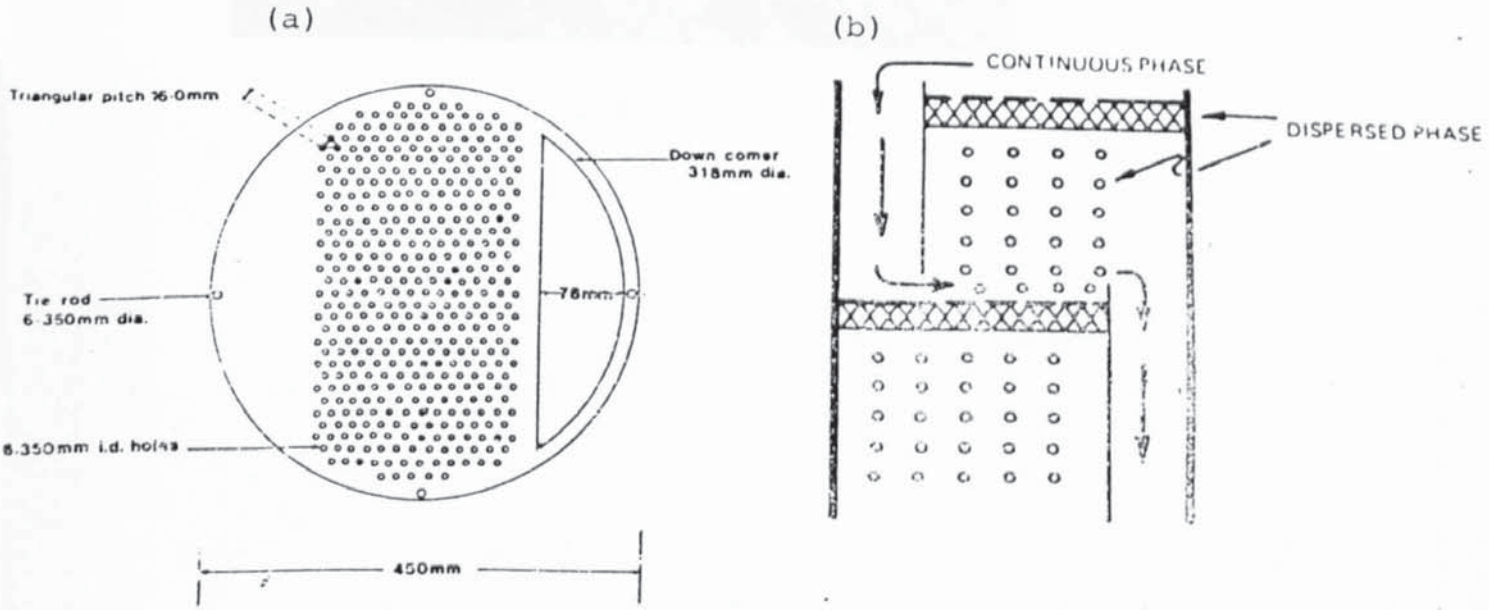

Figure 2 Plate layout (a) and Idealised Flow (b) in Sieve Plate Column

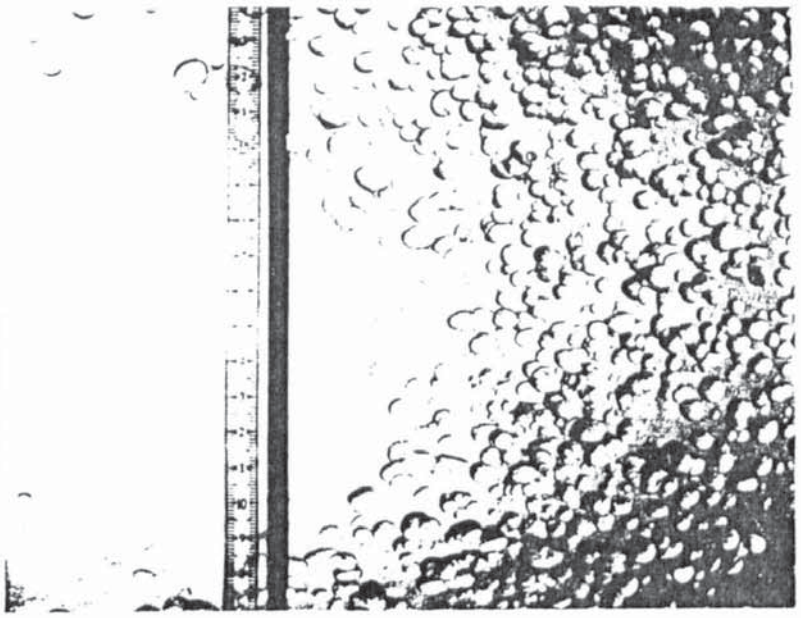

(a)

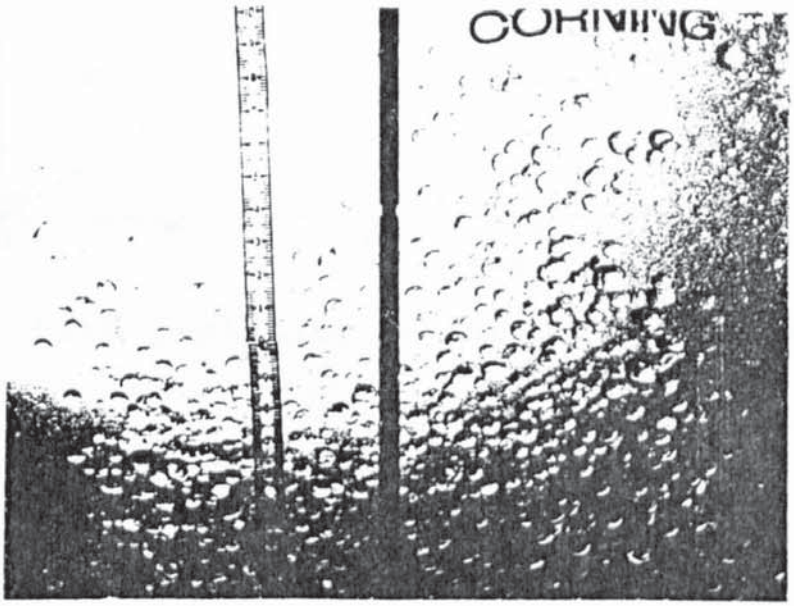

(b)

Figure 3

Droplet Swarm Flow Patter

U_c = 0.27cm/s

U_d = 0.18cm/s

(a) Plate Spacing = 380mm
Showing swarm
recirculation

(b) Plate Spacing = 300m
Reduced
recirculation

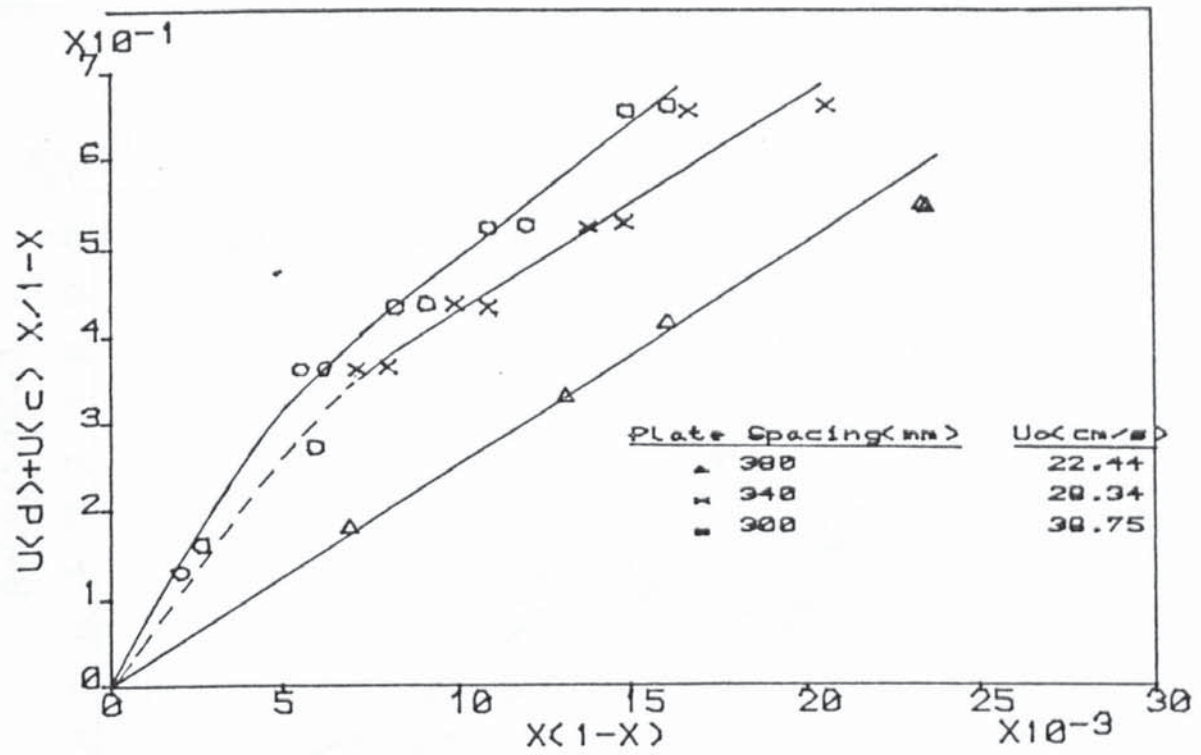

Fig4 Variation of Uo with plate-spacing

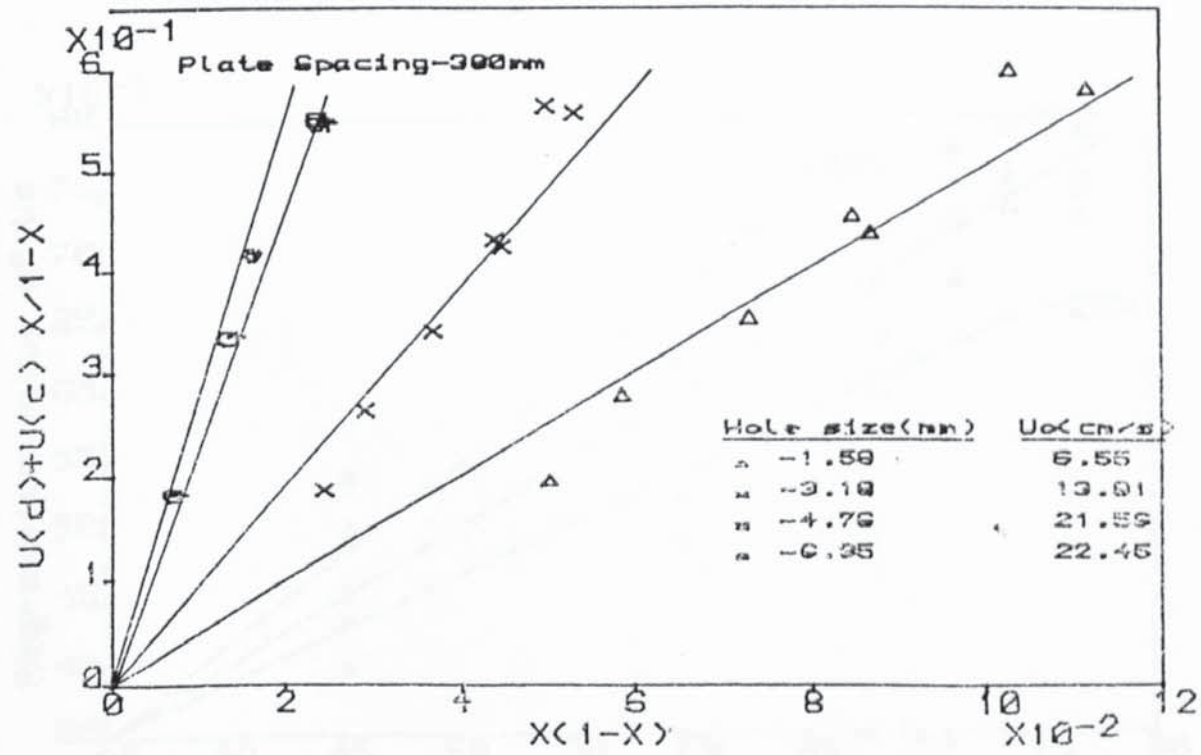

Fig5 Variation of Uo with plate hole-size

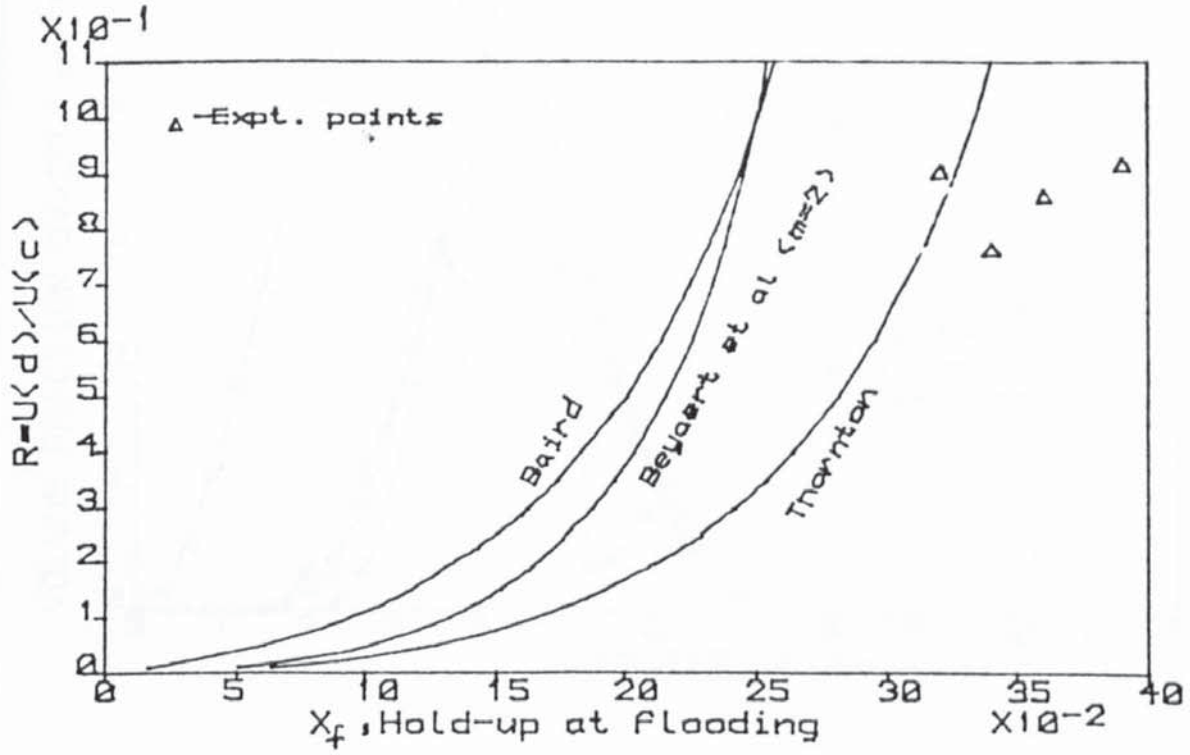

Fig6 Comparison of Flooding correlations

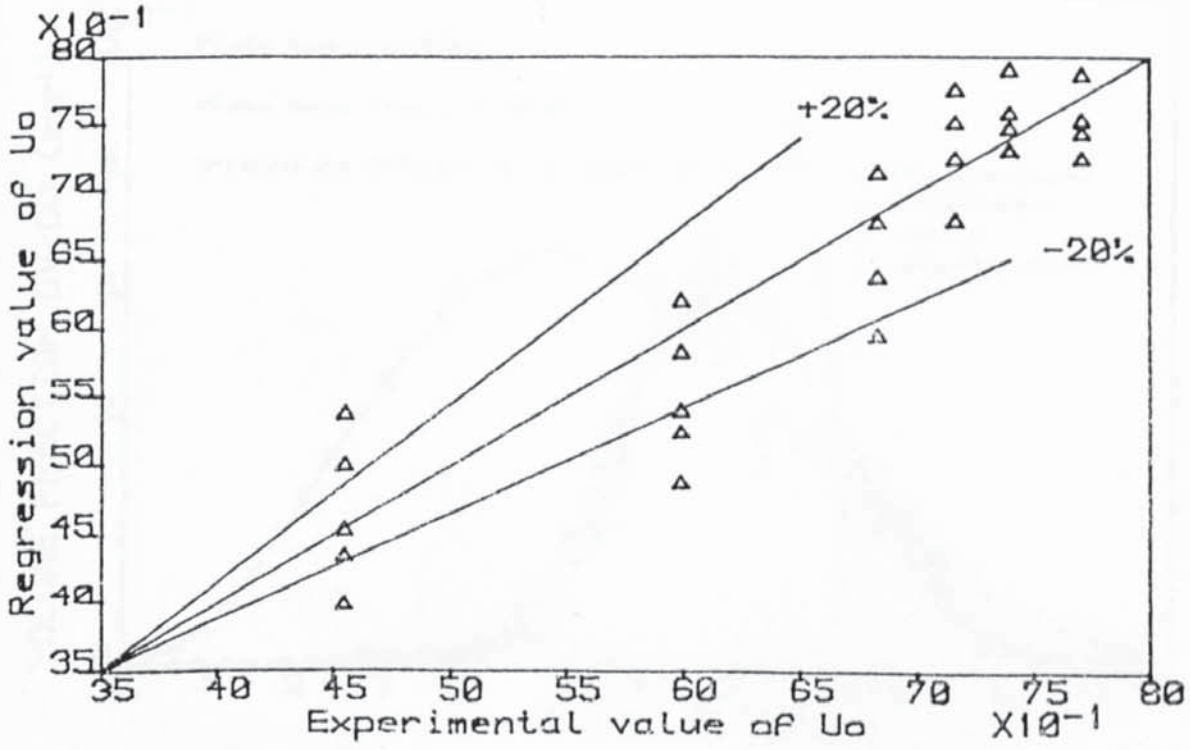

Fig7 Correlation of experimental Uo data with equation34

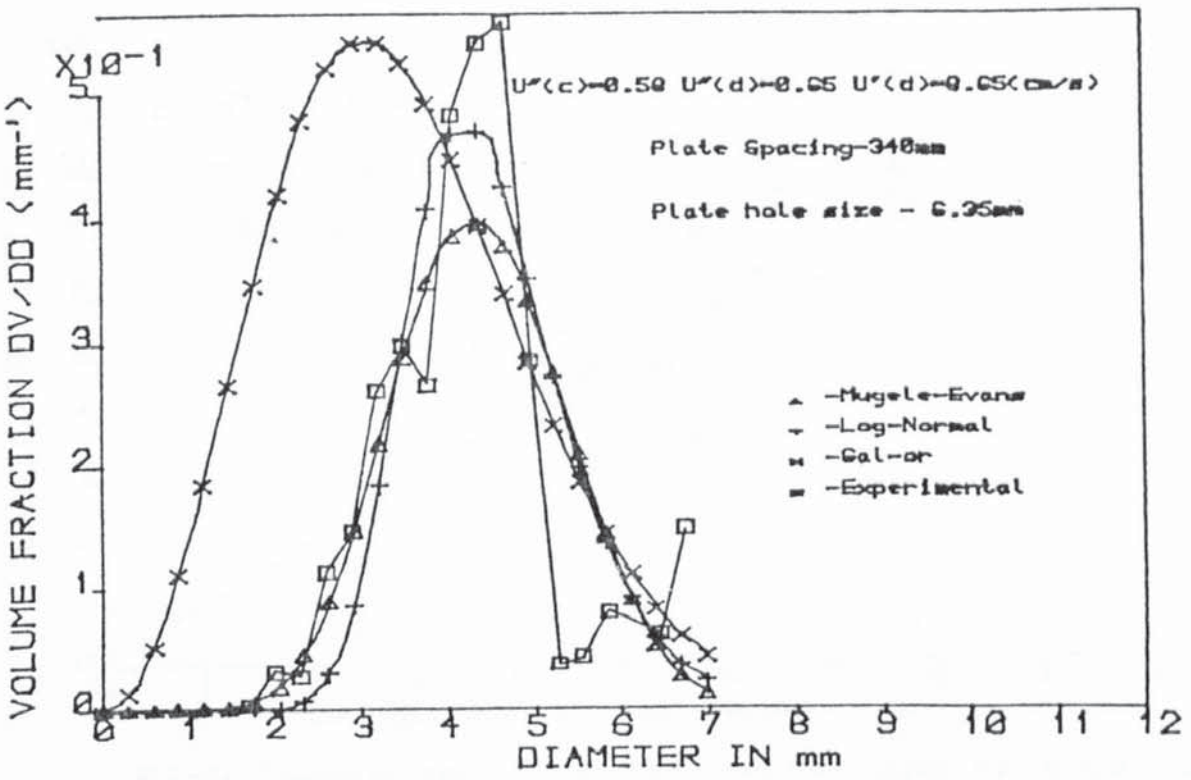

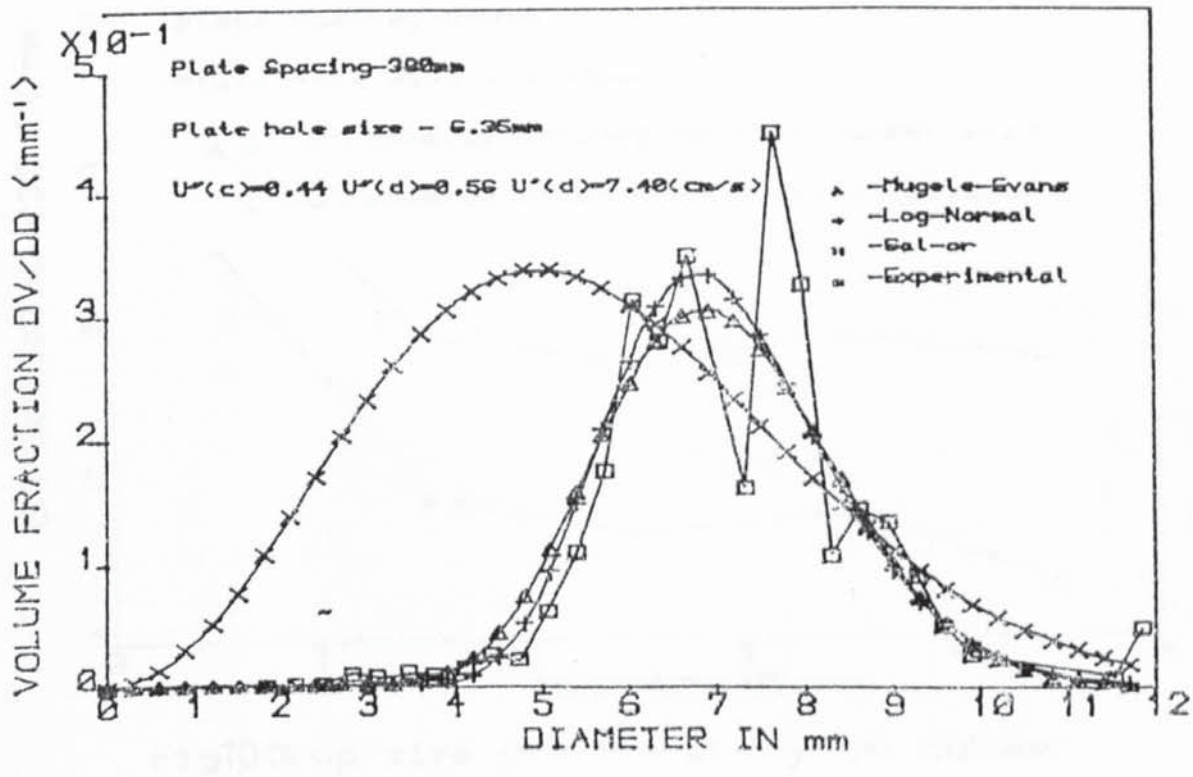

Fig8 Experimental and Theoretical distribution functions curves

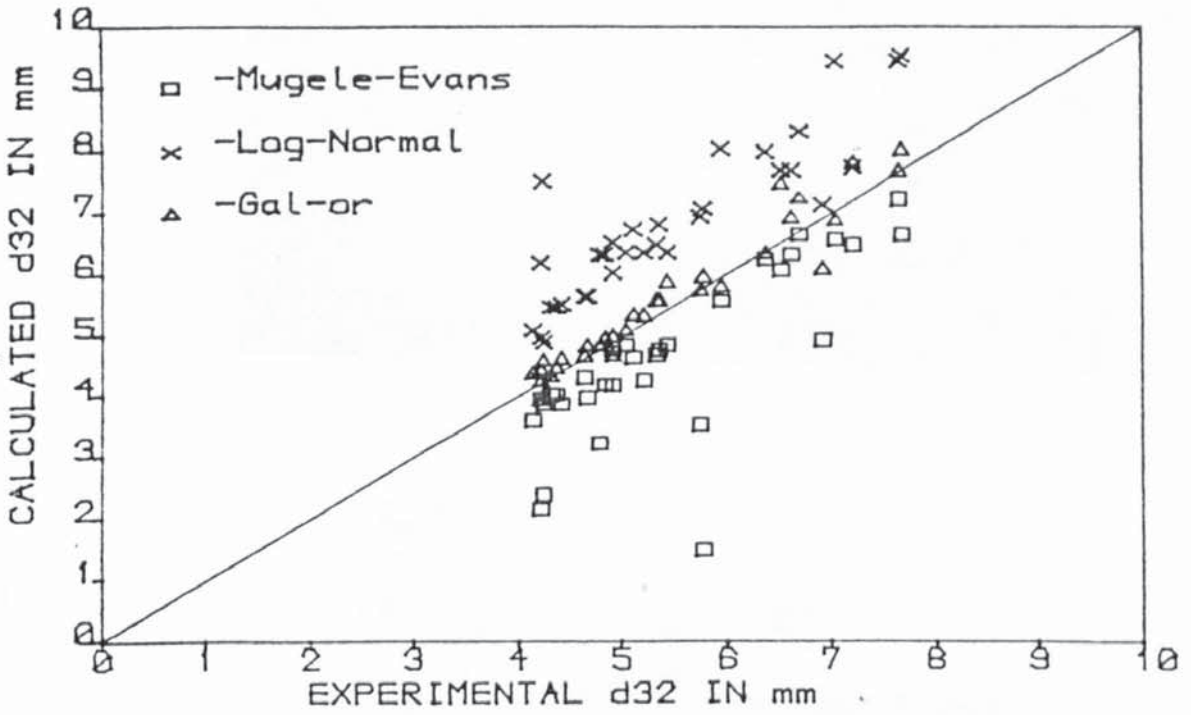

Fig9 Comparison of experimental and calculated values of d32

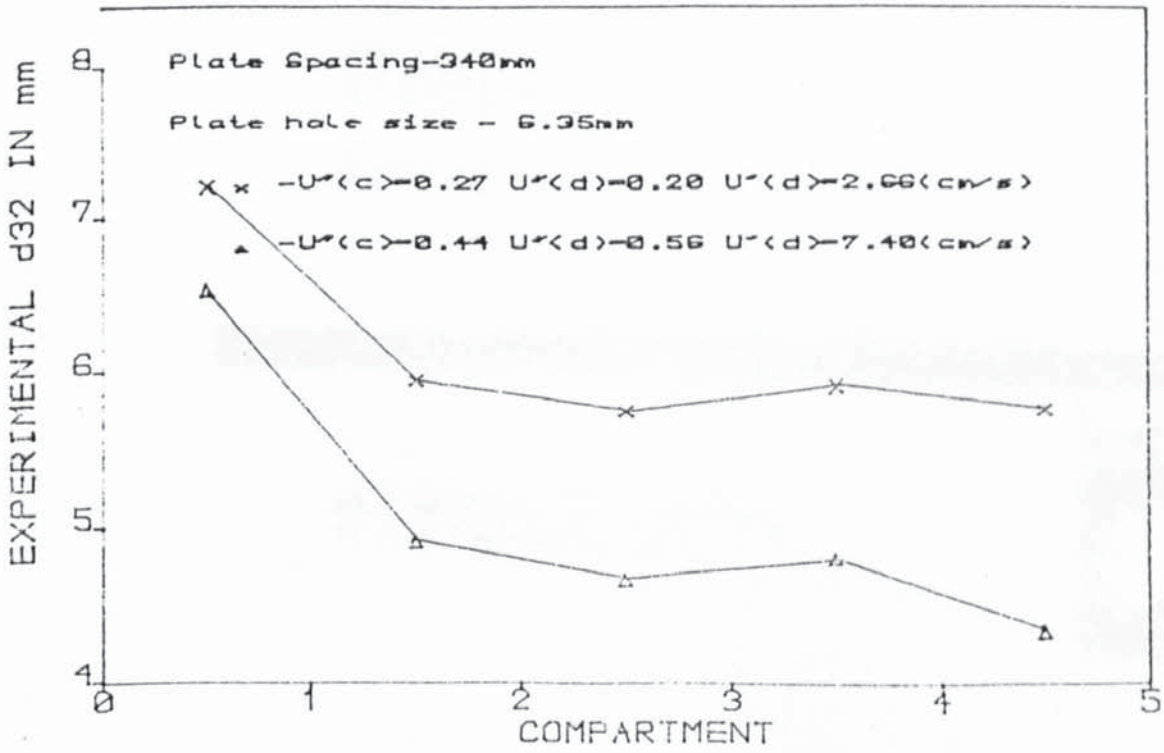

Fig10 Drop size profile along the column

NOMENCLATURE

A	Total interfacial area,cm^2
A_n	Parameter Constant Table 5.2
a	Specific interfacial area,cm^2/cm^3
a	Constant Eqn. 5.27
a'	Distribution parameter (Skewness parameter).
a_d	Drop surface area,cm^2
b	Constant Eqn. 5.27
ΔC	Concentration driving force ,g/cm^2
ΔC_m	Concentration driving force,g/cm^2
C	Solute concentration,g/cm^3
C^*	Equilibrium concentration,g/cm^3
C_D	Drag coefficient
D	Molecular diffusivity,cm^2/s
d	Drop diameter,cm
d_c	Critical drop size,cm
d_e	Diameter of sphere having the same volume as the droplet,cm
d_{gm}	Geometric mean diameter,cm
d_m	Maximum stable drop size,cm
d_n	Plate hole diameter,cm
d_o	Sauter mean drop diameter,cm
d_1	Diameter of major drop axis,cm
d_2	Diameter of minor drop axis,cm

d_{32}	Volume-surface or Sauter mean drop diameter,cm
$d_{10,50,90}$	Drop sizes at 10%,50% and 90% cummulative volume
E_o	Eotvos number, $\Delta\rho d^2 g/\sigma$
E_o	Overall stage efficiency
E_m	Extraction efficiency Eqns. 5.57 & 5.58
Ga	Galileo Number $(d_e^3\rho^2 g/\mu^2)$
g	Acceleration due to gravity,cm/s^2
H	Coalesccence/Flocculation zone height,cm Eqn.3.1
H	Variable parameter Eqn.4.16
H_t	Plate spacing,cm Eqns. 5.57 &5.58
H_c	Compartment height or Plate spacing,cm
h_e	Effective height of the column,cm
h_t	Coalescence height,cm
J	Variable parameter Eqn. 4.17
K	Overall mass transfer coefficient,cm/s
Ka	Overall volumetric mass transfer coefficient,cm/s
K_{cal}	Theoretical overall mass transfer coefficient,cm/s
K_{expt}	Experimental overall mass transfer coefficient,cm/s
k_c	Continuous phase mass transfer coefficient,cm/s
$k_{c.c}$	Continuous phase mass transfer coefficient of circulating drops,cm/s
$k_{c.o}$	Continuous phase mass transfer coefficient of oscillating drops,cm/s
k_d	Dispersed phase mass transfer coefficient,cm/s

$k_{d.c}$	Dispersed phase mass transfer coefficient of circulating drops,cm/s
$k_{d.o}$	Dispersed phase mass transfer coefficient of oscillating drops,cm/s
$K_{o.c}$	Overall mass transfer coefficient of circulating drops,cm/s
$K_{o.o}$	Overall mass transfer coefficient of oscillating drops,cm/s
$K_{c.c}$	Mass transfer coefficient during drop coalescence,cm/s
K_{df}	Mass transfer coefficient during drop formation,cm/s
L_j	Jet length,cm
M	Morton number, $\frac{g\mu^4 \Delta\rho}{\rho^2\sigma^3}$
m	Equilibrium distribution coefficient
m	Constant Eqn.5.27
N	Rate of mass transfer ,gm/s
N_c	Total number of compartments
N_s	Number of stages
N.T.U.	Number of transfer units
n	Number of drops/mode of oscillation
n	Constant Eqn.5.27
P	Power, kg/ms
P_c	Volume fraction of circulating drops in dispersion
Pe	Peclet Number, ($d_e U/D$)
P_o	Volume fraction of oscillating drops in dispersion
R	Flow ratio,U_d/U_c
R	Effective diffusivity defined by Eqn. 5.24

Re	Droplet Reynolds Number ($dU_s\rho_c/\mu_c$)
$r_{s.d}$	Stable drop radius,cm
r_o	Initial drop radius of drop,cm
Sc	Schmidt Number ($\mu/\rho D$)
Sh	Sherwood Number (kd/D)
T	Time dimensionless group $4Dt/d_e$
t	time,s
t_f	time of formation,s
U	Phase superficial velocity,cm/s
U_j	Jetting velocity,cm/s
U_K	Characteristic velocity of droplet swarm,cm/s
U_{max}	Maximum jet velocity,cm/s
U_n	Dispersed phase hole velocity,cm/s
U_s	Slip velocity,cm/s
U_t	Terminal velocity,cm/s
We	Weber Number ($\rho\mu^2 d/\sigma$)
V	Volume of the column,cm^3
v	Volume,cm^3
X	Solute concentration in dispersed phase gm/100g Sol.
x	Dispersed phase hold-up
x_f	Dispersed phase hold-up at flooding
y	Solute concentration in continuous phase gm/100g Sol.
y_v	mean diameter from Rosin-Rammler function Table 4.1

GREEK SYMBOLS

δ	Uniformity distribution parameter, Skewness parameter
β	Degree of impurity defined by Eqn.5.42
β	Ratio of drop diameter d_2/d_1 in coalescence
ϕ	Contact angle
γ	Retardation Coefficient Eqn. 5.42
ρ	Density,g/m^3
$\Delta\rho$	Density difference,g/cm^3
μ	Viscosity,g/cms
ν	Cummulative volume of the drops
σ	Interfacial tension,mN/m (dynes/cm)
σ	Index in Mugele-Evans distribution function Table 4.1
τ	Dimensionless time
ω	Frequency of oscillation 1/sec
π	Constant 3.1416
ε	Amplitude of oscillation
ε_o	Function of amplitude of oscillation
λ_n	Eigen value

SUBSCRIPTS

c	Continuous phase and /or Circulating drop
Cal	Calculated or Theoretical
d	Drop and / or Dispersed phase
exp	Experimental
f	Flooding condition
HB	Handlos and Baron
m	mean
o	Overall and/ Oscillation drop
s	Stagnant

SUPERSCRIPTS

* Equilibrium condition

REFERENCES

1. Adinarayana,T.,Sinha,R.and Jagannahha Rao,R.
   Chem.Petro.Chem.Jl. 8(10),27 (1977).

2. Al-Aswad,K.K.M.
   'Liquid-liquid Extraction in A Pilot Scale Rotating Disc Contactor'
   Ph.D. Thesis, University of Aston. (1982).

3. Al-Faize,M.M.
   "Mass Transfer to Large Oscillating Drops'
   Ph.D Thesis,University of Aston. (1986).

4. Al-Hassan,T.S.
   'A Study Of Mass Transfer From Large Oscillating Drops'
   Ph.D.Thesis,University of Aston. (1979).

5. Allak,A.M.A.and Jeffreys,G.V.
   A.I.Ch.E.J. 20,564 (1974).

6. Allerton,J.,Storm,B.O.and Treybal,R.E.
   Trans.A.I.Ch.Eng. 39,361 (1943)

7. Angelo,J.B.and Lightfoot,E.N.
   A.I.Ch.E.J. 14,531 (1968).

8. Angelo,J.B.,Lightfoot,E.N.and Howard,D.W.
   A.I.Ch.E.J. 12,751 (1966).

9. Bailes,P.J.,Godfrey,J.C.and Slater,M.J.
   Trans.Inst.Chem.Engr. 61,321 (1983).

10. Baird,M.H.I.and Hamielec,A.O.
    Can.Jl.Chem.Eng. 40,119 (1962).

11. Baird,M.H.I.,McGinnis,R.S.and Tan,G.C.
    Proc.Int.Sol.Ext.Conf.(Hague) Vol.1, 251 (1971).

12. Baird,M.H.I.,Lo,T.C.and Hanson,C.
    'Handbook Of Solvent Extraction'(Part ii).
    John Wiley and Sons, New York. (1983).

13. Baird,M.H.I.and Shen,R.J.
    Can.Jl.Chem.Eng. 62,218 (1984).

14. Barnea,E.and Mizrahi,E.
    Can.Jl.Chem.Eng. 53(5),461 (1975).

15. Barnea,E.and Mizrahi,E.
    Ind.Eng.Chem.Fundamental 15(2),120 (1976).

15a. Batey,W.,Lonie,S.J.Thompson,P.J.and Thornton,J.D.
Int.Sol.Ext.Conf.(ISEC `86) Vol.1 pg.371
Munich,W.Germany Sept.(1986).

15b. Batey,W.,Lonie,S.J.Thompson,P.J.and Thornton,J.D.
Chem. Eng. Res. and Design 64,396 (1987)

16. Beardmore,F.S.and Kosters,W.C.G.
Jl.Inst.Petro. 49(Jan.) (1963.

17. Bensalem,A.,Steiner,L.and Hartland,S.
Sol.Ext.& Ion.Exch. 3(5),697 (1985).

18. Beyaert,B.O.,Lapidus,L.and Elgins,J.C.
A.I.Ch.E.J. 7,46 (1961).

19. Boussinesq,J.
Copt.Rend.Acad.Sci.(Paris) 156,1124 (1913).

20. Boyadzhiev,L.,Elenkov,D.and Kyuchukova,G.
Can.Jl.Chem.Eng. 47,42 (1969).

21. Boyotiotis,B.A.and Thornton,J.D.
I.Ch.E.(Lond.) Symp.Series 26,43 (1967).

22. Bright,A.
Chem.Eng.Res.and Dev. 63(1),59 (1985).

23. Brown,A.A.and Hanson,C.
Inst.Chem.Eng.Symp.Series No.26,57 (1967).

24. Brown,A.H.and Hanson,C.
Chem.Eng.Sci. 23,841 (1968).
Nature 214,76 (1967).

25. Brunson,R.J.and Wellek,R.M.
Can.Jl.Chem.Eng. 48,267 (1970).

26. Burkhart,L.,Westerps,P.W.and Sharer,P.C.
A.I.Ch.E.J. 22,1090 (1976).

27. Burkholder,H.C.and Berg,J.C.
A.I.Ch.E.J. 20(5),872 (1974).

28. Bulatov,S.N.,Planovsky,A.N.and Adamov,A.P.
The Sov.Chem.Ind.(Khim.Prom.) 48(3),183 (1972).

29. Bushnell,J.D.and Fiocco,J.R.
Hydrocarbon process 5,119 (1980).

30. Bussolari,R.S.,Schiff,S.and Treybal,R.E.
Ind.Eng.Chem. 45,2413 (1953).

31. Calderbank,P.H.and Korchinski,I.J.O.
Chem.Eng.Sci. 6,65 (1956).

32. Calderbank,P.H.and Moo-Young,M.R.
Chem.Eng.Sci. 16,39 (1961).

33. Carless Solvent Manual (1986).

34. Chao,B.T.
Physic Fluids 5,69 (1962).

35. Charles,G.E.and Mason,S.G.
Jl.Collloid Sci. 15,105,235 (1960).

36. Chartres,R.H.and Korchinsky,W,J.
Trans.Inst.Chem.Engs. 53,247 (1975).

37. Chartres,R.H.and Korchinsky,W.J.
Trans.Inst.Chem.Eng. 56,91 (1978).

38. Chen,H.T.and Middleman,S.
A.I.Ch.E.J. 13,989 (1967).

39. Christiansen,R.M.and Hixson,A.N.
Ind.Eng.Chem. 49,1017 (1957).

40. Chu,T.C.,Taylor,C.C.and Levy,D.J.
Ind.Eng.Chem. 42,1157 (1950).

41. Clift,R.and Grace,J.R.and Weber,M.E.
`Bubbles,Drops and Particles'
Academic Press,New York (1978).

42. Colburn,A.P.
Trans.A.I.Ch.E. 35,211 (1939).

43. Coulson,J.H.and Skinner,S.J.
Chem.Eng.Sci. 1,197 (1951).

44. Cruz-Pinto,J.J.C.and Korchinsky,W.J.
Chem.Eng.Sci. 35,2213 (1980).

45. Damon,K.G.,Angelo,J.B.and Dark,R.W.
Chem.Eng.Sci 21,813 (1966).

46. Danckwerts,P.V.
Ind.Eng.Chem. 43,466 (1951).

47. Davies,G.A.and Jeffreys,G.V.
Filtration and Separation 6,349 (1969)

48. Davies,G.A.,Jeffreys,G.V.,Smith,D.V.and Ali,F.A.
Can.Jl.Chem.Eng. 48,328 (1970).

49. Davies,G.A.,Jeffreys,G.V.and Afzal,M.
Bri.Chem.Eng.Pro.Tech. 17(9),709 (1972).

50. Davies,G.A.,Jeffreys,G.V.and Afzal,M.
Chem.Eng.(Lond) p392 (1972).

51. Davies,G.A.,Juma,S.and Jeffreys,G.V.
Chem.Eng.Jl. 4,21 (1972).

52. Dawodu,F.A.
'Mechanism of Liquid Extraction in A Pilot Plant Sieve Plate Column' Ph.D. Thesis, University Of Aston.(1983).

53. Dawodu,F.A.,Mumford,C.J.and Jeffreys,G.V.
I.Ch.E. Symp.Series No.88,Dounreay (1984).

54. de Chazal,E.L.M.and Ryan,J.T.
A.I.Ch.E.J. 17,1226 (1971).

55. Defrawi,M.and Heideger,W.J.
A.I.Ch.E.J. 19,179 (1973).

56. Defrawi,M.and Heideger,W.J.
Chem.Eng.Sci. 33,35 (1978).

57. Dixon,B.E.and Russel,A.A.
Jl.Soc.Chem.Ind.(Lond.) 69,284 (1950).

58. Dixon,B.E.and Swallow,J.E.
Jl.Appl.Chem. 4,86 (1954).

59. Dzubur,I.and Sawistowski,H.
Proc.Int.Sol.Ext.Conf.,Lyon (1974).

60. Edge,R.M.and Grant,C.D.
Chem.Eng.Sci. 27,709 (1972).

60a. Eldridge,R.B.Humphrey,J.L.and Fair,J.R.
Int.Sol.Ext.Conf.(ISEC `86) Vol.3 pg55
Munich,W.Germany.Sept.(1986).

61. Elgin,J.C.and Browning,F.M.
Trans.A.I.Ch.E. 31,639 (1935).

62. Elgin,J.C.and Foust,C.F.
Ind.Eng.Chem. 42,1127 (1950).

63. Elzinga,E.and Banchero,J.
Chem.Eng.Prog.Symp.Seri. 55(29),149 (1959).

64. Elzinga,E.and Banchero,J.
A.I.Ch.E.J. 7,394 (1961).

65. Flemming,J.T.and Johnson,H.F.
Chem.Eng.Prog. 49,497 (1953).

66. Francis,A.W.and King,C.
Ad.Pet.Chem.Ref. 1,429 (1954).

67. Freshwater,D.C.
'Chemical Engineering Practice',,Vol.5 Chap.8.
Cremer,H.W.and Davis,T.(Edt.)
Butterworths,London (1958).

68. Fujinawa,K.,Maruyama,T.and Nakaike,Y.
Kagaku Kikai 21,194 (1957).

69. Fujita,S.,Tanizawa,E.and Kang,C.
Chem.Eng. (Japan) 17(3),111 (1953).

70. Gal-or,B.and Hoescher,H.E.
A.I.Ch.E.J. 12,499 (1966).

71. Garner,F.H.
Trans.Inst.Chem.Eng. 28,28 (1950).

72. Garner,F.H.,Ellis,S.R.M.and Frosbury,D.W.
Trans.Inst.Chem.Eng. 31,348 (1953).

73. Garner,F.H.,Ellis,S.R.M.and Hill,J.W.
A.I.Ch.E.J. 1,185 (1955).

74. Garner,F.H.,Foord,A.and Tayeban.M.
Jl.Appl.Chem. 9,315 (1959).

75. Garner,F.H.and Haycock,P.J.
Proc.R.Soc. 252,457 (1959).

76. Garner,F.H.and Skelland,A.H.P.
Chem.Eng.Sci.4,149 (1955).

77. Garner,F.H.and Skelland,A.H.P.
Ind.Eng.Chem. 46,,1255 (1954).

78. Garner,F.H.and Tayeban,M.
An.R.Soc.Esp.Fis.Quin (Madrid) B56,479,491 ((1960).

79. Garwin,L.and Smith,D.D.
Chem.Eng.Prog. 49(11),591 (1953).

80. Gaylor,R.,Roberts,N.N.and Pratt,H.R.C.
Trans.I.Ch.E. 31,57 (1953).

81. Giles,J.W.,Hanson,C.and Marsland,J.G.
Int.Sol.Ext.Conf. Hague,p94 (1971).

82. Gillespie,T.and Rideal,E.K.
Trans.Fara.Soc. 52,173 (1956).

83. Goldberger,W.M.and Benenati,R.F.
Ind.Eng.chem. 51,64 (1959).

83a. Golob,J.and Grilic,V.
Int.Sol.Ext.Conf.(ISEC `86) Poster Sess.34.
Munich,W.Germany.Sept.(1986).

84. Grace,J.R.,Wairegi,T.and Nguyen,T.H.
Trans.Inst.Chem.Eng. 54,167 (1976).

85. Graham,E.E.,Ooi,K.L.and Odell,M.H.
Chem.Eng.Jl. 18,189 (1979).

86. Graham.E.E.and Tregurtha,D.J.
Chem. Eng.Jl. 23,63 (1982).

87. Grant,R.P.and Middleman,S.
A.I.Ch.E.J. 12,669 (1966).

88. Grober,H.
Z.Ver.dt.Ing. 69,705 (1925).

89. Groothius,H.and Kramers,H.
Chem.Eng.Sci. 4,17 (1955).

90. Groothuis,H.and Zuiderweg,F.J.
Chem.Eng.Sci. 12,288 (1960).

91. Hadamard,J.
Acad.Sci.Paris 152,1735 (1912).

92. Hamielec,A.E.and Johnson,A.I.
Can.Jl.Chem.Eng. 40,41 (1962).

93. Hamielec,A.E.,Storey,S.H.and Whithead,J.M.
Can.Jl.Chem.Eng. 41,426 (1963).

94. `Handbook Of Chemistry and Physics' 66$^{th.}$ Ed.
R.C.Weast Edt.
Chemical Rubber Company,Florida,U.S.A.

95. Handlos,A.E.and Baron,T.
A.I.Ch.E.J. 3,127 (1957).

96. Hanson,C.
Chem.Eng. 75,76 (1968).

97. Hanson,C. (Ed.)
'Recent Advances in Liquid-Liquid Extraction'
Pergamon Press,New York (1971).

98. Haramarty,T.Z.
A.I.Ch.E.J. 6,281 (1960).

99. Harrington,P.J.
U.S. patent 1 943 822 (1934).

100. Harriot,P.
Can.Jl.Chem.Eng. 40,60 (1962).

101. Hasson,D.and Mizrahi,J.
Trans.I.Ch.E. 39,415 (1961).

102. Haynes,L.G.,Himmelblau,D.M.and Schechter,R.S.
Ind.Eng.Chem.Proc.Des.& Dev. 7,508 (1968).

103. Hayworth,C.B.and Treybal,R.E.
Ind.Eng.Chem. 42,1174 (1950).

104. Heertjes,P.M.and De Nie,L.H.
Chem.Eng.Sci. 21,755 (1966).

105. Heertjes,P.M.and De Nie,L.H.
Chem.Eng.Sci. 26,697 (1971).

106. Heertjes,P.M.,Holve,W.A.and Thalsma,H.
Chem.Eng.Sci. 3,122 (1954).

107. Heertjes,P.M.and De Nie,L.H.
In `Recent Advances In Liquid-Liquid Extraction` Chapter10.
Ed.Hanson,C. Pergamon Press,New York (1971).

108. Hemanth Kumar,C.,Ayyanna,C.and Krishna Murty,R.
Chemical Era 14(2),7 (1978).

109. Higbie,R.
Trans.A.I.Ch.E. 31,365 (1935).

110. Hirschmann,K.and Blass,E.
Germ.Chem.Eng. 7,280 (1984).

111. Hitit,H.A.
'Mechanism Of Phase Separation For Dispersion In Continuous Flow'
Ph.D. Thesis,University of Aston. (1972).

112. 'The Highly Flammable Liquids and Liquefied Petroleum Gas Regulations'Statutory Instruments No.917 (1972) HMSO

113. Horvath,M.,Steiner,L.and Hartland,S.
Can.Jl.Chem.Eng. 56,9 (1978).

114. Hozawa,M.and Tadaki,T.
Kogaku kogaku 37,827 (1973).

115. Hu,S.and Kintner,R.C.
A.I.Ch.E.J. 1,42 (1955).

116. Hughmark,G.H.
Ind.Eng.Chem.Fund. 6,408 (1967).

117. Humphery,J.H.,Rocha,R.A.and Fair,J.R.
Chem.Eng.Prog. (Sept.),76 (1984).

118. Ilkovic,C.D.
Coll.Czech.Chem.Comm. 6,498 (1934).

119. Ingham,J.
In `Recent Advances In Liquid-Liquid Extraction` Chapter 8.
Ed.Hanson,C. Pergamon Press,New York (1971).

120. Izard,J.A.
A.I.Ch.E.J. 18,634 (1972).

121. Jeffreys,G.V.and Lawson,G.B.
Trans.I.Ch.E. 43,294 (1965).

122. Jeffreys,G.V.and Hawksley,J.L.
A.I.Ch.E.J. 11,413 & 418 (1965).

123. Jeffreys,G.V.
Chem.and Proc.Eng. 49,111 (1968).

124. Jeffreys,G.V.and Davies,G.A.
In `Recent Advances In Liquid-Liquid Extraction` Chapter 14.
Ed.Hanson,C. Pergamon Press,New York (1971).

125. Jeffreys,G.V.,Al-Aswad,K.K.M.and Mumford,C.J.
Sep.Sci.and Tech. 16(9),1217 (1981).

126. Johns,J.C.and Beckman,R.B.
A.I.Ch.E.J. 12,10 (1966).

127. Johns,L.E.,Beckman,R.B.and Ellis,W.D.
Brit.Chem.Eng. 10,86 (1965).

128. Johnson,A.I.and Braida,C.
Can.Jl.Chem.Eng. 35,165 (1957).

129. Johnson,A.I.and Hamielec,A.C.
A.I.Ch.E.J. 6,145 (1960).

130. Johnson,H.F.and Bliss,H.
Trans.I.Ch.E. 42,331 (1946).

131. Jordan,D.G.
`Chemical Process Development' Pt.2 pg. 653 (1968).
Interscience Publishers.

132. Kagan,S.Z.,Kovalev,Yu.N.and Zakharychev,A.P.
Theoretical Foundations Chem.Eng. 7,514 (1973).

132a. Kawase,Y.A.and Ulbrech,J.J
Ind.Eng.Chem.Proc.Dev.& Des. 20,636 (1981).

133. Keith,F.W.and Hixson,A.N.
Ind.Eng.Chem. 49,1017 (1957).

134. Kesava Rao,C.,Sinha,R.and Jagannahha Rao,R.
Chem.Era 13(12),391 (1978).

135. Khemangkom,V.,Muratet,G.and Angelo,H.
Int.Sol.Ext.Conf.(Toronto) 429 (1977).

136. Kinard,G.E.,Manning,F.S.and Manning,W.P.
Bri.Chem.Eng. 8,326 (1963).

137. King,C.J.,Hsuch,I.and Mao,K.W.
Chem.Eng.Data 10,348 (1965).

138. Kitamura,Y.,Mishima,H.and Takahashi,T.
Can.Jl.Chem.Eng. 60,723 (1982).

139. Klee,A.J.and Treybal,R.E.
A.I.Ch.E.J 2,444 (1956).

140. Korchinsky,W.J.and Azinzadsh-Khataylo,S.
Chem.Eng.Sci. 31,871 (1976).

141. Krishna Murty,R.,Jagannadha Rao,R.and Venkata Rao,C.
Indian Jl.Tech. 5,271 (1967).

142. Krishna Murty,R. and Venkata Rao,C.
Indian Jl.Tech. 5,205 (1967).

143. Krishna Murty,R.,Reddy,M.S.and Venkata Rao,C.
Indian Jl.Tech. 6,53 (1968).

144. Krishna Murty,R. and Venkata Rao,C.
Ind.Eng.Chem.Proc.Des.& Dev. 7,166 (1968).

145. Krishna Murty,R.and Venkata Rao,C.
Chem.Age of India 19(2),106 (1968).

146. Krishna Murty,R.and Venkata Rao,C.
Chem.Age of India 19(7),513 (1968).

147. Krishna Murty,R.,Reddy,M.S.and Venkata Rao,C.
Indian Chem.Eng. 12,64 (1970).

148. Krishna Murty,R.,Ramalingasastry,A.and Dakshnamurty,P. and Chirandivi,C.
Ind.Chem.Manuf. 12(7),21 (1974).

149. Krishna,P.M.,VenkateSwarlu,D.and Narasimhamurty,G.S.R.
Jl.Chem.Eng.Data 4,336 (1959).

150. Kronig,R.and Brink,J.C.
Appl.Sci.Res. A42,142 (1950).

150a. Kuester,J.C.and Mize,J.H.
`Optimization Techniques With Fortran'
McGraw Hill Book Co.(1973).

151. Kumar,A.,Voitira,D.K.and Hartland,S.
Can.Jl.Chem.Eng. 58,154 (1980).

152. Kumar,A.and Hartland,S.
Trans.Inst.Chem.Eng. 60,35 (1982).

153. Kumar,A.and Hartland,S.
Can.Jl.Chem.Eng. 63,368 (1985).

154. Kumar,R.
Chem.Eng.Sci. 26,177 (1971).

155. Kumar,R.and Saradhy,Y.P.
Ind.Eng.Chem.Fund. 11(3),307 (1972).

156. Laddha,G.S.and Dagallesan,T.E.
'Transport Phenomena In Liquid Extraction' Chapter 11.
Tata McGraw-Hill,New Delhi,India (1974).

157. Laddha,G.S.and Smith,J.M.
Chem.Eng.Prog. 46(4),195 (1950).

158. Laird,W.G.
U.S.Patent 1 320 306 (1919).

159. Lawson,G.B.
Chem.Eng.Proc. 63,May,45 (1967).

160. Lee,J.C.and Lewis,G.
I.Ch.E.Symp.on Liquid Extraction,Newcastle,U.K. (1967).

161. Letan,R.and Kehat,E.
A.I.Ch.E.J. 13,443 (1967).

162. Levich,V.G.
`Physicochemical Hydrodynamics'
Prentice Hall Publications (1962).

163. Lewis,J.B.,Jones,I.and Pratt,H.R.C.
Trans.I.Ch.E. 29,126 (1951).

164. Licht,W.and Conway,J.B.
Ind.Eng.Chem. 42,1151 (1950).

165. Licht,W.and Pensing,W.F.
Ind.Eng.Chem. 45,1885 (1953).

166. Linton,M.and Sutherland,K.L.
Chem.Eng.Sci. 12,214 (1960).

167. Lo,T.C.
Liquid Extraction In 'Kirk-Othmer Encyclopedia Of Chemical Tech.' Vol.9. Pg.672 3rd. Ed. Wiley-Interscience New York (1978).

168. Lochiel,A.C.and Calderbank,P.H.
Chem.Eng.Sci 19,471 (1964).

169. Lode,T.and Heideger,W.J.
Chem.Eng.Sci. 25,1081 (1970).

170. Lodh,B.B.and Raja Rao,M.
Indian Jl.Tech.4,163 (1966).

171. Logsdail,D.H.,Thornton,J.D.and Pratt,H.R.C.
Trans.I.Ch.E. 35,301 (1957).

172. Logsdail,D.H.and Lowes,L
In 'Recent Advances in Liquid-Liquid Extraction' Chapter 5 Pergamon Press,New York (1971). Hanson,C. (Ed.)

173. Lykov,A.V.and Mikhaylon,Y.A.
`Theory of Energy and Mass Transfer'
Prentis Hall Publ. (1961).

174. MacKay,G.D.M.and Mason.S.G.
Nature 191,488 (1961).

175. MacKay,G.D.M.and Mason,S.G.
Jl.Colloid Sci. 16,632 (1961).

176. MacKay,G.D.M.and Mason,S.G.
Can.Jl.Chem.Eng. 41,203 (1963).

177. Madden,A.J.and Damerell,G.L.
A.I.Ch.E.J. 8,223 (1962).

178. Major,C.J.and Hertzog,R.R.
Chem.Eng.Prog. 51,17J (1955).

179. Marsh,B.D.and Heiderger,W.J.
Ind.Eng.Chem.Fund. 4,129 (1965).

180. Mayfield,F.D.and Church,W.L.
Ind.Eng.Chem. 44,2253 (1952).

181. McAvoy,R.M.,Weigard,W.A.,Tomkin,E.C.and Kintner,R.C.
Adv.Sep.Tech. 1,16 (1965).

182. McAvoy,R.M.and Kintner,R.C.
Jl.Colloid Sci. 20,188 (1965).

183. Meister,B.J.and Scheele,G.F.
A.I.Ch.E.J. 14(1),9 (1968).

184. Meister,B.J.and Scheele,G.F.
A.I.Ch.E.J. 15,700 (1969).

185. Meister,B.J.and Scheele,G.F.
A.I.Ch.E.J. 15,689 (1969).

186. Mekasut,L.,Molinie,J.and Angelino,H.
Chem.Eng.Sci. 33,821 (1978).

187. Mewes,D.and Kunkel,W.
Ger.Chem.Eng. 1,111 (1978).

188. Mewes,D.and Pilhofer,T.
Ger.Chem.Eng. 2,69 (1979).

189. Misek,T
Coll.Czech.Chem.Comm. 28,1631 (1963).
Proc.Int.Sol.Ext.Conf.,Lyon, 2,1591 (1974).

190. Misek,T.and Marek,J.
British Chem.Eng. 1,202 (1970).

191. Misek,T.
"Rotating Disk Extractors and Their Design"
(Czch),SNTL, Prague (1964).

192. Misek,T.and Rod,V.
In `Recent Advances In Liquid-Liquid Extraction` Chapter 7.
Ed.Hanson,C. Pergamon Press,New York (1971).

193. Misek,T. (Edt.)
'Recommended Systems For Liquid-Liquid Extraction Studies,EFCE Working Party on Distillation,Absorption and Extraction.
Inst. Chem. Engr. London (1978).

194. Miller,R.S.,Ralph,R.L.,Curl,R.L.and Towell,G.D.
A.I.Ch.E.J. 9,196 (1963).

195. Mok,Y.and Treybal,R.E.
A.I.Ch.E.J 17,916 (1971).

196. Morrello,V.S.and Poffenberger,N.
Ind.Eng.Chem. 42(6),1021 (1950).

197. Moulton,R.W.and Walkey,J.E.
Trans.A.I.Ch.Eng. 40,695 (1944).

198. Mugele,R.A.and Evans,H.D.
Ind.Eng.Chem. 43(6),1317 (1955).

199. Mumford,C.J.and Al-Hemeri,A.A.A.
Proc.Int.Sol.Ext.Con.,Lyon 2,1591 (1974).

199a. Mumford,C.J.
British Chem.Eng.13,337 (1968)

200. Murali,K.and Raja Rao,M.
Jl.Chem.Eng.Data 7,468 (1962).

201. Murrucci,G.,Apuzzo,G.and Astarita,G.
A.I.Ch.E.J. 16,538 (1970).

202. Nandi,S.K.and Ghosh,S.K.
Jl.Indian Chem.Soc.& News 13(2&3),93 (1950).

203. Nandi,S.K.and Ghosh,S.K.
Jl.Indian Chem.Soc.& News 13(2&3),103 (1950)

205. Neilsen,L.E.,Wall,R.and Adams,G.
Jl.Colloid Sci. 13,441 (1958).

206. Newman,A.B.
Trans.A.I.Ch.E. 27,310 (1931).

207. Null,H.R.and Johnson,H.F.
A.I.Ch.E.J. 3,273 (1958).

208. Oberg,A.G.and Jones,S.C.
Chem. Eng. 70(15),119 (1963).

209. Olander,D.R.
A.I.Ch.E.J 7,175 (1961).

210. Olander,D.R.
A.I.Ch.E.J. 12,1018 (1966).

211. Oliver,E.D.
'Diffusional Separation Process'
Wiley, New York (1966).

212. Oliveri Del Casstillo,G.
Chem-Ing-Tech. 56,9 (1984).

213. Oloidi,J.O.and Mumford,C.J.
Paper Presented at Research Meeting,Society Of Chemical Industry,Sol.Ext& Ion.Exch.Group,University Of Aston 5th . May (1985).

214. Oloidi,J.O.,Jeffreys,G.V.and Mumford,C.J.
Int.Sol.Ext.Conf. (ISEC '86) Vol.3 pg.157 Munich,W.Germany,Sept.(1986).

215. Olney,R.B.
A.I.Ch.E.J. 10,827 (1964).

216. Orella,A.and Westwater,J.W.
A.I.Ch.E.J 8,350 (1962).

217. Patel,J.M.and Wellek,R.M.
A.I.Ch.E.J. 13,384 (1967).

218. Perrut,M.and Loutaty,R.
Chem.Eng.Jl. 3,286 (1972).

219. Perrut,M.and Loutaty,R.
Chem.Eng.Sci. 27,669 (1972).

220. Perry,R.C.and Chilton,C.H. (Ed.)
'Chemical Engineer`s Handbook'
McGraw-Hill Kogakusha 5th. Ed. (1973).

221. Ponikarov,I.I.,Nikolaev,A.M.and Zhavronkov.N.M.
Int.Chem.Eng. 2,546 (1962).

222. Prabhu,N.,Agarwal,A.K.,Degallesan,T.E.and Laddha,G.S.
Indian Jl.Tech. 14(2),55 (1976).

223. Pratt,H.R.C.
Ind.Chem. 30,597 (1954).

224. Pratt,H.R.C.
Ind.Chem. 31,505 (1955).

226. Pritchard,C.L.and Biswas,S.K.
Brit.Chem.Eng. 10,86 (1965).

225. Princen,H.M.
Jl.Colloid Sci. 18,178 (1963).

227. Pistor,H.
Die Petroxoverhuolinge In 'Chem.Technologie' Winnacker,K.and Luchler,L.(Edt).
Vol.1,513 (1969).

228. Pyle,C.,Colburn,A.P.and Duffey,H.R.
Ind.Eng.Chem. 42,1042 (1950).

229. Rajan,S.M.and Heiderger,W.J.
A.I.Ch.E.J. 17,203 (1971).

230. Raju,J.,Sagar,D.V.and Sripathi,T.
Chem.Petro.Chem.Jl. 11(8),3 (1980).

231. Rammond,D.R.and Ziemiski,S.A.
A.I.Ch.E.J. 17,57 (1971).

232. Rao,E.V.,Kumar,R.and Kuloor,N.R.
Chem.Eng.Sci. 21,867 (1966).

233. Reddy,K.A.and Doraiswarmy,L.K.
Ind.Eng.Chem.Fund. 6(1),77 (1967).

234. Reman,G.H.
'Joint Symposium Of The Scale-Up Of Chemical Plant and Process'.Inst.Chem.Engrs.London (1957).

235. Reman,G.H.
Chem.Eng.Prog. 62(9),56 (1966).

236. Rietema,K.
`Advances In Chem.Engineering Chap.7 Pg.237 vol.5' Academic Press,New York (1964).

237. Rod,V.
Bri.Chem.Eng. 11(6),483 (1966).

238. Rose,P.M.and Kintner,R.C.
A.I.Ch.E.J. 12,530 (1966)..

239. Rosin,P.and Rammler,E.
Jl.Inst.Of Fuel 7,29 (1933).

240. Rod,V.
Paper Presented At The Euro.Fed.Chem.Engrs. Prague,Czechoslovakia (1970).

241. Rodger,W.A.,Trice,V.G.and Rushton,J.H.
Chem.Eng.Prog. 52(12),515 (1956).

242. Row,S.B.,Koffolt,J.H.and Withrow,J.R.
Trans.A.I.Ch.Eng. 37,559 (1941).

243. Rowe,P.N.,Claxton,K.T.and Lewis,J.B.
Trans.Int.Chem.Engs. 43,14 (1965).

244. Ruby,C.L.and Elgin,J.C.
Chem.Eng.Prog.Symp.Ser. 51(15),17 (1955).

245. Ruff,K.,Pilhofer,T.and Mersman,A.
Int.Chem.Eng. 18,395 (1978).

246. Ryan,J.P.
Ph.D Thesis,University Of Missouri, St.Louis.(1966).

247. Rybczynski,W.
Bul.Int.Acad.Sci.Lett.Cracovie,Sierie A,40 (1911).

248. Sainth,G.S.and Saga,D.V.
Chem. and Petro. Chem.Jl. 7(10),23 (1976).

249. Saradhy,Y.P.and Kumar,R.
Ind.Eng.Chem.Proc.Des.Dev.5(1),75 (1976).

250. Sastry,T.V.,Rama Murty,M.,Rao,J.and Venkata Rao,C.
Chem.and Petro.Chem.Jl. 11(8),25 (1980).

251. Satapathy,R.and Smith,W.
Jl.Fluid.Mech. 10,561 (1961).

252. Sawistowski,H.and Goltz,G.G.
Trans.I.Ch.E. 41,174 (1963).

253. Sawistowski,H.
In "Recent Advances In Liquid-Liquid Extraction" Chapter 9
C.Hanson. Ed.Pergamon ,Oxford (1971).

254. Sawistoswski,H.
Chem-Ing-Tech. 45,1114 (1973).

255. Sawistowski,H.
NATO Adv.Std.Inst.Series,Series E,72,613 (1983).

256. Schiebel,E.G.
Ind.Eng.Chem. 46,2007 (1954).

257. Schroeder,R.R.and Kintner,R.C.
A.I.Ch.E.J. 11,5 (1965).

258. Schulz,L.and Pilhofer,T.
Int.Chem.Eng. 22(1),61 (1982).

259. Schweitzer,P.A. (Ed.)
'Handbook of Separation Techniques For Chemical
Engineers' Pt.(i) Pg.283 MaGraw-Hill, New York (1979).

260. Sherwood,T.K.,Pigford,R.L.and Wilke,C.R.
`Mass Transfer' pp188
McGraw-Hill, New York (1975).

261. Sherwood,T.,Evans,J.E.and Longer,J.W.
Trans.A.I.Ch.E. 35,597 (1939).

262. Shiffler,D.A.
Ph.D. Thesis, Cornell University, Itach,N.Y.(1965)

263. Shrotsuka,T.and Murakami,A.
Kagaku Kogaku (Japan) 30,727 (1966).

264. Seidell,A. and Linke,W.F.
'Solubilities Of Inorganic and Organic Compounds'
Supple. to 3rd Ed. Pg.821
D. Van. Nostrand co. Inc. New York (1952)

265. Sims,L.L.and Bolme,D.W.
Jl.Chem.Eng.Data 10,111 (1965).

266. Skelland,A.H.P.and Wellek,R.M.
A.I.Ch.E.J. 10,491, (1964).

267. Skelland,A.H.P.and Cornish,A.R.H
Can. Jl. Chem. Eng. 43,302 (1965).

268. Skelland,A.H.P.and Minhas,W.J.
A.I.Ch.E.J. 17,1316 (1971).

269. Skelland,A.H.P.and Conger,W.L.
Ind.Eng.Chem.Proc.and Dev. 12(4),448 (1973).

270. Skelland,A.H.P.
'Diffusional Mass Transfer'
Wiley-Interscience (1974).

271. Skelland,A.H.P.and Johnson,K.R.
Can.Jl.Chem.Eng. 52,732 (1974).

272. Skelland,A.H.P.and Shah,A.V.
Ind.Eng.Chem.Proc.Des.& Dev. 14,379 (1975).

273. Skelland,A.H.P.and Huang,Y.F.
A.I.Ch.E.J. 23(5),701 (1977).

274. Skelland,A.H.P.and Huang,Y.F.
A.I.Ch.E.Jl. 25,80 (1979).

275. Skelland,A.H.P.and Vasti,N.C.
Can.Jl.Chem.Eng. 63,390 (1985).

276. Smith,A.R.,Caswell,J.E.,Larsen,P.P.and Cavers,S.D.
Can.Jl.Chem.Eng. 41,150 (1963).

277. Smith,D.V.and Davies,G.A.
Can.Jl.Chem.Eng. 45,628 (1970).

278. Smith,D.V.and Davies,G.A.
A.I.Ch.E. Symp.Ser. 68(124),1 (1972).

279. Slater,M.J.
Chemie Ing.Technik 46(15),663 (1974).

280. Slater,M.J.
Jl.Sep.Proc.Tech.5 (1984).

281. Sleicher,C.A.
A.I.Ch.E.J. 5,145 (1959).

282. Steinour,H.
Ind.Eng.Chem. 36,618 (1944).

283. Sternling,C.V.and Scriven,L.G.
A.I.Ch.E.J. 5,514 (1959).

284. Sturke,B.
Naturnissenschaften 39,325 (1952).

285. Susanov,E.Ya.,Novozhilova,A.P.and Feolorov,E.A.
Int.Chem. Eng. 7,423 (1967).

286. Tadaki,T.and Maeda,S.
Kogaku-Kagaku 25,254 (1961).

287. Thakar,N.S.and Othmer,D.F.
Ind.Eng.Chem. 45,589 (1953)

288. Thornton,J.D.and Pratt,H.R.C.
Trans.I.Ch.E. 31,289 (1953).

289. Thornton,J.D.
Jl.Chem.Eng.Japan 8,361 (1975).

290. Thorsen,G.and Terjersen,S.G.
Chem. Eng. Sci. 17,137 (1962).

291. Thorsen,G.and Storolalem,R.M. and Terjersen,S.G.
Chem.Eng.Sci. 23,413 (1968).

292. Todd,D.B.
Chem Eng.69(14),,156 (1962).

293. Toor,H.L.and Marcello,J.M.
A.I.Ch.E.J. 4,97 (1958).

294. Treybal,R.E.and Dumoulin,F.E.
Ind.Eng.Chem. 34,709 (1943).

295. Treybal,R.E.
'Liquid Extraction' 2nd Ed.McGraw-Hill (1963).

296. Treybal,R.E.
'Mass Transfer Operations' 2nd Ed.McGraw-Hill (1968)

297. Treybal,R.E.
'Chemical Engineers Handbook' 5th.Ed.(Chapter 15)
Perry,R.H.and Chilton,C.H.(Edt.)
McGraw-Hill Kogakusha (1973).

298. Ueyama,K.and Hatanaka,A.
Kogaku Kogaku 35,605 (1971).

299. Van der Akker,H.E.A.
Chem.Eng.Jl. 19,255 (1980)

300. Vedaiyan,S.,Degallesan,T.E.,Laddha,G.S.and Hoelscher,H.E.
A.I.Ch.E.Jl. 18,161 (1972).

301. Vedaiyan,S.,Degallesan,T.E.and Laddha,G.S.
Indian Jl.Tech. 12(4),135 (1974).

302. Vermeulen,T.J.
Ind.Eng.Chem. 45,1664 (1953).

303. Vijayan,S.,Furrer,M.and Ponter,A.B.
Can. Jl.Chem.Eng. 54,296 (1976).

304. Von Berg,R.L.and Weigandt,H.F.
Chem.Eng. 59,189 (1952).

305. Wagner,C.
Metal Trans. 4,91 (1952).

306. Walla,D.S.and Vir,D.
Chem.Eng.Sci. 31,525 (1976).

307. Warshay,M.,Bogusz,E.,Johnson,M.and Kintner,R.C.
Can.Jl.Chem.Eng. 37,29 (1959).

308. Waslo,S.and Gal-or,G.
Chem.Eng.Sci. 26, 829 (1971).

309. Wellek,R.M.and Skelland,A.H.P.
A.I.Ch.E.Jl. 11,557 (1965).

310. Weissermel,K.and Arpe,H.J.
'Industrille Orgausche Chemie'
Verlag Chemis,Weinhein (1976).

311. West,F.B.,Robinson,P.A.,Morgenthaler,A.C.,Beck,J.R.
and McGregor,D.K.
Ind.Eng.Chem. 44,625 (1951).

312. West,F.B.,Heerman,A.J.,Chong,A.T.and Thomas,L.E.K.
Ind.Eng.Chem. 44,625 (1952).

313. Whitman,W.G.
Chem.and Mett.Eng. 29,147 (1923).

314. Wilke,C.R.and Chang,P.
A.I.Ch.E.Jl. 1,264 (1955).

315. Winnikow,S.and Chao,B.T.
Physic Fluids 9,50 (1966).

316. Wongswan,S.,Perez de Ortiz,E.S.and Sawistowski,H.
Proc.Hydromatallurgy,D4 (Soc.Chem.Eng.)(1981)

317. Yamaguchi,M.,Watambe,S.and Katayama,T.
Jl.Chem.Eng.Japan 8,415 (1975).

318. Yamaguchi,M.,Fujamato,T.and Katayama,T.
Jl.Chem.Eng.Japan 8,361 (1975).